INVESTIGATING MACROPHAGE DYSFUNCTION IN PULMONARY FIBROSIS

CIGARETTE SMOKE EXPOSURE AND IMPAIRED ENDOPLASMIC RETICULUM STRESS RESPONSES UNDERLIE ALTERED PULMONARY MACROPHAGE COMPOSITION AND FUNCTION DURING LUNG INJURY, FIBROSIS, AND REPAIR

BY OLIVIA MAGED MILAD ANIES MEKHAEL, HON. B.SC.

A Thesis Submitted to the School of Graduate Studies in Partial Fulfilment of the Requirements for the Degree Doctor of Philosophy

DOCTOR OF PHILOSOPHY (2021) McMaster University

Department of Medical Sciences Hamilton, Ontario, Canada

TITLE:

Cigarette smoke exposure and impaired endoplasmic reticulum stress responses underlie altered pulmonary macrophage composition and function during lung injury, fibrosis, and repair.

AUTHOR:

Olivia Mekhael, Hon. B.Sc. in Life Sciences (McMaster University)

SUPERVISOR:

Dr. Kjetil Ask

NUMBER OF PAGES:

xxi, 221

LAY ABSTRACT

Fibrotic interstitial lung diseases (ILDs) comprise a wide array of devastating, irreversible, and ultimately fatal heterogeneous disorders of known and unknown etiology. Pulmonary fibrosis constitutes the late phase of ILDs. Pulmonary fibrosis is characterized by progressive lung scarring due to excessive wound healing. The exact triggers which initiate fibrotic processes remain unknown. Nevertheless, it is currently believed that in the genetically pre-disposed lung, cigarette smoke exposure contributes to the development of pathogenic fibrosis. Notably, central to the pathogenesis of cigarette smoke-associated pulmonary fibrosis is the macrophage. In addition to smoking, intrinsic processes mediated by protein misfolding, prolonged endoplasmic reticulum (ER) stress, and chronic unfolded protein response (UPR) perform vital roles in macrophage activation in pulmonary fibrosis. To date, the mechanisms by which continuous smoking and altered ER stress/UPR affect pulmonary macrophage composition, function and consequently pulmonary fibrosis development, progression, and immunopathogenesis are yet to be elucidated. This Ph.D. thesis begins by assessing the impact of smoking on the survival and pulmonary function outcomes of patients diagnosed with fibrotic ILDs. Subsequently, the thesis investigates the effects of smoking and aberrant ER stress/UPR on pulmonary macrophage composition and function in the setting of lung injury, tissue remodelling, and fibrogenesis using preclinical experimental mouse models.

ABSTRACT

RATIONALE. Fibrotic interstitial lung diseases (ILDs) comprise a wide array of heterogeneous disorders of known and unknown etiology. Pulmonary fibrosis constitutes the late phase of ILDs. A variety of extrinsic and intrinsic risk factors are implicated in fibrotic ILD development and pathogenesis, with macrophages considered central orchestrators of disease pathogenesis. Particularly, cigarette smoking, protein misfolding, endoplasmic reticulum (ER) stress, and the unfolded protein response (UPR), have been associated with impaired macrophage activation and function. However, a comprehensive understanding of the impact of these processes on the composition and function of pulmonary macrophage subpopulations and subsequently on tissue remodelling in pulmonary fibrosis is yet to be elucidated. In this Ph.D. thesis, we assessed the impact of cigarette smoke (CS) exposure and the myeloid-specific deletion of *Atf6α*, one of the UPR mediators, on pulmonary macrophage subpopulation composition and function during lung injury, tissue remodelling, and fibrogenesis.

METHODS. Current literature to date demonstrates conflicting evidence regarding the impact of smoking status on long-term outcomes in the setting of fibrotic ILDs. Therefore, to further understand the impact of smoking status on fibrotic ILD patients' survival, we began by assessing a prospective observational cohort, the Canadian Registry for Pulmonary Fibrosis (CARE-PF). This included 3062 patients with fibrotic ILD who were considered smokers or never smokers. Next, we used a preclinical experimental mouse model of concurrent bleomycin-induced lung injury and CS exposure to investigate the

effect of CS on macrophage subpopulation composition and function during tissue remodelling processes. Lastly, given that CS is known to stimulate the UPR and that an impaired UPR is a potential mechanism for macrophage dysfunction, we specifically addressed the impact of altered UPR on pulmonary macrophage composition and function during bleomycin-induced lung injury. To achieve that, we utilized the myeloid-specific deletion of *Atf6α*, one of the UPR mediators, experimental approach.

MAIN RESULTS. Findings from subgroup analysis of CARE-PF patient cohort demonstrated that overall, there was a significant interaction between smoking and fibrotic ILD diagnosis (p-value for interaction is 0.039), with respect to mortality. Specifically, the subgroup analysis has shown that smoking was an effect modifier and significantly increased mortality in connective tissue disease-associated ILD and unclassifiable ILD patients, but did not have a significant effect on mortality in idiopathic pulmonary fibrosis and chronic hypersensitivity pneumonitis patients. Furthermore, preclinical findings demonstrated that cigarette smoke exposure impaired the composition of pulmonary macrophages increasing $CD11b^{+}$ subpopulations including monocyte-derived alveolar macrophages (Mo-AM) as well as interstitial macrophage (IM)1, -2 and -3, at multiple CS exposure timepoints. The expansion of Mo-AM and IM3 was dependent on IL-1α and likely reflective of increased cell recruitment. Compositional changes in macrophage subpopulations were associated with impaired induction of fibrogenesis including decreased α-smooth muscle actin positive myofibroblast following intratracheal bleomycin treatment. Mechanistically, *in vivo* and *ex vivo* assays demonstrated predominant

macrophage M1 functional status and reduced matrix metallopeptidase 9 activity in cigarette smoke-exposed mice. Lastly, following bleomycin administration, the myeloid-specific deletion of *Atf6α* altered pulmonary macrophage composition, expanding $CD11b^+$ populations with dual polarized $CD38^+CD206^+$ expressing macrophages. Compositional changes were associated with an aggravation of fibrogenesis including increased myofibroblast and collagen deposition. Further mechanistic *ex vivo* investigation revealed that ATF6α was required for CHOP induction and for the apoptotic death of bone marrow-derived $CD11b^+$ macrophages during chronic ER stress, a process we speculate to be crucial for the attenuation of fibrogenesis.

CONCLUSION. CS and aberrant ER stress/UPR disturbed pulmonary macrophage subpopulation composition and function, expanding $CD11b^+$ macrophages, and resulted in alterations in wound healing and repair processes. Further investigation of $CD11b^+$ macrophages in clinical samples obtained from fibrotic ILD patients enrolled in CARE-PF is required. Targeting these populations through the UPR might offer a potential therapeutic approach to halt fibrotic ILD progression. We believe that a better understanding of the complex interplay of CS, UPR, and macrophage will identify potential intervention strategies to restore conventional macrophage and UPR functions and mitigate disease exacerbation.

ACKNOWLEDGEMENTS

"Nothing in life is to be feared. It is only to be understood. Now is the time to understand more, so that we may fear less." (Marie Curie)

I would like to start by taking this opportunity to extend my sincerest gratitude and appreciation to the exceedingly supportive learning environment **McMaster University** has provided me. At McMaster, I completed 4 years of undergraduate studies in Honours Life Sciences and 4 years of Ph.D. studies in Medical Sciences. During these past 8 years, McMaster has been my second home where I grew up as a scientist and more importantly as a person. At McMaster, I have learned a lot, achieved a lot, and I have failed a lot. I am mostly grateful for the challenges I have experienced; these challenges and failures built my perseverance, constructed my resilience, and have been enabling me to take on future adversities bravely.

Throughout my Ph.D. journey, I have been blessed with working with many people that have diverse skills, knowledge, education, backgrounds, and culture. I had the opportunity to work with research assistants, laboratory and animal technicians, undergraduate and graduate students, postdoctoral fellows, pathologists, chemical biologists, engineers, clinicians, professors, and scientists on collaborative health research projects. Reflecting back to my time in China as part of a research exchange program, I am grateful that I had the opportunity to work with peers who had a different culture and language. I have to admit that my Ph.D. thesis is a product of the knowledge I have acquired from a wide array of mentors and colleagues with different expertise and life perspective.

I would like to recognize the invaluable diverse talents, gifts, and skills that each member of my team has brought to contribute to my intellectual and personal growth. I wish to express my deepest gratitude and appreciation to all the people whose assistance was imperative in the completion of this thesis.

I would like to pay special regards to my supervisor, **Dr. Kjetil Ask**, who has guided, led, and encouraged me. Without his continuing help, feedback, positive attitude, and trust, these studies would not have been materialized. Thank you for taking a chance on me and allowing me to be part of your team.

I wish to show my gratitude to my Ph.D. supervisory committee members, Dr. Anthony Rullo, Dr. Jeremy Hirota, and Dr. Nathan Hambly for all the continuous feedback they have given me throughout the past 4 years. Thank you for your generosity and meaningful insights on my work. Thank you **Dr. Nathan Hambly** for the opportunity you have given me to be part of the CARE-PF clinical project. Thank you **Dr. Anthony Rullo** for the opportunity you have given me to be part of the "cell-specific drug targeting in the lung" review. *"Be comfortable being uncomfortable"*, is one of the many insights I have received from **Dr. Jeremy Hirota** and the one that influenced me the most at both the professional and personal level. Thank you very much **Dr. Jeremy Hirota, Dr. Carl Richards, and Dr. Ali Askhar** for all the feedback you have provided me on my comprehensive examination, committee reports, and committee meeting presentations.

To **Dr. Manel Jordana**, I whole-heartedly appreciate your great advice for my studies, it has proven indispensable towards the success of my work. I would like to thank you very much for all the feedback you have given me. Your positive comments after my WIP presentations, advanced immunobiology course presentation, and comprehensive examination were the motivation I needed to keep me going during very stressful times. You have always encouraged and driven me to embrace science passionately.

To **Dr. Martin Stämpfli**, thank you very much for giving me the opportunity to TA Immunology 3I03, for all the feedback and advice, and for allowing me to be part of your team. I owe a very important debt to Dr. Stämpfli's team; **Dr. Steven Cass**, **Dr. Joshua McGrath**, and **Dr. Danya Thayaparan**. In addition to your mentorship, guidance, and continuous feedback on my work, you taught me the meaning of team spirit, unity, and synergy. You are extremely brilliant and yet the humblest people I have met. Thank you very much for being great mentors, I learned a lot from all your insightful comments and suggestions.

I wish to express my sincere gratitude and appreciation to **Dr. Tereza Martinu** who saw my potential and gave me the opportunity to be part of the CLAD team by offering me a postdoctoral fellowship. Thank you for believing in me and I will make sure that I do not let you down. I would like to offer my special thanks to **Dr. Robert Matthew Tighe** for agreeing to be the external examiner of the Ph.D. oral defence.

I wish to express my sincere appreciation to **Dr. Anna Dvorkin-Gheva** and **Dr. Malik Farooqi** for their assistance with bioinformatics and statistics. Without their

expertise, this thesis would have been incomplete. The technical contribution of **Jane Ann Smith, Joanna Kasinsj, Mary Jo Smith, Mary Bruni, Christine Mader (King), Leanne Blanchard, Liliana De Sousa, and Hong Liang** is truly appreciated. Without their support, this project could not have reached its true potential.

I am indebted to **Dr. Jewel Imani, Dr. Ehab Ayaub, and Hemisha Patel**, who believed in me and allowed me to get exposed to the research world, the world that I immediately became passionate about. To my former and current lab mates, **Spencer Revill, Amir Reihani, Nafis Wazed, and Dr. Anmar Ayaub**, thank you very much for all your assistance and for providing me with great support.

To my colleagues and friends, **Dr. Manreet (Sonia) Padwal, Aaron Hayat, and Megan Vierhout**. Thank you for not giving up on me and for lending an ear to support during my toughest times. Thank you for all the technical help and moral support.

I am deeply grateful for the support and great love of my family**, my mother, Nancy; my father, Maged; and my sister, Julia**. Their sacrifices and faith in me kept me going on and this thesis would not have been possible without their input, encouragement, love, and trust.

DEDICATION

In memory of my grandfather, Milad, who always believed in me, but never saw this adventure. I hope I kept my promise.

TABLE OF CONTENTS

LIST OF FIGURES AND TABLES

None

LIST OF ABBREVIATIONS AND SYMBOLS

Activating transcription factor 6 - **ATF6**

Acute exacerbation - **AE**

Alpha smooth muscle actin - **α-SMA**

Alveolar epithelial cell - **AEC**

Arginase-1 - **Arg-1**

Basic leucine zipper - **bZIP**

Binding immunoglobulin protein - **BiP**

Bronchoalveolar lavage - **BAL**

cAMP-response-element-binding protein-related protein - **CREB-RP**

CCAAT/enhancer binding proteins (C/EBP) homologous protein - **CHOP**

CC chemokine ligand 18 - **CCL18**

Cellular FADD-like IL-1β–converting enzyme–inhibitory protein - **c-Flip**

Chinese hamster ovary - **CHO**

Chronic obstructive pulmonary disease - **COPD**

Cigarette smoke extract - **CSE**

cJUN NH2-terminal kinase (JNK)-IRE1-TNF receptor-associated factor 2 (TRAF2)-apoptosis signal-regulating kinase1 (ASK1) complex - **IRE1/ASK1/JNK**

Composite physiologic index - **CPI**

Computed tomography - **CT**

Confidence interval - **CI**

Connective tissues disease-associated ILD - **CTD-ILD**

Diffusing capacity for carbon monoxide - **D_{LCO}**

Endoplasmic reticulum - **ER**

Extracellular matrix - **ECM**

Forced expiratory volume (1 second) - **FEV1**

Forced vital capacity - **FVC**

Glucose-regulated protein 78 - **GRP78**

Human bronchial epithelial cell - **hBEC**

Hypersensitivity pneumonitis - **HP**

Hypoxia-inducible factor 1α - **HIF-1α**

Idiopathic pulmonary fibrosis - **IPF**

Inositol-requiring enzyme 1 - **IRE1**

Interferon gamma - **IFN-γ**

Interleukin - **IL**

Interstitial lung disease - **ILD**

Interstitial macrophage - **IM**

Lipopolysaccharide - **LPS**

Macrophage colony-stimulating factor [M-CSF] receptor - **Csfr1**

Monocyte-derived alveolar macrophage - **Mo-AM**

Nuclear factor kappa-light-chain-enhancer of activated B cell - **NF-kB**

Odds ratio - **OR**

Pattern recognition receptor - **PRR**

4-phenylbutyrate - **4-PBA**

Protein kinase R (PKR)-like endoplasmic reticulum kinase - **PERK**

Reactive oxygen species - **ROS**

Resident alveolar macrophage - **Res-AM**

Smooth muscle cell - **SMC**

T helper -**Th**

Toll-like receptor - **TLR**

Transforming growth factor beta - **TGF-β**

Tumour necrosis factor-α - **TNF-α**

Unfolded protein response - **UPR**

Usual interstitial pneumonia - **UIP**

DECLARATION OF ACADEMIC ACHIEVEMENT/ PREFACE

The present Ph.D. thesis has been prepared in a "sandwich" thesis format according to the instructions described in the "Guide for the Preparation of Master's and Doctoral Theses" provided by the School of Graduate Studies at McMaster University. The present Ph.D. thesis consists of five chapters. Chapter 1 is an introduction for the three primary research projects conducted for this Ph.D degree. Specifically, chapter 1 contains the background information and the current knowledge in the literature which aim to facilitate the understanding of the rationale of the primary studies discussed later in chapters 2-4. Chapters 2-4 are three independent and yet interconnected primary research projects that investigate the contribution of extrinsic risk factor (smoking), cell type (macrophage), intrinsic molecular mechanisms and biological processes (ER stress and the UPR) to the immunopathogenesis and pathophysiology of fibrotic lung diseases. The thesis ends with chapter 5 which discusses the interplay of major findings from the primary research illustrated in chapters 2-4, the significance of the findings, and clinical implications.

Chapter 1: This section includes all the general information and the most recent beliefs and thoughts on the major themes of this thesis. Understanding the concepts illustrated in this chapter is essential to better recognize the rationale and objectives of our studies. A discussion of the current gaps in the field, the major issues, and controversies which require further investigation has also been highlighted.

Chapter 2: Olivia Mekhael, M. Malik Farooqi, Anna Dvorkin-Gheva, Kathryn Donohue, Ciaran Scallan, Fahad Alobaid, Deborah Assayag, Kerri A. Johannson, Charlene D.

Fell, Veronica Marcoux, Helene Manganas, Julie Morisset, Jolene H. Fisher, Shane Shapera, Andrea S. Gershon, Teresa To, Alyson Wong, Mohsen Sadatsafavi, Pearce G. Wilcox, Andrew J. Halayko, Nasreen Khalil, Debarati Chakraborty, Gerard Cox, Christopher J. Ryerson, Kjetil Ask, Martin R.J. Kolb, Nathan Hambly[#]. Effect of Smoking Status on Fibrotic Interstitial Lung Disease: Novel Insights from the Prospective Canadian Registry for Pulmonary Fibrosis. *An unpublished brief communication clinical report*.

In this chapter, we hypothesize that smoking will be associated with poorer survival and more severe pulmonary function outcomes in patients diagnosed with fibrotic interstitial lung diseases. This work has been carried out over the period of December 2019 – June 2021. This chapter includes a clinical project that was conducted in collaboration with clinicians, scientists, and statisticians. As the primary author, I developed the main hypothesis, research questions, and objectives of the study, analysed and interpreted most of the generated data obtained from a registry of fibrotic ILD patients, and drafted the manuscript. Database development and statistical analysis were carried out by Dr. M. Malik Farooqi and Dr. Anna Dvorkin-Gheva. Collecting patients' clinical information from multiple clinical centres across Canada and constructing the prospective Canadian registry for pulmonary fibrosis were performed by a team of clinicians and researchers including Kathryn Donohue, Ciaran Scallan, Fahad Alobaid, Deborah Assayag, Kerri A Johannson, Charlene D Fell, Veronica Marcoux, Helene Manganas, Julie Morisset, Jolene H Fisher, Shane Shapera, Andrea S Gershon, Teresa To, Alyson Wong, Mohsen Sadatsafavi, Pearce G Wilcox, Andrew J Halayko, Nasreen Khalil, Debarati Chakraborty, and Gerard Cox. Dr.

Christopher J. Ryerson, Dr. Kjetil Ask, and Dr. Martin R.J. Kolb oversaw the project. Dr. Nathan Hambly supervised the project, critically appraised the work, and edited the manuscript.

Chapter 3: Steven P. Cass[†], Olivia Mekhael[†], Danya Thayaparan, Joshua JC. McGrath, Spencer D. Revill, Matthew F. Fantauzzi, Peiyao Wang, Amir Reihani, Aaron I. Hayat, Christopher S. Stevenson, Anna Dvorkin-Gheva, Fernando M. Botelho, Martin R. Stämpfli[†], and Kjetil Ask[†]. Increased monocyte-derived $CD11b^{+}$ macrophage subpopulations following cigarette smoke exposure are associated with impaired bleomycin-induced tissue remodelling. *An original research article submitted to and in review in Frontiers in Immunology*.

In collaboration with Dr. Stämpfli's group, we hypothesize that cigarette smoke exposure expands monocyte-derived alveolar and interstitial macrophage subpopulations. We hypothesize further that these expanded monocyte-derived macrophages will exacerbate immunopathology and tissue remodelling in a mouse model of lung injury. This work has been performed over the period of November 2019 – June 2021. Steven P. Cass and I have contributed equally to the work described in this chapter. As primary authors, we designed and performed all the experiments, analysed, and interpreted all the generated data, drafted, edited, and revised the manuscript. Experimental and technical assistance was provided by Danya Thayaparan, Joshua JC. McGrath, Spencer D. Revill, Matthew F. Fantauzzi, Peiyao Wang, Amir Reihani, Aaron I. Hayat, and Dr. Fernando M. Botelho. Bioinformatic and statistical assessments were performed by Dr. Anna Dvorkin-Gheva.

Resources were provided by Christopher S. Stevenson. Dr. Martin R. Stämpfli and Dr. Kjetil Ask provided resources, supervised the project and the experiments, edited, and critically appraised the manuscript.

Chapter 4: Olivia Mekhael, Spencer D. Revill, Aaron I. Hayat, Steven P. Cass, Kyle MacDonald, Megan Vierhout, Anmar Ayoub, Amir Reihani, Manreet Padwal, Jewel Imani, Ehab Ayaub, Anna Dvorkin-Gheva, Anthony Rullo, Jeremy A. Hirota, Carl D. Richards, Darren Bridgewater, Martin R. Stämpfli, Nathan Hambly, Asghar Naqvi, Martin R.J. Kolb, and Kjetil Ask[#]. Myeloid-specific deletion of activating transcription factor 6 alpha increases $CD11b^{+}$ macrophage subpopulations and aggravates lung fibrosis. *An original research article submitted to and in review in Immunology and Cell Biology*.

In this chapter, we hypothesize that the myeloid-specific deletion of *Atf6α* will halt the pro-fibrotic function of pulmonary macrophage subpopulations during lung injury and tissue remodelling. This work has been carried out over the period of September 2017 – June 2021. I initiated this work when I started my Masters in 2017 and continued working on it after transferring to Ph.D. in 2019. As the primary author, I conceptualized, designed, and carried out all the experiments, analysed and interpreted all the generated data, drafted, edited, and revised the manuscript. Experimental and technical assistance was provided by Spencer D. Revill, Aaron I. Hayat, Steven P. Cass, Kyle MacDonald, Megan Vierhout, Dr. Anmar Ayoub, Amir Reihani, Dr. Manreet Padwal, Dr. Jewel Imani, and Dr. Ehab Ayaub. Bioinformatic and statistical assessments were performed by Dr. Anna Dvorkin-Gheva. Drs. Anthony Rullo, Jeremy A. Hirota, Carl D. Richards, Darren Bridgewater, Martin R.

Stämpfli, Nathan Hambly, Asghar Naqvi, and Martin R.J. Kolb critically appraised the work and provided scientific input. Dr. Kjetil Ask provided resources, supervised the project and the experiments, edited, and critically appraised the manuscript.

Chapter 5: This chapter discusses the interplay of the major findings obtained from the three primary research projects. The chapter also highlights the significance of the work presented in this thesis and how the findings might be supporting or adding to the current knowledge in pulmonary fibrosis research field. A discussion of the potential clinical implications of the presented Ph.D. studies has also been included in this chapter.

Chapter 1

Introduction

- Fibrotic interstitial lung diseases - Overview and pathophysiology
  Multifaceted complex interplay of genetic and environmental risk factors

- Extrinsic risk factor: Smoking in fibrotic interstitial lung diseases

- Cell type: Pulmonary macrophages
  Pulmonary macrophage composition and phenotype
  Pulmonary macrophage contribution to cigarette smoke-induced inflammation
  Pulmonary macrophage contribution to tissue remodelling and fibrosis

- Intrinsic molecular mechanism: Role of protein misfolding, endoplasmic reticulum stress, and the unfolded protein response in pulmonary fibrosis
  Endoplasmic reticulum stress and the unfolded protein response – Overview
  Impact of endoplasmic reticulum stress on pro-fibrotic feature of alveolar epithelial cells in pulmonary fibrosis
  Impact of endoplasmic reticulum stress on pro-fibrotic feature of macrophages in pulmonary fibrosis
  Impact of endoplasmic reticulum stress on pro-fibrotic feature of myofibroblasts in pulmonary fibrosis

- Activating transcription factor 6 alpha

- Mouse models of lung fibrosis, a published book chapter

- Central Aim and Thesis Objectives

Fibrotic interstitial lung diseases - Overview and pathophysiology

Multifaceted complex interplay of genetic and environmental risk factors

Diffuse parenchymal lung diseases comprise a wide array of heterogeneous disorders of known and unknown etiology[1,2]. These disorders are characterized by a variety of pathological abnormalities which predominately appear in the lung interstitium, hence, they are termed interstitial lung diseases **(ILDs)**[1]. Pulmonary fibrosis constitutes the late phase of ILDs[3]. Fibrotic ILD is characterized by progressive scarring of the alveolar interstitium[4], destruction of the pulmonary parenchyma, deposition of extracellular matrix **(ECM)**, and significant alterations in the phenotype and function of fibroblasts and alveolar epithelial cells[3]. Collectively, this results in progressive decline in lung function and respiratory failure[5]. Major fibrotic ILD subtypes include idiopathic pulmonary fibrosis **(IPF)**, connective tissue disease-associated ILD **(CTD-ILD)**, and chronic hypersensitivity pneumonitis **(HP)**[5,6]. IPF is the most common fibrotic ILD[1] that occurs primarily in older adults[7]. The etiology of IPF has not been identified, but the disease is known to be characterized by the presence of an imaging and pathological pattern of usual interstitial pneumonia **(UIP)**[1].

A broad range of "early phase" disease-specific pathogenic insults result in the "late phase" shared self-perpetuating pulmonary fibrosis[1]. These early inflammatory insults include autoimmunity as detected in CTD-ILD and chronic granulomatous inflammation resulting from the persistent exposure to an inhaled antigen as in the case of chronic HP[1]. Unlike the inflammation-driven fibrosis occurring in CTD-ILD and HP, disorders

characterized by unresolved chronic inflammatory processes, IPF is currently believed to manifest as a fibrotic disorder from the beginning[2]. IPF has been proposed to be an epithelial-driven disorder that results from a complex interaction of genetic and environmental risk factors, and aging-associated processes[2]. Particularly, in the genetically predisposed aged lung, multiple environmental risk factors (tobacco smoking, occupational exposures, air pollution, microaspiration, and viral infection) result in recurrent injuries to the alveolar epithelial cell **(AEC)** and this may initiate the early pathogenic mechanisms in IPF[1,2,8–10]. Consequently, alveolar epithelial cells undergoing aberrant activation and phenotypic and functional changes, eventually result in maladaptive repair processes characterized by excessive apoptosis[1,2,8–10]. Notably, both inflammation- and epithelial-driven disorders trigger similar fibrotic signaling pathways involving fibroblast and myofibroblast activation, tissue remodelling, persistent secretions of extracellular matrix components, and finally fibrosis[1,2,8–10]. Specifically, following repeated alveolar epithelial cell injuries or chronic immune inflammation, pro-fibrotic cytokines promote fibroblast activation, followed by proliferation and differentiation into myofibroblasts[1]. Subsequently, myofibroblasts migrate to the alveolar interstitium[1] and are characterized as the main drivers of pathological tissue fibrosis[11,12]. Myofibroblasts can originate from multiple different precursors including the proliferation of resident fibroblasts, the differentiation of epithelial cells, endothelial-to-mesenchymal transition, and bone marrow–derived circulating fibrocytes[1,12]. The later phase of fibrogenesis involves extracellular matrix production, resulting in lung tissue remodelling and subpleural microscopic honeycombing. Tissue stiffness and hypoxia associated with remodelling

further promote myofibroblast activation and pro-fibrotic cytokine pathways[1]. To note, structural components such as fibrillar collagens and elastin perform vital roles in the ECM stiffness which in turn enhances myofibroblast activity through positive feedback loops, including the secretion and activation of matrix-bound latent transforming growth factor beta **(TGF-β)**[2]. TGF-β activates multiple transcriptional pathways promoting the expression of pro-fibrotic genes, including TGF-β itself and this subsequently leads to a progressive pro-fibrotic loop[2] and, thereby perpetuating fibrogenesis[1].

Pathological lung fibrosis is irreversible and managing the disease is currently the only option. Management strategies include supplemental oxygen, smoking cessation, pulmonary rehabilitation[7], antifibrotic drugs (pirfenidone or nintedanib for IPF patients), or immunomodulation with glucocorticoids and immunosuppressive therapy (for inflammation-driven fibrotic ILD)[1]. While managing fibrotic ILD aims to ameliorate disease symptoms or slow down disease progression while maintaining quality of life[1], there is currently no cure for pulmonary fibrosis. This suggests the need to further investigate the ***extrinsic risk factors***, the different ***cell types***, the ***intrinsic molecular mechanisms and biological processes*** which contribute to fibrotic ILD immunopathogenesis and pathophysiology. Understanding the complex interplay of risk factors and cellular and molecular mechanisms will enable the identification of interventions and therapeutic approaches that would eventually halt and reverse pulmonary fibrosis.

Extrinsic risk factor: Smoking in fibrotic interstitial lung diseases

Tobacco smoking is *"the single most preventable cause of death in the world"* (World Health Organization, 2008)[13]. Cigarette smoke, an aerosol (a mixture of solid and liquid particles) and gases[14], contains approximately 7,357 chemical compounds[15], including many well-characterized toxins and carcinogens[14]. The tobacco leaf is composed of a variety of alkaloid chemicals[15]. Nicotine, an addictive compound in humans, is the most abundant[15]. It has been estimated that the lungs of a 60-year-old person with a 40-pack-year smoking history commencing at age 20 years, have inhaled the smoke from approximately 290,000 cigarettes[14]. The significant amount of carcinogens and toxins distributed to the respiratory system place this smoker at substantial risk for chronic obstructive pulmonary disease **(COPD)**, lung cancer, and other nonmalignant diseases affecting all components of the respiratory tract including the mouth[14].

The role of smoking in COPD and lung cancer has already been established[16,17]. In contrast, the link between smoking and fibrotic ILDs is not yet well defined[18]. Principally, in a multicenter case-control study, a history of smoking was associated with an increased risk of developing IPF, with an odds ratio **(OR)** for ever-smokers (current and ex-smokers) of 1.6 (95% Confidence Interval **(CI)**: 1.1 to 2.4)[19,20]. In a meta-analysis of observational studies, cigarette smoking and other environmental and occupational exposures were significantly associated with IPF development. In these studies, the overall OR for ever-smoking as IPF risk factor was 1.58 (95% CI: 1.27–1.97)[21]. Paradoxically, reports also suggest that concurrent smoking status with IPF is positively associated with improved

prognosis and survival compared to never or ex-smokers[22,23]. Nonetheless, this phenomenon is not fully conserved across all cohorts. Following age and disease status adjustment, multiple cohorts observed no significant survival benefit with current smoking status[24,25]. These conflicting research findings might be partially due to the fact that indices utilized to measure IPF severity such as the diffusing capacity for carbon monoxide **(D_{LCO})** and the forced vital capacity **(FVC)** are affected by the coexistence of smoking-related damage[24]. In an attempt to resolve this issue, the composite physiologic index **(CPI)** was developed and has been used to account for the confounding functional effects of coexisting emphysema[24] *"a major confounding influence on pulmonary function indices"*[26]. The CPI measures the functional damage related to pulmonary fibrosis, while excluding that attributable to emphysema[26]. As a case in point, using a cohort of 249 patients with IPF (current smokers, n=20; former smokers, n=166; never smokers, n=63), Antoniou *et al.* (2008) reported that within IPF patients, current smokers had higher survival than former smokers, but this difference was eliminated when adjusted for disease severity, using the CPI[24]. Moreover, never smokers had better survival than former smokers and this difference was enhanced when adjusted for baseline disease severity, using the CPI[24]. Additionally, it was found that IPF patients who were current smokers had better pulmonary function outcomes at presentation[23,24]. Explicitly, Antoniou *et al.* (2008) demonstrated that FVC and D_{LCO} levels were lower, and computed tomography **(CT)** disease extent and CPI scores were greater in IPF patients who were ex-smokers than in IPF patients who were current smokers[24]. Similarly, FVC and D_{LCO} levels were lower, and CT disease extent and CPI scores were higher in never smokers than in current smokers

among IPF patients[24]. Furthermore, King *et al.* (2001) have shown that the honeycombing pattern was significantly higher in IPF patients who were former smokers than in IPF patients who were considered current or never smokers in addition to showing that FVC and forced expiratory volume (1 second) **(FEV1)** were significantly lower and the FEV1/FVC ratio was significantly higher in never smokers than former smokers[23]. Lastly, FVC and FEV1 were significantly greater and FEV1/FVC ratio was significantly lower in current smokers compared with never and former smokers[23]. These less severe pulmonary function indices detected in IPF patients who were current smokers compared to IPF patients who were former smokers might be caused by *"healthy smoker effect"* which states that patients with more critical disease symptoms are more likely to cease smoking for recognized health reasons[24]. Hence, current smoking might be considered as a marker of less severe disease, correlated with better outcome and survival[24]. Interestingly, in a cohort of IPF patients (never smokers, n=32; smokers, n=66), Kishaba *et al.* (2016) have found that 50% and 18% of the never smoker and smoker patients, respectively, experienced acute exacerbation **(AE)** and that after adjusting for CPI and prednisolone use, never smoker patients showed tendency to develop AE more frequently and late than that of smoker patients[22]. In addition, within IPF patients, the median survival period of never smokers and smokers was 18.5 and 26.3 months, respectively. Surprisingly, after the adjustment of baseline CPI, IPF patients who were never smokers showed worse prognosis than that of IPF patients who were considered smokers[22]. Lastly, Song *et al.* (2011) revealed that never smoking and reduced FVC were significant risk factors for AE in IPF[27]. Interestingly, cigarette smoking has been proposed to protect from developing HP[28]. It has been

suggested that the protective effect of smoking in this disease is caused by the suppression of T helper **(Th)** 1 cell immunity by cigarette smoking, but this functional impairment of the immune system may potentially result in alternative lung diseases[18].

The present Ph.D. thesis's primary goal was to shed light on these clinical controversies and contradicting research findings by further investigating the impact of smoking status on the survival and pulmonary function decline in fibrotic ILD patients enrolled in a Canadian registry. Moreover, using preclinical experimental mouse models, advanced flow cytometry-based techniques, and *ex vivo* approaches, the present Ph.D. studies aimed to untangle the cellular and molecular mechanisms by which smoking influences pulmonary fibrosis development, progression, and immunopathogenesis. We believe that this will ultimately enable the development of drugs that will specifically target cells and pathways that are activated or impaired by cigarette smoke-associated fibrogenesis.

Cell type: Pulmonary macrophages

Pulmonary macrophage composition and phenotype

Pulmonary macrophages are highly heterogeneous. They are composed of multiple subpopulations with independent and diverse functional roles and phenotypes, and express different cell surface proteins. Pulmonary macrophages can be stratified into two broad populations; resident alveolar macrophages **(Res-AM)** and interstitial macrophages **(IM)**[29,30]. Resident alveolar macrophages, the most abundant macrophage populations[30], perform vital roles in both stimulating and suppressing the immune response, as well as in

surfactant/lipid processing and iron homeostasis[31]. Specifically, AMs are critical for immune defence mechanisms such as phagocytosis, the production of inflammatory mediators such as reactive oxygen species **(ROS)**, and the secretion of inflammatory cytokines such as interleukin **(IL)**-1, IL-2, IL-4, IL-6, IL-8, tumour necrosis factor-α **(TNF-α)**, and interferon gamma **(IFN-γ)**. In addition, AMs produce anti-inflammatory mediators and remove apoptotic bodies (efferocytosis) to resolve inflammatory processes[31]. Mechanistic mouse work has indicated that AMs are derived from yolk sac precursors of fetal monocytes during embryogenesis, which populate the alveoli shortly after birth and persist over the lifespan via self-renewing embryo-derived cells independently of bone marrow-derived cells under homeostatic conditions[31–41]. Conversely, during inflammation or injury states, there is an expansion in inflammatory monocyte recruitment from the circulation[41]. Recruited monocytes have been proposed to differentiate into monocyte-derived alveolar macrophages **(Mo-AM)**[42] or monocyte-derived IM populations[43]. Both macrophage subtypes were shown to persist in the lung over a sustained period of time and contribute to immunopathogenesis and fibrosis[42,43]. IMs, constituting 30-40% of lung macrophages, are crucial for tissue remodelling and maintenance, as well as antigen presentation[29,30]. Together with AMs, IMs contribute to barrier immunity in the lung[29]. Although AM origin is well-characterized, IM ontogeny is more complicated and less studied. Currently, interstitial macrophages are believed to originate from an embryonic yolk-sac-derived origin and are maintained by postnatal bone marrow-derived cells[30,35]. Furthermore, Gibbings *et al.* (2017) have identified three distinct subpopulations of interstitial macrophages, displaying different transcriptional profiles in C57BL/6 mouse

lung at steady state[32]. Using flow cytometry, Gibbings *et al.* (2017) have isolated $MerTK^{+}CD64^{+}$ total pulmonary macrophages from which $siglecF^{+}CD11c^{+}CD11b^{-}$ AMs and $SiglecF^{-}CD11b^{+}$ IMs were gated[32]. Subsequently, IMs were further divided into three different IM subtypes based on the expression levels of CD11c and MHCII. They termed the different IM subpopulations as follows: "IM1" ($CD11c^{low}MHCII^{low}$); "IM2" ($CD11c^{low}MHCII^{high}$); and "IM3" ($CD11c^{+}MHCII^{high}$)[32]. Gibbings *et al.* (2017) provided evidence that the three IMs were clearly distinguishable from AMs and from each other. Unique cell surface markers that are commonly expressed on AMs (Marco, SiglecF, and Csf2r) were not detected on any of the three IMs and IMs, but not AMs were found to express genes that repress self-renewal, such as *Mafb* and *Maf*[32]. Additionally, monocyte-related genes such as *Cd14*, *Cd163*, and *Csfr1* (macrophage colony-stimulating factor **[M-CSF]** receptor) were greatly expressed on IMs compared with AMs and this further reinforces findings suggesting that IMs arise from postnatal circulating monocytes[32].

In addition to the stratification of pulmonary macrophage populations into Res-AM, Mo-AM, IM1, IM2, and IM3, studies further suggest that the functional status of macrophage subpopulations is influenced by the immune environment. In particular, depending upon the specific mediators and micro-environmental stimuli and signals, monocyte-derived macrophages can be skewed toward two distinct polarised phenotypes *in vitro*[31,44,45]. Pro-inflammatory "M1 macrophages" are classically activated typically by lipopolysaccharide **(LPS)**, IFN-γ and/or TNF-α, and are responsible for pathogen clearance, produce pro-inflammatory cytokines, and generate a Th1-cell environment. Pro-

fibrotic "M2 macrophages" are alternatively activated by IL-4, IL-13, and IL-10 and are essential for suppressing inflammation, promoting tissue remodelling, resolution and tissue repair, mediating wound healing and fibrogenesis, and establishing a Th2-cell environment[31,44,45]. M1 markers include CD80, toll-like receptor **(TLR)** 4, MHCII, CD86[44], and CD38[46], whereas M2 is characterized by the high expression of arginase-1 **(Arg-1)**, the family of proteins chitinase-like Ym1/2 and Fizz1/RELM-α (found in inflammatory zone 1), and mannose receptor (CD206)[44]. *In vivo*, however, macrophages are highly plastic, have a spectrum of differentiation, and can co-express both M1 and M2 markers[31].

Pulmonary macrophage contribution to cigarette smoke-induced inflammation

Cigarette smoke exposure results in oxidative stress leading to a chronic low-grade inflammation and recruitment of inflammatory cells to the airways by the stimulation of epithelial cells, alveolar macrophages, neutrophils, and T lymphocytes[31]. Cigarette smoking impairs the development, cytokine secretion, and effector function of both innate immune cells, including dendritic cells, macrophages and natural killer cells, and adaptive immune cells, such as cytotoxic $CD8^+$ T cells, $CD4^+$ T helper cells, regulatory T cells and B cells, resulting in aggravated pro-inflammatory responses and/or dysfunction of immune cells[47]. To this end, cigarette smoke can either exacerbate pathological immune responses or dampen the normal defensive function of the innate and adaptive immunity[47]. Particularly, cigarette smoke attenuates immunity against infections, but paradoxically enhances autoimmunity[47]. Further research is warranted to better understand the

mechanisms underlying immunopathology associated with smoking. Notably, central to cigarette smoke-associated immunopathology is the macrophage.

The impact of cigarette smoke exposure on each individual macrophage subpopulation is yet to be elucidated. Nevertheless, it has been shown that the number of bronchoalveolar lavage **(BAL)** macrophages was significantly higher in humans who are considered current smokers compared to former and never smoker subjects[48]. Although smoke exposure is associated with an expansion in the number of BAL macrophages, smoke-exposed macrophage function is supressed. Gaschler *et al.* (2008) have provided evidence that although increased in the BAL of smoke-exposed mice, macrophages had significantly attenuated production of inflammatory cytokines (TNF-α and IL-6) and the chemokine RANTES and that was associated with decreased nuclear translocation of the pro-inflammatory transcription factor "nuclear factor kappa-light-chain-enhancer of activated B cells" **(NF-kB)**, in response to innate pattern recognition receptors **(PRRs)** *ex vivo* stimulation which normally activates pathways associated with bacterial and viral infections[49]. In line with preclinical mouse findings, alveolar macrophages obtained from humans who were healthy smokers, produced lower levels of pro-inflammatory cytokines (TNF-α, IL-1β, and IL-6) in response to LPS (TLR4 agonist) stimulation compared to never smoker macrophages[50]. An increase in the size of alveolar macrophages has been reported in both smoker subjects and COPD patients who were current smokers compared to never smoker subjects[51]. This has been proposed to be caused by lipid accumulation in smoke-exposed macrophages, resulting in their foamy feature[52], which in turn increased IL-1α

production contributing to cigarette smoke-induced inflammation[52,53]. Other smoke-induced macrophage dysfunction includes; impaired phagocytosis and ROS production, enhanced proteinase release, damaged iron metabolism, and altered efferocytosis[31].

The impact of cigarette smoke on macrophage M1/M2 polarization status remains inconclusive. Some findings suggest that cigarette smoke up-regulates pro-fibrotic M2-like characteristics of macrophages[54], while others propose that cigarette smoke enhances pro-inflammatory M1-like characteristics of macrophages[55]. Specifically, a study conducted by Shaykhiev *et al.* (2009) revealed that genes associated with M1 polarization were down-regulated in AM of healthy smokers compared to healthy non-smokers and that genes associated with M2-like polarization were up-regulated in healthy smokers[54]. Similarly, M1-related genes were further down-regulated and M2-related genes were further up-regulated in AM of COPD patients who were smokers when compared to healthy smokers[54]. In contrast, Karimi *et al.* (2006) have shown that human monocyte-derived macrophages produced the pro-inflammatory cytokine IL-8 upon exposure to cigarette smoke medium[55]. Lastly, Eapen *et al.* (2017) have reported different macrophage polarization status depending on the location within the lung. Macrophages were found to predominantly acquire the M1 phenotype in small airways in both healthy smokers and COPD patients who were smokers compared to non-smokers[56]. On the other hand, BAL AMs were mostly of the M2 phenotype and BAL cytokines were skewed towards an M2 profile in both healthy smokers and COPD patients who were smokers[56].

Taken together, despite the recent advances in the understanding of pulmonary macrophage composition and phenotypic plasticity under homeostatic conditions and during ongoing inflammation, the exact manner in which cigarette smoke exposure impacts the relative composition and function of pulmonary macrophage subpopulations during tissue remodelling and fibrogenesis has not been elucidated.

Pulmonary macrophage contribution to tissue remodelling and fibrosis

Recruited monocyte-derived macrophages are considered central orchestrators of pulmonary fibrosis pathogenesis. Particularly, a distinct population of macrophages was found to be associated with impaired tissue remodelling in pulmonary fibrosis lung explants[57–60]. Further, an expansion in monocyte-derived macrophage subpopulations was associated with enhanced fibrogenesis in mouse experimental models of lung fibrosis[42,61,62]. In particular, using a genetic lineage tracing system, Misharin *et al.* (2017) have demonstrated that the genetic depletion of Mo-AM following their recruitment to the lung significantly reduced the severity of bleomycin-induced lung fibrosis, whereas the deletion of Res-AM had no effect on fibrogenesis[42]. Similarly, Joshi *et al.* (2020) have illustrated that the genetic deletion of Mo-AM but not Res-AM, attenuated asbestos-induced lung fibrosis[61]. In addition, Mo-AM subpopulations, expressing pro-fibrotic genes, were located in a fibrotic niche in the proximity of fibroblasts[61].

Notably, studies further provided evidence of the contributions of M2-polarized alternatively activated macrophages in the development of fibrotic lung diseases[43,63–67]. Specifically, Prasse *et al.* (2006) have shown that the secretions of an M2 marker known

as CC chemokine ligand 18 **(CCL18)** were significantly higher in the supernatant of cultured BAL macrophages collected from IPF patients compared to healthy donor BAL supernatant[63]. Additionally, flow cytometry analysis revealed that the % of $CCL18^+$ BAL-derived cells was significantly higher in IPF patients compared to healthy control subjects[63]. Furthermore, Gibbons *et al.* (2011) have demonstrated that the *in vivo* depletion of lung macrophages during the fibrotic phase of bleomycin-induced pulmonary fibrosis, dramatically attenuated the fibrotic response in mice and that was associated with a reduction in the expression of M2 markers such as Ym1 and Arg-1[64]. Similarly, the depletion of $Ly6C^{high}$ circulating monocytes during the fibrotic phase significantly reduced pulmonary fibrosis and the number of Ym1-positive cells[64], suggesting the critical roles of both circulating monocytes and M2-polarized macrophages in lung fibrogenesis. Moreover, Ji *et al.* (2014) and Misharin *et al.* (2013) studies have provided evidence that during the fibrotic phase of the bleomycin model in mice, IMs acquired a pro-fibrotic phenotype, characterized by elevated expression of CD206[43,65]. Lastly, our group has previously found that the overexpression of IL-6, in combination with bleomycin in mice, resulted in increased lung elastance, collagen content, and fibrotic score and that was associated with the accumulation of $Arg\text{-}1^+CD206^+$ M2-like macrophages[66].

To date, the mechanisms by which macrophage composition and function are altered during fibrogenesis are yet to be investigated. We believe that having a better understanding of the extrinsic factors and the intrinsic cellular and molecular pathways

involved in macrophage pro-fibrotic function during tissue remodelling will enable the identification of potential therapeutic targets.

Intrinsic molecular mechanism: Role of protein misfolding, endoplasmic reticulum stress, and the unfolded protein response in pulmonary fibrosis

Endoplasmic reticulum stress and the unfolded protein response - Overview

The endoplasmic reticulum **(ER)** is essential for the synthesis, modification and processing, folding, and assembly of secretory and membrane proteins[68,69]. Proteostasis, also known as protein homeostasis, can be altered by internal or external stressors resulting in an accumulation of unfolded or misfolded proteins within the ER lumen[68]. When the ER protein folding capacity is exhausted, cells undergo a condition termed ER stress[70]. In an attempt to restore proteostasis, cells have evolved an evolutionary conserved signal transduction pathway called the unfolded protein response **(UPR)**[70]. UPR is composed of three ER transmembrane sensors: inositol-requiring enzyme 1 **(IRE1)**, activating transcription factor 6 **(ATF6)**, and protein kinase R (PKR)-like endoplasmic reticulum kinase **(PERK)**[68,71,72]. In an unstressed cell, binding immunoglobulin protein **(BiP)** also called glucose-regulated protein 78 **(GRP78)**, a molecular chaperone that facilitates protein folding, is bound to IRE1, ATF6, and PERK to maintain these sensors in an inactive state[68,71,72]. Due to the higher affinity of GRP78 to the hydrophobic regions of the misfolded or unfolded proteins, it dissociates from these sensors during ER stress, stimulating the downstream UPR signaling pathways[68,71,72]. UPR sensors work independently to alleviate ER stress by terminating protein translation, enhancing misfolded protein degradation,

upregulating the expression of chaperones, and expanding the size of the ER[68]. This response leads to cellular survival. However, if UPR fails to restore proteostasis and the normal functions of the ER fail to recover, chronic UPR activation can lead to pathologic reprogramming of the cell or cellular dysfunction and initiation of pro-apoptotic pathways resulting in cell death[69,73]. Prolonged UPR-mediated apoptosis occurs via three primary pathways including; the activation of the cJUN NH2-terminal kinase **(JNK)** pathway, which is mediated by the formation of the IRE1-TNF receptor-associated factor 2 **(TRAF2)**-apoptosis signal-regulating kinase1 **(ASK1)** complex **(IRE1/ASK1/JNK)**, the activation of the caspase-12 kinase pathway, and the stimulation of the CCAAT/enhancer binding proteins (C/EBP) homologous protein **(CHOP)**/GADD153 pathway[69,74]. In the case of prolonged ER stress and UPR, apoptosis occurs when functions of the ER are rigorously disrupted, in order to protect the organism by destroying the damaged cells[74].

In pulmonary fibrosis, stressors such as hypoxia, cigarette smoke, particulate matter, asbestos, bacterial, fungal, and viral pathogens may stimulate aberrant ER stress and UPR in a genetically predisposed lung[71]. ER stress and UPR processes have been proposed to contribute to pulmonary fibrosis through the stimulation of epithelial cell apoptosis, skewed polarization of macrophages, and differentiation of fibroblasts to myofibroblasts[68,72].

Impact of endoplasmic reticulum stress on pro-fibrotic feature of alveolar epithelial cells in pulmonary fibrosis

Burman *et al.* (2018) have found that CHOP-deficient mice were protected from lung fibrosis following repetitive intratracheal bleomycin administration via the attenuation of AEC apoptosis[75]. Localized hypoxia might be a potential mechanism for inducing ER stress as hypoxia was detected in type II AECs found in mice treated with repetitive intratracheal bleomycin[75]. In human IPF lungs, CHOP and the hypoxia marker, hypoxia-inducible factor 1α **(HIF-1α)**, were upregulated in type II AECs, further providing evidence that localized hypoxia resulted in ER stress–mediated CHOP expression, thus promoting type II AEC apoptosis and initiating lung fibrosis[75]. Similarly, Delbrel *et al.* (2018) have demonstrated that HIF-1α and CHOP were both co-localized in hyperplastic AECs found in IPF patients' lung biopsies and in bleomycin-treated mice, but not in controls[76]. They have also found that hypoxia and HIF-1α can induce ER stress and CHOP-mediated apoptosis in AEC[76]. These results further suggest that localized hypoxia and the expression of HIF-1α contribute to UPR activation, CHOP induction, and AEC apoptosis, thereby leading to alveolar epithelial cell impairment and eventually aggravating lung fibrosis[76].

Impact of endoplasmic reticulum stress on pro-fibrotic feature of macrophages in pulmonary fibrosis

It has been previously demonstrated that the genetic deletion of UPR regulators resulted in either protection or aggravation of the fibrotic responses mediated by the modulation of UPR-mediated macrophage apoposis[77]. Specifically, the haploinsufficiency of GRP78 led

to the apoptosis of M2-like macrophages and that was associated with protection from pulmonary fibrosis[77]. Conversely, CHOP deficiency led to an accumulation of the M2-like macrophage subpopulations and an enhanced fibrotic response[77]. Additionally, UPR is believed to be critical in the differentiation of a wide array of cell types from inactive states to synthetic cells with high secretory capacities, including macrophages, plasma cells, adipocytes, and myofibroblasts[77]. We previously demonstrated that the addition of IL-6 to macrophages led to a hyperpolarized pro-fibrotic M2 phenotype associated with increases in the activation of both IRE1-XBP1 and cleaved ATF6 pathways[78]. Inhibition studies targeting the IRE1-XBP1 arm of the UPR reduced the ER expansion program of macrophage, a process required for their activation toward the hyperpolarized M2 phenotype[78]. However, the contribution of the ATF6α arm previously shown to also be responsible for the expansion of the endoplasmic reticulum and activation of Chinese hamster ovary **(CHO)** cells and mouse embryo fibroblasts in the absence of XBP1-splicing[79], has not yet been investigated in the context of macrophage activation.

Impact of endoplasmic reticulum stress on pro-fibrotic feature of myofibroblasts in pulmonary fibrosis

In human and mouse lung fibroblasts, pharmacological inhibition of ER stress through the usage of a chemical chaperone, sodium 4-phenylbutyrate **(4-PBA)** suppressed TGFβ1-induced alpha smooth muscle actin **(α-SMA)** and collagen production, suggesting the involvement of ER stress in myofibroblast differentiation[80]. Similar to macrophage alternative activation, treatment of fibroblasts with an IRE1 inhibitor attenuated TGFβ1-

induced collagen 1α2 and fibronectin production in IPF lung fibroblasts but not in those from non-IPF donors[81].

Collectively, current data provide evidence of the involvement of ER stress and the UPR in regulating alveolar epithelial cells, macrophages, and myofibroblasts, however, conflicting findings suggest both protective and detrimental effects of these internal processes during fibrogenesis. Therefore, further investigation is required to determine whether the net effect of ER stress and the UPR is pathogenic or protective in lung fibrosis and to decipher the lung cell type that is affected the most by the alterations of these processes and thereby, will represent the main cell contributor to the immunopathogenesis and pathophysiology of fibrotic lung diseases.

Activating transcription factor 6 alpha

p90ATF6 encoded by the *Atf6* gene, is a type II transmembrane glycoprotein localized in the ER. p90ATF6 is synthesized as a precursor protein in unstressed cells and undergoes proteolytic cleavage into the soluble nuclear active form p50ATF6 in response to ER stress[82]. Additionally, there is another protein that is closely related to ATF6, which is encoded by the G13 or cAMP-response-element-binding protein-related protein **(CREB-RP)** gene. Haze *et al.* (2001) named the ATF6 gene product "p90ATF6α" and the G13/CREB-RP gene product as "p110ATF6β"[83]. Both isoforms are ubiquitously synthesized ER-localised basic leucine zipper **(bZIP)** transcription factors, which are composed of an ER luminal domain that senses ER-stress, a transmembrane segment, and an N-terminal cytoplasmic domain with transcriptional activity[84]. In response to ER stress,

both isoforms relocate from the ER to the Golgi apparatus where cleaved by Site-1 and Site-2 proteases, giving rise to the cytoplasmic N-terminal regions, designated as p50ATF6α(N) and p60ATF6β(N) which enter the nucleus and induce the transcription of target genes[83–85]. Yamamoto *et al.* (2007) have previously developed full body ATF6α-or ATF6β- knockout mice with no observed pathological phenotype, whereas, their double knockout resulted in embryonic mortality[86]. We here focused on studying ATF6α as it was previously shown that in MEFs, ATF6α but not ATF6β was required for the transcription induction of ER chaperones that augmented ER protein folding capacities[86,87]. Moreover, previous findings have demonstrated that the overexpression of ATF6α upregulated myocardin induction and its depletion reduced myocardin expression during the differentiation of embryonic stem cell towards the smooth muscle cell **(SMC)** lineage[88]. These findings indicated that ATF6α may have a role in cell differentiation likely via the ER expansion program[89].

To date, the role of ATF6α arm of UPR in macrophage activation, pro-fibrotic function, and apoptosis during lung injury, tissue remodelling, and fibrogenesis has not been determined.

Mouse models of lung fibrosis, a published book chapter

Note:

This section of the present thesis' introduction includes a reprint version of a currently published book chapter which discusses preclinical mouse models of lung fibrosis and relevant research methodologies utilized to assess fibrotic measures. Preclinical fibrosis mouse models and methods described in detail in this book chapter, have been used in all primary research work conducted in the present thesis and depicted primarily in chapters 3 and 4 which include two original research articles.

Status of the work:

First Online: 25 May 2021

Citation: Mekhael O. et al. (2021) Mouse Models of Lung Fibrosis. In: Hinz B., Lagares D. (eds) Myofibroblasts. Methods in Molecular Biology, vol 2299. Humana, New York, NY. https://doi.org/10.1007/978-1-0716-1382-5_21

Chapter 21

Mouse Models of Lung Fibrosis

Olivia Mekhael, Safaa Naiel, Megan Vierhout, Aaron I. Hayat, Spencer D. Revill, Soumeya Abed, Mark D. Inman, Martin R. J. Kolb, and Kjetil Ask

Abstract

The drug discovery pipeline, from discovery of therapeutic targets through preclinical and clinical development phases, to an approved product by health authorities, is a time-consuming and costly process, where a lead candidates' success at reaching the final stage is rare. Although the time from discovery to final approval has been reduced over the last decade, there is still potential to further optimize and streamline the evaluation process of each candidate as it moves through the different development phases. In this book chapter, we describe our preclinical strategies and overall decision-making process designed to evaluate the tolerability and efficacy of therapeutic candidates suitable for patients diagnosed with fibrotic lung disease. We also describe the benefits of conducting preliminary discovery trials, to aid in the selection of suitable primary and secondary outcomes to be further evaluated and assessed in subsequent internal and external validation studies. We outline all relevant research methodologies and protocols routinely performed by our research group and hope that these strategies and protocols will be a useful guide for biomedical and translational researchers aiming to develop safe and beneficial therapies for patients with fibrotic lung disease.

Key words Pulmonary fibrosis, Experimental models of pulmonary fibrosis, Target engagement, Lung, Cytokines, Collagen deposition, Smooth muscle actin, Myofibroblast, Primary/secondary endpoints, Antifibrotic agents, Bleomycin

1 Introduction

The drug discovery and development pipelines are a crucial part of medicine and healthcare. The pharmaceutical industry has identified and implemented many steps and milestones that need to be successfully passed throughout the path toward the final approval of a novel medication [1]. The process usually starts with observational studies examining biological mechanisms of the disease, including its origin, development, resolution, or progression of

Olivia Mekhael and Safaa Naiel contributed equally to this work.

Boris Hinz and David Lagares (eds.), *Myofibroblasts: Methods and Protocols*, Methods in Molecular Biology, vol. 2299, https://doi.org/10.1007/978-1-0716-1382-5_21,

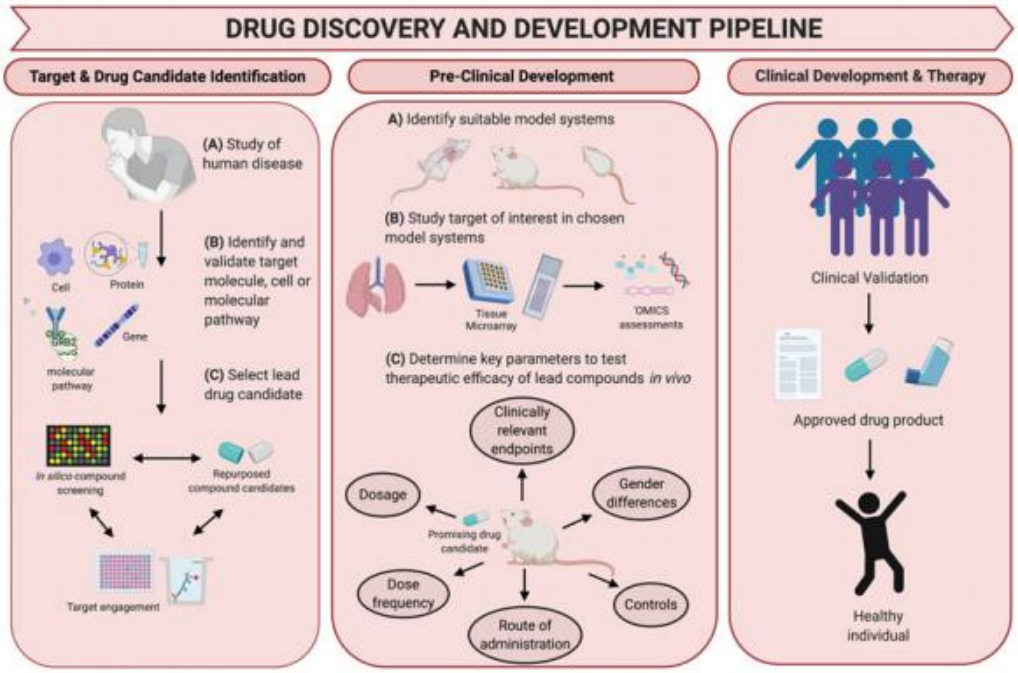

Fig. 1 *Drug discovery and development pipeline.* Promising drug candidates must pass through three key developmental phases of the pipeline before approval: (1) target and drug candidate identification: observational studies examining the molecular and cellular mechanisms of the disease of interest (A) will identify relevant targets (B) and drug candidates (C) that will initiate the pipeline; (2) preclinical development: in vivo studies will be conducted on appropriate experimental models that replicate human disease phenotype (A) and express the target of the interest (B), to ultimately test preclinical efficacy of the lead candidate by measuring clinically relevant outcomes (C); (3) clinical development and therapy: a lead candidate that has passed the preclinical stages and demonstrated preclinical efficacy must be clinically validated before being approved as a therapeutic product

the condition. Although the events that encompasses the cellular and molecular underpinnings of the disease and its resolution may be observed in this type of study, their exact nature may only be predicted, not tested. Hypothesized mechanisms may then be tested with specific interventional studies, and lead to improved understanding of the disease. Once a putative target, cell or molecular pathway is identified, that is believed to play a key role in the pathogenesis or progressive nature of the disease, the drug development pipeline starts [1–4] (Fig. 1). This process is often initiated by in silico or physical screening processes aimed at identifying lead compounds that have achieved a desired activity at the target site, and that can progress to the preclinical and clinical phases of the pipeline [2, 4]. Due to the significant time in development, high costs, and failure rates in the conventional drug development process, compound screens have evolved to also include health agency approved drugs with known toxicity and safety profiles [5, 6]. The

preclinical stage involves proof-of-principle studies aimed to demonstrate safety, target engagement and therapeutic modulation that results in the amelioration of experimental disease-like outcomes [7–9]. Although both in vitro and in vivo models can be utilized to investigate target modulation and engagement, in vivo models are required for the validation of in situ target engagement within a live host organism and therapeutic efficacy in meaningful models of human disease [9]. In this book chapter, we describe current considerations and strategies to investigate the effect of therapeutic candidates in experimental models of pulmonary fibrosis. We will focus on the following: (1) selection of experimental rodent models that express the target(s) of interest; (2) selection of route of administration, dose and frequency; (3) selection of control groups and control treatments, statistical and species sex considerations; (4) analyzing a discovery cohort and selection of primary and secondary outcomes; and (5) design and execution of validation experiments. We have chosen to describe in detail the methodology of the well-known and widely used bleomycin model of pulmonary fibrosis. We believe that the overall principles and strategies outlined within this chapter, with slight modifications, can be relatively easily translated to investigate therapeutic efficacy in other experimental models of pulmonary fibrosis.

1.1 Selection of Experimental Rodent Models That Express The Target(s) of Interest

To successfully assess target validity and preclinical efficacy of any drug candidate, the first and most important consideration is the selection of the most appropriate experimental model system [10, 11]. To be labeled as a clinically relevant model for therapeutic efficacy studies, the experimental model would ideally need to replicate key elements of the human disease phenotype and express a clinically relevant target molecule or molecular pathway that a lead candidate intends to modulate [1, 12]. To date, many experimental models of pulmonary fibrosis have been reported, including bleomycin model, fluorescein isothiocyanate (FITC), irradiation, silica, overexpression of viral vectors, humanized models, asbestosis, age-dependent models, targeted type II alveolar epithelial cell (AEC) injury models, and various other lung injury models [10, 13–16]. Although no model on its own fully recapitulate progressive pulmonary fibrosis observed in the clinical setting, each of these models have been shown to share part of the fibrotic features observed in patients and could be useful candidate models, depending on the therapeutic target and pathway studied [10, 11, 15]. To achieve this, preliminary information about the temporal expression level of target molecules in each model needs to be available, as well as reasonable claims that the selected targets could be critically involved in the fibrogenic process [4, 17–19]. If the pathway or therapeutic target has not been formally studied and reported within the model, a formal investigation across model systems may be required to select the most suitable

approach [15]. Ideally, standardized kinetic "multi-omic" datasets, including gene arrays (bulk and single-cell RNA sequencing—scRNAseq), proteomic, metabolomic, and lipidomic, would be generated and accessible from each model, so that subsequent bioinformatic assessments would help to select the appropriate model systems [4, 15, 18, 20, 21]. In-house repositories can also be developed, including the generation of tissue micro arrays (TMA) containing several model systems on a single block, with lungs extracted from multiple time-courses [15]. This is a relatively low-cost tool that can be developed and used to rapidly screen several model systems (depending on TMA design and available models) at the protein or mRNA level to select the most appropriate model [15]. In Subheading 3, we describe the methodology to develop a screening TMA containing four distinct experimental models of lung fibrosis, to allow for rapid evaluation of model suitability.

1.2 Selection of Route of Administration, Dose, and Frequency

The overall objective of therapeutic assessment trials in preclinical experimental models is to demonstrate a beneficial effect of the intervention. How do we ensure that our therapy reaches the right area, at the right time, with the right amount and adequate frequency? How do we make sure that the putative therapeutic target is engaged, and modulated appropriately? These are some of the pharmacodynamic questions that need to be carefully assessed before preclinical trials are designed. For experimental models of lung disease, most therapeutic options are formulated for oral or inhaled delivery [22–24]. Animal inhaled aerosols are a novel vehicle for the delivery of high concentrations of drugs into the airways[25]. Recent advancements in flexiVent technology allow for simultaneous lung function assessment and drug delivery. Regardless of the chosen method, when a new therapy is to be evaluated, we recommend that tolerability studies are conducted to address the safety levels of the drug and to determine whether the drug displays any short- or long-term toxic effects, followed by pharmacokinetic (PK) and pharmacodynamic (PD) studies, to address the kinetic profile of the drug [26, 27]. These experiments can be performed on a reduced number of animals, and both in naïve animals as well as in the appropriate model systems. When direct lung delivery is performed, we usually monitor animals for acute (same day) or latent (up to one week) distress signs post-administrations. Once a tolerable dose has been identified, PK and PD assessments need to be established. This is preferably performed in the model system where the drug will be evaluated as the injured and fibrotic lung might have a different drug metabolism and PK/PD capacities [24, 26, 28]. The timing of drug intervention also needs careful consideration and has been subject to extensive debates and review [16, 17, 29, 30]. Although many preclinical trials administer therapeutic options in a prophylactic

regimen, where the therapy is given prior or at the same time as the agent inducing the disease, we have over the past decade seen a shift in the timing, where more therapeutic modalities have been introduced [11, 16, 30]. The latter is thought to better mimic the clinical setting, where the diagnosis of fibrotic lung disease and therapy are only given after diagnosis, and so far not to prevent the onset of the disease [11, 16, 17, 30].

1.3 Selection of Control Groups and Control Treatments, Statistical and Species Sex Considerations

Well-designed experimental trials benefit from the addition of treatment groups containing already approved therapies (nintedanib or pirfenidone) [10, 31, 32], and established benchmark candidates in various experimental models of lung fibrosis [28, 32, 33]. Other important considerations that need to be determined before the start of the trial are the number of treatment groups required and the appropriate group size, based on a priori power calculations [11, 34]. As an example, we consider a case where an investigational drug (X) is hypothesized to prevent the accumulation of myofibroblasts and subsequent pulmonary fibrosis (Fig. 2). In our hypothetical example, X will be delivered as an inhaled formulation and administered daily, with vehicle Y, at two concentrations to potentially establish a dose-dependent effect. The control drug to include (either nintedanib or pirfenidone) will be administered as per previously published studies, per os and with daily administrations using appropriate (and likely different) vehicle formulations. Taking into consideration the research question outlined above, the following additional questions should be addressed: How many control groups do we need in this case? How many mice should be included in each group? Which statistical tests should be used to examine outcomes? Should we perform the experiment in both male and females? Due to the significant costs of these trials, often times one sex is used for initial assessments. To account for sex influences, it is recommended to replicate experiments for the interventional aims in the opposite sex [17]. Based on our hypothetical example, a negative control group is required to establish the baseline level in the parenchyma of naïve mice (group 1). A positive control group will be required to establish the maximal amount of parenchymal fibrosis (group 2). Two potentially different vehicle control groups are required, one with the inhaled vehicle formulation (group 3) and one with oral vehicle formulation (nintedanib/pirfenidone arm, group 4), to account for potential effects of the formulations alone. Two treatment arms of the investigational, inhaled drug (X) may be required (group 5, 6) if a potential dose-dependency is to be examined. The result of these arms should be compared to the positive treatment arm (nintedanib/pirfenidone, oral administration, group 7). In all, based on this simple example, 7 investigational groups may be required. As described in depth in Subheadings 1.4 and 1.5, establishing the primary outcomes prior to the initiation of the study is essential as it

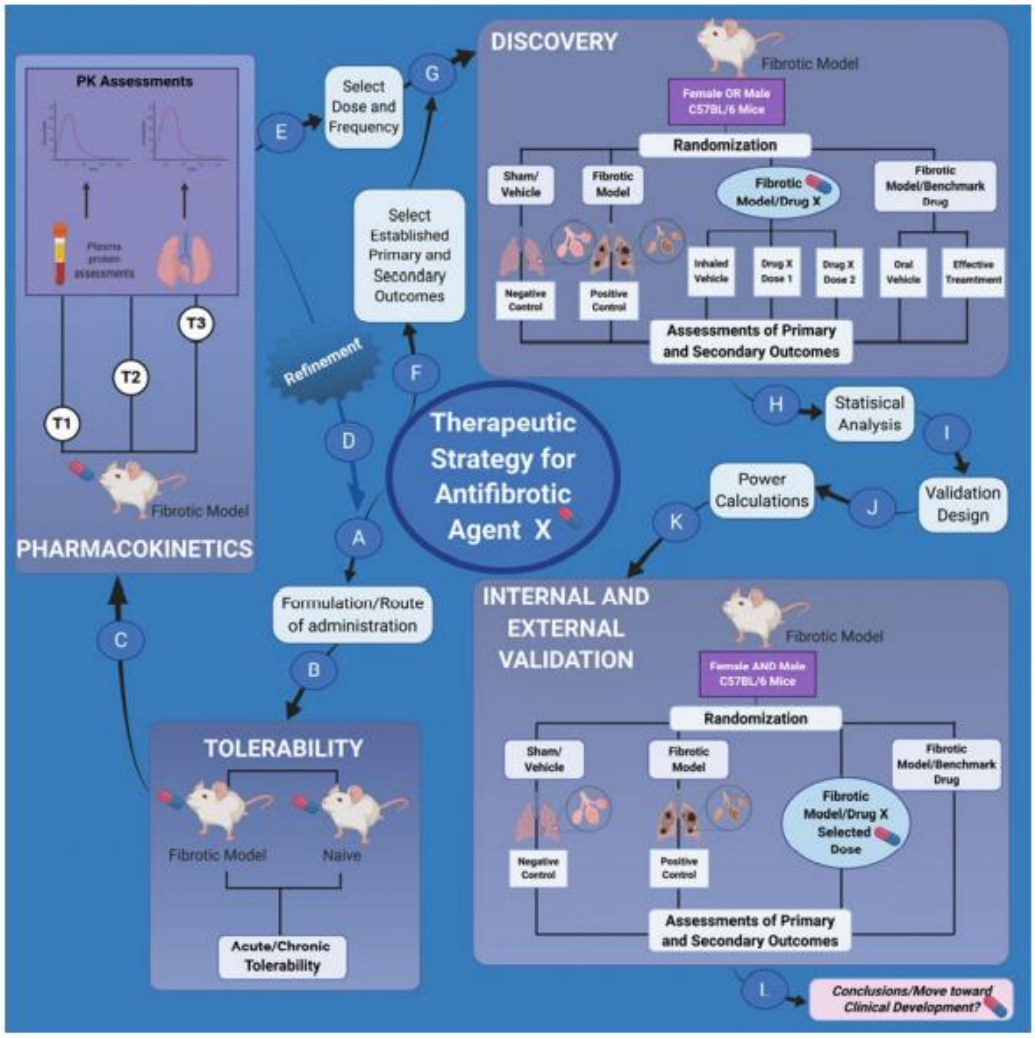

Fig. 2 *Therapeutic study design strategy for antifibrotic agent X.* To investigate whether the lead candidate, drug X, has antifibrotic properties, it must pass through several preclinical phases. To evaluate the efficacy of Drug X, the formulation (A) is initially tested in a tolerability study (B) to address the safety levels of the drug. When direct lung delivery is performed, animals are monitored for acute (same day) or latent (up to one week) distress signs post-administration to determine if the drug displays any short- or long-term effects, respectively. This is ideally tested in both naïve and in the fibrotic model system. Once a safe and tolerable dose is established, pharmacokinetic studies (PK) (C) are conducted to establish a kinetic profile of the drug. PK studies are preferably performed in the model system where the drug will be evaluated as the injured and fibrotic lung might have different drug metabolism and PK properties. PK studies for Drug X is usually performed by administering the drug at various time-points (T1, T2, T3) and collecting samples, such as plasma and lung, that are processed and analyzed for drug and relevant metabolites. If a favorable PK profile is not achieved, the formulation and administration route may require further optimization (D). A favorable PK profile will determine the selection of drug X dose(s) and frequency (E) and, after selection of established primary and secondary outcomes (F), a discovery cohort can be designed and evaluated (G). Based on this hypothetical example, a negative control group is required to establish the baseline level (group 1). A positive

prevents the researcher from mining through the measured study outcomes in search of a statistically significant effect, often referred to as "p-hacking" [34, 35]. When having many primary outcomes, it is difficult to perform power calculations for each readout as standard deviations may vary between the different assessments [36]. This will lead to the requirement of larger sample sizes to conclude that an observed effect is a true effect [34, 36]. In general, and as outlined in Fig. 2, we recommend that preclinical studies are conducted in several phases, and that after careful tolerability and PK evaluations, a smaller discovery cohort is designed and evaluated. This discovery cohort could be performed with a minimum sample size of five for all control and test groups, and that the data generated from this study is used to refine the design, consolidate the selected primary and secondary outcomes, and conduct appropriate power analysis calculations before a validation study is initiated. Other important considerations include animals to be randomly allocated to the treatment groups, where intervention initiation and assessments follow, and to practice operator and data analyst blindness before and during the study to deter experimental and observer biases [34, 37]. If at times operator blindless cannot occur, then analyst blindness with data uniquely coded is encouraged [34]. Sample and data elimination during the analysis process should be strongly discouraged and only in the case of a validated outlier test recommends the removal of select data points [38]. Furthermore, biases and outlier handling can be better managed by establishing solid inclusion and exclusion criteria during the planning of the study and prior to the initiation of the treatments [34, 38].

1.4 Analyzing a Discovery Cohort and Selection of Primary and Secondary Outcomes

For preclinical studies in lung fibrosis, it is not unusual to assess a multitude of outcomes. These outcomes can include the assessment of pulmonary physiology, various biochemical assessments of lung tissues, histological examinations, bronchoalveolar lavage fluid, or blood-borne components [17] (Fig. 3). With recent advances of "omics" technology, including, but not limited to, gene arrays,

Fig. 2 (continued) control group will be required to establish the level of fibrosis (group 2). Two potentially different vehicle control groups may be required, one with the inhaled vehicle formulation (group 3) and one with oral vehicle formulation (nintedanib/pirfenidone arm, group 4). Two treatment arms of the investigational, inhaled drug (X) may be required (group 5, 6) if a potential dose-dependency is to be examined. The result of these arms should be compared to the positive treatment arm (nintedanib/pirfenidone, oral administration, group 7). The data generated and analyzed (H) from this study is used to refine the design (I), primary and secondary outcomes and to conduct appropriate power analysis calculations (J) before an internal or external validation study is initiated (K). Due to the lack of reproducibility often observed in the preclinical field, and to improve translation to the clinical settings, we recommend sharing study designs and associated data with the scientific community to allow for external assessments and further validations. If Drug X displayed preclinical efficacy, it may facilitate the move toward clinical development (L)

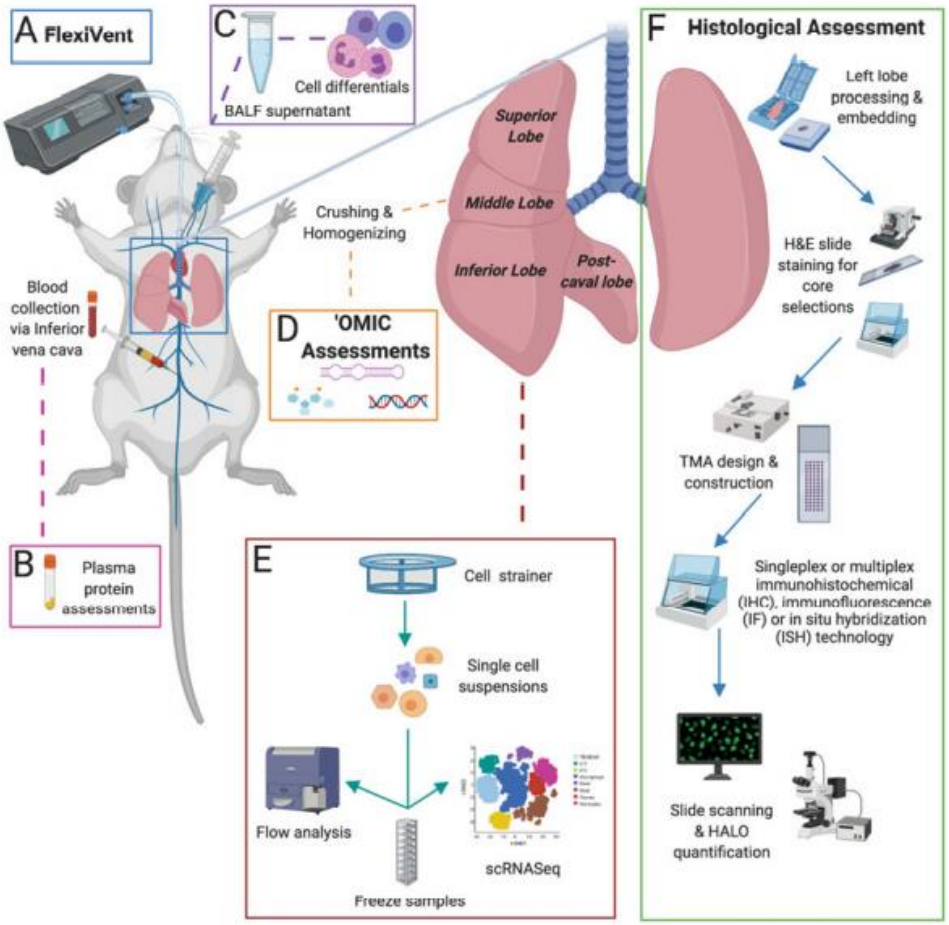

Fig. 3 *Processing and archiving of biological samples.* (A) Lung function assessments using a flexiVent mechanical respirator. (B) Blood is collected via the inferior vena cava and plasma isolated for potential protein analysis. (C) BALF is collected and processed for cell differential assessments. (D) Middle and post-caval lobes are snap-frozen for potential "omics" assessment. (E) Superior and inferior lobes are digested and single-cell suspensions are frozen for later flow cytometry and potential scRNAseq processing and assessments. (F) Left lung is fixed in formalin, embedded for TMA generation and downstream histological assessments (such as α-Smooth Muscle Actin, Masson's Trichrome, Picrosirius Red, and Hematoxylin and Eosin)

metabolomics, lipidomic and proteomic assessments on bulk or single-cell suspensions, plasma or in bronchoalveolar lavage (BAL) supernatant, single-cell RNAseq and multiplex strategies on histology specimens, gives the possibility to measure an endless number of variables [4, 19, 39]. Due to technological advances in the past decades, whole-body animal imaging, such as miniaturized X-ray and ultrasound, are being utilized more frequently to track the effects of the drug candidates in live animals, providing clinically relevant information and ultimately shortening the preclinical

phase of the pipeline [17, 40–42]. Depending on the target engagement profile of the lead candidate and the research hypothesis being addressed, one quantifiable primary endpoint may not be sufficient to link preclinical to clinical readouts [8, 43]. For instance, when testing lead antifibrotic candidates in experimental models of lung fibrosis, certain studies have considered the quantification of collagen via hydroxyproline assessment as the primary readout for disease severity and success of antifibrotic therapy [17]. In other antifibrotic therapeutic trials, the combination of multiple primary endpoints such as respiratory mechanics assessment and histopathology has been used. A composite index has been developed in other fibrotic systems [44] and is strongly warranted for use in preclinical therapeutic interventions studies in lung fibrosis. Overall, limiting the number of primary outcomes will increase the robustness of the trial, allow for proper power-calculations, decrease the number of animals required, and decrease the chances of reporting false positive findings [36, 38, 45]. Secondary outcomes are additional variables that can be assessed and support primary outcomes [43]. Frequently, exciting findings are observed when analyzing secondary outcomes. For example, an anti-fibrotic intervention is seen to also reduce the extent of inflammatory cell infiltration. It is important to recognize that as a researcher increases the number of secondary outcome measurements there will be a proportional increase in the number of false positive observations. When this happens, there is obviously a temptation to switch the aim of the study, to the new, exciting data with strong statistical significance. While that is obviously an error, it is likely that this occurs frequently and contributes to a biased and false state of "knowledge." However, analyzing secondary outcome is likely the source of exciting new hypotheses. What is important, and this responsibility lies with the basic scientist, is that exciting observations made on secondary outcomes need to be confirmed with a brand new experiment or clearly declared as secondary findings, in need of validation, when presented in the final publication. To avoid this, we recommend here that discovery experiments are used to analyze multiple outcomes and to formally identify primary and secondary outcomes. Appropriate power calculations can then be conducted before internal or external validation experiments are conducted, as discussed below.

1.5 Design and Execution of Validation Experiments

Since 2004, based on recommendation made by the International Committee of Medical Journal Editors (ICMJE), all clinical trials must be registered online prior to enrolling the first trial participant. This achieves several aims, perhaps the most important of which is the declaration of the primary outcome variable before the data is analyzed. As mentioned above, this prevents authors from selecting the outcome that best supports the pre-trial hypothesis, and thereby markedly reduces bias and the extent to which knowledge is influenced by chance, or false positive results

[36, 46]. Currently, this same systematic oversight is not currently applied to basic or preclinical research. A basic researcher is still free to pick whichever outcome he/she chooses to include in the publication at the end of a research project. It is therefore the responsibility of the researcher to ensure that the data presented, and the conclusions drawn from that data, are the best attempt at representing the underlying truth, as opposed to the best attempt to support the pre-study hypothesis. Therefore, it is recommended that the primary outcomes (or pre-defined composite of multiple outcomes) should be selected and appropriately powered prior to the validation analysis, thereby imposing the same control that is systematically imposed in clinical research. In addition, we recommend validation studies to include both male and female groups and to potentially focus on specific groups identified in the discovery cohort and as shown in Fig. 2. Finally, validation studies executed by external research groups increase the confidence that "real" effects are seen, provided that shared protocols and methodologies are available[46]. To this effect, we have here assembled the different methodologies used in our research laboratory to assess the effect of anti-fibrotic therapies, focusing on the bleomycin-model of lung fibrosis.

2 Materials

2.1 Intratracheal Administration of Drugs

1. Biological safety cabinet (BSC).
2. Autoclave machine.
3. Anesthetic machine with an accompanying anesthetic chamber.
4. Gaseous isoflurane anesthetic.
5. Mouse scale.
6. Ear notcher.
7. 70% Ethanol.
8. Intratracheal intubation equipment: Intubation board, otoscope handle, operating otoscope that attaches to the handle, mouse intubation specula that fits on the end of the operating otoscope, 22G 1 inch Insyte IV catheter needle with the sharp end of the needle blunted, 200μL extended length gel loading pipette tips, blunt end forceps, and masking tape.
9. Bleomycin: Reconstitute bleomycin to a stock concentration of 1.6 units/mL by adding 9.38 mL of saline to a vial containing 15 units of bleomycin. Aliquot 500μL of bleomycin in 1.5 mL Eppendorf tubes and store in −80 °C. On the day of bleomycin instillation, dilute stock concentration to obtain the required doses of either 0.04 or 0.05 or 0.06 units (U)/mouse of bleomycin in a volume of 50μL sterile saline per mouse, and

gently vortex. Keep on ice throughout the procedure (*see* **Note 1**).

2.2 Endpoint Measures: Respiratory Mechanics

1. FlexiVent® mechanical respirator (flexiVent® SCIREQ, Montreal, PQ, Canada).
2. Ketamine hydrochloride/xylazine anesthesia in mice: To prepare a cocktail, in a sterile vial combine 0.75 mL (75 mg) of ketamine (100 mg/mL concentration), 0.25 mL (5 mg) of xylazine (20 mg/mL), and 4 mL of sterile water. For mouse, recommended dose for ketamine is 80–100 mg/kg and for xylazine is 10 mg/kg. Cocktail can be stored in a cool place protected from light for a maximum of 1 month.
3. Mouse cannula.
4. 25G Needle.
5. 1 mL Syringe.
6. Heating blanket.
7. Straight forceps.
8. 70% Ethanol.
9. Micro forceps.
10. Rocuronium bromide (paralytic): To prepare a total volume of 500µL, sufficient for 10 mice [40µL per mouse (1:5 dilution)], in a labeled 1.5 mL Eppendorf tube, add 400µL of sterile phosphate-buffered saline (PBS) to a 100µL of rocuronium (10 mg/mL) (extract using a 25-gauge (G) needle and a 1 mL syringe) and gently vortex. Prepare the working concentration on the day of experiment. Paralytic is sufficient for one day. Keep on ice throughout the procedure.

2.3 Endpoint Measures: Blood Collection for Plasma Analysis

1. 1 mL Syringe.
2. Heparin.
3. 23G Needle.
4. K2EDTA vacutainer blood collection tube.
5. Ice box.
6. 200µL pipette.

2.4 Endpoint Measures: BALF Collection for Immune Cell Differentials

1. Mouse cannula.
2. Phosphate-buffered saline (PBS): 137 mM NaCl, 2.7 mM KCl, 8 mM Na_2HPO_4, and 2 mM KH_2PO_4. Adjust pH to 7.4.
3. 1 mL Syringe.
4. Hemocytometer.
5. Trypan blue 0.4%
6. Centrifuge.
7. 200µL Pipette.

8. −80 °C.
9. Microscope slides.
10. Cytocentrifugation.
11. Wright-Giemsa stain kit.

2.5 Endpoint Measures: Lung Processing for Histopathology, Flow Cytometry, and Single-Cell RNA Sequencing

1. Surgical sutures.
2. Digestion Media: To a complete Roswell Park Memorial Institute (RPMI) media containing 10% fetal bovine serum (FBS), 1% L-glutamine, and 1% penicillin streptomycin (pen-strep), add the following: 50 U/mL deoxyribonuclease I from bovine pancreas (DNase I), and 300 U/mL collagenase type I.
3. Cell shaker.
4. Syringe plunger.
5. 40µm Cell strainer.
6. 50 mL Falcon tube.
7. RMPI media: 10% FBS, 1% L-glutamine, and 1% pen/strep.
8. Hemocytometer.
9. Centrifuge.
10. Fluorescence activated cell sorting (FACS) buffer: 0.5% bovine serum albumin (BSA) in PBS.
11. Freezing Media: Consists of 50% of complete RPMI media (10% FBS, 1% L-glutamine, and 1% pen-strep), 40% of FBS, and 10% of dimethyl sulfoxide (DMSO).
12. Cryovials.
13. Freezing materials: cold ice, dry ice, 1 large supply of liquid nitrogen, and freezing containers.
14. –80 °C Freezer.
15. 10% Formalin.
16. 70% Ethanol.
17. Histology cassettes.
18. Paraffin wax.
19. TMA.
20. Bond RX (Leica).
21. Lung crushing equipment for snap-frozen lung processing and assessment: Metal chamber (to localize the sample), piston (cylindrical metal piece to crush the sample, placed in metal chamber), wooden block, hammer, several metal spatulas, 1 Styrofoam container for freezing equipment and instruments, 1 Styrofoam container containing dry ice, 14 mL polypropylene tubes, tin foil, and a balance.
22. Lung homogenization equipment for snap-frozen lung processing and assessment: Mechanical homogenizer, a beaker, and

1 50 mL falcon tube of 70% ethanol, and 1 50 mL falcon tube of distilled water.

23. Radioimmunoprecipitation assay (RIPA) buffer containing protease inhibitor (*see* **Note 2**): To prepare 100 mL of RIPA buffer stock solution, in a sterile glass bottle combine 93 mL of PBS (1×), 1 mL of octylphenoxypolyethoxyethanol (IGEPAL CA-630) (100%), 5 mL of Na-deoxycholate (10%), and 1 mL of sodium dodecyl sulfate (SDS) (10%). To prepare inhibitor, per 1 mL of RIPA buffer, add: 5μL Na_3VO_4 (200 mM), 30μL aprotinin, 5μL phenylmethylsulfonyl fluoride (PMSF) (20 mg/mL), and 1μL of 1,4-Dithiothreitol (DTT) (1 M).
24. 1.5 mL Eppendorf tubes.
25. RNA assessments reagents/equipment: Nucleospin RNA Plus Isolation Kit, NanoDrop spectrophotometer, Bioanalyzer, NanoString, and RNA sequencing technologies.
26. Reagents and equipment for collagen quantification assessment: Sircol™ Soluble collagen assay, Hydroxyproline assay, and a microplate reader.

2.6 Analysis of Homogenized Tissue Samples

1. Histology cassettes.
2. Hot paraffin wax.
3. TMA coring tools.
4. Small oven (research only).
5. 4 °C Refrigerator.
6. Microscope slide digitizer and scanner.

2.7 Quantification Using Digitalized TMAs

1. Picrosirius red (PSR) stain kit.
2. Masson's trichrome stain kit.
3. Hematoxylin and Eosin (H&E) stain kit.
4. Alpha-smooth muscle actin (α-SMA) stain kit.

3 Methods

3.1 Intratracheal Administration of Drugs

Intratracheal intubation is a simple and reliable method of instilling drugs into mouse lungs [47]. This procedure involves putting mice under inhalable anesthesia, visualizing the trachea through the opening of vocal cords, inserting a catheter through the tracheal opening, and delivering drug in a syringe through the catheter [48]. Once a researcher has some experience with this method, it can be carried out with little damage to the soft tissues of the upper respiratory tract [47, 48]. Evaluating the presence of a fibrotic response brought about by intratracheal intubation of bleomycin shows all lobes to be affected, referring to even dispersal of drug

into the lungs when procedure is done proficiently [47]. In this chapter, we describe how pulmonary fibrosis is induced in 8-12-week-old female C57BL/6J mice (Jackson Laboratories) by a single intratracheal instillation of bleomycin. Mice are anesthetized with gaseous isoflurane anesthesia prior to the procedure. The step-by-step procedure is outlined below:

1. After preparing the BSC (*see* **Note 3**), anesthetize mice with isoflurane using the anesthetic machine. Turn the oxygen to 1.5 L/min and isoflurane setting to 5%. Place the mouse (or mice) into the anesthetic chamber.
2. Ensure that the intubation board is set up at an angle of 60° relative to the working area (BSC counter), often referred to as a semi-suspended dorsal recumbency position [49].
3. When the mouse is deeply anesthetized (breathing rate is around one inhalation every two or 3 s), hang it on the intubation board by its teeth (upper incisors). Place a strip of masking tape over the mouse's ribcage to hold the chest in a position that ensures the airways are easily detected when looking inside with the otoscope.
4. Use the forceps to gently pull the mouse's tongue to the side of the mouth (*see* **Note 4**).
5. Turn on the otoscope and insert the assembled otoscope (*see* **Note 5**) into the mouse's mouth, looking for the vocal cords. They will appear as flaps of muscle that are opening and closing relative to the respiratory rate. If they cannot be seen, then the specula may have gone down too far, pull back and reinsert.
6. When the vocal cords can be seen, insert the syringe-catheter (*see* **Note 6**) ensemble through the vocal cord opening. Once through, hold the syringe steady and place the otoscope on the bench. Remove the needle and syringe from the catheter, leaving only the catheter in place.
7. To confirm the catheter is in the trachea, take the 200μL pipette containing water and air (*see* **Note 7**) and hold its pipette tip securely inside the catheter to form a tight seal. If the catheter is in the trachea, the water in the pipette tip will be drawn up and down by the mouse's breathing. Place this pipette back on the bench. If there is no movement of water, remove the catheter and start again. Proceed to **step 10** if you are confident the catheter is in the trachea.
8. While holding the catheter steady, take the 200μL pipette containing bleomycin (*see* **Note 8**) and hold its pipette tip securely inside the catheter to form a tight seal. The breathing of the mouse will draw the fluid into its airways. As this happens, gently push down on the pipette plunger to prevent fluid from coming back up the tip (*see* **Note 9**).

9. When all the fluid has been inhaled, hold the catheter in the trachea and place the blunt-ended needle into the catheter. This will expel any fluid remaining in the catheter.
10. Remove the catheter from the mouse. Remove the mouse from the intubation board. Place the mouse in the cage on its back in an upright position using the bedding to elevate its head; this will prevent suffocation. This also helps to prevent any fluid from draining from the lungs.
11. Monitor the mouse until it is conscious and has a normal respiration rate and activity level.

3.2 Endpoint Measures: Respiratory Mechanics

Lung function assessments are conducted using a flexiVent® mechanical respirator. FlexiVent® enables the measurement of lung compliance, or its inverse, lung elastance, which is a functional parameter derived from the pressure-driven pressure–volume loops. Instructions on flexiVent® procedures are previously described [50] and provided below:

1. Fully anesthetize mice via an intraperitoneal (i.p.) injection of a ketamine hydrochloride and xylazine cocktail at a dose of 0.06–0.07 mL/10 g of body weight using a 25G needle and 1 mL syringe (*see* **Notes 10** and **11**).
2. Place mouse on a heating blanket set on low to maintain body temperature.
3. Pinch the toes with straight forceps to verify that the subject has no reflexes.
4. Spray mouse with 70% ethanol solution.
5. Perform tracheal cannulation according to the following **steps 6–11**:
6. Using sterile surgical scissors and straight forceps, make a small incision of the skin in the throat area and cut laterally to expose a section of the anterior side of the neck.
7. Gently separate the submaxillary glands, separate muscle layer and any adhesive tissue, and remove the skin around the tracheal area to expose the trachea (*see* **Note 12**).
8. Gently slide sterile curved micro-forceps underneath the trachea.
9. Make a small incision at the top of the trachea, below the cricoid cartilage between two rings of cartilage.
10. Insert a 18G cannula into the incision and push the cannula into the trachea past 3–5 tracheal rings.
11. Place a surgical suture over the cannula and tie two knots over it.

12. Connect the mouse to the mechanical ventilator controlled by the SCIREQ software (FlexiWare 7.6.6) (*see* **Note 13**) and start ventilation.
13. To paralyze subjects and inhibit respiratory effort, administer rocuronium bromide (*see* **Note 14**) (10 mg/mL) at a dose of 4 mg/kg i.p. (40μL per mouse) using a 25G needle connected to a 1 mL syringe.
14. Ventilate subject for 10–30 s and then hyperinflate the lung to total lung capacity in order to attain standardized baseline conditions [51].
15. Start the flexiVent® script and the lung perturbations as previously described [50]. Mice are ventilated with 10 mL/kg of air at a rate of 150 breaths per min in between forced oscillation waveforms maneuvers. The changes in flow, volume, and pressure within the airways are recorded and the raw data is fit to the *single-compartment model* to assess lung elastance resistance, and the *pressure-volume loop Salazar Knowles equation* to assess quasi-static elastance [51].

3.3 Endpoint Measures: Blood Collection for Plasma Analysis

Following flexiVent® assessments, 0.5–1 mL of blood can be obtained from mouse inferior vena cava as follows:

1. Load heparin (or another appropriate anticoagulant) into 1 mL syringe to coat the surface.
2. Lift the abdomen skin and cut laterally from mouse pelvis/prepuce to the xiphoid.
3. Gently move the intestines to the left side of the mouse to expose the inferior vena cava.
4. Gently insert a 23G needle attached to the 1 mL heparinized syringe into the inferior vena cava and slowly withdraw the blood.
5. Place extracted blood in a K2EDTA vacutainer blood collection tubes and immediately store on ice until later processing and plasma collection.
6. To collect plasma, spin blood at 1500 g for 10 mins at 4 °C.
7. Draw plasma from each tube using a 200μL pipette (*see* **Note 15**).
8. Store plasma at −80 °C in sterile cryovials for downstream assessments (*see* **Note 16**).

3.4 Endpoint Measures: BALF Collection for Immune Cell Differentials

Following blood collection, BALF can be harvested for immune cell differentials as follows:

1. Puncture and cut away diaphragm to stop breathing of mouse.
2. Open the thoracic cavity of the mouse.

3. As described in detail in Subheading 3.2, insert a cannula in the incision made on top of the trachea.
4. Inject 600μL of PBS into the lungs using a 1 mL syringe via the cannula for a first wash.
5. Briefly massage the lungs to wash out lung infiltrate cells and then extract PBS through negative pressure using the same 1 mL syringe.
6. Place the recovered lavage fluid (~400–500μL) in a 1.5 mL Eppendorf tube.
7. Inject 400μL of PBS into the lungs using a 1 mL syringe via the cannula for a second wash.
8. Repeat **steps 4** and **5** above.
9. Following BALF collection, place the tubes immediately on ice until later processing.
10. Perform total cell count using a hemocytometer from an aliquot of 20μL from each sample and add trypan blue stain 0.4% to these tubes to test for cellular viability.
11. Centrifuge each Eppendorf tube at 400 × *g* for 8 mins at 4 °C.
12. Draw supernatant from each tube using a 200μL pipette and store it at −80 °C in sterile cryovials for downstream assessments (*see* **Note 17**).
13. Suspend the cell pellet in 300–600μL (depending on cell density of each sample) of sterile cold PBS.
14. Use 120μL aliquot to cytospin onto a microscope slide.
15. Prepare smears by cytocentrifugation at a speed of 22 g for 3 min.
16. Stain the developed cytospin slides with Wright–Giemsa stain according to the manufacturer's protocol.
17. Conduct differential cell count in BALF under 40× magnification using a microscope. A sample size of 200 is chosen and morphological characteristics are assessed to identify the different cell types in the lung BALF (*see* **Note 18**).
18. Present each cell type as total numbers, based on the corresponding total cell count calculated from each sample.

3.5 Lung Processing for Histopathology, Flow Cytometry, and Single-Cell RNA Sequencing

3.5.1 Processing of the Right Superior and Inferior Lobes for Flow Cytometry or scRNAseq Assessment

1. Following collection of the BALF, heart and lungs are disconnected from mouse carcass and the four lobes of the right lung are separated from the left lung by tying them up with a surgical suture and excising them. The lung lobes are separated and processed as described below (*see* **Notes 19** and **20**).
2. Mince the superior and inferior lobes into small pieces, immediately place them into 5 mL of digestion media (refer to Subheading 2.5).
3. Keep lobes on a cell shaker at 37 °C for 1–2 h.
4. Subsequently, using a sterile syringe plunger, crush the digested lobes and push them through a 40μm cell strainer placed on a 50 mL falcon tube (*see* **Note 21**).
5. Centrifuge cells drained through filters at 400 × *g* for 5 min at 4 °C.
6. Decant supernatant and suspend pellets in 10 mL of complete RPMI medium (10% FBS, 1% L-glutamine, and 1% pen/strep) or PBS.
7. Perform cell count using a hemocytometer from an aliquot of 20μL from each sample and add trypan blue stain 0.4% to these tubes to test for cellular viability.
8. Centrifuge cells at 350 × *g* for 5 min at 4 °C.
9. Decant supernatant and resuspend pellets in cell staining FACS buffer (refer to Subheading 2.5) or PBS (*see* **Note 22**) at a concentration of 40 × 10^6 cells/mL to be stained for flow cytometry assessment of different cell markers.
10. Freeze remaining cells in freezing media (refer to Subheading 2.5) and place samples into cryovials (1 mL of freezing medium per each sample) (*see* **Note 23**).
11. Immediately, place cryovials into cold freezing containers and store containers at −80 °C for 24–48 h.
12. After 24–48 h, transfer frozen lung cells from −80 °C to liquid nitrogen for later flow or scRNAseq processing and analysis.

3.5.2 Processing of the Right Middle and Post-Caval Lung Lobes for RNA Analysis

1. Immediately snap-freeze the middle and post-caval lobes in liquid nitrogen.
2. Store the lobes at –80 °C for further protein and RNA analysis.

3.5.3 Processing of the Left Lung Lobe for Histology

1. Inflate the left lung with 10% formalin at a 30 cm H_2O of pressure for 3–5 min.
2. Submerge the left lung into 15 mL falcon tube filled with 10% formalin and fix them for 24 h before transferring them to 70% ethanol.

3. Later, cut each left lung (2 tissues per lung) and place them into histology cassettes.
4. Process and embed all tissue-containing cassettes in paraffin wax.
5. Generate a tissue microarray (TMA) as described in Subheading 3.7.
6. Following the development of a TMA containing mouse lung tissues, cut and stain with a Bond RX (Leica), as described previously [51, 52].

3.5.4 Crushing of Snap-Frozen Lung and Homogenization for RNA and Protein Assessment

1. Snap-frozen right middle and post-caval lungs can be retrieved from −80 °C and processed for further RNA and protein assessments. Processing and assessment protocols are as follows:
2. Prepare two sets of 14 mL polypropylene tubes labeled with animal identification numbers (*see* **Note 24**).
3. Add 1 mL each of RIPA buffer (refer to Subheading 2.4) into one set of tubes only.
4. Take and record weights of all tubes using a balance.
5. Place the snap-frozen lungs (removed from −80 °C freezer and stored in tin foil) in liquid nitrogen (*see* **Note 25**).
6. Freeze equipment (metal chamber, piston, and spatulas) by placing them in a Styrofoam container filled with liquid nitrogen (*see* **Note 26**).
7. Remove frozen metal chamber from Styrofoam container and place on wooden block. Add small amount of liquid nitrogen to frozen metal chamber.
8. Remove frozen tissue sample from tin foil and take the weight using a balance.
9. Place tissue in frozen metal chamber and slide piston into chamber on top of tissue (*see* **Note 27**).
10. Hammer the top of the piston approximately 10 times until lungs have been crushed into a fine powder.
11. Remove the piston and scrape any powder left on piston surface into the metal chamber using a frozen spatula (*see* **Note 28**).
12. Use spatula to stir and scrape tissue powder to ensure adequate mixing.
13. Quickly invert metal chamber onto a piece of clean tin foil to remove the tissue. Hammer the bottom of the metal chamber approximately 10–15 times to remove all powder (*see* **Note 29**).

14. Transfer the tin foil containing the powder to dry ice. Using frozen spatula, remove one scoop of powder and place into corresponding RIPA containing tube. Store tube on dry ice.
15. Place remaining powder in the respective empty 14 mL tube (for RNA analysis). Store the tube on dry ice (*see* **Note 30**).
16. Take weights of tubes now containing powder and subtract prior tube weights without tissue (taken in **step 3**) to determine the respective tissue weights (*see* **Note 31**).
17. Store all tubes at −80 °C.
18. For lung homogenization (*see* **Note 32**), place all tissue sample tubes on wet ice and let thaw.
19. After assembling the homogenizer, clean the metal cylindrical wand by dipping it into a 50 mL falcon tube of 70% ethanol and letting the homogenizer run for 10 s. Repeat this with distilled water and then wipe the wand dry.
20. Place the first tube containing tissue powder and RIPA buffer in a beaker containing ice and insert the metal wand of the homogenizer into the tube. Homogenize the sample for 10 s, followed by a 10 s pause, and another 10 s of homogenization. Remove the tube from the beaker and place on ice (*see* **Note 33**).
21. Clean the homogenizer with 70% ethanol and distilled water as described in **step 19**.
22. Centrifuge samples at 1500 rpm for 8 min.
23. Collect supernatant and store in 1.5 mL Eppendorf tubes.
24. Resuspend the pellet in PBS and store in 1.5 mL Eppendorf tubes.
25. Store the supernatant and pellet tubes at −80 °C.

3.6 Analysis of Homogenized Tissue Samples

If desired, powdered lung tissue stored at -80°C as described in Subheading 3.2.7 can be processed to extract RNA for downstream analysis.

3.6.1 RNA Extraction

1. Isolate RNA using a commercially available spin column RNA kit, according to the manufacturer's instructions.
2. With 1–2μL of isolated RNA use the Nanodrop spectrophotometer to determine the RNA concentration in each sample.
3. Examine RNA integrity and quality using Bioanalyzer.
4. Submit RNA samples to a core facility for gene expression analysis, NanoString Technologies, or bulk RNA sequencing.

3.6.2 Collagen Assessment

1. To quantify the levels of soluble collagen in the supernatant from the RIPA-homogenized lung tissues, the Sircol™ soluble collagen assay can be utilized. Perform the assay using

supernatants from lung homogenates, according to the manufacturer's protocol. Read absorbance using a microplate reader at a wavelength of 555 nm and determine the test sample collagen concentrations from the standard curve. Results are expressed as μg soluble collagen/mL solution.

2. To quantify the levels of insoluble collagen in the pellet from the RIPA-homogenized lung tissues, the colorimetric hydroxyproline assay can be utilized: Perform the assay as previously described [53] by reading absorbance using a microplate reader at a wavelength of 550 nm and determining the test sample collagen concentrations from standard curve. Results are expressed as μg hydroxyproline/ml solution.

3.7 Histology Tissue Microarray (TMA) Production and Digitization

3.7.1 Creation of a TMA

Assessing all formalin-fixed paraffin-embedded murine tissues on an individual basis is time consuming and can be quite costly. Extracting these tissues from each individual paraffin block and consolidating them into a single paraffin block provides the ability to analyze whole lung slices for all experimental mice in a single paraffin slice, as illustrated previously [15]. Creating a tissue microarray requires planning and knowledge of the precise location(s) the core(s) should be extracted. In this case, by using a puncher with a sufficiently large diameter size (1.5–2.0 mm), 1–2 cores are enough to extract the entirety of the mouse lung. Thus, deciding on a location for punching is not required as most of the tissue is included.

1. Organize all formalin-fixed paraffin-embedded tissue blocks from which cores will be extracted, ensuring each one has a meaningful block identifier (*see* **Note 34**).
2. Determine the limiting factor: what aspect of the TMA must or must not take place, such as the minimum core diameter not being less than 1.5 mm or ensuring that all animal tissues are present on a single TMA (as opposed to being spread out over 2 or 3 TMAs).
3. Design TMA layout(s) with limiting factor(s) in mind (*see* **Note 35**).
4. Prepare the paraffin receiving block as this is what will become the TMA: Fill a 37 mm × 24 mm block mold with hot paraffin wax to a depth of approximately 8 mm and place an empty tissue cassette face down and remove the fresh receiving block from mold once paraffin has solidified.
5. Drill out the designated number of holes into the receiving block with the desired diameter drill bit at a depth of approximately 7 mm according to the TMA layout design.
6. Once drilling is complete, remove excess wax filings by inverting drilled receiving block upside-down and tapping the

underside of the cassette lightly causing the filings to fall out of the drilled holes.

7. If specific areas of the specimen are required, ensure that these locations are chosen and identified ahead of time to allow for an accurate and smooth extraction of tissue from the donor to the recipient block (*see* **Note 36**).
8. With the receiving block drilled and all of the regions on the donor tissue blocks identified, begin punching.
9. Punch a tissue core in each designated donor tissue block and transfer these formalin-fixed paraffin-embedded cores into the receiving block's designated location, according to the TMA layout design. Continue until all desired tissues have been punched and all receiving block holes have been filled.
10. Once the receiving block (now a TMA) is full, place a new microscope slide on top such that it covers all the tissue cores, and invert the receiving block plus microscope slide such that the TMA is lying flat on the microscope slide (*see* **Note 37**).
11. Set the oven to 45 °C.
12. Place the new TMA inverted on a microscope slide directly onto one of the oven racks, and let it sit for 24 h. The gentle heat will cause a very slight melting of the paraffin filling in the gaps caused by the drilling and sealing the tissue cores into one cohesive unit. The weight of the cassette will also press the paraffin slightly, compacting the TMA.
13. Remove from the oven and place the TMA on the slide directly into a 4 °C refrigerator for a few hours. The paraffin should be hard to the touch.
14. Remove the TMA from the refrigerator. The microscope slide will be stuck to the top of the TMA; pull it off and discard.
15. The top of the TMA will be uneven from the drying process. Run the TMA through a microtome to smooth out the top, as this will ensure each successive cut will contain tissue.
16. The TMA is now ready for slicing onto a microscope slide and staining.

3.7.2 Tissue Array Digitization

Viewing tissue slides utilizing a microscope is limited by experience with a microscope, time of viewing, equipment availability and inability to utilize for assessment. Digitizing these slides enables easy viewing, without requiring experience with a microscope, on any computer. This allows for more people to view the slide simultaneously, even remotely, and side-by-side comparison of stains.

1. Load desired slides into a slide digitizer (*see* **Note 38**).
2. Once the digitizer has gone through a quick low magnification overview scan of the slide, select the region of the slide where

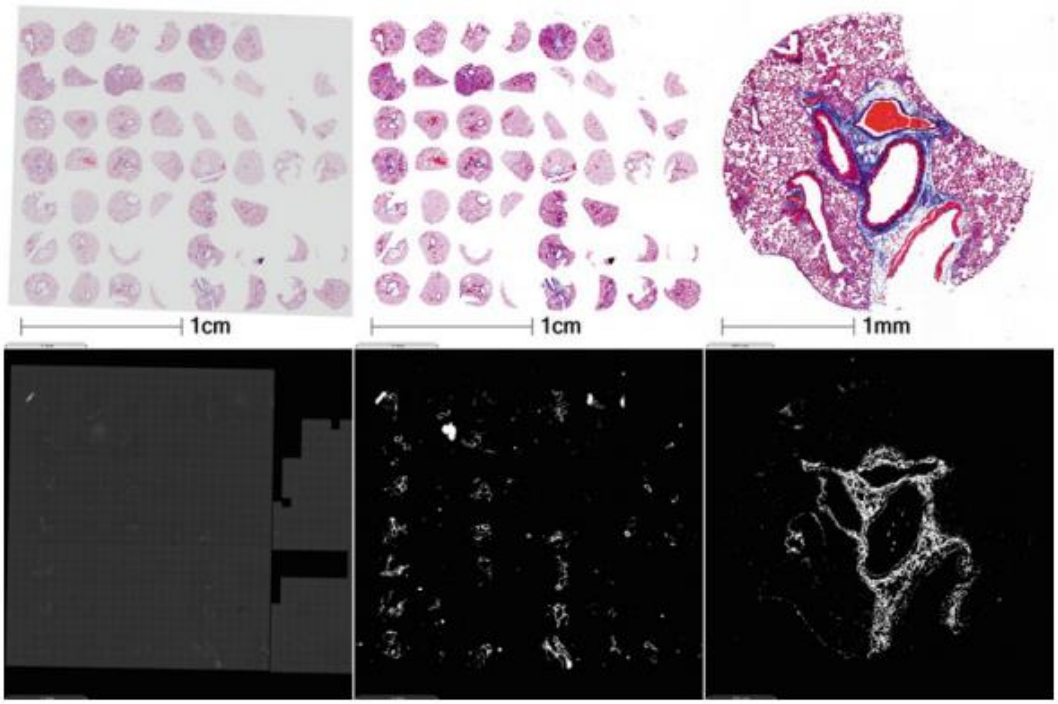

Fig. 4 *Importing and contrast-correcting images in HALO®*. (Top-Left) Tissue Microarray (TMA) stained with Masson's Trichrome, digitized and directly imported into HALO. (Top-Center) Pixel black input increased from 0 to 125 and white input decreased from 255 to 220. End result removes background and increases color vividness. (Top-Right) Zoom in on one specific core to see mouse lung tissue in reddish-purple and collagen in blue. (Bottom-Left) Same TMA serially sliced and stained with Picrosirius Red, digitized using polarized white light and directly imported into HALO. (Bottom-Center) Pixel black input increased from 0 to 13 and white input decreased from 255 to 15. End result removes background and increases whiteness. (Bottom-Right) Zoom in on the same specific core to see mouse lung collagen in white and everything else in black

the high magnification scan will take place, that being the tissue of interest.

3. Different stains require also different imaging techniques (*see* **Note 39**).
4. Once the scanning is complete, the slide has been digitized and is ready for viewing and/or quantification.

3.8 Quantification Using Digitized TMAs

With digitized tissues, image analyses can be performed to extract further quantifiable and qualitative information. The power of digital pathology made possible here is immense, however our foci here are the number of cells within the tissue as defined by nuclear staining, the proportion of cells that are positive for a protein or mRNA transcript as defined by Immunohistochemistry or ISH staining, respectively, and their proximity to previously defined cells. There is also the quantification of protein area with

respect to the total tissue area, such as with Picrosirius red or Masson's trichrome staining for the detection of collagen (Fig. 4).

1. Import the digitized tissue images into the tissue quantification software.
2. Contrast correct the digitized images by adjusting the pixel input black and white levels. Doing so will shift the balance of color to increase the image contrast more accurately.
3. The colors should be more vibrant for H&E, IHC, immunofluorescence, C-ISH, and FISH.
4. The white fluorescence should be brighter for Picrosirius red-POL.
5. The background noise should be eliminated.
6. Recreate the design map within the quantification software, by adding the rows and columns according to the TMA layout.
7. Assign each core useful information for quantification, such as animal ID, group #, and potential drug treatment.

3.8.1 Protein and mRNA Quantification from Digitized TMAs

1. The algorithms used will require assigning a color for nuclei, which can be done by selecting a range of nuclear pixels on-screen and averaging those pixel colors, as well as colors for the protein(s)/mRNA(s) for which the image is stained (*see* **Note 40**).
2. Adjust the cellular parameters such that the nuclear size, shape, contrast threshold, and minimum optical density properly reflect the cells on-screen (*see* **Note 41**).
3. Adjust the protein/mRNA parameters such that the cellular compartment and minimum positive threshold(s) properly reflect the stain(s) on-screen.
4. The stain must present itself within the proximity of the cell for the algorithm to consider that cell to be positive for the selected protein/mRNA transcript (*see* **Note 42**).
5. The stain must also be of sufficient pixel intensity or minimum optical density for it to be considered true staining (*see* **Note 43**).
6. Run the protein/mRNA quantification software over the entire image for single tissue slides, or for TMAs, run it through the TMA layout so that each core is analyzed individually, and results are assigned on a core-by-core basis instead of treating the image as a single tissue.
7. Using the raw data (total cells, stain + cells, etc.), determine the proportion of cells that are positive for your stain of interest according to the experimental groups and perform statistical analyses.

3.8.2 Picrosirius Red Quantification

1. The fluorescence area quantification algorithm used will require assigning a fluorescence channel (POL-MONO) as the selected dye (*see* **Note 44**).
2. Adjust the dye minimum intensity such that only the white fluorescence of the collagen passes the positivity threshold (*see* **Note 45**).
3. Annotate the tissue region to determine the total tissue area.
4. Run the fluorescence area quantification algorithm to determine the total POL-MONO area (*see* **Note 46**).
5. If desired, excise the major airways and blood vessels from the lung by means of annotation and then run the algorithm again (*see* **Note 47**).
6. Using the raw data (POL-MONO area, total area, etc.), determine the proportion of the lung that is composed of collagen according to the experimental groups and perform statistical analyses.

4 Notes

1. It is recommended to test the aliquoted vial prior to each use, as the strength of drug and its response may vary depending on the provider, lot/batch number, the mouse (strain, gender, and age), and more. Subsequently, these tests will help determine the proper dose.
2. Protease inhibitor should be made fresh on the day of the experiment.
3. Ensure that the working area around the biological safety cabinet (BSC) is sterilized and approved for animal work and autoclave all materials listed in Subheading 2.1.
4. It is important to not pinch the tip of the animal's tongue to avoid injury.
5. Prior to use, attach the operating otoscope to the otoscope handle, and then attach the specula to the operating otoscope.
6. Prior to injection, blunt the ends of several 22G, 1-inch insyte IV catheter needles. Then, attach the 22G, 1-inch insyte IV catheter/blunt ended needle to a 1 mL syringe.
7. Prior to the start of the experiment, adjust a 200μL pipette to the 150μL setting and attach a standard-length pipette tip. Then, draw 150μL of double-distilled water into the pipette tip and leave a space at the end of the tip for a large volume of air. Set aside until use.
8. Prior to the start of the experiment, adjust an extended length gel loading pipette tip to a second 200μL and draw 50μL of bleomycin into the pipette tip. Set aside until use.

9. It is important the agent is inhaled and not forced into the lungs. Forced fluid can come out the nose, potentially being fatal.
10. If needed, top-up the anesthesia with 1/3 dose of ketamine only.
11. With this ketamine/xylazine cocktail, animals will remain surgically anesthetized for 20–30 min.
12. Carefully remove any fur and skin around the trachea, avoid cutting the jugular veins, and ensure that there is no excess blood in tracheal area as it is critical to not have blood entering the airways.
13. Software will differ depending on the flexiVent® provider.
14. Refer to Subheading 2.2 to prepare a working concentration of rocuronium bromide (1:5 dilution).
15. 0.5 mL—1.0 mL of blood results in a volume of approximately 200–500μL of plasma.
16. It is critical to aliquot the plasma (for example, in a volume of 50μL) and to avoid freeze-thaw cycles.
17. It is critical to aliquot the BALF supernatant and to avoid freeze-thaw cycles.
18. The following morphological characteristics are assessed to identify the different cell types in the lung BALF: Macrophages are the largest of the white blood cells with large purple kidney-shaped nucleus, abundant cytoplasm, and fine pink/purple granules. Lymphocytes are slightly larger than red blood cells (RBC), look like monocytes but with small spherical purple nucleus and not much cytoplasm. Neutrophils contain multi-lobed purple nuclei, cytoplasm contains purplish granules, and are the smallest of granulocytes but bigger than RBC. Eosinophils are larger than neutrophils, contain two lobed purple nuclei, and cytoplasm with pink granules. Bronchial epithelial cells are ciliated and columnar with purple nucleus.
19. To avoid red blood cells contamination with cells of interest in lungs, heart perfusion might be conducted. Perform heart perfusion prior to BALF collection as follows: After opening the thoracic cavity of the mouse, expose lungs and heart as much as possible by removing surrounding tissues and rip cage. Insert a 26G1/2 needle, connected to a 5 mL syringe that contains sterile PBS, into the right ventricle of mouse heart. Slowly inject 5 mL of PBS until lung color changes and turns white.
20. Caution must be taken while performing heart perfusion as lungs might be very fragile at specific timepoints. The fragility of the lungs depends on the time of investigation and the amount of injury. For instance, during inflammatory phase

(seven days following bleomycin administration), perfusing heart to remove blood might result in leakage in the lungs.

21. Immediately, place 50 mL falcon tube containing digested cells on ice.
22. Resuspending pellets in FACS buffer or PBS depends on the respective flow cytometry staining protocol.
23. To maximize total number of cells to be processed for flow cytometry, it is recommended to stain fresh viable cells before the freezing process. Following one freeze-thaw cycle, approximately 50% of total number of viable frozen cells are lost.
24. One set of tubes containing RIPA buffer will be for protein analysis, and the other empty set of tubes will be used for RNA analysis.
25. It is always important to keep tissues frozen throughout the entire procedure. Perform steps quickly when tissues are not in liquid nitrogen or dry ice.
26. Freeze the inside of the metal chamber by adding, swirling, and pouring out the liquid nitrogen.
27. Ensure that liquid nitrogen has evaporated from inside of chamber prior to adding the piston.
28. It is important to keep returning the piston back into Styrofoam freezing container.
29. Once sample is crushed and powder is transferred over onto a tin foil, quickly return the metal chamber back into the Styrofoam freezing container.
30. All tubes on dry ice should be transferred and stored in −80 °C as soon as possible.
31. To ensure that tissue is being properly conserved, store the tubes on dry ice when they are not being weighed.
32. This protocol should be performed in a fume hood.
33. All tissue powder must be dissolved in the RIPA buffer. Often, longer than 10 s homogenization cycles, or extra homogenization cycles, are required.
34. If multiple mice are present on a single block, include identifiers for each separate mouse whose tissues are present in the block.
35. In the case of an animal model TMA, it is likely more desirable to have tissues from each animal be present within a single TMA. Also, multiple TMAs can be made with this in mind [15]: One TMA could have tissues from all animals present in a single 2.0 mm core, allowing for larger field of views for visual phenotyping. Another could have tissues from all animals

present as 3 replicate 1.0 mm cores to allow for statistical analyses as well as analyses set over multiple regions in a single lung.

36. If regions must be determined by microscopic examination, have digitized images of full tissue slices annotated to making finding these locations during punching efficient.
37. This is done to ensure none of the cores accidentally slide out of the TMA during the inversion process, as the paraffin has not yet molded to the cores which will occur during the heating process.
38. Provide a descriptive, searchable file name that can be distinguished from other slides that may have similar tissues and/or stains.
39. For example, hematoxylin and eosin (H&E) slides should be scanned using the 40× objective lens, as this magnification is needed when pathologists need to determine cell types and tissue phenotypes; Immunohistochemistry (IHC) slides should be scanned using the 20× objective lens; less detail is required as compared to the H&E slide, since labeled proteins are very dark and spacious within or around cells, making them easily viewable and quantifiable; In situ hybridization (ISH) slides, both colorimetric and fluorescent, should be scanned using the 40× objective lens, as labeled mRNA transcripts are much smaller than labeled proteins.
40. For nuclear stains, the prevalent counterstains in the histology performed leaves the nuclei with a blue color. For IHC stains, such as α-smooth muscle actin, this is a deep brown color. Care must be made so as not to select a color that is too dark, as gray/black artifacts may be accidentally categorized as IHC stain, when they should be excluded.
41. For example, based on the average volume of alveolar macrophages [54] and the average diameter of lung cell nuclei [55], with the whole cell diameter being calculated from the volume and the nuclear diameter being subtracted from that value, the resultant diameter (and thus, radius) is found to be approximately 6.5μm.
42. Based the previous example and **Note 41**, we have defined the radius of the cytoplasm to be 6.5μm surrounding the nucleus.
43. This is often done with the assistance of the resident pathologists that have agreed to assist the laboratory with these situations.
44. POL-MONO is the specific term used by Olympus to refer to using the mono-color channel in conjunction with a polarizer filter lens.

45. Picrosirius Red staining enhances the natural birefringence of collagen making it shine white under polarized fluorescent light.
46. Under polarized fluorescent light, the image will only display black and white; white is the total amount of collagen present in the image, black is everything else.
47. By removing vasculature and airways, all the collagen present is considered as being part of the parenchyma only.

References

1. Hughes J, Rees S, Kalindjian S, Philpott K (2011) Principles of early drug discovery. Br J Pharmacol 162:1239–1249. https://doi.org/10.1111/j.1476-5381.2010.01127.x
2. Sioud M (2007) Main approaches to target discovery and validation. In: Sioud M (ed) Target discovery and validation reviews and protocols: volume 1, emerging strategies for targets and biomarker discovery. Humana Press, Totowa, NJ, pp 1–12
3. Naiel S, Tat V, Padwal M et al (2019) Protein misfolding and er stress in chronic lung disease: will cell-specific targeting be the key to the cure? Chest. https://doi.org/10.1016/j.chest.2019.11.009
4. Kaminski N, Rosas IO (2006) Gene expression profiling as a window into idiopathic pulmonary fibrosis pathogenesis: can we identify the right target genes? Proc Am Thorac Soc 3:339–344. https://doi.org/10.1513/pats.200601-011TK
5. Cha Y, Erez T, Reynolds IJ et al (2018) Drug repurposing from the perspective of pharmaceutical companies. Br J Pharmacol 175:168–180. https://doi.org/10.1111/bph.13798
6. Karatzas E, Bourdakou MM, Kolios G, Spyrou GM (2017) Drug repurposing in idiopathic pulmonary fibrosis filtered by a bioinformatics-derived composite score. Sci Rep 7. https://doi.org/10.1038/s41598-017-12849-8
7. Durham TB, Wiley MR (2017) Target engagement measures in preclinical drug discovery: theory, methods, and case studies. In: Bhattachar SN, Morrison JS, Mudra DR, Bender DM (eds) Translating molecules into medicines: cross-functional integration at the drug discovery-development interface. Springer International Publishing, Cham, pp 41–80
8. Durham TB, Blanco M-J (2015) Target engagement in lead generation. Bioorg Med Chem Lett 25:998–1008. https://doi.org/10.1016/j.bmcl.2014.12.076
9. Steinmetz KL, Spack EG (2009) The basics of preclinical drug development for neurodegenerative disease indications. BMC Neurol 9:S2. https://doi.org/10.1186/1471-2377-9-S1-S2
10. Tashiro J, Rubio GA, Limper AH et al (2017) Exploring Animal models that resemble idiopathic pulmonary fibrosis. Front Med (Lausanne) 4. https://doi.org/10.3389/fmed.2017.00118
11. Denayer T, Stöhr T, Van Roy M (2014) Animal models in translational medicine: validation and prediction. New Horizons Transl Med 2:5–11. https://doi.org/10.1016/j.nhtm.2014.08.001
12. Justice MJ, Dhillon P (2016) Using the mouse to model human disease: increasing validity and reproducibility. Dis Model Mech 9:101–103. https://doi.org/10.1242/dmm.024547
13. Moore BB, Hogaboam CM (2008) Murine models of pulmonary fibrosis. Am J Physiol Lung Cell Mol Physiol 294:L152–L160. https://doi.org/10.1152/ajplung.00313.2007
14. B Moore B, Lawson WE, Oury TD et al (2013) Animal models of fibrotic lung disease. Am J Respir Cell Mol Biol 49:167–179. https://doi.org/10.1165/rcmb.2013-0094TR
15. Yanagihara T, Chong SG, Vierhout M et al (2020) Current models of pulmonary fibrosis for future drug discovery efforts. Expert Opin Drug Discovery:1–11. https://doi.org/10.1080/17460441.2020.1755252
16. Kolb P, Upagupta C, Vierhout M et al (2020) The importance of interventional timing in the bleomycin model of pulmonary fibrosis. Eur Respir J. https://doi.org/10.1183/13993003.01105-2019
17. Jenkins RG, Moore BB, Chambers RC et al (2017) An official American thoracic society

workshop report: use of animal models for the preclinical assessment of potential therapies for pulmonary fibrosis. Am J Respir Cell Mol Biol 56:667–679. https://doi.org/10.1165/rcmb.2017-0096ST

18. Bauer Y, Tedrow J, de Bernard S et al (2015) A novel genomic signature with translational significance for human idiopathic pulmonary fibrosis. Am J Respir Cell Mol Biol 52:217–231. https://doi.org/10.1165/rcmb.2013-0310OC
19. Adams TS, Schupp JC, Poli S et al (2019) Single Cell RNA-seq reveals ectopic and aberrant lung resident cell populations in idiopathic pulmonary fibrosis. bioRxiv:759902. https://doi.org/10.1101/759902
20. Yu G, Ibarra GH, Kaminski N (2018) Fibrosis: lessons from OMICS analyses of the human lung. Matrix Biol 68–69:422–434. https://doi.org/10.1016/j.matbio.2018.03.014
21. Herazo-Maya JD, Kaminski N (2012) Personalized medicine: applying 'omics' to lung fibrosis. Biomark Med 6:529–540. https://doi.org/10.2217/bmm.12.38
22. Patil JS, Sarasija S (2012) Pulmonary drug delivery strategies: a concise, systematic review. Lung India 29:44–49. https://doi.org/10.4103/0970-2113.92361
23. Strong P, Ito K, Murray J, Rapeport G (2018) Current approaches to the discovery of novel inhaled medicines. Drug Discov Today 23:1705–1717. https://doi.org/10.1016/j.drudis.2018.05.017
24. Epstein-Shochet G, Pham S, Beck S et al (2020) Inhalation: a means to explore and optimize nintedanib's pharmacokinetic/pharmacodynamic relationship. Pulm Pharmacol Ther:101933. https://doi.org/10.1016/j.pupt.2020.101933
25. Darquenne C (2012) Aerosol deposition in health and disease. J Aerosol Med Pulm Drug Deliv 25:140–147. https://doi.org/10.1089/jamp.2011.0916
26. Tuntland T, Ethell B, Kosaka T et al (2014) Implementation of pharmacokinetic and pharmacodynamic strategies in early research phases of drug discovery and development at Novartis Institute of Biomedical Research. Front Pharmacol 5. https://doi.org/10.3389/fphar.2014.00174
27. Polson AG, Fuji RN (2012) The successes and limitations of preclinical studies in predicting the pharmacodynamics and safety of cell-surface-targeted biological agents in patients. Br J Pharmacol 166:1600–1602. https://doi.org/10.1111/j.1476-5381.2012.01916.x
28. Schaefer CJ, Ruhrmund DW, Pan L et al (2011) Antifibrotic activities of pirfenidone in animal models. Eur Respir Rev 20:85–97. https://doi.org/10.1183/09059180.00001111
29. Bonniaud P, Fabre A, Frossard N et al (2018) Optimising experimental research in respiratory diseases: an ERS statement. Eur Respir J 51:1702133. https://doi.org/10.1183/13993003.02133-2017
30. Moeller A, Ask K, Warburton D, et al (2008) The bleomycin animal model: a useful tool to investigate treatment options for idiopathic pulmonary fibrosis? Int J Biochem Cell Biol 40:362–382. doi: 10.1016/j.biocel.2007.08.011
31. King TE, Bradford WZ, Castro-Bernardini S et al (2014) A phase 3 trial of pirfenidone in patients with idiopathic pulmonary fibrosis. N Engl J Med 370:2083–2092. https://doi.org/10.1056/NEJMoa1402582
32. Richeldi L, du Bois RM, Raghu G et al (2014) Efficacy and safety of nintedanib in idiopathic pulmonary fibrosis. N Engl J Med 370:2071–2082. https://doi.org/10.1056/NEJMoa1402584
33. Richeldi L, Costabel U, Selman M et al (2011) Efficacy of a tyrosine kinase inhibitor in idiopathic pulmonary fibrosis. N Engl J Med 365:1079–1087. https://doi.org/10.1056/NEJMoa1103690
34. Curtis MJ, Bond RA, Spina D et al (2015) Experimental design and analysis and their reporting: new guidance for publication in BJP. Br J Pharmacol 172:3461–3471. https://doi.org/10.1111/bph.12856
35. Head ML, Holman L, Lanfear R et al (2015) The extent and consequences of p-hacking in science. PLoS Biol 13:e1002106. https://doi.org/10.1371/journal.pbio.1002106
36. Aban IB, George B (2015) Statistical considerations for preclinical studies. Exp Neurol 270:82–87. https://doi.org/10.1016/j.expneurol.2015.02.024
37. Huang W, Percie du Sert N, Vollert J, Rice ASC (2020) General principles of preclinical study design. In: Bespalov A, Michel MC, Steckler T (eds) Good research practice in non-clinical pharmacology and biomedicine. Springer International Publishing, Cham, pp 55–69
38. Festing MFW (2006) Design and statistical methods in studies using animal models of development. ILAR J 47:5–14. https://doi.org/10.1093/ilar.47.1.5
39. Kulkarni MM (2011) Digital multiplexed gene expression analysis using the NanoString nCounter system. Curr Protoc Mol Biol 25.

Unit25B.10. https://doi.org/10.1002/0471142727.mb25b10s94

40. Ask K, Labiris R, Farkas L et al (2008) Comparison between conventional and "clinical" assessment of experimental lung fibrosis. J Transl Med 6(16). https://doi.org/10.1186/1479-5876-6-16
41. Beckmann N, Kneuer R, Gremlich H-U et al (2007) In vivo mouse imaging and spectroscopy in drug discovery. NMR Biomed 20:154–185. https://doi.org/10.1002/nbm.1153
42. Schambach SJ, Bag S, Schilling L et al (2010) Application of micro-CT in small animal imaging. Methods 50:2–13. https://doi.org/10.1016/j.ymeth.2009.08.007
43. Vetter TR, Mascha EJ (2017) Defining the primary outcomes and justifying secondary outcomes of a study: usually, the fewer, the better. Anesth Anal 125:678–681. https://doi.org/10.1213/ANE.0000000000002224
44. Liang W, Menke AL, Driessen A et al (2014) Establishment of a general NAFLD scoring system for rodent models and comparison to human liver pathology. PLoS One 9. https://doi.org/10.1371/journal.pone.0115922
45. Noordzij M, Tripepi G, Dekker FW et al (2010) Sample size calculations: basic principles and common pitfalls. Nephrol Dial Transplant 25:1388–1393. https://doi.org/10.1093/ndt/gfp732
46. Bert B, Heinl C, Chmielewska J et al (2019) Refining animal research: the animal study registry. PLoS Biol 17. https://doi.org/10.1371/journal.pbio.3000463
47. Cai Y, Kimura S (2013) Noninvasive intratracheal intubation to study the pathology and physiology of mouse lung. J Vis Exp. https://doi.org/10.3791/50601
48. Vandivort TC, An D, Parks WC (2016) An improved method for rapid intubation of the trachea in mice. J Vis Exp. https://doi.org/10.3791/53771
49. Puri S, Li J, Xiong M et al (2015) Method for single intravenous anesthetic infusion in a rodent model. Open J Anesthesiol 05:96–104. https://doi.org/10.4236/ojanes.2015.55019
50. McGovern TK, Robichaud A, Fereydoonzad L et al (2013) Evaluation of respiratory system mechanics in mice using the forced oscillation technique. J Vis Exp e50172. https://doi.org/10.3791/50172
51. Ayaub EA, Kolb PS, Mohammed-Ali Z et al (2016) GRP78 and CHOP modulate macrophage apoptosis and the development of bleomycin-induced pulmonary fibrosis. J Pathol 239:411–425. https://doi.org/10.1002/path.4738
52. Ayaub EA, Dubey A, Imani J et al (2017) Overexpression of OSM and IL-6 impacts the polarization of pro-fibrotic macrophages and the development of bleomycin-induced lung fibrosis. Sci Rep 7:13,281. https://doi.org/10.1038/s41598-017-13511-z
53. Brown S, Worsfold M, Sharp C (2001) Microplate assay for the measurement of hydroxyproline in acid-hydrolyzed tissue samples. Biotechniques 30:38–40, 42. https://doi.org/10.2144/01301bm06
54. Krombach F, Münzing S, Allmeling AM et al (1997) Cell size of alveolar macrophages: an interspecies comparison. Environ Health Perspect 105:1261–1263. https://doi.org/10.1289/ehp.97105s51261
55. Crapo JD, Barry BE, Gehr P et al (1982) Cell number and cell characteristics of the normal human lung. Am Rev Respir Dis 126:332–337. https://doi.org/10.1164/arrd.1982.126.2.332

Central Aim and Thesis Objectives

The central aim of the present Ph.D. thesis is to investigate the contribution of extrinsic risk factors (smoking), cell types (macrophages), intrinsic molecular mechanisms and biological processes (ER stress/UPR) to the immunopathogenesis and pathophysiology of fibrotic lung diseases. The present thesis has three specific hypothesises. First of all, we hypothesize that smoking will be associated with poorer survival and more severe pulmonary function outcomes in patients diagnosed with fibrotic ILD. Second, we hypothesize that CS exposure expands monocyte-derived AM and IM subpopulations. We hypothesize further that expanded monocyte-derived macrophages will exacerbate immunopathology in a mouse model of lung injury. Third, we hypothesize that the myeloid-specific deletion of *Atf6α* will halt the pro-fibrotic function of pulmonary macrophage subpopulations during lung injury and tissue remodelling. To test these hypothesises, we have developed the following three objectives: **1)** To investigate the effect of smoking status on the survival and pulmonary function decline in fibrotic ILD patients enrolled in the Canadian Registry for Pulmonary Fibrosis, a prospective observational cohort. **2)** To assess the impact of CS exposure on macrophage subpopulation composition using a whole-body CS exposure system for mice. To examine the functional consequences of altered macrophage subpopulations, we used a model of concurrent bleomycin-induced lung injury and cigarette smoke exposure to assess tissue remodelling processes. **3)** To investigate the impact of the myeloid-specific deletion of *Atf6α*, one of the UPR mediators, on pulmonary macrophage subpopulation composition and function during lung injury, tissue remodelling, and fibrogenesis.

Chapter 2

Effect of Smoking Status on Fibrotic Interstitial Lung Disease: Novel Insights from the Prospective Canadian Registry for Pulmonary Fibrosis

Olivia Mekhael[1], M. Malik Farooqi[2], Anna Dvorkin-Gheva[3], Kathryn Donohue[4], Ciaran Scallan[2], Fahad Alobaid[2], Deborah Assayag[5], Kerri A. Johannson[6], Charlene D. Fell[6], Veronica Marcoux[7], Helene Manganas[8], Julie Morisset[8], Jolene H. Fisher[9], Shane Shapera[9], Andrea S. Gershon[9], Teresa To[9], Alyson Wong[10], Mohsen Sadatsafavi[10], Pearce G. Wilcox[10], Andrew J. Halayko[11], Nasreen Khalil[10], Debarati Chakraborty[12], Gerard Cox[2], Christopher J. Ryerson[10], Kjetil Ask[2,3], Martin R.J. Kolb[2], Nathan Hambly[#2]

[1]Medical Sciences Graduate Program, Department of Medicine, McMaster University, Hamilton, ON, Canada, [2]Department of Medicine, Firestone Institute for Respiratory Health, McMaster University and The Research Institute of St. Joe's Hamilton, Hamilton, ON, Canada, [3]Department of Pathology and Molecular Medicine, McMaster Immunology Research Centre, McMaster University, Hamilton, ON, Canada, [4]Centre for Heart Lung Innovation, St. Paul's Hospital, Vancouver, BC, Canada, [5]Department of Medicine, McGill University, Montreal, QC, Canada, [6]Department of Medicine, University of Calgary, Calgary, AB, Canada, [7]Department of Medicine, University of Saskatchewan, Saskatoon, SK, Canada, [8]Department of Medicine, Université de Montréal, Montréal, QC, Canada, [9]Department of Medicine, University of Toronto, Toronto, ON, Canada, [10]Department of Medicine, University of British Columbia, Vancouver, BC, Canada, [11]Department of Internal Medicine, University of Manitoba, Winnipeg, MB, Canada, [12]Department of Medicine, Western University, London, ON, Canada.

An unpublished brief communication clinical report

Effect of Smoking Status on Fibrotic Interstitial Lung Disease: Novel Insights from the Prospective Canadian Registry for Pulmonary Fibrosis

Olivia Mekhael[1], M. Malik Farooqi[2], Anna Dvorkin-Gheva[3], Kathryn Donohue[4], Ciaran Scallan[2], Fahad Alobaid[2], Deborah Assayag[5], Kerri A. Johannson[6], Charlene D. Fell[6], Veronica Marcoux[7], Helene Manganas[8], Julie Morisset[8], Jolene H. Fisher[9], Shane Shapera[9], Andrea S. Gershon[9], Teresa To[9], Alyson Wong[10], Mohsen Sadatsafavi[10], Pearce G. Wilcox[10], Andrew J. Halayko[11], Nasreen Khalil[10], Debarati Chakraborty[12], Gerard Cox[2], Christopher J. Ryerson[10], Kjetil Ask[2,3], Martin R.J. Kolb[2], Nathan Hambly[#2]

1. *Medical Sciences Graduate Program, McMaster University, Hamilton, ON, Canada.*
2. *Department of Medicine, Firestone Institute for Respiratory Health, McMaster University and The Research Institute of St. Joe's Hamilton, Hamilton, ON, Canada.*
3. *Department of Medicine, McMaster Immunology Research Centre, McMaster University, Hamilton, ON, Canada.*
4. *Centre for Heart Lung Innovation, St. Paul's Hospital, Vancouver, BC, Canada.*
5. *Department of Medicine, McGill University, Montreal, QC, Canada.*
6. *Department of Medicine, University of Calgary, Calgary, AB, Canada.*
7. *Department of Medicine, University of Saskatchewan, Saskatoon, SK, Canada.*
8. *Department of Medicine, Université de Montréal, Montréal, QC, Canada.*
9. *Department of Medicine, University of Toronto, Toronto, ON, Canada.*
10. *Department of Medicine, University of British Columbia, Vancouver, BC, Canada.*
11. *Department of Internal Medicine, University of Manitoba, Winnipeg, MB, Canada.*
12. *Department of Medicine, Western University, London, ON, Canada.*

[#]**Corresponding author:** E-mail: hamblyn@mcmaster.ca

Running head: Impact of smoking on survival and lung function in fibrotic ILD.

Keywords: Fibrotic interstitial lung disease, smoking status, survival, pulmonary function outcome, hazard ratio, ILD-GAP.

Abbreviations:

Acute exacerbation - **AE**

Canadian registry for pulmonary fibrosis - **CARE-PF**

Composite physiologic index - **CPI**

Computed tomography - **CT**

Confidence interval - **CI**

Connective tissue diseases - **CTD**

Connective tissue disease-associated interstitial lung disease - **CTD-ILD**

Desquamative interstitial pneumonitis - **DIP**

Diffusing capacity for carbon monoxide - **DL_{CO}**

Forced expiratory volume (1 second) - **FEV_1**

Forced vital capacity - **FVC**

Hazard ratio - **HR**

Hypersensitivity pneumonitis - **HP**

Idiopathic pulmonary fibrosis - **IPF**

Interstitial lung disease - **ILD**

Interstitial lung disease-Gender-Age-Physiology - **ILD-GAP**

Odds ratio - **OR**

Pulmonary Langerhans cell histiocytosis - **PLCH**

Respiratory bronchiolitis ILD - **RB-ILD**

Smoking-related interstitial fibrosis - **SRIF**

Unclassifiable ILD - **U-ILD**

Usual interstitial pneumonia - **UIP**

ABSTRACT

Rationale. A direct causal link or strong association can be made with smoking and many interstitial lung diseases (ILDs). Current literature to date, however, demonstrates conflicting evidence regarding the impact of smoking status on long-term outcomes in the setting of ILD. We here describe the impact of smoking status on the survival and pulmonary function decline in patients enrolled in the Canadian Registry for Pulmonary Fibrosis (CARE-PF), a prospective observational cohort study.

Methods. Participants were studied from Nov 2015 to Nov 2020. Prospective data were collected, and patients were categorized according to fibrotic ILD diagnosis and smoking status. Survival was evaluated against smoking status, using time-to-event models. Time-to-event analysis was also used to assess whether smoking history impacted the rate of forced vital capacity (FVC) and diffusing capacity for carbon monoxide (DL_{CO}) decline. Of note, we examined time to 10% decline in percent predicted FVC and time to 15% decline in DL_{CO} in the initial 27 months following the first visit after the ILD diagnosis.

Main Results. The study group consisted of 3062 patients diagnosed with key CARE-PF diagnostic subgroups: Idiopathic pulmonary fibrosis (IPF), connective tissue disease-associated interstitial lung disease (CTD-ILD), hypersensitivity pneumonitis (HP), and unclassifiable ILD (U-ILD). IPF patients were more likely to have a smoking history compared to the other fibrotic ILDs ($P<0.0001$). Hazard ratio assessments demonstrated that CTD-ILD, HP, and U-ILD patients had lower mortality than IPF patients whether they belonged to the never smoker or smoker categories. Subgroup analysis showed that there

was a significant interaction between smoking and fibrotic ILD diagnosis, with respect to mortality, with smoking affecting the risk of death in CTD-ILD and U-ILD patients more than IPF and HP patients. We also found that in all subtypes of fibrotic ILD examined, time to 15% DL_{CO} decline was significantly shorter in smokers (HR: 1.21, 95% CI: 1.06-1.39), whereas no significant difference was seen in time to 10% FVC decline between smokers and never smokers (HR: 1.12, 95% CI: 0.98-1.28).

Conclusion. IPF patients were more likely to have a smoking history and were found to have higher mortality compared to the other fibrotic ILD patients. However, the high mortality rate detected in IPF patients might not necessary be mediated by smoking. Notably, among fibrotic ILD patients, smoking affected DL_{CO} decline, but not FVC decline. Research is warranted to offer insight into mechanisms by which continuous smoke and smoke cessation affect fibrotic ILD development, immunopathogenesis, and progression.

INTRODUCTION

Interstitial lung disease **(ILD)** is a group of lung diseases defined by the occurrence of cellular proliferation, cellular infiltration, and/or aberrant fibrogenesis of the lung parenchyma which are not caused by infection or neoplasia[90]. ILDs may result from a wide array of causes including; environmental, occupational, medication-related exposures, or from one of the several systemic autoimmune or connective tissue diseases **(CTDs)**[91]. If no etiology is identified, patients with interstitial fibrosis receive a classification of idiopathic interstitial pneumonia[7]. The most common idiopathic interstitial pneumonia is idiopathic pulmonary fibrosis **(IPF)**, a chronic, progressive, fibrotic ILD[7]. Smoke exposure has been reported to be associated with the development of various subtypes of ILD, such as respiratory bronchiolitis ILD **(RB-ILD)**, desquamative interstitial pneumonitis **(DIP)**, pulmonary Langerhans cell histiocytosis **(PLCH)**, smoking-related interstitial fibrosis **(SRIF)**, and idiopathic pulmonary fibrosis[18,28,91,92].

Principally, in a multicenter case-control study, a history of smoking was associated with an increased risk of developing IPF, with an odds ratio **(OR)** for ever-smokers (current and ex-smokers) of 1.6 (95% Confidence Interval **(CI)**: 1.1 to 2.4)[19,20]. In a meta-analysis of observational studies, cigarette smoking and other environmental and occupational exposures were significantly associated with IPF development. In these studies, the overall OR for ever-smoking as IPF risk factor was 1.58 (95% CI: 1.27–1.97)[21]. Paradoxically, reports suggest that concurrent smoking status with IPF is positively associated with improved prognosis and survival compared to never or ex-smokers[22,23]. Nonetheless, this

phenomenon is not fully conserved across all cohorts. Following age and disease status adjustment, multiple cohorts observed no significant survival benefit with current smoking status[24,25].

To shed light on these clinical controversies, our study aims to further investigate the impact of smoking status on the survival and pulmonary function decline in fibrotic ILD patients by examining the Canadian Registry for Pulmonary Fibrosis **(CARE-PF)**, a national, mutli-centre, and prospective registry.

METHODS

Study population

Patients enrolled in the CARE-PF were studied from Nov 2015 to Nov 2020. As previously described, CARE-PF is the first prospective multi-centre registry for fibrotic ILD patients in Canada[5,93]. Consenting patients with incident or prevalent fibrotic ILD who met eligibility criteria, were recruited from specialized Canadian ILD clinics at Vancouver, Calgary, Hamilton, Toronto, Montreal, and Saskatoon as previously described[5,93]. Diagnostic criteria for fibrotic ILDs, baseline clinical data (demographics, smoking history, comorbidities,…), patient-reported outcomes (dyspnea,…), and quality of life were recorded prospectively and pulmonary function tests were measured as previously described[5]. Measurements of pulmonary symptoms and quality of life were conducted at baseline and at approximately six monthly intervals, or more frequently during periods of rapidly changing health status[5]. The impact of smoking status on survival and pulmonary function decline was examined in the complete population and amongst key CARE-PF diagnostic subgroups: idiopathic pulmonary fibrosis, connective tissue disease-associated interstitial lung disease **(CTD-ILD)**, hypersensitivity pneumonitis **(HP)**, and unclassifiable ILD **(U-ILD)**.

Outcome assessment

Survival

Assessing the impact of smoking status on survival was our primary outcome. Survival was evaluated against smoking status, using time-to-event curves analyzed by Cox proportional

hazards regression. Data were depicted with Kaplan-Meier survival curves. Unadjusted hazard ratio **(HR)** was reported along with HR adjusted for the interstitial lung disease-Gender-Age-Physiology **(ILD-GAP)** score which incorporates known prognostic risk factors for ILD: age, sex, lung function, and ILD diagnosis. Survival time was reported as the number of years from the patient's initial visit until death or lung transplant.

Pulmonary function decline

Time-to-event analysis was used to assess whether smoking history impacted the rate of forced vital capacity **(FVC)** and diffusing capacity for carbon monoxide **(DL_{CO})** decline. A relative 10% decline in percent predicted FVC and 15% decline in DL_{CO} in the initial 27 months following the first visit after the ILD diagnosis was used to denote physiologic progression.

Statistical analysis

Statistical analyses were performed using STATA version 15 (Stata Corporation, College Station, TX, USA). A chi-squared test was performed using GraphPad Prism 9.1 (GraphPad Software, Inc) and was used to compare the frequency of smoking history between all the fibrotic ILD diagnosis. A P value less than 0.05 was considered statistically significant.

RESULTS

Fibrotic ILD patient demographic characteristics, clinical data, and smoking history

The study group consisted of 3062 patients with fibrotic ILD prospectively enrolled into the Canadian Registry for Pulmonary Fibrosis. Fibrotic ILD patients' demographic and clinical characteristics are shown in **Table 1.** Out of 3062 patients with fibrotic ILD, 961 (31%) were diagnosed with IPF *(never smokers, n=230; smokers, n=731 (76%))*, 1175 (38%) with CTD-ILD *(never smokers, n=594; smokers, n=581 (49%))*, 264 (9%) with HP *(never smokers, n=115; smokers, n=149 (56%))*, and 662 (22%) patients with U-ILD *(never smokers, n=228; smokers, n=434 (66%))* **(Table 1 and Figure 1)**. Throughout the whole study, current smokers and ex-smokers have been combined into one category (smokers) given the low number of patients categorized as current smokers **(Table 1)**. Chi-squared test demonstrated that IPF patients were more likely to have a smoking history compared to the other fibrotic ILDs ($P<0.0001$). Notably, within IPF and CTD-ILD patients, never smokers had significantly lower FVC and significantly higher DL_{CO} in the first visit compared to current or former smokers **(Table 1)**. Within HP patients, no differences were detected in initial FVC or DL_{CO} measures between never, ex-, and current smokers **(Table 1)**. Within U-ILD patients, never smokers had significantly lower initial FVC measure compared with current and former smokers, whereas smoking status did not affect DL_{CO} measure **(Table 1)**. Furthermore, CTD-ILD patients who were current smokers were significantly younger compared to never and former smokers. However, there was no

significant age difference between current, former, and never smokers in the other fibrotic ILD patients **(Table 1)**.

Impact of smoking status on survival in fibrotic ILD

Time-to-event analysis was used to assess the relationship between smokers and never smokers adjusted for the ILD-GAP score which incorporates known prognostic risk factors for ILD: age, sex, lung function, and ILD diagnosis. Within all subtypes of fibrotic ILD examined, smokers had a significantly higher mortality compared to non-smokers, after adjusting for age, sex, and lung function (HR: 1.36, 95% CI: 1.16-1.61). These relationships were evaluated by an unadjusted Kaplan-Meier survival curve which showed better survival in never smokers compared with ever-smokers (current and ex-smokers) among fibrotic ILD patients **(Figure 2)**. Furthermore, data from an unadjusted Kaplan-Meier survival curve provided evidence that IPF patients had a higher mortality compared to the other fibrotic ILD patients **(Figure 3)**. Subsequently, the mortality of CTD-ILD, HP, and U-ILD patients was compared to IPF patients by assessing unadjusted hazard ratio (stratified by subgroup (smokers vs non-smokers)). HR values shown in **Table 2** provided evidence that mortality was significantly higher in IPF patients who were smokers compared to each of the other fibrotic ILD subtypes who belonged to the smoker group. Similarly, mortality was significantly higher in never smoker IPF patients compared to each of the other never smoker fibrotic ILD subtypes **(Table 2)**. Lastly, we determined whether smoking was an effect modifier in the relationship between ILD diagnosis and mortality by conducting a subgroup analysis of mortality in smokers compared to non-smokers,

stratified by ILD diagnosis. Findings from subgroup analysis of smokers versus never smokers by diagnosis demonstrated that overall, there was a significant interaction between smoking and fibrotic ILD diagnosis (p-value for interaction is 0.039), with respect to mortality **(Figure 4)**. Specifically, the subgroup analysis has shown that smoking was an effect modifier and significantly increased mortality in CTD-ILD and U-ILD patients but did not have a significant effect on mortality in IPF and HP patients **(Figure 4)**.

Impact of smoking status on pulmonary function decline in fibrotic ILD

Further, time-to-event analysis was used to assess whether smoking history impacted the rate of FVC and DL_{CO} decline. A relative 10% decline in percent predicted FVC and 15% decline in DL_{CO} in the initial 27 months following the first visit after the ILD diagnosis was used to denote physiologic progression. We found that within all fibrotic ILD patients, time to DL_{CO} decline was significantly shorter in smokers (HR: 1.21, 95% CI: 1.06-1.39), whereas no significant difference was seen in time to FVC decline between smokers and never smokers (HR: 1.12, 95% CI: 0.98-1.28) **(Figure 5)**.

DISCUSSION

Our findings have shown that IPF patients were more likely to have a smoking history compared to the other fibrotic ILD patients. Additionally, we demonstrated that IPF patients had higher mortality compared to CTD-ILD, HP, and U-ILD patients whether they belonged to the never smoker or smoker categories. Subgroup analysis showed that there was a significant interaction between smoking and ILD diagnosis, with respect to mortality, with smoking affecting the risk of death in CTD-ILD and U-ILD patients more than IPF and HP patients. We also found that in all subtypes of fibrotic ILD examined, time to 15% DL_{CO} decline was significantly shorter in smokers, whereas no difference was seen in time to 10% FVC decline. Overall, our data suggest that smoking has a significant negative impact on the survival of fibrotic ILD patients, but this negative effect is stronger in CTD-ILD and U-ILD patients compared to IPF and HP patients whose mortality does not seem to be significantly associated with the smoking status. DL_{CO} decline associated with smoking might be caused by the smoke-related emphysema.

Findings described in the present clinical report validate observations from previous studies which investigated the impact of smoking status on survival and outcomes in IPF patients. In particular, Antoniou *et al.* (2008) have previously examined 249 patients with IPF (current smokers, n=20; former smokers, n=166; never smokers, n=63) and they have reported that within IPF patients, current smokers had higher survival than former smokers, but this difference was eliminated when adjusted for disease severity, using the composite physiologic index **(CPI)**[24]. Moreover, within IPF patients, never smokers had better

survival than former smokers and this difference was enhanced when adjusted for baseline disease severity, using the CPI[24]. Within IPF patients, current smokers were found to have higher mortality than never smokers, however, current smokers were shown to have better pulmonary function outcomes at presentation[23,24]. Interestingly, Antoniou *et al.* (2008) demonstrated that FVC and D_{LCO} levels were lower, and computed tomography **(CT)** disease extent and CPI scores were greater in IPF patients who were ex-smokers than in current smokers. Similarly, FVC and D_{LCO} levels were lower, and CT disease extent and CPI scores were higher in never smokers than in current smokers[24]. This suggests that while current smoking status is associated with higher mortality, current smoking is surprisingly associated with improved lung function. In line with these findings, King *et al.* (2001) have studied 238 IPF patients (current smokers, n=33; former smokers, n=121; and never smokers, n=84) and shown that honeycombing pattern was significantly higher in IPF patients who were former smokers than in the current and never smokers[23]. In addition, within IPF patients, FVC and forced expiratory volume (1 second) **(FEV_1)** were significantly lower and the FEV_1/FVC ratio was significantly higher in never smokers than in former smokers[23]. Lastly, among IPF patients, FVC and FEV_1 were significantly greater and FEV_1/FVC ratio was significantly lower in current smokers compared with never and former smokers[23]. One of the limitations in Antoniou *et al.* (2008) and King *et al.* (2001) studies is that the number of former smokers is greater than the number of current smokers. This makes the current smoker group under-powered. To prevent the under-powering effect of the current smoker group, our present study combined the current and former smokers who were diagnosed with fibrotic ILDs into one category. Furthermore, the less severe

pulmonary function indices detected in IPF patients who were current smokers compared to former smokers might be caused by the *"healthy smoker effect"* which states that patients with more critical disease symptoms are more likely to cease smoking for recognized health reasons[24]. Hence, current smoking might be considered as a marker of less severe disease, correlated with better outcome and survival[24].

Moreover, Kärkkäinen *et al.* (2017) assessed 45 non-smokers, 66 ex-smokers, and 17 current smokers diagnosed with IPF and found that current smokers were significantly younger at baseline (58.1 ± 8.74 years) compared to non-smokers (71.4 ± 8.74, $p< 0.001$) and ex-smokers (72.5 ±7.95, $p <0.001$)[25]. This study highlighted the impact of smoking status on the course of disease in IPF since current smokers were diagnosed with the disease at a younger age in comparison to non-smokers and ex-smokers[25]. In Kärkkäinen *et al.* (2017) study, ex-smokers had significantly higher mortality compared with non-smokers and current smokers among IPF patients[25]. However, following age and severity adjustment, smoking was not associated with survival[25]. These findings are in line with the data presented here which further suggest that there is no significant interaction between IPF diagnosis and smoking status with respect to mortality.

In contrast, using a cohort of IPF patients who were never smokers (n=32) or smokers (n=66), Kishaba *et al.* (2016) have found that 50% and 18% of the never smoker and smoker patients, respectively, experienced acute exacerbation **(AE)** and that after adjusting for CPI and prednisolone use, never smoker IPF patients showed tendency to develop AE more frequently and late than that of IPF patients who were smokers[22]. In

addition, the median survival of never smoker and smoker IPF patients was 18.5 and 26.3 months, respectively. Surprisingly, after the adjustment of baseline CPI, never smoker IPF patients showed worse prognosis than that of IPF patients who were smokers[22]. Lastly, a study conducted by Song *et al.* (2011) revealed that never smoking status and reduced FVC were significant risk factors for AE in IPF[27].

Although multiple studies have examined the impact of smoking status on IPF patients' survival and lung function, the effect of smoking on the survival and outcome of patients diagnosed with other fibrotic ILDs remains to be investigated. However, cigarette smoking has been suggested to protect from developing HP[28]. It has been proposed that the protective effect of smoking in this disease is caused by the suppression of T helper 1 cell immunity by cigarette smoking, but this functional impairment of the immune system may potentially result in alternative lung diseases[18].

Taken together, our data support previous thoughts that smoking status might not be significantly associated with survival and lung function outcomes in IPF patients. The present study also provides novel findings on the strong association between smoking status and the mortality of CTD-ILD and U-ILD patients. The current conflicting research findings regarding the effect of smoking status on IPF patients' survival and outcomes might be partially due to the fact that indices utilized to measure IPF severity such as D_{LCO} and FVC are affected by the coexistence of smoking-related damage[24]. Therefore, further investigation is required to identify the most accurate index to be utilized to account for major confounding factors and disease severity. Additionally, further analysis is required

to describe the impact of smoking status on incidence of acute exacerbation, dyspnea, health outcome and quality of life, usual interstitial pneumonia **(UIP)** pattern (definite UIP, UIP, or not UIP), and requirement for lung transplantation among CARE-PF patients. Studies that aim to investigate comorbidities, such as pulmonary hypertension, cardiovascular disease, chronic obstructive pulmonary disease, uroepithelial tumors, congestive heart failure, and lung cancer in relation to smoking status within fibrotic ILD patients enrolled in CARE-PF are required.

TABLES

Table 1. Demographic characteristics of fibrotic ILD patients, clinical data, and selected pulmonary indices obtained in the first visit after the fibrotic ILD diagnosis.

	Never smokers	Ex-smokers	Current smokers	# p-value
IPF (n=961)	**n=230**	**n=680**	**n=51**	
Sex (% males)	67.83	75.11	66.67	N/A
Age (years)	69.81 (9.49)	69.35 (7.89)	64.68 (9.56)	0.1296
Pack years	N/A	27.88 (21.83)	38.11 (22.40)	N/A
Smoking cessation (years)	N/A	25.87 (15.50)	N/A	N/A
Duration of smoking (years)	N/A	28.71 (14.23)	48.53 (12.69)	N/A
Initial FVC	73.26 (19.10)	77.66 (18.69)	79.20 (17.81)	0.001553
Initial DL_{CO}	57.85 (18.61)	52.96 (17.93)	51.24 (16.65)	0.002054
CTD-ILD (n=1175)	**n=594**	**n=522**	**n=59**	
Sex (% males)	22.39	34.87	33.9	N/A
Age (years)	55.10 (13.83)	59.80 (11.10)	50.63 (13.10)	4.81E-07
Pack years	N/A	19.48 (20.43)	24.73 (18.42)	N/A
Smoking cessation (years)	N/A	24.42 (14.80)	N/A	N/A
Duration of smoking (years)	N/A	22.18 (13.83)	37.85 (13.20)	N/A
Initial FVC	73.47 (19.74)	77.71 (19.23)	79.38 (21.56)	0.0003579
Initial DL_{CO}	60.25 (19.65)	57.91 (19.38)	57.54 (19.20)	0.0373
HP (n=264)	**n=115**	**n=138**	**n=11**	
Sex (% males)	40	46.38	45.45	N/A
Age (years)	62.01 (12.97)	63.50 (10.34)	56.13 (4.44)	0.758
Pack years	N/A	23.65 (23.01)	23.36 (16.39)	N/A
Smoking cessation (years)	N/A	26.99 (14.50)	N/A	N/A
Duration of smoking (years)	N/A	22.81 (14.36)	39.91 (12.51)	N/A
Initial FVC	70.64 (19.67)	74.06 (17.73)	78.88 (13.99)	0.1486
Initial DL_{CO}	56.17 (18.92)	57.24 (16.48)	60.13 (15.19)	0.6268
U-ILD (n=662)	**n=228**	**n=393**	**n=41**	
Sex (% males)	38.6	60.97	63.41	N/A
Age (years)	65.93 (12.59)	68.15 (10.29)	62.19 (8.35)	0.4637
Pack years	N/A	26.06 (22.82)	40.92 (31.05)	N/A
Smoking cessation (years)	N/A	26.82 (16.25)	N/A	N/A
Duration of smoking (years)	N/A	26.50 (14.20)	47.98 (12.44)	N/A
Initial FVC	72.97 (23.20)	79.52 (19.93)	86.19 (19.86)	0.0001244
Initial DL_{CO}	62.22 (20.96)	59.43 (19.67)	60.73 (18.06)	0.1329

Notes: All calculations were conducted on available data (not all variables were available in the registry for all patients). For age, pack years, smoking cessation, duration of smoking, initial FVC, and initial DL_{CO}: mean (SD). # For age, initial FVC, and initial DL_{CO}: mean (SD) - Mann Whitney Test.

Table 2. Hazard ratio of mortality by diagnosis for never smokers and smokers.

Fibrotic ILD diagnosis	HR for mortality in never smokers (95% CI)	HR for mortality in smokers (95% CI)
IPF	Reference	Reference
CTD-ILD	0.30 (0.21-0.42)	0.44 (0.35-0.56)
HP	0.39 (0.22-0.70)	0.56 (0.38-0.83)
U-ILD	0.49 (0.33-0.72)	0.78 (0.62-0.98)

FIGURES

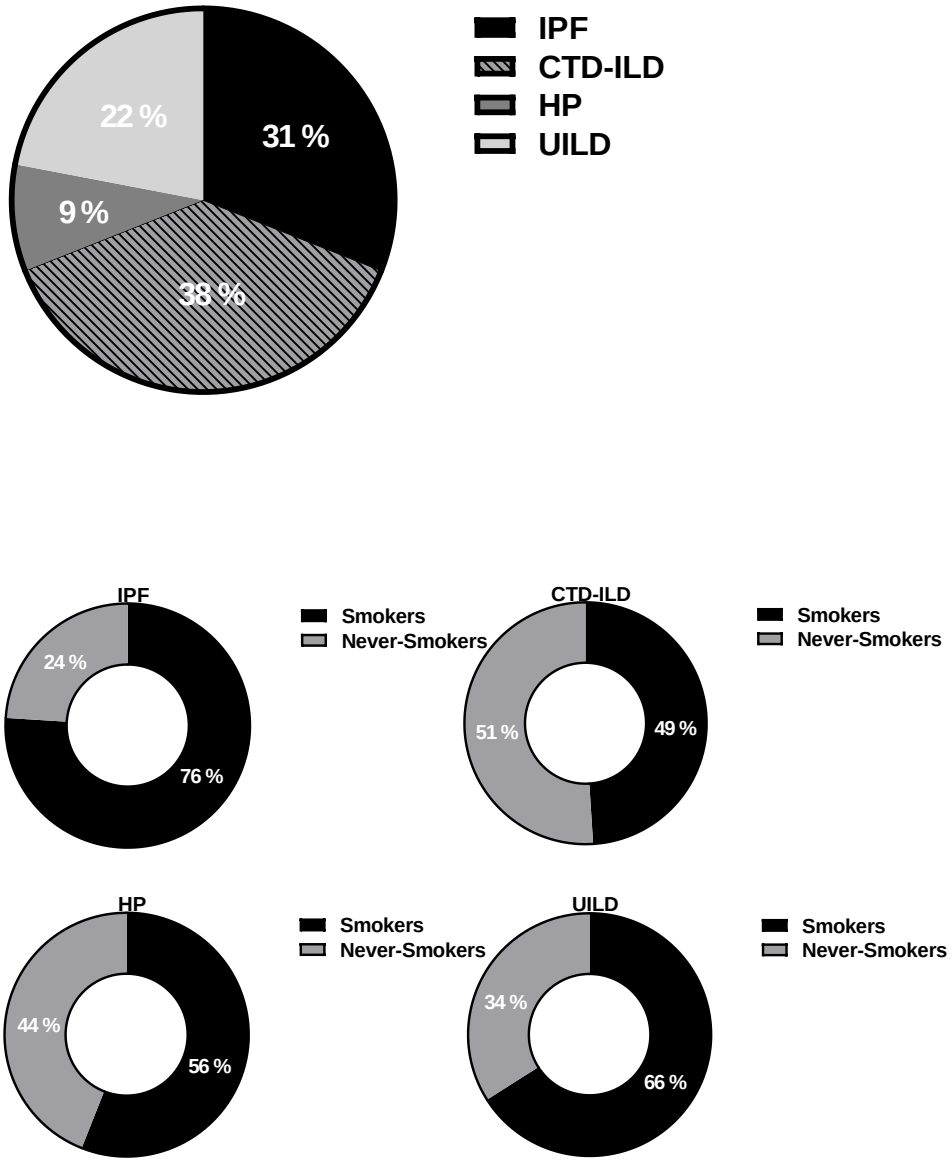

Figure 1. Fibrotic ILD smoking history.

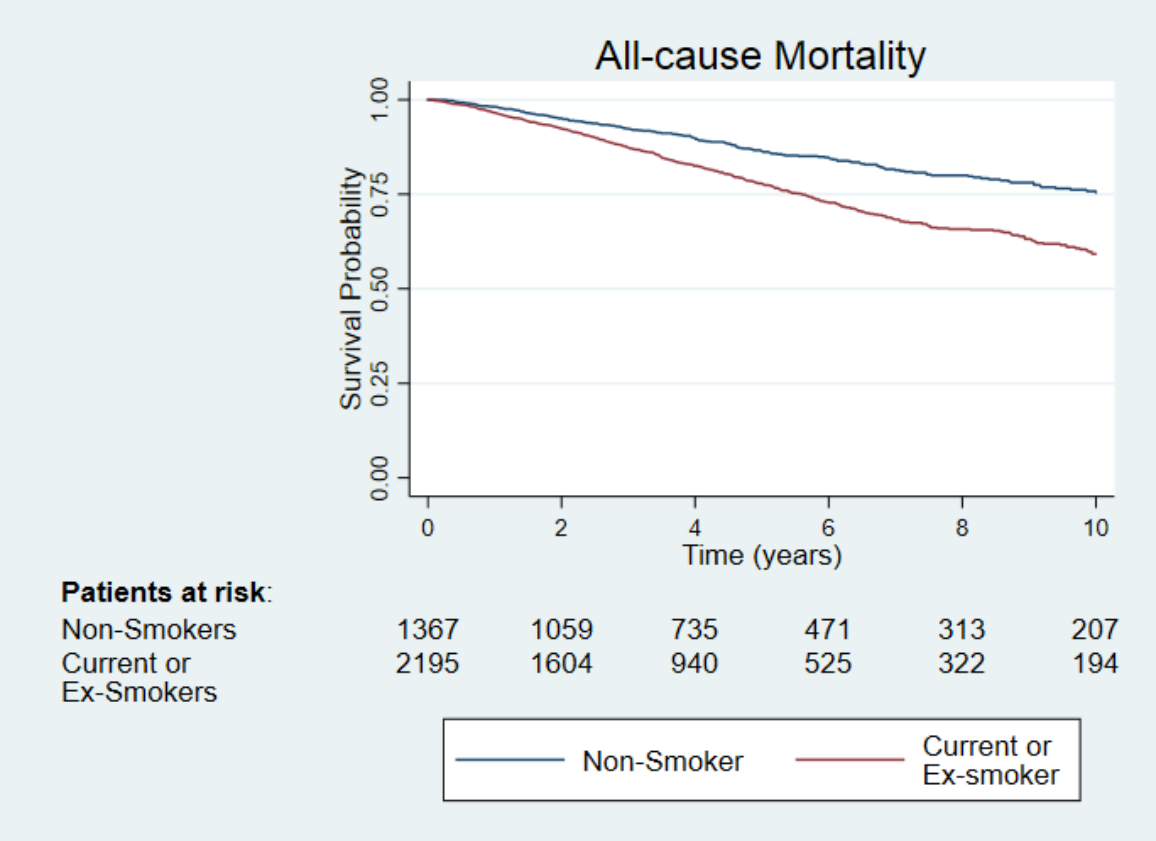

Figure 2. Unadjusted Kaplan-Meier plot of survival probability stratified by smoking status among all the diagnosis subgroups.

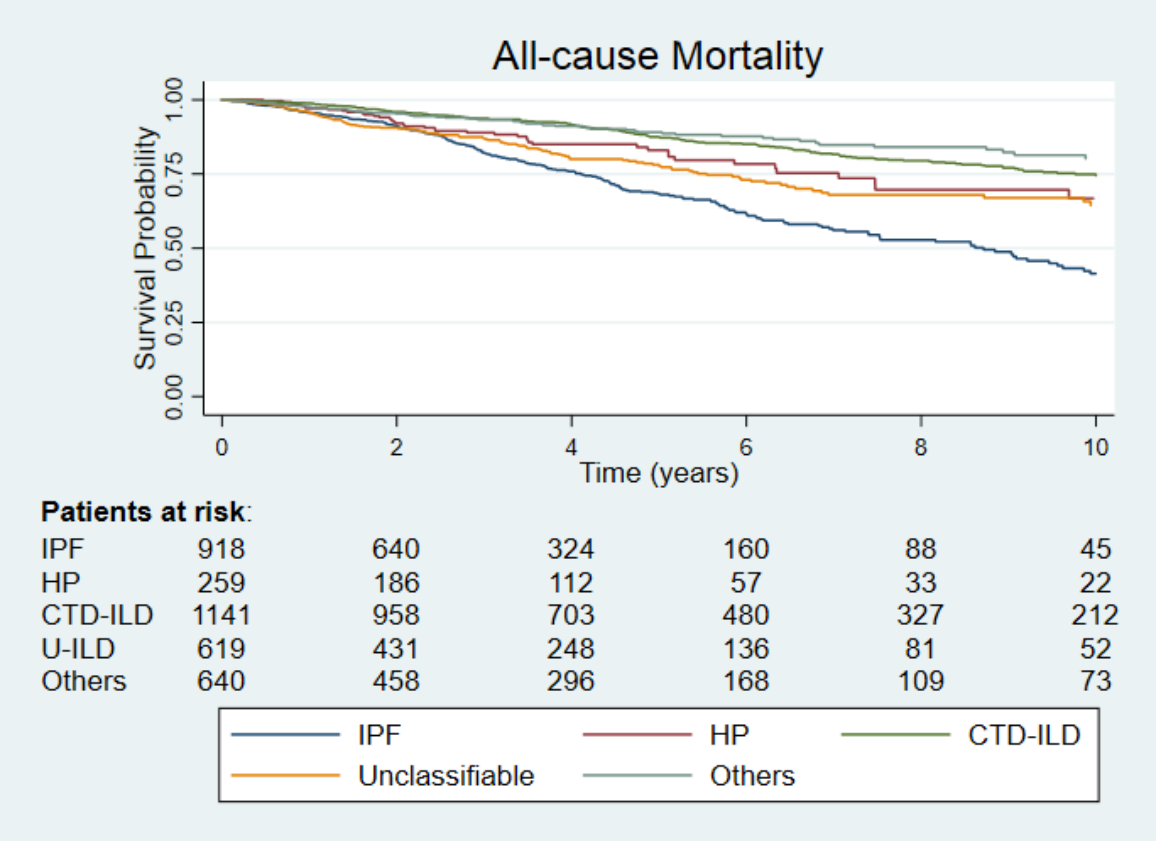

Figure 3. Unadjusted Kaplan-Meier plot of survival probability stratified by fibrotic ILD diagnosis.

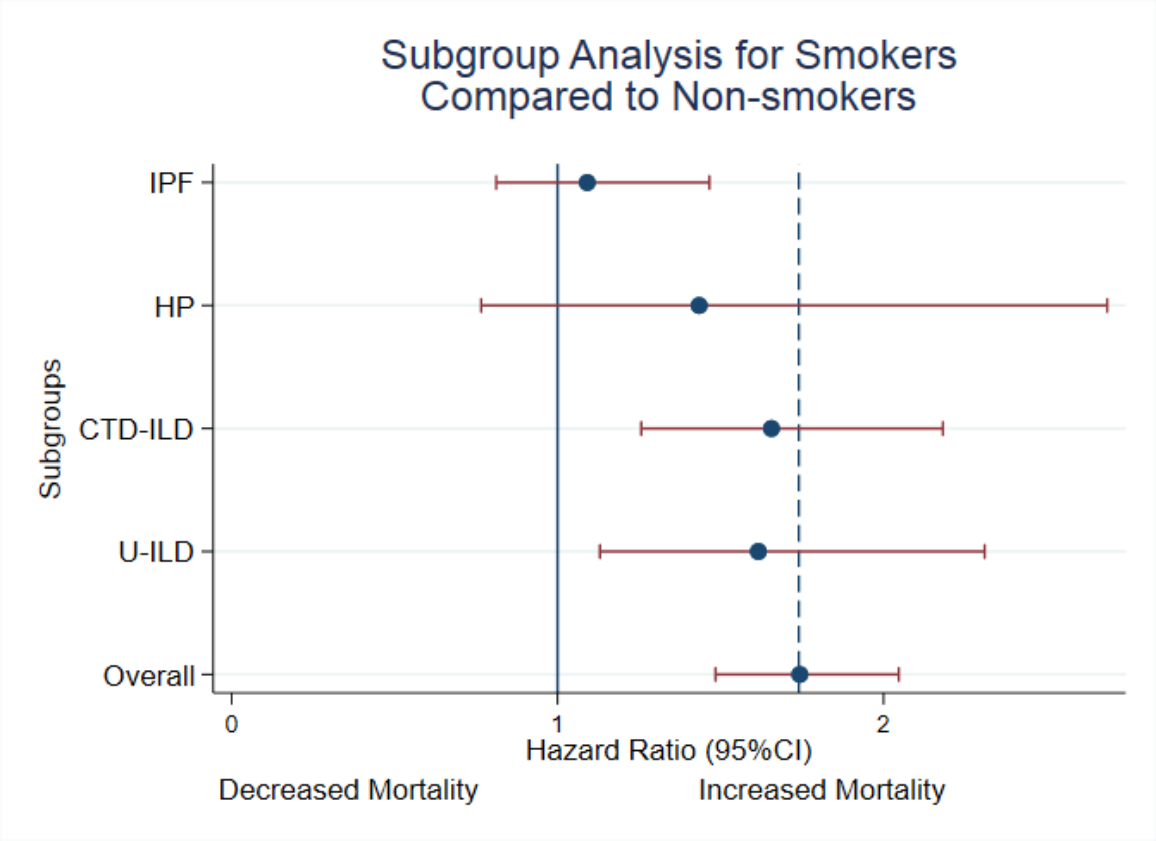

Figure 4. Subgroup analysis of smokers compared to never smokers stratified by fibrotic ILD diagnosis.

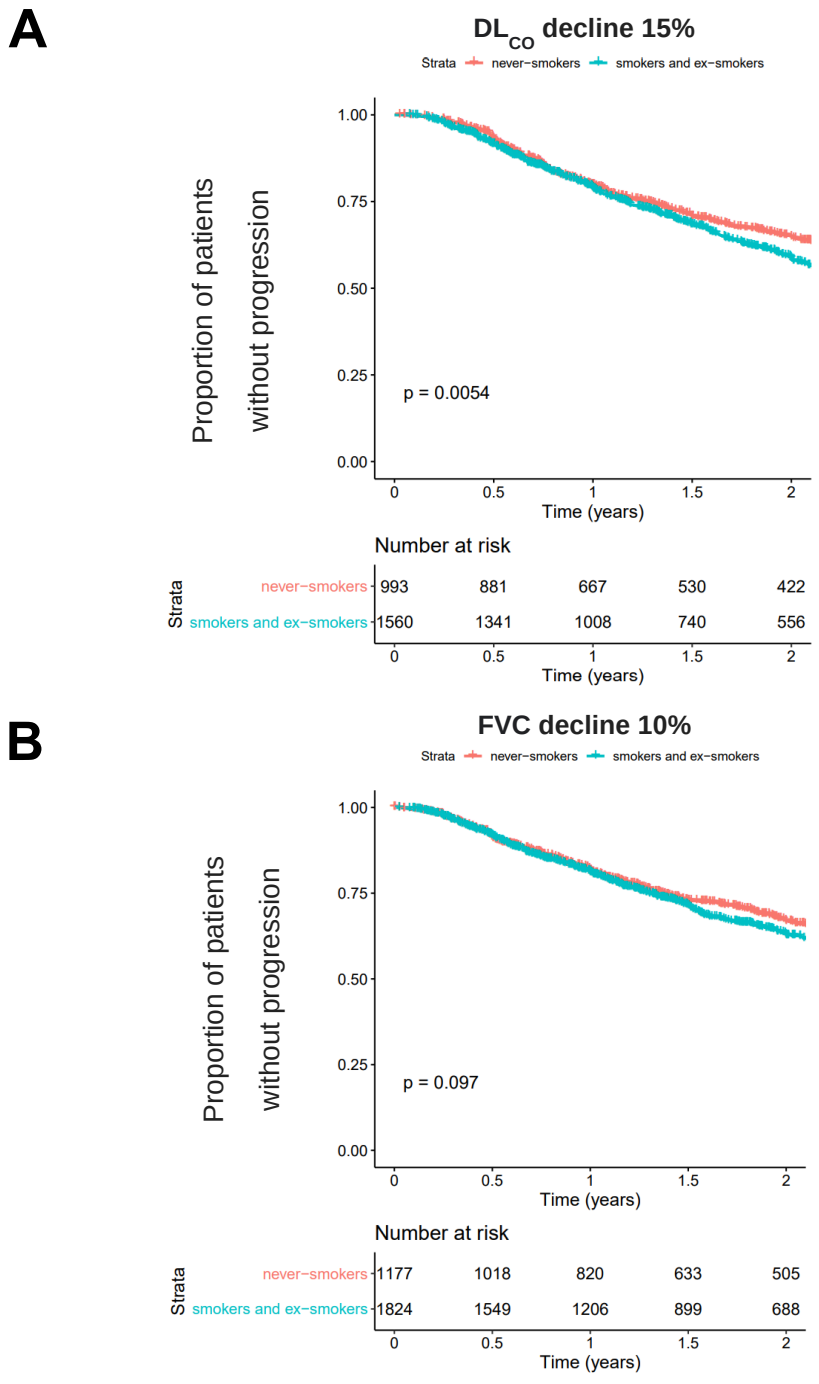

Figure 5. Analysis of (A) DL_{CO} and (B) FVC decline in the initial 27 months following the first visit after the fibrotic ILD diagnosis stratified by smoking status.

Chapter 3

Increased monocyte-derived CD11b^{+} macrophage subpopulations following cigarette smoke exposure are associated with impaired bleomycin-induced tissue remodelling

Steven P. Cass[1†], Olivia Mekhael[1†], Danya Thayaparan[1], Joshua JC. McGrath[1], Spencer D. Revill[1,2], Matthew F. Fantauzzi[1], Peiyao Wang[3], Amir Reihani[2], Aaron I. Hayat[1], Christopher S. Stevenson[4], Anna Dvorkin-Gheva[5], Fernando M. Botelho[5], Martin R. Stämpfli[†2,5], and Kjetil Ask[†*2,5]

[1]Medical Sciences Graduate Program, McMaster University, Hamilton, ON, Canada, [2]Department of Medicine, Firestone Institute for Respiratory Health, McMaster University and The Research Institute of St. Joe's Hamilton, Hamilton, ON, Canada, [3]Department Biochemistry and Biomedical Sciences, McMaster University, Hamilton, ON, Canada, [4]Janssen Disease Interception Accelerator, Janssen Pharmaceutical Companies of Johnson and Johnson, Raritan, NJ, USA, [5]Department of Medicine, McMaster Immunology Research Centre, McMaster University, Hamilton, ON, Canada.

Submitted to Journal:
Manuscript is in review in Frontiers in Immunology

Specialty Section:
Inflammation

Article type:
Original Research Article

Received on:
12 Jul 2021

Increased monocyte-derived CD11b^{+} macrophage subpopulations following cigarette smoke exposure are associated with impaired bleomycin-induced tissue remodelling

Steven P. Cass[1†], Olivia Mekhael[1†], Danya Thayaparan[1], Joshua JC. McGrath[1], Spencer D. Revill[1,2], Matthew F. Fantauzzi[1], Peiyao Wang[3], Amir Reihani[2], Aaron I. Hayat[1], Christopher S. Stevenson[4], Anna Dvorkin-Gheva[5], Fernando M. Botelho[5], Martin R. Stämpfli[†2,5], and Kjetil Ask[†*2,5]

1. *Medical Sciences Graduate Program, McMaster University, Hamilton, ON, Canada.*
2. *Department of Medicine, Firestone Institute for Respiratory Health, McMaster University and The Research Institute of St. Joe's Hamilton, Hamilton, ON, Canada.*
3. *Department Biochemistry and Biomedical Sciences, McMaster University, Hamilton, ON, Canada.*
4. *Janssen Disease Interception Accelerator, Janssen Pharmaceutical Companies of Johnson and Johnson, Raritan, NJ, USA.*
5. *Department of Medicine, McMaster Immunology Research Centre, McMaster University, Hamilton, ON, Canada.*

[†]**Authors contributed equally to this work and share first authorship.**

[†]**Authors contributed equally to this work and share senior authorship.**

[#]**Corresponding author:** Dr. Kjetil Ask, Department of Medicine, McMaster University and The Research Institute of St. Joe's Hamilton, Firestone Institute for Respiratory Health, Luke Wing, Rm L314-5, 50 Charlton Ave East, Hamilton, Ontario, Canada L8N 4A6, Ph. (905) 522 1155 ext. 33683; Fax (905) 521 6183; E-mail: askkj@mcmaster.ca .

Running head: Cigarette smoke-exposed macrophage composition in tissue remodelling

Key words: Macrophage, cigarette smoke, immunopathology, tissue remodelling, fibrogenesis.

Abbreviations:

alpha-Smooth muscle actin - **α-SMA**

Alveolar macrophage - **AM**

Bromodeoxyuridine - **BrdU**

Chronic obstructive pulmonary disease - **COPD**

Common monocyte progenitor - **cMoP**

Cigarette smoke - **CS**

Cigarette smoke extract - **CSE**

Embryonic day – **E**

Hematoxylin & eosin - **H&E**

Immunohistochemistry - **IHC**

Interstitial macrophage - **IM**

Lactose dehydrogenase - **LDH**

Lineage negative $Sca1^{+}c\text{-}Kit^{+}$ - **LSK**

Matrix metallopeptidase 9 - **MMP9**

Monocyte-derived alveolar macrophages - **Mo-AM**

Monocyte-macrophage dendritic cell progenitor - **MDP**

Phosphate-buffered saline - **PBS**

Principal component analysis - **PCA**

Resident alveolar macrophage - **Res-AM**

Room air - **RA**

Tissue microarray - **TMA**

Transforming growth factor beta 1 - **TGF-β1**

CONTRIBUTIONS TO THE FIELD

Emerging evidence demonstrates a role for specific macrophage subpopulations in the pathogenesis of respiratory disease. To date, the impact of cigarette smoke on the composition and function of pulmonary macrophage subpopulations is not fully understood. In this study, we explore the composition, origin and function of macrophage subpopulations in a mouse model of whole-body smoke exposure. Cigarette smoke-induced the expansion of all $CD11b^+$ subpopulations including monocyte-derived alveolar macrophages as well as interstitial macrophages 1, -2 and -3. The expansion of monocyte-derived alveolar macrophages and interstitial macrophages 3 was IL-1α dependent and associated with transient changes to monocytes. Moreover, cigarette smoke impaired matrix metallopeptidase-9 release from all macrophage subpopulations and inhibited exacerbated monocyte-derived alveolar macrophage expansion following lung injury impairing fibrogenesis. This study characterises the impact of cigarette smoke on pulmonary macrophage subpopulations and offers insight into impaired tissue repair responses which may lead to respiratory disease in cigarette smokers.

ABSTRACT

Rationale. The accumulation of macrophages in the airways and the pulmonary interstitium is a hallmark of cigarette smoke-associated inflammation. Notably, pulmonary macrophages are not a homogenous population but consist of several subpopulations. To date, the manner in which cigarette smoke exposure affects the relative composition and functional capacity of macrophage subpopulations has not been elucidated.

Methods. Using a whole-body cigarette smoke exposure system, we investigated the impact of cigarette smoke on macrophage subpopulations in C57BL/6 mice using flow cytometry-based approaches. Moreover, we used bromodeoxyuridine labelling plus *Il1a*$^{-/-}$ and *Il1r1*$^{-/-}$ mice to assess the relative contribution of local proliferation and monocyte recruitment to macrophage accumulation. To assess the functional consequences of altered macrophage subpopulations, we used a model of concurrent bleomycin-induced lung injury and cigarette smoke exposure to examine tissue remodelling processes.

Main Results. Cigarette smoke exposure altered the composition of pulmonary macrophages increasing CD11b^{+} subpopulations including monocyte-derived alveolar macrophages (Mo-AM) as well as interstitial macrophages (IM)1, -2 and -3. The increase in CD11b^{+} subpopulations was observed at multiple cigarette smoke exposure timepoints. Bromodeoxyuridine labelling and studies in *Il1a*$^{-/-}$ mice demonstrated that increased Mo-AM and IM3 turnover in the lungs of cigarette smoke-exposed mice was IL-1α dependent. Compositional changes in macrophage subpopulations were associated with impaired induction of fibrogenesis including decreased α-smooth muscle actin positive cells

following intratracheal bleomycin treatment. Mechanistically, *in vivo* and *ex vivo* assays demonstrated predominant macrophage M1 polarisation and reduced matrix metallopeptidase 9 activity in cigarette smoke-exposed mice.

Conclusion. Cigarette smoke exposure modified the composition of pulmonary macrophage by expanding $CD11b^{+}$ subpopulations. These compositional changes were associated with attenuated fibrogenesis, as well as predominant M1 polarisation and decreased fibrotic activity. Overall, these data suggest that cigarette smoke exposure altered the composition of pulmonary macrophage subpopulations contributing to impaired tissue remodelling.

INTRODUCTION

A strong association has been shown between cigarette smoking and respiratory diseases such as, chronic obstructive pulmonary disease (**COPD**), lung cancer, and interstitial lung disease. Central to the pathogenesis of these cigarette smoke (**CS**)-associated respiratory diseases is the macrophage (1–3). Increased in the lungs following CS exposure (4,5), macrophages perform a vital role in CS-induced inflammation (6). Of note, pulmonary macrophages consist of several subpopulations with independent and diverse functional roles (7–11). The composition and functional consequences of CS exposure on pulmonary macrophage subpopulations is yet to be elucidated.

Pulmonary macrophages can be stratified into two broad populations, alveolar macrophages (**AM**) and interstitial macrophages (**IM**). In mice, the first developmental wave occurs in the yolk sac on embryonic day (**E**)10-12 producing primitive AM (12,13). The longevity of primitive AM is unclear; however, a second developmental wave arises from the foetal liver and enter the lungs by E12-16 (12,13). These pre-AM enter the lumen postnatally(12,13) and mature into long-lived tissue resident alveolar macrophages (**Res-AM**). These mature Res-AM are predominately self-maintained with limited contribution from circulating monocytes(14). A third AM subpopulation, monocyte-derived alveolar macrophages (**Mo-AM**), are recruited from the bone marrow after birth (14). Mo-AM share 99.9% of genes with Res-AM(15) but contribute to less than 5% of the alveolar population under homeostatic conditions(13). In addition to AM populations, IM are present and constitute approximately 20% of the pulmonary macrophage environment at steady state

(13,16). The majority of IM are produced postnatally in the bone marrow and populate the lung parenchyma throughout life (12,17). Notably, a proportion of IM are derived from the yolk sac and are self-maintained similar to Res-AM populations (11). IM are further divided into three subpopulations based on CD11c and MHCII expression (IM1 - $CD11c^{Neg}MHCII^{Neg}$, IM2 - $CD11c^{Neg}MHCII^{Hi}$, IM3 - $CD11c^{Hi}MHCII^{Hi}$) (17). In total five pulmonary macrophage populations, Res-AM, Mo-AM plus IM1, -2 and -3 are detectable by flow cytometry-based techniques in mice.

The developmental origin of macrophage subpopulations is associated with differing function. At steady state, the phagocytic capacity is greatest in AM populations, followed by IM1, IM2 and poorest in IM3 (17). In contrast, IM populations are enriched for inflammatory mediators and monocyte-related genes distinct from AM (17). These observations have been replicated in COPD, wherein IM were found to be more proinflammatory, but less phagocytic, than AM counterparts (7). Macrophages are key in tissue remodelling processes and interstitial CX_3CR1 mononuclear phagocytes, encompassing IM1, -2 and -3 populations (17), have been reported to promote CS-induced emphysema (18). Moreover, in pre-clinical pulmonary fibrosis models, aberrant tissue remodelling has been specifically associated with increased Mo-AM (9,10,19) and reduced IM1 (8). Given that macrophage subpopulations instigate inflammation that can lead to respiratory disease, further investigation of the impact of CS on individual macrophage subpopulations is warranted.

In this study, we investigated the impact of CS exposure on macrophage subpopulation composition and function. Using a whole-body CS exposure system, we assessed CS-induced alterations in macrophage populations, including $CD11b^+$ subpopulations Mo-AM, IM1, -2 and -3, in the lungs. Moreover, we evaluated the impact of concurrent bleomycin treatment and CS exposure to understand macrophage subpopulation polarisation and ability to facilitate tissue remodelling. These data explored the impact of CS exposure on macrophage subpopulation composition, origin and function to offer insight into CS-associated respiratory disease.

MATERIALS AND METHODS

Animals. 6- to 8-week-old female C57BL/6 mice were purchased from Charles River Laboratories (PQ, Canada). Female IL-1α-deficient (*Il1a*$^{-/-}$) mice were obtained from MiceCenter for Experimental Medicine and Systems Biology, University of Tokyo, Japan and bred in-house. Female IL-1R1-deficient (*Il1r1*$^{-/-}$) mice (C57BL/6 background) with respective wild-type controls were obtained from The Jackson Laboratories (Maine, USA). Mice were subjected to a 12-hour light–dark cycle and had ad libitum access to food and water and housed under specific pathogen-free conditions. All experiments were approved by the Animal Research Ethics Board at McMaster University (#19-08-23).

Experimental CS exposure model. Mice were exposed to twelve 3R4F reference cigarettes with filters removed (University of Kentucky, Lexington, USA) or room air (**RA**), twice daily for five days per week. Mice were exposed for up to 24-weeks using a whole-body CS exposure system SIU-48 (Promech Lab AB, Vintrie Sweden). Upon exposure completion, mice were euthanized by exsanguination and cardiac puncture.

Tissue processing for flow cytometric analysis. Single cell suspensions were produced as follows. Mouse right middle, inferior, and post-caval lobes were enzymatically digested (150U/mL collagenase type I) for 1-hour shaking at 37°C. Bronchoalveolar lavage (**BAL**) was collected following 2x 500µL phosphate-buffered saline (**PBS**) washes of the single left lung lobe and BAL samples were then spun at 300 g for 5-minutes to pellet cells. To assess bone marrow, a single femur was removed and cells were flushed out using 5mL RPMI. Digested lung, flushed bone marrow, and harvested spleens were all crushed

through 40µm mesh. Lung cells were treated with ACK lysis buffer (1mL, 1-minute) to lyse red blood cells. Approximately 80µL of blood was drawn using retro-orbital bleeding, lysed using 1x Red Blood Cell lysis buffer (#00-4333-57, eBioscience) and spun at 300 g for 5-minutes. All single cell suspensions were stained for flow cytometric analysis using antibodies shown in **Table S1**. Gating strategies are shown in **Figure S1A-D**. All samples were run on a BD LSRFortessa (BD Biosciences, ON, Canada).

Bromodeoxyuridine delivery. CS- or RA-exposed mice were intraperitoneally injected with bromodeoxyuridine (**BrdU**) for three consecutive days prior to sacrifice. 200µg on day -3 then subsequently 100µg on day -2 and -1 to assess macrophage turnover. BrdU incorporation into cells was assessed by flow cytometry.

Experimental pulmonary fibrosis model. Tissue remodelling was induced with a single intratracheal instillation of bleomycin (0.05U/mouse in a volume of 50µl sterile saline) by oropharyngeal administration. Control animals received 50µl vehicle alone. Weights of animals were monitored regularly, and tissue harvest was conducted 7 (inflammatory phase) or 21 (fibrotic phase) days following bleomycin intubation. Lung function assessments were conducted using a flexiVent® mechanical respirator according to manufacturer's protocol at day 21 (flexiVent®, SCIREQ, Montreal, PQ, Canada)(20).

Isolation and stimulation of lung CD45$^+$ adhered cells. CD45$^+$ cells from lung single-cell suspensions were positively selected using mouse CD45 microbeads and LS columns (#130-052-301 and #130-042-401, Miltenyi Biotech) and cultured on a flat 96-well plate for 90-minutes. Non-adherent cells were stringently washed with PBS before remaining

adherent cells were treated for 24-hours with recombinant murine transforming growth factor beta 1 (**TGF-β1**) (30ng/mL; BioLegend, USA), IL-4 (20ng/mL; PeproTech, Canada) and IL-6 (5ng/mL; PeproTech, Canada). Macrophage "M2" polarisation was assessed by arginase activity in cell lysates, as described previously(21). Matrix metallopeptidase 9 (**MMP9**; #DY6718 R&D Systems, ON, Canada) ELISA, and CyQUANT™ lactose dehydrogenase (**LDH**; #C20301 ThermoFisher Scientific, ON, Canada) cytotoxicity assay, and soluble collagen assessed using sircol assay (Sircol™ Soluble Collagen Assay #CLRS1000, Biocolor, UK) were performed on cell culture supernatant.

Tissue collection for protein and RNA multiplex analysis. Lung (right superior lobe) homogenate was processed using Bullet Blender 24 Gold (Next Advance, Troy NY USA) either in PBS or RLT lysis buffer (Qiagen, Valencia, CA, USA) for protein and RNA analysis respectively. Protein from lung homogenate supernatant was assessed using the Discovery Assay® Mouse Cytokine Array/Chemokine Array 31-Plex (MD31; Eve Technologies Corp, Calgary, AB, Canada). Total RNA from RLT lysed lung homogenate was extracted using the RNeasy mini kit (Qiagen, Valencia, CA, USA, #74104). Following RNA integrity and quantity quality control the nCounter Elements system (NanoString Technologies, Seattle, WA, USA) was employed to quantify the expression levels of 25 mouse genes (**Table S2**).

Lung processing for histopathology. Mouse single left lungs were inflated and fixed in 10% formalin for 24-hours prior to embedment in paraffin wax. A tissue microarray (**TMA**) was generated containing 5µm lung sections cut and stained on a Bond RX fully automated

research Stainer (Leica Biosystems)(21). Immunohistochemistry (**IHC**) staining on lung serial sections was performed for hematoxylin & eosin (**H&E**), α-smooth muscle actin (**α-SMA**), and Masson's trichrome blue **(MTri)**. IHC stained-microscope slides were digitalised using an Olympus VS120-L100-W slide scanner at a 20× magnification and quantified using HALO™ Image Analysis Software (Halo Plus 3.2, Indica Labs).

Statistical analysis. Results expressed as mean ± standard error of the mean. Graphs and statistical tests were performed using GraphPad Prism 9.1 (GraphPad Software, Inc) and R (www.r-project.org). For RNA analysis samples were preprocessed and normalised using nSolver 2.5 software (www.nanostring.com) using three housekeeping genes *Actb, Pgk1, and Ywhaz* plus negative and positive controls. 25 mouse genes (**Table S2**) were used to perform principal component analysis (**PCA**), hierarchical clustering and differential expression analysis in R. Two-way ANOVA followed by Tukey's multiple comparisons test was used to determine significance when two concurrent variables were compared. Unpaired t test with Welch's correction was used to assess significance between only two groups. A $p < 0.05$ was considered statistically significant.

RESULTS

CD11b$^+$ macrophage subpopulations increase in the lungs of CS-exposed mice. CS is known to cause the expansion of the total lung macrophages (4,5) but the impact on macrophage subpopulation diversity is not known. Using the nomenclature proposed by Gibbings *et al.*(17) (**Table 1**), we demonstrated an expansion of all CD11b$^+$ populations including Mo-AM and IM1, -2 and – 3 at all CS timepoints (**Figure 1A**). Res-AM were unchanged at 2 and 12 weeks of CS but decreased at 24-weeks. The alterations in macrophage subpopulation numbers were not driven by changes in total lung cellularity but represent changes to each subpopulation individually (**Figure S2A**). Independent of CS exposure length, each CD11b$^+$ macrophage subpopulation was increased in CS-exposed mice.

The size and location of macrophages has been associated with phagocytic and inflammatory differences (7). In this study, CD11b$^+$ populations, Mo-AM (16.0%), IM1 (8.2%), and IM3 (7.1%), decreased in size at 12 weeks of CS (**Figure S2B**), corresponding to clinical observations of expanded small macrophages in COPD lung sections(7). We further assessed the presence of macrophage subpopulations in the BAL as a measure of macrophage location within the airways. While Res-AM decreased, each CD11b$^+$ subpopulation, including all IM, were increased in the BAL of CS-exposed mice at 8 weeks of CS (**Figure 1B**). Clinically, airway macrophages are reported to be lipid-laden, and thus more granular (22). In our model, Res-AM became 197.9% and CD11b$^+$ subpopulations 121.5-150.1% more granular than respective RA populations in the BAL (**Figure S2C**).

Overall, we observed increased number of small, more granular, $CD11b^+$ macrophages subpopulations following CS exposure.

Increased $CD11b^+$ macrophage turnover in CS-exposed mice. To elucidate mechanisms contributing to increased $CD11b^+$ macrophage populations, we assessed immune mediators associated with macrophage recruitment and survival in the lung homogenate. At 12 weeks of CS exposure myeloid chemoattractants CCL2 and CCL3 increased, as well as IL-1α (**Figure 2A**). IL-1α has previously been associated with CS-mediated myeloid cell recruitment (6,23). Next, we measured immune mediators associated with monocyte differentiation and macrophage survival, M-CSF, GM-CSF and IL-6, all of which increased in the lung tissue of CS-exposed mice (**Figure 2B**). Immune mediators associated with macrophage recruitment and survival were increased in CS-exposed mice.

To understand pulmonary lung dynamics, we assessed macrophage subpopulation turnover using thymidine analogue BrdU. BrdU uptake can be used as a surrogate measure of cell turnover and the balance between local proliferation and cell recruitment. While the total Res-AM trended to decrease following CS exposure the percentage of Res-AM positive for BrdU increased (**Figure 2C**). Of note, the decreasing trend in total Res-AM was associated with increased cell death in CS-exposed mice as measured by flow cytometry Live/Dead positive staining (**Figure 2D**). Taken together, this suggests Res-AM proliferated in response to CS exposure to refill the environmental niche opened by increased Res-AM cell death. In contrast, $CD11b^+$ populations had proportionally equal or fewer percentage $BrdU^+$ cells, but increased total $BrdU^+$ cells, following CS exposure

(**Figure 2E-H**). The fixed percentage of BrdU positive cells indicated a stable rate of BrdU incorporation. Consequently, the increase in total $BrdU^+$ Mo-AM and IM3 likely reflected a predominant recruitment of cells to the lungs. Total lung cell numbers were equivalent in RA and CS mice suggesting that changes were reflective of compositional shifts within the lung. Overall, CS was associated with Res-AM proliferation and a recruitment of Mo-AM and IM3 cells to the lung.

Monocytes and macrophage-lineage bone marrow progenitor cells are transiently decreased at 12 weeks of CS exposure. Given the expansion of $CD11b^+$ populations including Mo-AM and IM3 in the lung, we next assessed the impact of CS on lung, blood, spleen, and bone marrow monocytes. In the lung, we observed that $Ly6C^{Lo}$ monocyte populations, primed for macrophage differentiation, were not altered by CS exposure at 12-weeks. In contrast, classical inflammatory $Ly6C^{Hi}$ monocytes were reduced by CS (**Figure 3A**). There was no change in either monocyte population in the circulation (**Figure 3B**). In the spleen, a known monocyte reservoir(24), CS resulted in decreased total spleen cells (**Figure S3A**) and consequently both monocyte populations (**Figure 3C**). CS exposure decreased both monocyte populations in the bone marrow at 12-weeks (**Figure 3D**). No changes in either monocyte population were observed in any tissue at 2- and 24-weeks CS exposure, with the exception of $Ly6C^{Lo}$ monocytes, which were decreased following 2 weeks of CS exposure in the bone marrow (**Figure S3B-E**).

Next, we assessed macrophage progenitor cells in the bone marrow. The linearity of commitment toward cell terminal differentiation in order is $Lineage^{Neg}Sca1^+c$-

Kit^+(**LSK**), monocyte-macrophage dendritic cell progenitor (**MDP**), common monocyte progenitor (**cMoP**) and finally monocyte populations (25–27). We observed all LSK progenitor cell populations were decreased in CS-exposed mice at 12 weeks (**Figure 3E**; **Figure S3F**). To note, more committed progenitor MDP and cMoP populations were unchanged by CS exposure (**Figure 3E**). CS exposure was associated with a transient reduction in lung, spleen and bone marrow monocyte and macrophage progenitor populations at 12 weeks of CS exposure.

CS-exposed pulmonary macrophage expansion is IL-1α dependent. The IL-1α axis is critical in the recruitment of myeloid cells to the lung following CS exposure (6,28,29). Consequently, we assessed the impact of IL-1α and IL1-R1 deficiency on macrophage subpopulations composition in CS-exposed mice. Res-AM were significantly attenuated in both *Il1a*$^{-/-}$ and *Il1r1*$^{-/-}$ mice following CS exposure (**Figure 4**; **Figure S4A**). Mo-AM and IM3, which were the predominant subpopulations increased in total $BrdU^+$ cells, had attenuated expansion in *Il1a*$^{-/-}$ mice following CS exposure (**Figure 4**). There was no change in Mo-AM or IM3 populations in *Il1r1*$^{-/-}$ mice following CS exposure (**Figure S4A**). Moreover, IL-1α- and IL1-R1-deficiency was not associated with changes in IM1 or IM2 populations (**Figure 4; Figure S4A**). Cell number changes were not driven by differences in total cell number (**Figure S4B-C**). Thus, CS was associated with IL-1α dependent expansion of Mo-AM, IM3, and Res-AMs.

CS exposure skews macrophage subpopulation composition during impaired bleomycin-induced tissue remodelling. Monocyte-derived macrophages, which contribute to the

expanded $CD11b^+$ macrophages in our model, have been shown to be necessary for fibrogenesis(9,10,19). Using a model of concurrent mild bleomycin-induced lung injury, we assessed the impact of CS on macrophage function at two timepoints, day 7 (pre-tissue remodelling and peak inflammation) and day 21 (peak fibrogenesis) (**Figure 5A**). While bleomycin-treated mice had equivalent weight loss regardless of exposure (**Figure S5A**), 3/5 (60%) and 4/5 (80%) myeloid lineage-related genes were enriched in CS-exposed compared to RA-exposed bleomycin-treated mice at day 7 and 21 respectively (**Table S3**; **Table S4**). These transcriptional changes, including the upregulation of the CD11b-encoding gene *Itgam*, were likely related to the observed expansion of all $CD11b^+$ subpopulations at day 7 in CS-exposed bleomycin-treated mice (**Figure 5B**). This compositional phenotype was not maintained in CS-exposed bleomycin-treated mice at day 21, with only IM2 remaining expanded (**Figure 5C**). In contrast, at day 21, Res-AM and Mo-AM populations were decreased and IM1/IM3 were equivalent in CS-exposed compared to RA-exposed bleomycin-treated mice (**Figure 5C**).

These alterations in macrophage composition at day 7 and 21 were associated with impaired fibrogenesis by day 21 as determined by biomechanical, transcriptional and histological measurements. CS-exposed compared to RA-exposed bleomycin-treated mice had reduced lung elastance (**Figure S5B**) at day 21. This decreased elastance was associated with the downregulation of 5/9 (55%) fibrotic/wound healing genes at day 7 and 3/9 (33%) at day 21 in CS-exposed compared to RA-exposed bleomycin-treated mice (**Table S3**; **Table S4**). Notably, overall transcriptional changes were sufficient to define

experimental groups by unsupervised hierarchical clustering analysis at day 7 but not at day 21, where clustering was split based on CS status (**Figure S5C-D)**. These altered transcriptional and lung biomechanics were associated with attenuated expansion of α-SMA^+ cells in CS-exposed compared to RA-exposed mice (**Figure 5D**). Moreover, while the percent of collagenous area increased in RA-exposed bleomycin-treated mice compared to non-treated RA controls, collagen deposition was variable in CS-exposed bleomycin-treated mice and did not increase compared to controls (**Figure 5E**). Thus, trichrome staining suggests impaired collagen production in CS-exposed mice. Representative H&E stains are shown in (**Figure S5E**). Overall, these data suggest CS alters the transcriptional environment and macrophage composition at day 7 post bleomycin in a manner conductive to impaired fibrogenesis, as evidenced by decreased α-SMA^+ myofibroblasts, elastance and collagen deposition at day 21.

Macrophage function and polarisation is skewed by CS exposure. Given that we observed concurrent changes in macrophage composition and fibrotic outcome, we next sought to address whether CS specifically alters macrophage fibrogenic phenotype and function. M2-polarised, alternatively activated macrophages are proposed to contribute to tissue remodelling and fibrogenesis (21,30). Consequently, using CD38 as a marker for M1-like and CD206 for M2-like macrophages, we assessed the polarisation state of each macrophage subpopulation at day 7 and 21 post bleomycin. While polarised macrophages comprised less than 30% of each subpopulation, of those cells polarised, $CD38^+$ macrophages formed the greatest proportion at both day 7 and 21. CD38 expression was

increased in all macrophage subpopulations of CS-exposed bleomycin-treated mice at day 7 (**Figure 6A; Figure S6A**). By day 21, polarised macrophages remained predominately $CD38^+$ but strikingly $CD206^+$ Res-AM decreased in CS-exposed compared to RA-exposed bleomycin treated mice (**Figure 6B; Figure S6B**). At both day 7 and day 21 CS-induced dual $CD38^+CD206^+$ expression, reflecting previous dual polarisation observations in CS only exposure models (31) (**Figure 6A-B**; **Figure S6A-B**). Of note, no difference in total cell number was observed between bleomycin-treated groups at either day 7 or 21 (**Figure S6C-D**). To explore the impact of CS on macrophage function further, adherent lung $CD45^+$ cells isolated following 12-weeks of CS or RA exposure were stimulated for 24-hours with a profibrotic cytokine mix (TGF-β1, IL-4, and IL-6). Comprising predominantly pulmonary macrophages, but not excluding monocytes or dendritic cells, we observed no difference in cell viability between experimental groups (**Figure S6E**). Arginase activity (as measured by urea production), a surrogate measure of alternatively-activated macrophage function, was equivalent in RA or CS-exposed cells following stimulation and demonstrating no loss in M2-like functionality (**Figure 6C**). In addition, while adherent $CD45^+$ cells produced soluble collagen, CS exposure did not alter production and therefore contribute to changes in collagen deposition (**Figure 6D**). However, CS exposure was sufficient to attenuate the induction of MMP9, a peptidase implicated in CS-mediated epithelial-mesenchymal transition and myofibroblast development in fibrogenesis (32). In summary, CS exposure elicited a shift toward a M1-dominant phenotype and decreased MMP9 release.

DISCUSSION

Macrophages perform a central role in the pathogenesis of several CS-associated respiratory diseases including COPD and interstitial lung disease (1–3). However, the composition of pulmonary macrophage subpopulations following CS exposure is poorly understood. Using a mouse model of CS exposure, we showed increased $CD11b^+$ macrophage populations, including Mo-AM and IM1, -2 and -3, in CS-exposed mice. The expansion of Mo-AM and IM3 populations was IL-1α dependent and was associated with a transient decrease in monocyte and progenitor populations in the bone marrow, spleen, and lungs, at 12 weeks of CS. These compositional changes were exacerbated in a model of bleomycin-induced lung injury. Moreover, CS exposure increased M1-polarised macrophages and was associated with impaired MMP9 release. Ultimately, these macrophage compositional and functional changes were associated with decreased fibrogenesis and impaired tissue remodelling in CS-exposed mice.

IM populations are reported to be located in the lung parenchyma and associated with vascular integrity and antigen presentation (8,11). In CS-exposed mice, we observed all IM populations in the BAL. It is possible that the greater epithelial permeability in cigarette smokers (33,34) enables greater recovery of IM from CS-exposed mice. To note, these cells likely do not reflect a transitioning IM cell into a Mo-AM as these populations are reported to have independent ontologies (10). Distinguishing IM and AM populations by histology is challenging due to the spectrum of cellular markers expressed which are shared between macrophage subpopulations. Further analysis is therefore warranted to

determine whether IM1, -2 and -3 populations continue to reside in interstitial spaces upon CS exposure. The presence and the functional consequence of IM in the alveolar space warrants further investigation.

CS exposure caused a robust expansion of $CD11b^+$ (Mo-AM, IM1, -2, -3) populations in the lung. These expanded $CD11b^+$ populations have been previously reported to be derived from monocytes (10,17). We observed transient decreases in macrophage/monocyte progenitor populations in the bone marrow and decreased monocytes in the lung and spleen following CS exposure. Moreover, we observed increased total $BrdU^+$ Mo-AM and IM3 cell turnover in CS-exposed mice. It is therefore plausible these observations represent a CS-induced recruitment of monocytes which differentiate into Mo-AM and IM3 populations in the lung. However, targeted lineage tracing experiments are needed to confirm the ontogeny of these macrophage subpopulations in CS-exposed lungs. Res-AM numbers were unchanged by CS exposure with an equal balance between increased cell death and cell proliferation. This paradigm is supported by previous data that showed Res-AM have minimal postnatal recruitment and are self-maintained at steady state (12). Taken together, these data suggest that CS exposure promotes the expansion of $CD11b^+$ populations, and specifically Mo-AM and IM3, altering pulmonary macrophage composition.

The IL-1α axis has been shown to be vital in CS-induced inflammation (6,28,29). In *Il1a*$^{-/-}$ mice, we observed reduced Mo-AM and IM3. Notably, these populations had increased numbers positive for BrdU which suggested increased cell turnover. Overall,

these data propose an IL-1α dependent recruitment of Mo-AM and IM3 populations to CS-exposed lungs. Furthermore, Res-AM expansion was also IL-1α dependent whereas IM1 and IM2 expansion was not. We speculate the smaller contribution of IL-1α to IM1 and IM2 populations is a consequence a proportion of yolk sac-derived to IM1 and IM2 populations. IM1 and IM2 populations share a cellular phenotype with self-maintained and long-lived yolk sac-derived IM cells (11). Thus, we speculate long-lived yolk sac-derived IM cells are less dependent on IL-1α than foetal liver- or bone marrow-derived macrophage subpopulations.

Macrophages perform a vital role in the repair and regeneration of the tissue following damage (35). Using a model of bleomycin-induced lung injury, we observed attenuated tissue remodelling following CS exposure which was associated with decreased Res-AM and Mo-AM populations at peak fibrogenesis. Mo-AMs are necessary for fibrogenesis in mouse models of fibrosis (9,10); thus, a reduction in Mo-AM in CS-exposed compared to RA-exposed bleomycin-treated mice may represent an impairment in fibrogenesis in our model. In addition, IM1 which have been reported to protect against fibrosis (8), were expanded in CS-exposed mice and therefore may also contribute to an anti-fibrotic environment. Notably, CS exposure induced phenotypically a greater number of M1-like compared to M2-like-polarised macrophages at both day 7 and 21 regardless of subpopulation. Lung transcriptional changes in fibrotic/wound healing and M2-realted genes were most discordant at the day 7 timepoint between bleomycin-treated groups. This phenotypic shift was not associated with any difference in arginase activity suggesting

macrophages remain capable of M2-like functional activity despite the increase in M1-like cells. Detailed investigation of the impact of CS on each macrophage subpopulation's function is needed to elucidate the precise mechanisms altered and that contribute to impaired tissue remodelling. Taken together, these data suggest that CS exposure alters pulmonary macrophage composition and polarisation, decreasing the accumulation of profibrotic macrophages early in fibrogenesis progression leading to an impaired tissue remodelling phenotype by day 21.

CS is well-known to compromise tissue repair through such processes as impaired myofibroblast differentiation (36). Specifically, MMP9 has been shown to contribute to TGF-β production (37) and epithelial-mesenchymal transition (32,38), processes central to myofibroblast differentiation (39). We observed impaired MMP9 expression in isolated adherent lung $CD45^+$ cells from 12-week CS-exposed mice. These data suggest an impaired, or delayed, ability for CS-exposed adherent $CD45^+$ cells to contribute to α-SMA^+ myofibroblast expansion. It is plausible the CS-mediated reduction in α-SMA^+ myofibroblasts, a major collagen producing cell (40), is critical in the impaired tissue remodelling and repair response observed in this bleomycin-induced lung injury model. Further investigation of processes that contribute to CS-induced impaired myofibroblast expansion in tissue remodelling is warranted.

In summary, we showed that CS altered pulmonary macrophage composition, increasing $CD11b^+$ subpopulations, including Mo-AM and IM1-2 and -3, at multiple CS exposure timepoints. The expansion of Mo-AM and IM3 was dependent on IL-1α and

likely reflective of increased cell recruitment. Compositional changes were associated with predominately M1-like macrophages, attenuated MMP9 release and decreased fibrogenesis in a model of bleomycin-induced lung injury. Taken together, these data propose that CS exposure skews pulmonary macrophage subpopulation composition and function predisposing the host to impaired tissue remodelling following lung injury.

ACKNOWLEDGMENTS

We sincerely thank Mary Jo Smith and Mary Bruni at McMaster Immunology Research Centre John Mayberry histology facility (McMaster University, ON, Canada) for their technical help in immunohistochemistry. We thank Christine Mader (Farncombe Metagenomics Facility, McMaster University, ON, Canada) for assistance with NanoString. This work was funded by Canadian Institutes of Health Research (PJT-159792), RespiVert Ltd. part of Janssen Pharmaceuticals, the Canadian Pulmonary Fibrosis Foundation, and the Lung Health Foundation.

AUTHOR CONTRIBUTIONS.

Conception and design: SPC, OM, MRS, KA; Performed experiments: SPC, OM, DT, JJCM, SDR, MFF, PW, AR, AIH, FB; Analysis and interpretations: SPC, OM, ADG, MRS, KA; Drafting the manuscript: SPC, OM; Provided resources: CSS, MRS, KA. Edited and revised manuscript: SPC, OM, DT, JJCM, SDR, MFF, FB, MRS, KA. All authors read and approved the final version.

TABLE LEGENDS

Table 1. Cell surface expression of pulmonary macrophage subpopulations. Expression profile for macrophage subpopulations, based on Gibbings *et al.*, used for flow cytometry analysis. Cells express marker (+), cells do not express (-), and cells have a spectrum of expression (-/+).

FIGURE LEGENDS

Figure 1. Cigarette smoke exposure alters pulmonary macrophage subpopulation composition expanding CD11b$^+$ populations. Female C57BL/6 mice were RA or CS-exposed for 2- to 24-weeks. Data show total numbers of Res-AM, Mo-AM, IM1, IM2, and IM3 populations in **(A)** lung tissue and **(B)** bronchoalveolar lavage (BAL). Data show mean ± SEM, n = 5. Unpaired t test with Welch's correction. RA – room air. CS – cigarette smoke

Figure 2. CD11b$^+$ macrophages are recruited to the lung during cigarette smoke exposure. Female C57BL/6 mice were RA or CS-exposed for 12-weeks. Lung homogenate **(A)** immune mediators (CCL2, CCL3, and IL-1α) and **(B)** monocyte differentiation and macrophage survival factors (M-CSF, GM-CSF, and IL-6). BrdU was used to assess macrophage subpopulation turnover in the lung at 6-weeks CS. Data show **(C)** total cells, % BrdU$^+$ and total BrdU$^+$ Res-AM and **(D)** total cells, total dead and % dead Res-AM. Shown in **(E)** Mo-AM, **(F)** IM1, **(G)** IM2, and **(H)** IM3 are total cells, % positive and total

$BrdU^+$ cells. Data show mean ± SEM, n = 4 - 5. Unpaired t test with Welch's correction. RA – room air. CS – cigarette smoke

Figure 3. Macrophage progenitor cells are transiently decreased at 12-weeks of cigarette smoke exposure. Female C57BL/6 mice were RA or CS-exposed for 12-weeks. Data show total numbers of $Ly6C^{Lo}$ and $Ly6C^{Hi}$ monocyte populations in **(A)** lungs, **(B)** blood, **(C)** spleen, and **(D)** bone marrow. Shown in **(E)** total numbers of macrophage progenitor cells in the bone marrow (lineage-negative Sca1 c-Kit (LSK), monocyte-macrophage dendritic cell progenitor (MDP), common monocyte progenitor (cMoP)). Data show mean ± SEM, n = 5. Unpaired t test with Welch's correction. RA – room air. CS – cigarette smoke

Figure 4. Macrophage expansion in cigarette smoke-exposed lung is IL-1α dependent. Data show total lung Res-AM, Mo-AM, IM1, -2 and -3 populations in *Il1a*$^{-/-}$ and C57BL6 wild type control mice at 8-weeks CS. Data show mean ± SEM, n = 5. Two-way ANOVA with Tukey's multi-comparison test. RA – room air. CS – cigarette smoke

Figure 5. Skewed macrophage subpopulation composition is associated with decreased fibrogenesis. (A) Schematic of CS exposure with bleomycin instillation. C57BL/6 female mice were administered bleomycin (0.05U/mouse) (grey bars) or saline

control (open bars) following 12-weeks of RA or CS exposure. Res-AM, Mo-AM, IM1, IM2, and IM3 populations in lung tissue following **(B)** 7 days or **(C)** 21 days of bleomycin administration. Data show representative image and HALO quantification for **(D)** α-SMA and **(E)** Masson's trichrome. Data show mean ± SEM, n = 5 - 10. Two-way ANOVA with Tukey's multi-comparison test. RA – room air. CS – cigarette smoke.

Figure 6. Macrophage subpopulation function and polarisation is altered by cigarette smoke exposure. C57BL/6 female mice were administered bleomycin (0.05U/mouse) (grey bars) or saline control (open bars) following 12-weeks of RA or CS exposure. Total number of Res-AM and Mo-AM expressing CD38, CD206 and CD38/CD206 in lung tissue following **(C)** 7 days or **(D)** 21 days post bleomycin administration. Adherent lung $CD45^+$ cells isolated from 12-week RA- or CS-exposed C57BL/6 cell supernatant **(C)** urea production, **(D)** soluble collagen and (**E**) MMP9 release following TGF-β1, IL-4, IL-6 stimulation. Data show mean ± SEM, n= 5-10. Two-way ANOVA with Tukey's multi-comparison test. RA – room air. CS – cigarette smoke.

SUPPLEMENTAL TABLE LEGENDS

Table S1. Flow cytometry panel. A panel of surface and intracellular markers to examine the myeloid cells in mouse lung, blood, spleen, and bone marrow.

Table S2. NanoString custom designed fibrogenesis panel. A panel to assess the expression of genes related to wound healing/fibrogenesis, monocytes/macrophages, M1 and M2 macrophage polarisation.

Table S3. mRNA differential expression of fibrogenesis-associated genes at day 7 post bleomycin. Fold change of genes related to wound healing/fibrogenesis, myeloid, M1 and M2 macrophage polarisation. Blank wells represent no significant differential expression between groups. Shown are genes significantly differentially expressed at day 7. Limma package, R.

Table S4. mRNA differential expression of fibrogenesis-associated genes at day 21 post bleomycin. Fold change of genes related to wound healing/fibrogenesis, myeloid, M1 and M2 macrophage polarisation. Blank wells represent no significant differential expression between groups. Shown are genes significantly differentially expressed at day 21. Limma package, R.

SUPPLEMENTAL FIGURE LEGENDS

Figure S1. Monocyte and macrophage subpopulations gating strategies. (A) Lungs were enzymatically digested and stained for flow cytometry. Diagrams showing gating strategies used to isolate total macrophage populations identified as Live autofluorescent

(FITC) +/-Lineage^{Neg}CD45^{+}MertK^{+}CD64^{+}. We further distinguished CD11c^{+}CD11b^{Neg}SiglecF^{Hi} resident alveolar macrophages (Res-AM), CD11c^{+}CD11b^{+}MHCII^{Neg} monocyte-derived alveolar macrophages (Mo-AM), CD11c^{Neg}CD11b^{+}MHCII^{Neg} interstitial macrophage 1 (IM1), CD11c^{Neg}CD11b^{+}MHCII^{+} (IM2), CD11c^{+}CD11b^{+}MHCII^{+} (IM3) plus Ly6C^{Lo}, Ly6C^{Hi} monocyte subsets. Blood **(B)** and spleen **(C)** monocyte populations were determined as CD45^{+}Ly6G^{Neg}CD11b^{+}CD115^{+} then Ly6C^{Lo} and Ly6C^{Hi}. **(D)** Bone marrow monocytes and progenitors were defined as CD45^{+}Lineage^{Neg}. Subsequently monocytes defined as CD11b^{+}CD115^{+}CD117^{Neg}CD135^{Neg} then Ly6C^{Lo} and Ly6C^{Hi}. Myeloid progenitors were defined as CD115^{+}CD117^{+}CD135^{Neg}CD11b^{Neg}Ly6C^{Hi} common monocyte progenitor (cMoP), CD115^{+}CD117^{+}CD135^{+}CD11b^{Neg}Ly6C^{Neg} monocyte-macrophage dendritic cell progenitor (MDP) plus CD115^{Neg}CD117^{+}Sca1^{Hi} Sca1 c-Kit (LSK), CD115^{Neg}CD117^{+}Sca1^{Neg} LS^{Neg}K and CD115^{Neg}CD117^{Neg}Sca1^{+} LSK^{Neg}. Fluorescence minus one was used to gate each of the population of interest.

Figure S2. Macrophage size and granularity following cigarette smoke exposure. Data show total numbers of **(A)** lung (2-, 12-, 24-weeks) and BAL (8-weeks) cells following CS exposure. **(B)** Res-AM, Mo-AM, IM1, IM2, and IM3 population size measured by forward scatter (FSC). **(C)** Res-AM, Mo-AM, IM1, IM2, and IM3 population granularity measured by side scatter (SSC). Data show mean ± SEM, n = 5. Unpaired t test with Welch's correction. RA – room air. CS – cigarette smoke.

Figure S3. Progenitor and monocyte populations at 2, 12 and 24-weeks following cigarette smoke exposure. Female C57BL/6 mice were RA or CS-exposed for 2, 12, or 24-weeks. Data show total cell numbers in **(A)** lung, blood, spleen, and bone marrow. Data also show total numbers of $Ly6C^{Lo}$ and $Ly6C^{Hi}$ monocyte populations in **(B)** lung, **(C)** blood, **(D)** spleen, and **(E)** bone marrow and **(F)** total numbers of macrophage progenitor cells in the bone marrow (lineage-negative Sca1 c-Kit (LSK), monocyte-macrophage dendritic cell progenitor (MDP), common monocyte progenitor (cMoP)). Data show mean ± SEM, n= 4 - 5. Unpaired t test with Welch's correction. RA – room air. CS – cigarette smoke.

Figure S4. Pulmonary macrophages are expanded via IL1α during cigarette smoke exposure. Female C57BL/6, *Il1a*$^{-/-}$ and *Il1r1*$^{-/-}$ mice were RA or CS-exposed for 8-weeks. **(A)** Data show total Res-AM, Mo-AM, IM1, -2, -3 numbers in *Il1r1*$^{-/-}$ mice and C57BL/6 wildtype controls. Total cell number in **(B)** *Il1a*$^{-/-}$ and **(C)** *Il1r1*$^{-/-}$ mice plus C57BL6 wildtype controls. Data show mean ± SEM, n = 5. Two-way ANOVA with Tukey's multi-comparison test. RA – room air. CS – cigarette smoke.

Figure S5. Fibrotic measurements at day 21 of bleomycin instillation. C57BL/6 female mice were administered bleomycin (0.05U/mouse) or control saline following 12-weeks of RA or CS exposure. Mice were monitored 21 days prior to flexiVent® lung measurements and tissue harvest. **(A)** Body weight was measured daily and shown as percentage change

in body weight. **(B)** Total lung elastance, a functional parameter derived from the pressure-driven pressure–volume loops, measured at day 21. Principal component analysis and heatmaps defined by 25 mouse genes from lung homogenate assessed by NanoString at **(C)** day 7 and **(D)** day 21. **(E)** Representative images for H&E-stained sections. Data show mean ± SEM, n= 4-10. Two-way ANOVA with Tukey's multi-comparison test. RA – room air. CS – cigarette smoke.

Figure S6. $CD38^+$ macrophages are increased in cigarette smoke-exposed bleomycin-treated mice. C57BL/6 female mice were administered bleomycin (0.05U/mouse) or control saline following 12-weeks of RA or CS exposure. Graphs demonstrate total numbers of IM1, IM2, and IM3 populations expressing CD38, CD206 and CD38/CD206 in lung tissue following **(A)** 7 days or **(B)** 21 days of bleomycin administration. Total lung cell counts **(C)** day 7 and **(D)** day 21. Adherent lung $CD45^+$ lactose dehydrogenase release in *ex vivo* TGF-β1, IL-6 and IL-4 stimulated cell supernatant from **(E)** 12-week room air (RA)- or cigarette smoke (CS)-exposed mice. Shown mean ± SEM, n = 4 - 10. Two-way ANOVA with Tukey's multi-comparison test. RA – room air. CS – cigarette smoke.

REFERENCES

1. Traves SL, Smith SJ, Barnes PJ, Donnelly LE. Specific CXC but not CC chemokines cause elevated monocyte migration in COPD: a role for CXCR2. *J Leukoc Biol* (2004) **76**:441–450. doi:10.1189/jlb.1003495

2. Sumitomo R, Hirai T, Fujita M, Murakami H, Otake Y, Huang C. M2 tumor-associated macrophages promote tumor progression in non-small-cell lung cancer. *Exp Ther Med* (2019) **38**:4490–4498. doi:10.3892/etm.2019.8068

3. Prasse A, Pechkovsky D V., Toews GB, Jungraithmayr W, Kollert F, Goldmann T, Vollmer E, Müller-Quernheim J, Zissel G. A vicious circle of alveolar macrophages and fibroblasts perpetuates pulmonary fibrosis via CCL18. *Am J Respir Crit Care Med* (2006) **173**:781–792. doi:10.1164/rccm.200509-1518OC

4. Gaschler GJ, Zavitz CCJ, Bauer CMT, Skrtic M, Lindahl M, Robbins CS, Chen B, Stämpfli MR. Cigarette smoke exposure attenuates cytokine production by mouse alveolar macrophages. *Am J Respir Cell Mol Biol* (2008) **38**:218–226. doi:10.1165/rcmb.2007-0053OC

5. Morissette MC, Shen P, Thayaparan D, Stämpfli MR. Disruption of pulmonary lipid homeostasis drives cigarette smoke-induced lung inflammation in mice. *Eur Respir J* (2015) **46**:1451–60. doi:10.1183/09031936.00216914

6. Nikota JK, Shen P, Morissette MC, Fernandes K, Roos A, Chu DK, Barra NG, Iwakura Y, Kolbeck R, Humbles AA, et al. Cigarette smoke primes the pulmonary

environment to IL-1α/CXCR-2-dependent nontypeable Haemophilus influenzae-exacerbated neutrophilia in mice. *J Immunol* (2014) **193**:3134–45. doi:10.4049/jimmunol.1302412

7. Dewhurst JA, Lea S, Hardaker E, Dungwa J V., Ravi AK, Singh D. Characterisation of lung macrophage subpopulations in COPD patients and controls. *Sci Rep* (2017) **7**:1–12. doi:10.1038/s41598-017-07101-2

8. Chakarov S, Lim HY, Tan L, Lim SY, See P, Lum J, Zhang XM, Foo S, Nakamizo S, Duan K, et al. Two distinct interstitial macrophage populations coexist across tissues in specific subtissular niches. *Science (80-)* (2019) **363**: doi:10.1126/science.aau0964

9. Misharin A V., Morales-Nebreda L, Reyfman PA, Cuda CM, Walter JM, McQuattie-Pimentel AC, Chen C-I, Anekalla KR, Joshi N, Williams KJN, et al. Monocyte-derived alveolar macrophages drive lung fibrosis and persist in the lung over the life span. *J Exp Med* (2017) **214**:2387–2404. doi:10.1084/jem.20162152

10. Joshi N, Watanabe S, Verma R, Jablonski RP, Chen CI, Cheresh P, Markov NS, Reyfman PA, Mcquattie-pimentel AC, Sichizya L, et al. A spatially restricted fibrotic niche in pulmonary fibrosis is sustained by M-CSF/M-CSFR signalling in monocyte-derived alveolar macrophages. *Eur Respir J* (2020) **55**: doi:10.1183/13993003.00646-2019

11. Ural BB, Yeung ST, Damani-Yokota P, Devlin JC, de Vries M, Vera-Licona P,

Samji T, Sawai CM, Jang G, Perez OA, et al. Identification of a nerve-associated, lung-resident interstitial macrophage subset with distinct localization and immunoregulatory properties. *Sci Immunol* (2020) **5**:1–15. doi:10.1126/sciimmunol.aax8756

12. Tan SYS, Krasnow MA. Developmental origin of lung macrophage diversity. *Development* (2016) **143**:1318–1327. doi:10.1242/dev.129122

13. Guilliams M, De Kleer I, Henri S, Post S, Vanhoutte L, De Prijck S, Deswarte K, Malissen B, Hammad H, Lambrecht BN. Alveolar macrophages develop from fetal monocytes that differentiate into long-lived cells in the first week of life via GM-CSF. *J Exp Med* (2013) **210**:1977–92. doi:10.1084/jem.20131199

14. Hashimoto D, Chow A, Noizat C, Teo P, Beasley MB, Leboeuf M, Becker CD, See P, Price J, Lucas D, et al. Tissue-resident macrophages self-maintain locally throughout adult life with minimal contribution from circulating monocytes. *Immunity* (2013) **38**:792–804. doi:10.1016/j.immuni.2013.04.004

15. Gibbings SL, Goyal R, Desch AN, Leach SM, Prabagar M, Atif SM, Bratton DL, Janssen W, Jakubzick C V. Transcriptome analysis highlights the conserved difference between embryonic and postnatal-derived alveolar macrophages. *Blood* (2015) **126**:1357–1366. doi:10.1182/blood-2015-01-624809

16. Nayak DK, Zhou F, Xu M, Huang J, Tsuji M, Hachem R, Mohanakumar T. Long-Term Persistence of Donor Alveolar Macrophages in Human Lung Transplant

Recipients That Influences Donor-Specific Immune Responses. *Am J Transplant* (2016) **16**:2300–2311. doi:10.1111/ajt.13819

17. Gibbings SL, Thomas SM, Atif SM, Mccubbrey AL, Desch AN, Danhorn T, Leach SM, Bratton DL, Henson PM, Janssen WJ, et al. Three Unique Interstitial Macrophages in the Murine Lung at Steady State. *Am J Respir Cell Mol Biol* (2017) **57**:66–76. doi:10.1165/rcmb.2016-0361OC

18. Xiong Z, Leme AS, Ray P, Shapiro SD, Lee JS. CX3CR1+ Lung Mononuclear Phagocytes Spatially Confined to the Interstitium Produce TNF- and IL-6 and Promote Cigarette Smoke-Induced Emphysema. *J Immunol* (2011) **186**:3206–3214. doi:10.4049/jimmunol.1003221

19. Henson PM, Barthel L, Danhorn T, McCubbrey AL, Mohning MP, Jakubzick C V., Redente EF, Leach SM, Mould KJ, Gibbings SL, et al. Deletion of c-FLIP from CD11b high Macrophages Prevents Development of Bleomycin-induced Lung Fibrosis. *Am J Respir Cell Mol Biol* (2018) **58**:66–78. doi:10.1165/rcmb.2017-0154oc

20. McGovern TK, Robichaud A, Fereydoonzad L, Schuessler TF, Martin JG. Evaluation of respiratory system mechanics in mice using the forced oscillation technique. *J Vis Exp* (2013) **75**: doi:10.3791/50172

21. Ayaub EA, Dubey A, Imani J, Botelho F, Kolb MRJ, Richards CD, Ask K. Overexpression of OSM and IL-6 impacts the polarization of pro- fibrotic

macrophages and the development of bleomycin-induced lung fibrosis. *Sci Rep* (2017) **7**:1–16. doi:10.1038/s41598-017-13511-z

22. Wilson AM, Nair P, Hargreave FE, Efthimiadis AE, Anvari M, Allen CJ. Lipid and smoker's inclusions in sputum macrophages in patients with airway diseases. *Respir Med* (2011) **105**:1691–1695. doi:10.1016/j.rmed.2011.07.011

23. Botelho FM, Gaschler GJ, Kianpour S, Zavitz CCJ, Trimble NJ, Nikota JK, Bauer CMT, Stämpfli MR. Innate immune processes are sufficient for driving cigarette smoke-induced inflammation in mice. *Am J Respir Cell Mol Biol* (2010) **42**:394–403. doi:10.1165/rcmb.2008-0301OC

24. Swirski FK, Al. E. Identification of Splenic Reservoir Monocytes and Their Deployment to Inflammatory Sites. *Science (80-)* (2009) **325**:612–616.

25. Oguro H, Ding L, Morrison SJ. SLAM family markers resolve functionally distinct subpopulations of hematopoietic stem cells and multipotent progenitors. *Cell Stem Cell* (2013) **13**:102–116. doi:10.1016/j.stem.2013.05.014

26. Hettinger J, Richards DM, Hansson J, Barra MM, Joschko AC, Krijgsveld J, Feuerer M. Origin of monocytes and macrophages in a committed progenitor. *Nat Immunol* (2013) **14**:821–830. doi:10.1038/ni.2638

27. Kumar R, Fossati V, Israel M, Snoeck H-W. Lin − Sca1 + Kit − Bone Marrow Cells Contain Early Lymphoid-Committed Precursors That Are Distinct from Common Lymphoid Progenitors . *J Immunol* (2008) **181**:7507–7513.

doi:10.4049/jimmunol.181.11.7507

28. Botelho FM, Bauer CMT, Finch D, Nikota JK, Zavitz CCJ, Kelly A, Lambert KN, Piper S, Foster ML, Goldring JJP, et al. IL-1α/IL-1R1 expression in chronic obstructive pulmonary disease and mechanistic relevance to smoke-induced neutrophilia in mice. *PLoS One* (2011) **6**:e28457. doi:10.1371/journal.pone.0028457

29. Pauwels NS, Bracke KR, Dupont LL, Pottelberge GR Van, Provoost S, Berghe T Vanden, Vandenabeele P, Lambrecht BN, Joos GF, Brusselle GG. Role of IL-1 a and the Nlrp3/caspase-1/IL-1 b axis in cigarette smoke-induced pulmonary inflammation and COPD. *Eur Respir J* (2011) **38**:1019–1028. doi:10.1183/09031936.00158110

30. Gibbons MA, MacKinnon AC, Ramachandran P, Dhaliwal K, Duffin R, Phythian-Adams AT, Van Rooijen N, Haslett C, Howie SE, Simpson AJ, et al. Ly6C hi monocytes direct alternatively activated profibrotic macrophage regulation of lung fibrosis. *Am J Respir Crit Care Med* (2011) **184**:569–581. doi:10.1164/rccm.201010-1719OC

31. Shaykhiev R, Krause A, Salit J, Harvey B, Connor TPO, Crystal RG, Harvey B, Connor TPO, Crystal RG. Smoking-Dependent Reprogramming of Alveolar Macrophage Polarization: Implication for Pathogenesis of Chronic Obstructive Pulmonary Disease. *J Immunol* (2009) **183**:2867–2883. doi:10.4049/jimmunol.0900473

32. Agraval H, Yadav UCS. MMP-2 and MMP-9 mediate cigarette smoke extract-induced epithelial-mesenchymal transition in airway epithelial cells via EGFR/Akt/GSK3β/β-catenin pathway: Amelioration by fisetin. *Chem Biol Interact* (2019) **314**: doi:10.1016/j.cbi.2019.108846

33. Burns AR, Hosford SP, Dunn LA, Walker DC, Hogg JC. Respiratory epithelial permeability after cigarette smoke exposure in guinea pigs. *J Appl Physiol* (1989) **66**:2109–2116. doi:10.1152/jappl.1989.66.5.2109

34. Jones JG, Lawler P, Crawley JCW, Minty BD, Hulands G, Veall N. Increased Alveolar Epithelial Permeability in Cigarette Smokers. *Lancet* (1980) **315**:66–68. doi:10.1016/S0140-6736(80)90493-6

35. Puttur F, Gregory LG, Lloyd CM. Airway macrophages as the guardians of tissue repair in the lung. *Immunol Cell Biol* (2019) **97**:246–257. doi:10.1111/imcb.12235

36. Silva D, Ca M, Arancibia R, Martı C, Martı J, Pc S. Effects of cigarette smoke and nicotine on cell viability, migration and myofibroblastic differentiation. *J Periodont Res* (2012) **47**:599–607. doi:10.1111/j.1600-0765.2012.01472.x

37. Lee CG, Homer RJ, Zhu Z, Lanone S, Wang X, Koteliansky V, Shipley JM, Gotwals P, Noble P, Chen Q, et al. Interleukin-13 Induces Tissue Fibrosis by Selectively Stimulating and Activating Transforming Growth Factor Beta 1. *J Exp Med* (2001) **194**:809–821. doi:10.1084/jem.194.6.809.

38. Lin C, Tsai P, Kandaswami CC, Lee P, Huang C, Hwang J, Lee M. Matrix

metalloproteinase-9 cooperates with transcription factor Snail to induce epithelial – mesenchymal transition. *Cancer Sci* (2011) **102**:815–827. doi:10.1111/j.1349-7006.2011.01861.x

39. Willis BC, Roland M, Borok Z. Epithelial Origin of Myofibroblasts during Fibrosis in the Lung. *Proc Am Thorac Soc* (2006) **3**:377–382. doi:10.1513/pats.200601-004TK

40. Tsukui T, Sun KH, Wetter JB, Wilson-Kanamori JR, Hazelwood LA, Henderson NC, Adams TS, Schupp JC, Poli SD, Rosas IO, et al. Collagen-producing lung cell atlas identifies multiple subsets with distinct localization and relevance to fibrosis. *Nat Commun* (2020) **11**:1–16. doi:10.1038/s41467-020-15647-5

TABLES

	Res-AM	**Mo-AM**	**IM1**	**IM2**	**IM3**
CD64/MertK	+	+	+	+	+
CD11c	+	+	-	-	+
CD11b	-	+	+	+	+
SiglecF	+	+/-	-	-	-
MHCII	+/-	-	-	+	+

Table 1.

Antibody Specificity	Conjugate	Clone	Supplier
CD11b	Pe Dazzle 594	M1/70	Biolegend
CD11c	BV650	N418	Biolegend
CD19	APCeFlour780	eBio1D3	eBioscience
CD24	BV421	M1/69	Biolegend
CD45	AlexaFluor700	30-F11	Biolegend
CD64	PeCy7	X54-5/71	Biolegend
EpCAM	APC Cy7	G8.8	Biolegend
LIVE/DEAD™	Fixable Yellow Stain		Thermo Fisher Scientific
Ly6C	BV711	HK1.4	Biolegend
Ly6G	APC Cy7	1A8	Biolegend
MerTk	APC	2B10C42	Biolegend
MHCII	PerCp Cy5.5	M5/114.15.2	Biolegend
NK1.1	APC Cy7	PK136	Biolegend
SiglecF	Pe	E50-2440	BD Pharmingen
SiglecF	BV421	S17007L	Biolegend
CD38	Pe	90	Biolegend
CD206	BV785	C068C2	Biolegend
CD115	BV421	AF598	Biolegend
CD115	PE/Cy7	AF598	Biolegend
CD117	APC	2B8	Thermo Fisher Scientific
CD135	BV421	A2F10	Biolegend
CD3	APCeFlour780	17A2	eBioscience
Sca1	BV650	D7	Biolegend
BrdU	APC		BD Biosciences

Table S1

Wound healing/Fibrogenesis	**Myeloid**	**M1**	**M2**
Fgf2	*Itgam*	*Nos2*	*Arg1*
Pdgfa	*Itgax*	*Tnf*	*Mrc1*
Tgfb1	*Ccl2*	*IL1b*	*IL4ra*
Lrrc32	*IL-10*	*IL1a*	*IL6ra*
Vegfa	*Cxcl1*		*Osmr*
Fn1			*IL6*
Col1a1			*Osm*
Col3a1			
Timp1			

Table S2

		RA Bleo - RA Saline	CS Bleo - CS Saline	CS Bleo - RA Bleo	CS Saline - RA Saline
Fibrosis/wound healing	*Fgf2*	1.46	1.18	-1.32	-
	Pdgfa	-1.33	-	1.17	-
	Tgfb1	-1.11	-1.08	1.11	-
	Lrrc32	-	-1.37	-	-
	Vegfa	-1.28	-	-	-1.19
	Fn1	2.82	1.84	-1.48	-
	Col1a1	2.71	2.13	-1.42	-
	Col3a1	2.45	2.16	-1.38	-1.22
	Timp1	11.18	3.73	-1.81	1.65
Myeloid	*Itgam*	-	1.36	1.83	1.44
	Itgax	1.34	-	1.67	2.68
	Ccl2	11.55	1.70	-	7.41
	Il10	-3.67	-3.49	-	-
	Cxcl1	2.36	-	2.14	7.64
M1	*Nos2*	1.81	1.43	-	-
	Tnf	1.72	-	1.50	2.79
	Il1b	-1.81	-	-	-1.41
	Il1a	-	-	1.71	1.75
M2	*Arg1*	4.53	3.14	-1.76	-
	Mrc1	-	-1.35	-	1.55
	Il4ra	1.31	1.21	-1.15	-
	Il6ra	-1.83	-1.58	-	-
	Osmr	1.62	1.12	-	1.34
	Il6	2.72	-	-	1.93
	Osm	1.39	-	-	1.40

Table S3

		RA Bleo - RA Saline	CS Bleo - CS Saline	CS Bleo - RA Bleo	CS Saline - RA Saline
Fibrosis/wound healing	*Fgf2*	-	-	-	-
	Pdgfa	-	1.17	-	-
	Tgfb1	-	-	-	1.17
	Lrrc32	-	-	-	-
	Vegfa	-	-	-	-1.45
	Fn1	1.29	-	-1.25	-
	Col1a1	1.65	-	-1.44	-
	Col3a1	2.15	-	-1.52	-
	Timp1	1.69	-	-	2.14
Myeloid	*Itgam*	-1.27	-	1.67	1.30
	Itgax	1.30	-	1.91	2.52
	Ccl2	-	-	7.82	8.78
	Il10	-	-	-	4.04
	Cxcl1	-	-	6.37	4.15
M1	*Nos2*	2.06	-	-	-
	Tnf	-	-	1.93	1.95
	Il1b	-1.40	-	-	-2.27
	Il1a	-	-	1.89	1.99
M2	*Arg1*	-	1.59	-	-2.09
	Mrc1	-	-	1.52	1.68
	Il4ra	-	-	-	-
	Il6ra	-1.58	-	-	-1.34
	Osmr	-	-	-	-
	Il6	-	-	-	-
	Osm	-	-	-	-1.44

Table S4

FIGURES

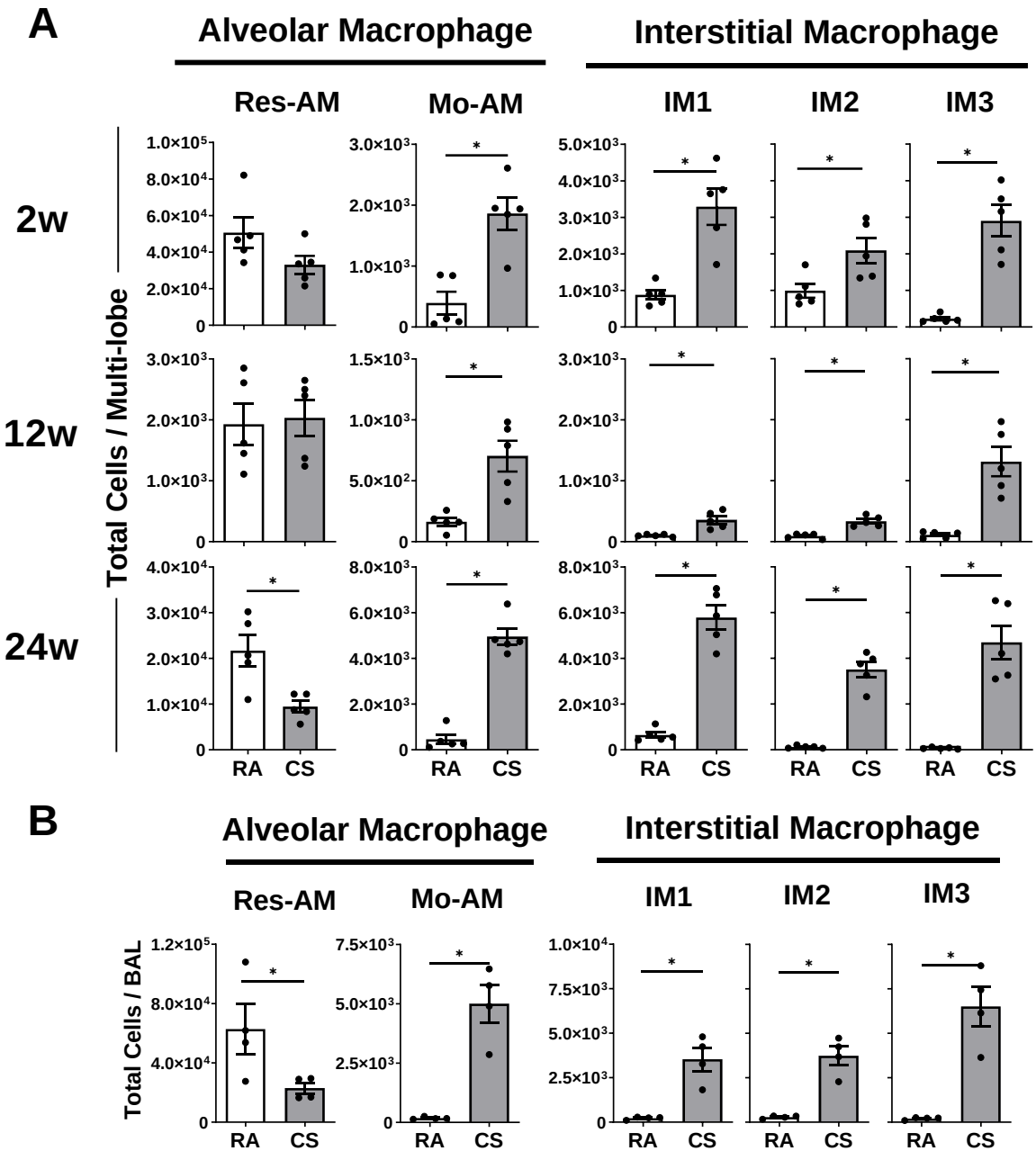

Figure 1

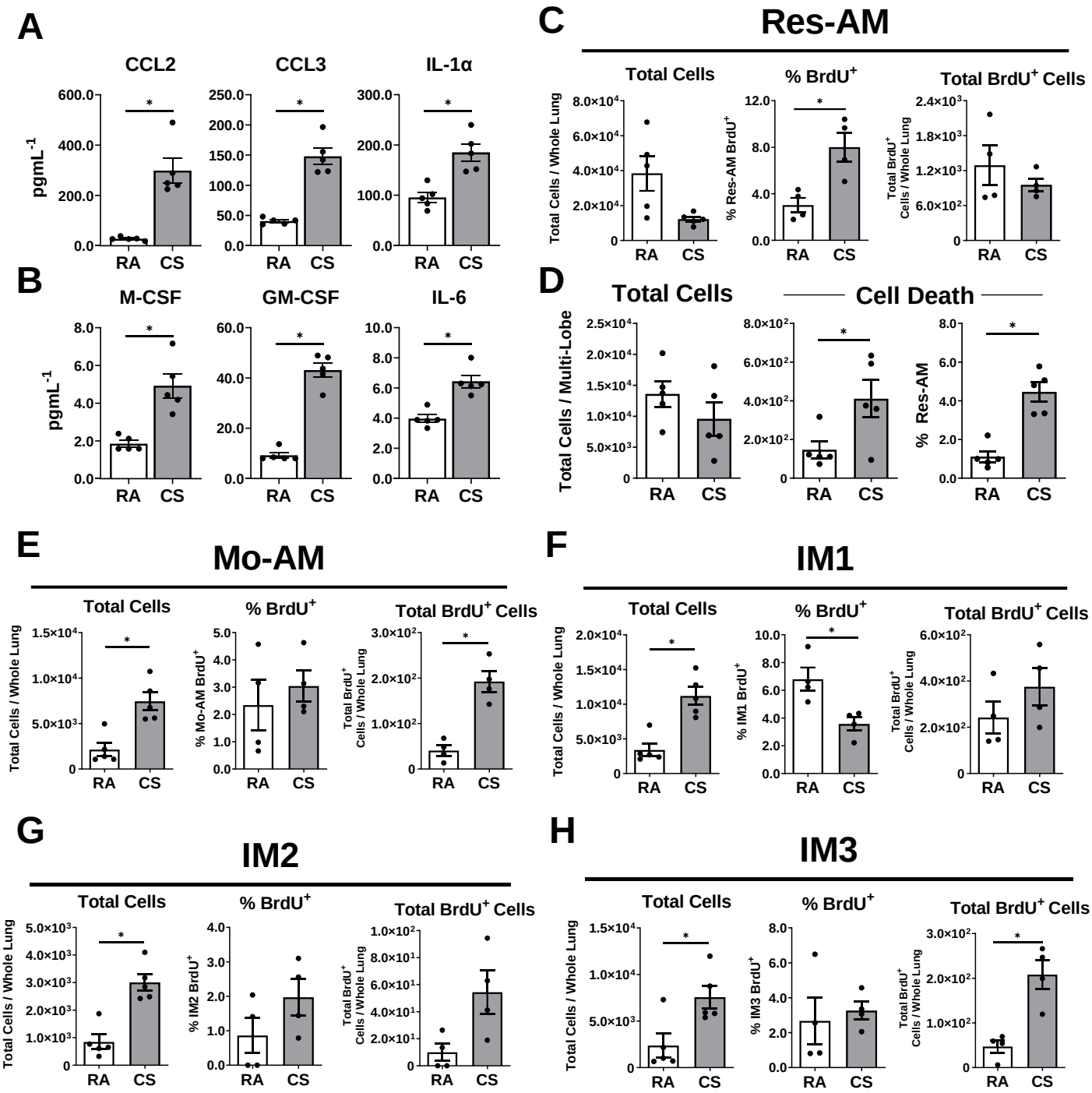
A
CCL2
CCL3
IL-1α
pgmL-1
RA
CS
B
M-CSF
GM-CSF
IL-6
C
Res-AM
Total Cells
% BrdU+
Total BrdU+ Cells
Total Cells / Whole Lung
% Res-AM BrdU+
Total BrdU+ Cells / Whole Lung
D
Total Cells
Cell Death
Total Cells / Multi-Lobe
% Res-AM
E
Mo-AM
% Mo-AM BrdU+
F
IM1
% IM1 BrdU+
G
IM2
% IM2 BrdU+
H
IM3
% IM3 BrdU+

Figure 2

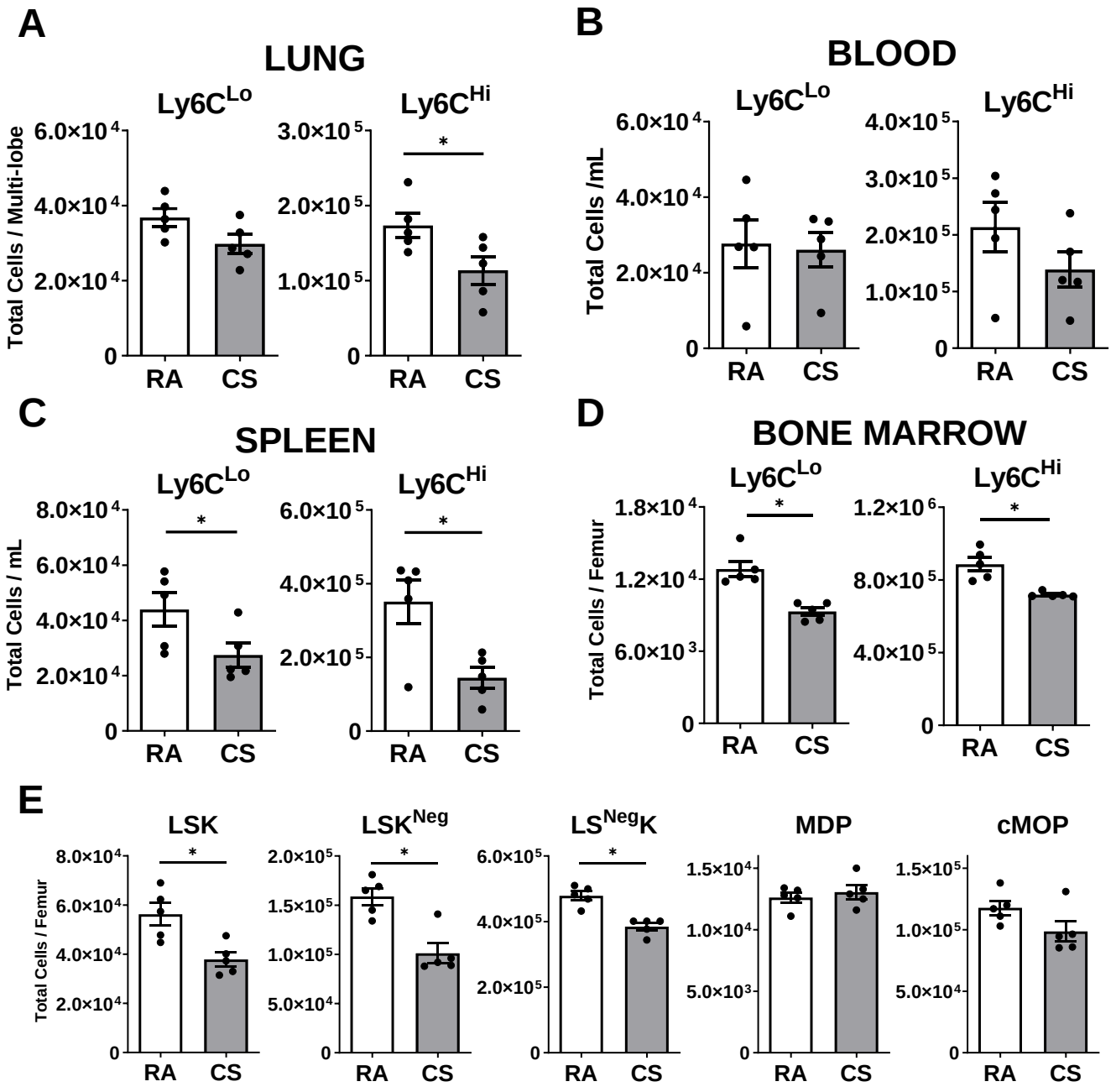
A
LUNG
Ly6C^Lo
Ly6C^Hi
Total Cells / Multi-lobe
6.0×10^4
4.0×10^4
2.0×10^4
0
3.0×10^5
2.0×10^5
1.0×10^5
*
RA
CS
B
BLOOD
Total Cells /mL
4.0×10^5
3.0×10^5
C
SPLEEN
Total Cells / mL
8.0×10^4
6.0×10^5
4.0×10^5
D
BONE MARROW
Total Cells / Femur
1.8×10^4
1.2×10^4
6.0×10^3
1.2×10^6
8.0×10^5
E
LSK
LSK^Neg
LS^NegK
MDP
cMOP
2.0×10^5
1.5×10^5
5.0×10^4
1.5×10^4
1.0×10^4
5.0×10^3
1.5×10^5

Figure 3

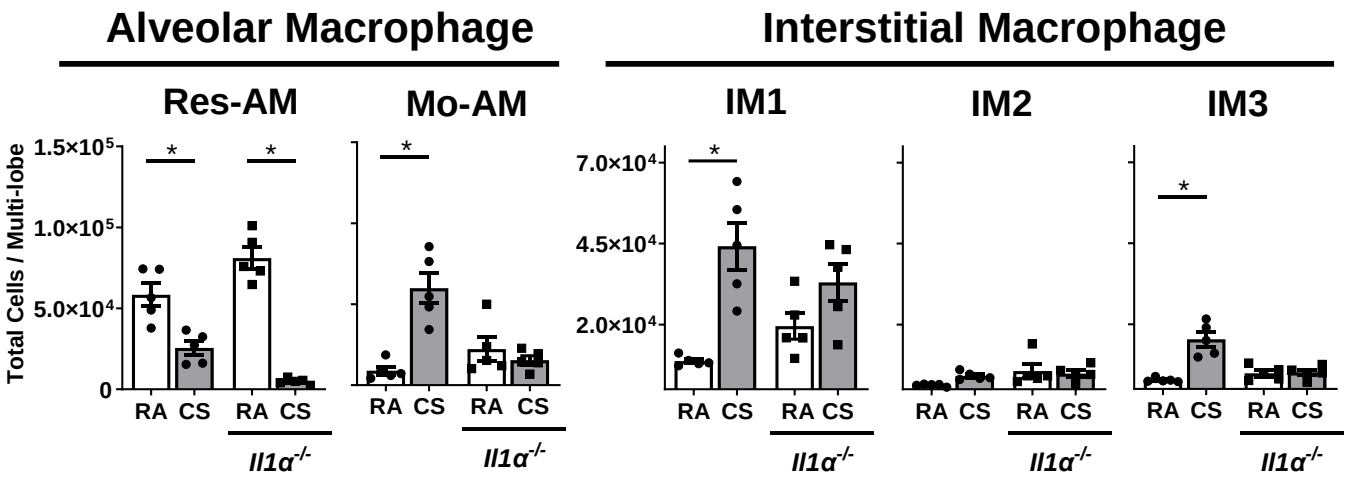
Alveolar Macrophage
Interstitial Macrophage
Res-AM
Mo-AM
IM1
IM2
IM3
Total Cells / Multi-lobe
1.5×10⁵
1.0×10⁵
5.0×10⁴
0
7.0×10⁴
4.5×10⁴
2.0×10⁴
*
RA CS RA CS
Il1α-/-

Figure 4

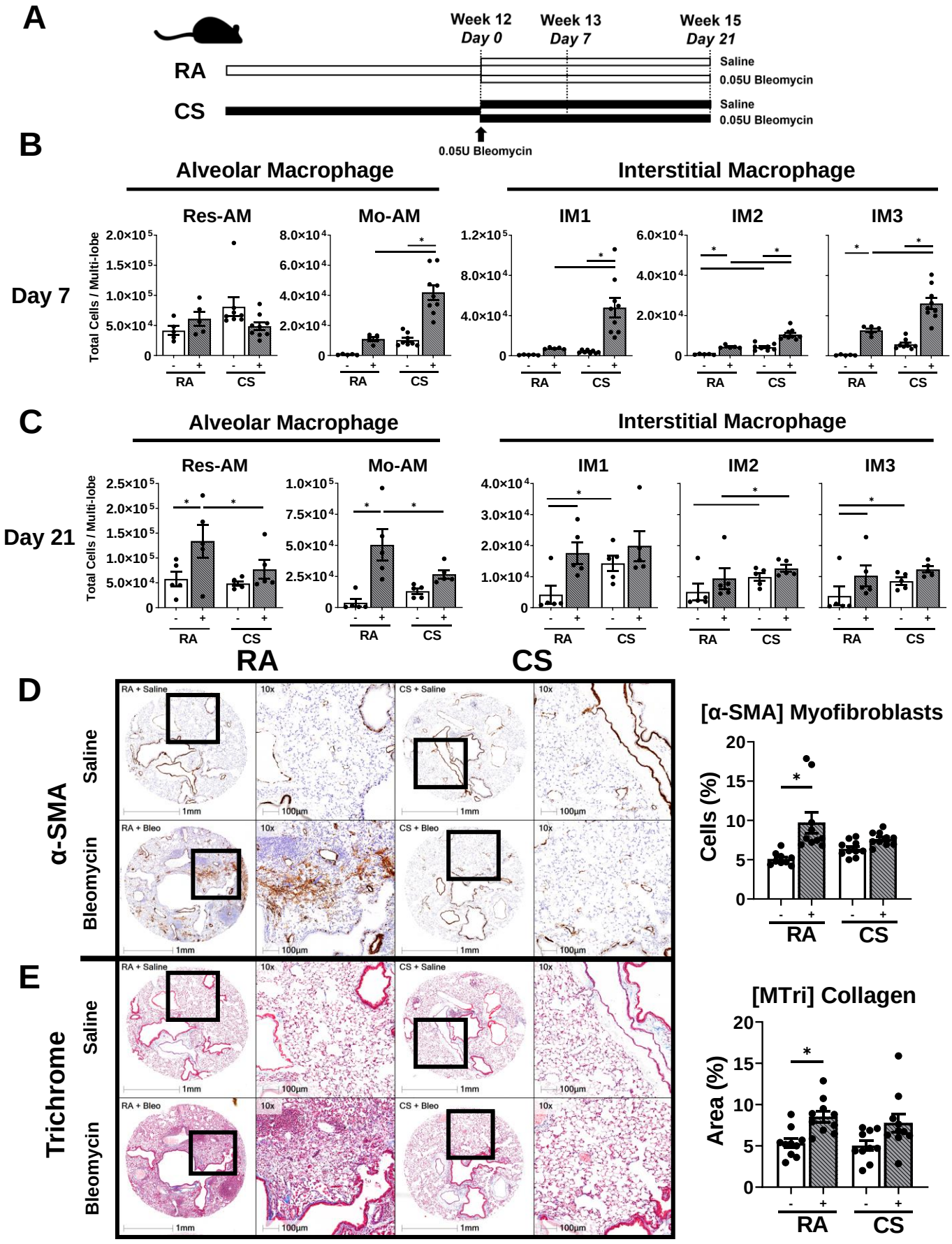
A
Week 12
Day 0
Week 13
Day 7
Week 15
Day 21
RA
CS
Saline
0.05U Bleomycin
Saline
0.05U Bleomycin
0.05U Bleomycin
B
Alveolar Macrophage
Interstitial Macrophage
Res-AM
Mo-AM
IM1
IM2
IM3
Day 7
Total Cells / Multi-lobe
RA
CS
C
Alveolar Macrophage
Interstitial Macrophage
Res-AM
Mo-AM
IM1
IM2
IM3
Day 21
Total Cells / Multi-lobe
RA
CS
D
α-SMA
Saline
Bleomycin
RA + Saline
CS + Saline
RA + Bleo
CS + Bleo
10x
1mm
100μm
[α-SMA] Myofibroblasts
Cells (%)
E
Trichrome
Saline
Bleomycin
[MTri] Collagen
Area (%)

Figure 5

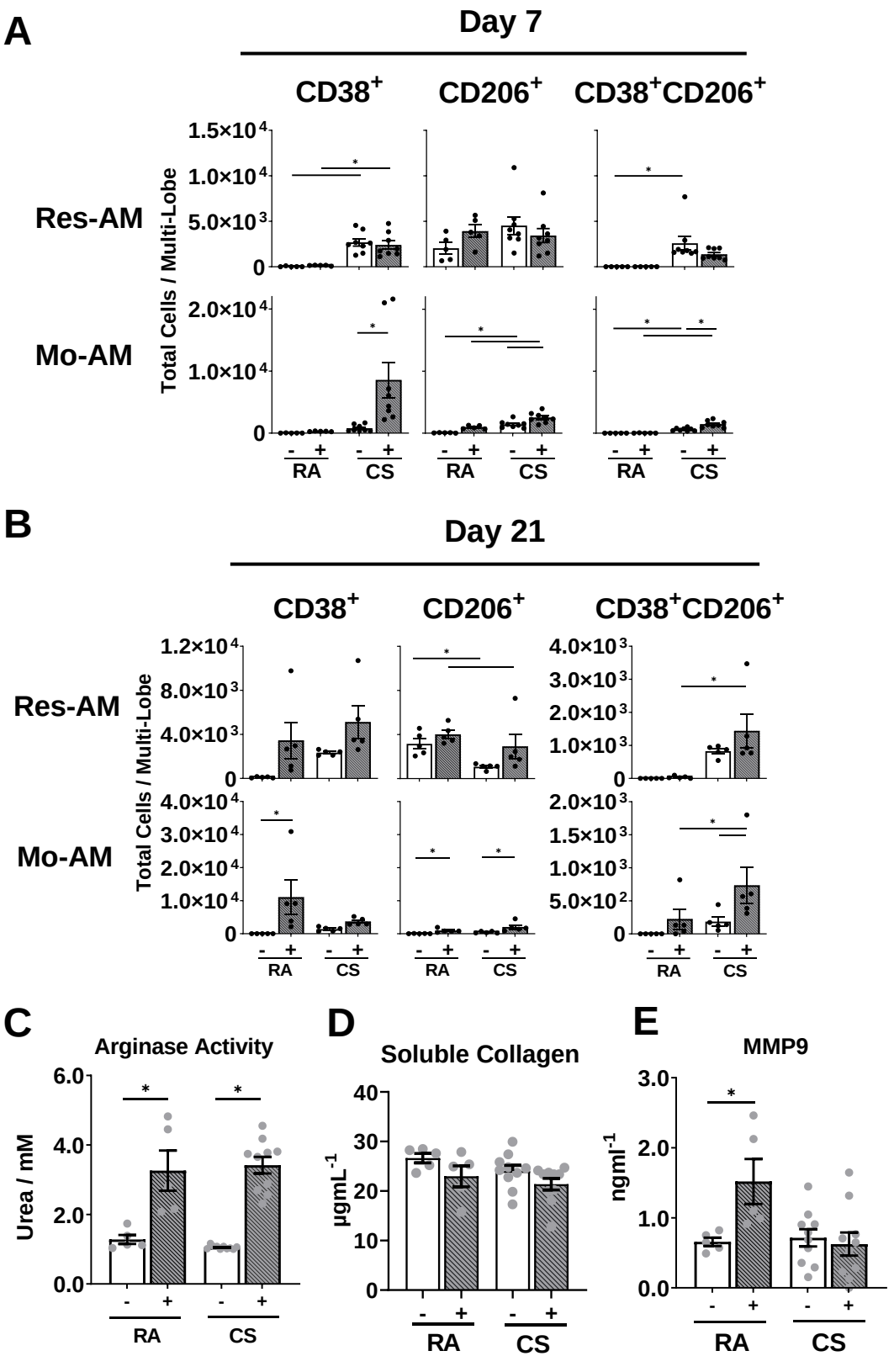
A
Day 7
CD38+
CD206+
CD38+CD206+
Res-AM
Mo-AM
Total Cells / Multi-Lobe
RA
CS
B
Day 21
C
Arginase Activity
Urea / mM
D
Soluble Collagen
µgmL-1
E
MMP9
ngml-1

Figure 6

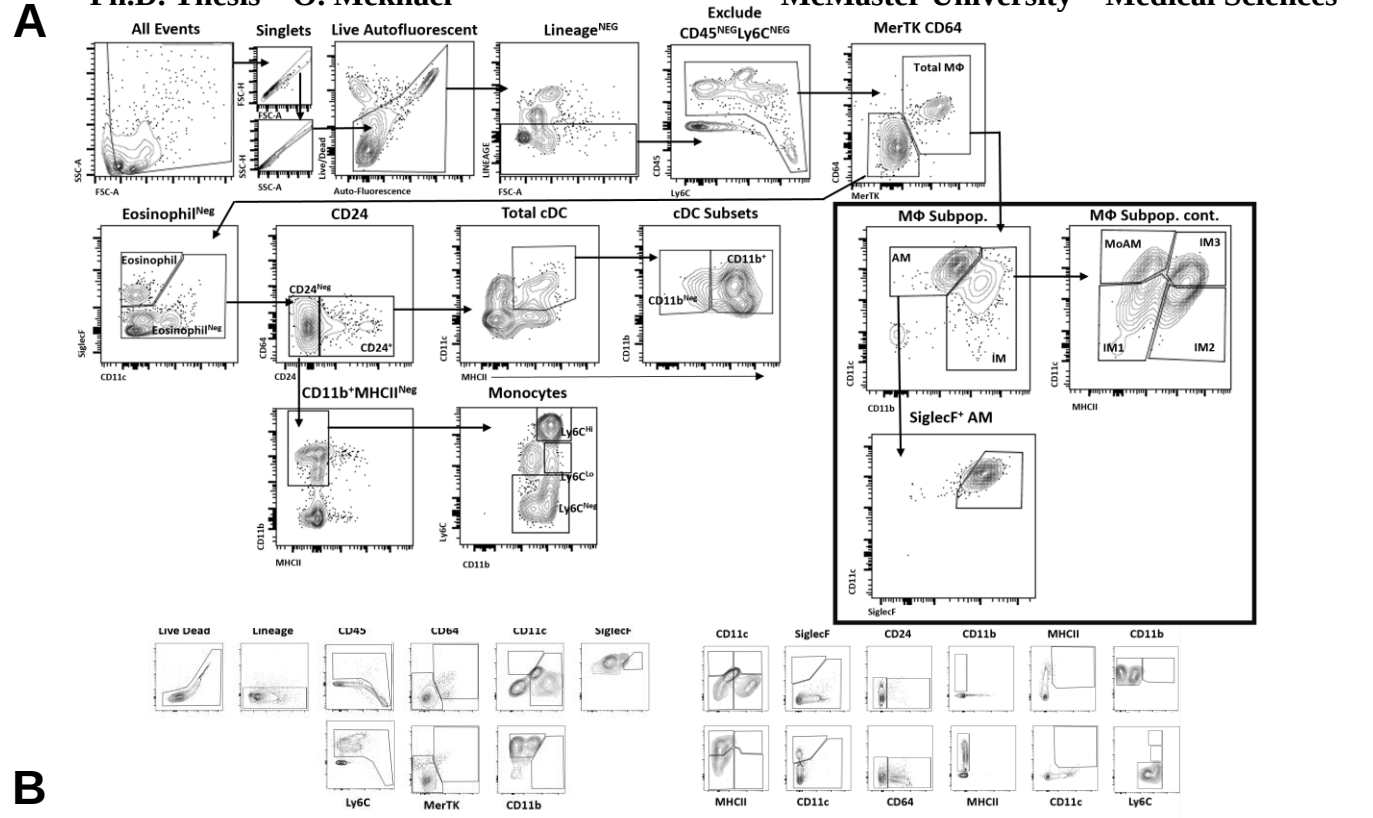
A
All Events
Singlets
Live Autofluorescent
Lineage^{NEG}
Exclude CD45^{NEG}Ly6C^{NEG}
MerTK CD64
Total MΦ
Eosinophil^{Neg}
CD24
Total cDC
cDC Subsets
MΦ Subpop.
MΦ Subpop. cont.
AM
iM
MoAM
IM3
IM1
IM2
SiglecF^{+} AM
CD11b^{+}MHCII^{Neg}
Monocytes
Ly6C^{Hi}
Ly6C^{Lo}
Ly6C^{Neg}
B
All Events
Singlets
Exclude CD45^{NEG}Ly6C^{NEG}
Ly6G^{Neg}
CD11b^{+}CD115^{+}
Monocytes
C
All Events
Singlets
Exclude CD45^{NEG}Ly6C^{NEG}
LINEAGE^{Neg}
CD11b^{+}CD115^{+}
Monocytes
D
All Events
Singlets
Exclude CD45^{NEG}Ly6C^{NEG}
Lineage^{NEG}
cMoP
MDP
Monocytes
LSK^{Neg}
LSK

Figure S1

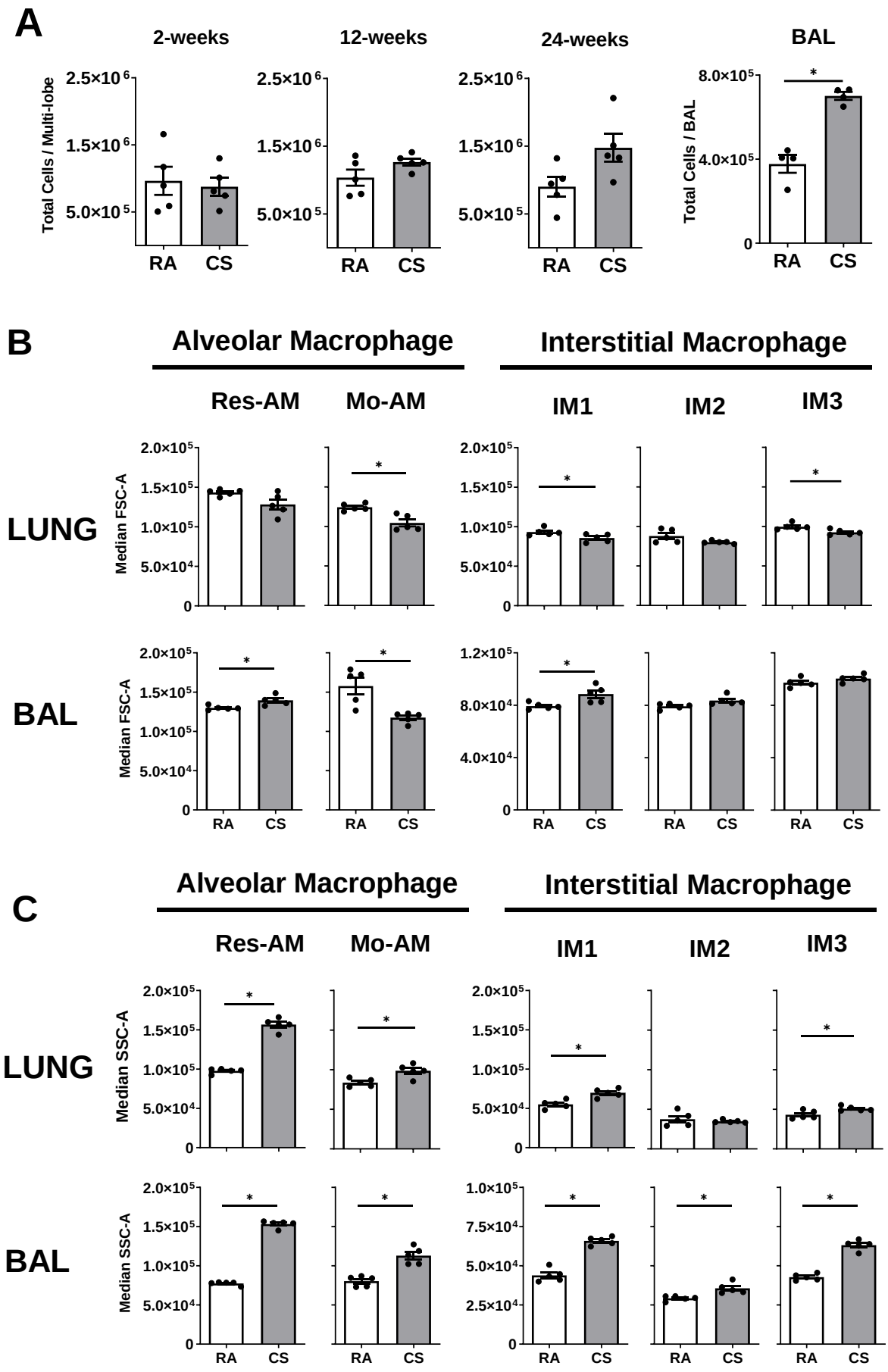
A
2-weeks
12-weeks
24-weeks
BAL
Total Cells / Multi-lobe
Total Cells / BAL
RA
CS
B
Alveolar Macrophage
Interstitial Macrophage
Res-AM
Mo-AM
IM1
IM2
IM3
LUNG
BAL
Median FSC-A
C
Median SSC-A

Figure S2

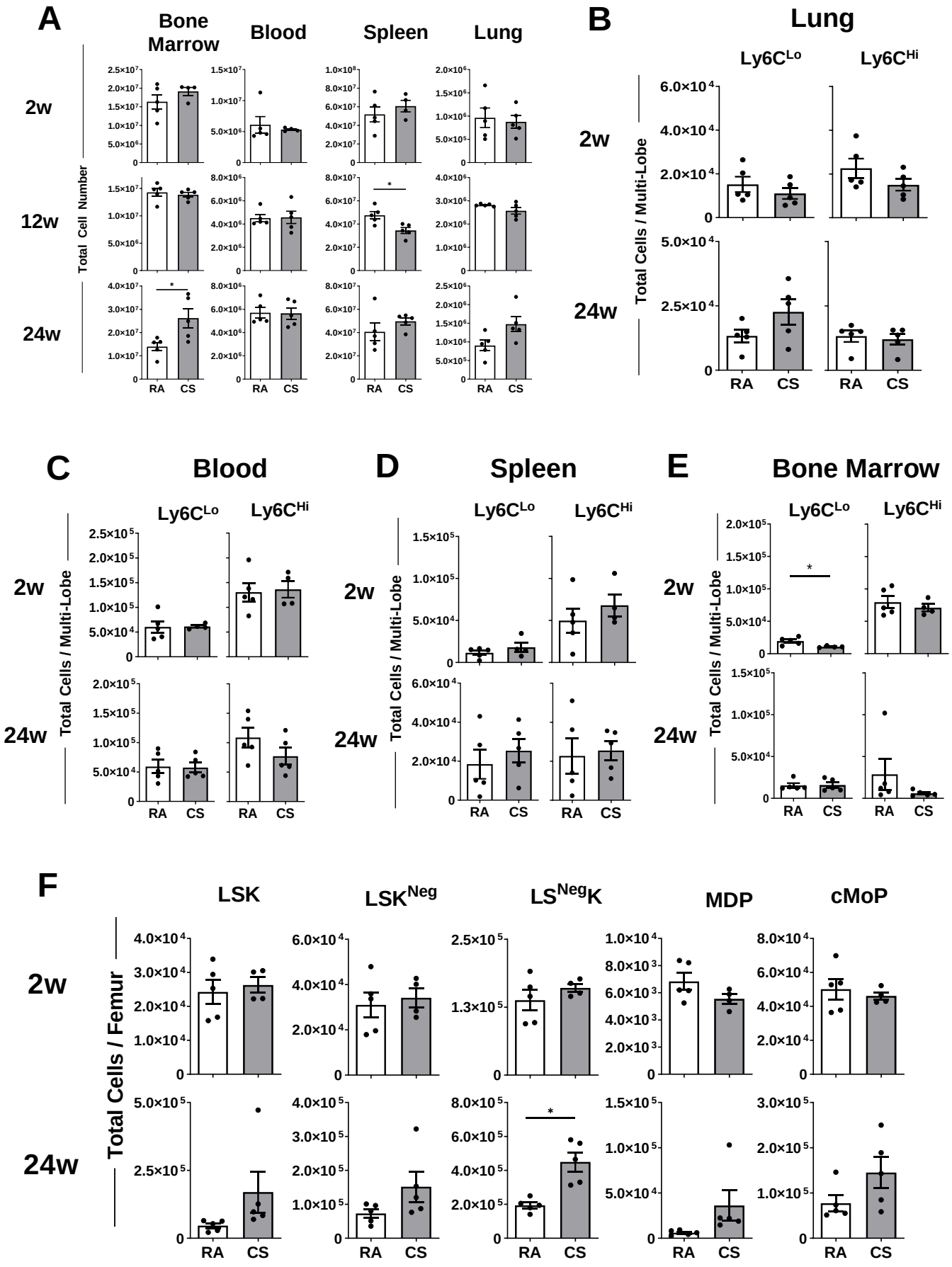
A
Bone Marrow
Blood
Spleen
Lung
2w
12w
24w
Total Cell Number
RA
CS
B
Lung
Ly6C^Lo
Ly6C^Hi
Total Cells / Multi-Lobe
C
Blood
D
Spleen
E
Bone Marrow
F
LSK
LSK^Neg
LS^NegK
MDP
cMoP
Total Cells / Femur

Figure S3

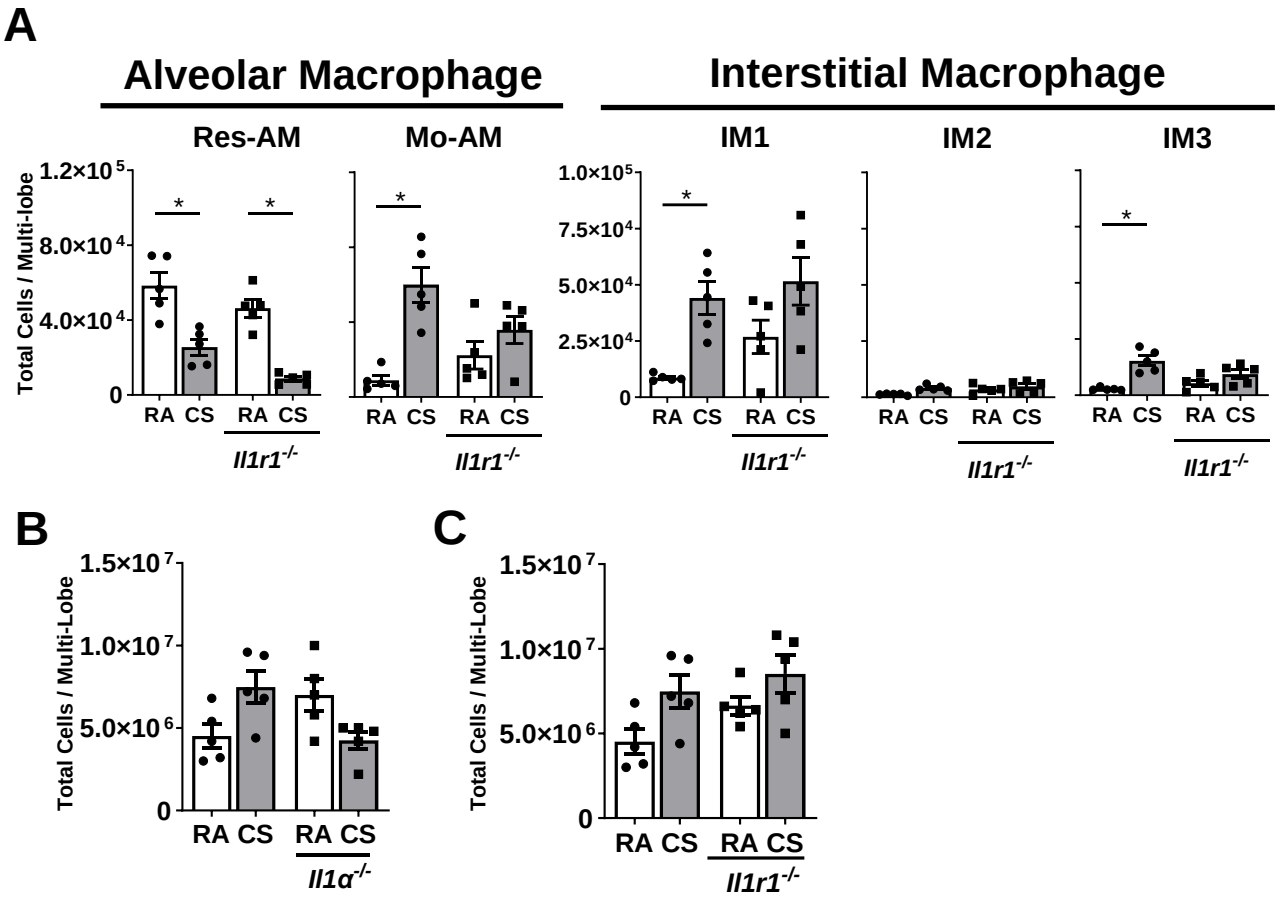
A
Alveolar Macrophage
Interstitial Macrophage
Res-AM
Mo-AM
IM1
IM2
IM3
Total Cells / Multi-lobe
1.2×10^5
8.0×10^4
4.0×10^4
0
7.5×10^4
5.0×10^4
2.5×10^4
RA CS RA CS
Il1r1-/-
B
C
Total Cells / Multi-Lobe
1.5×10^7
1.0×10^7
5.0×10^6
Il1α-/-

Figure S4

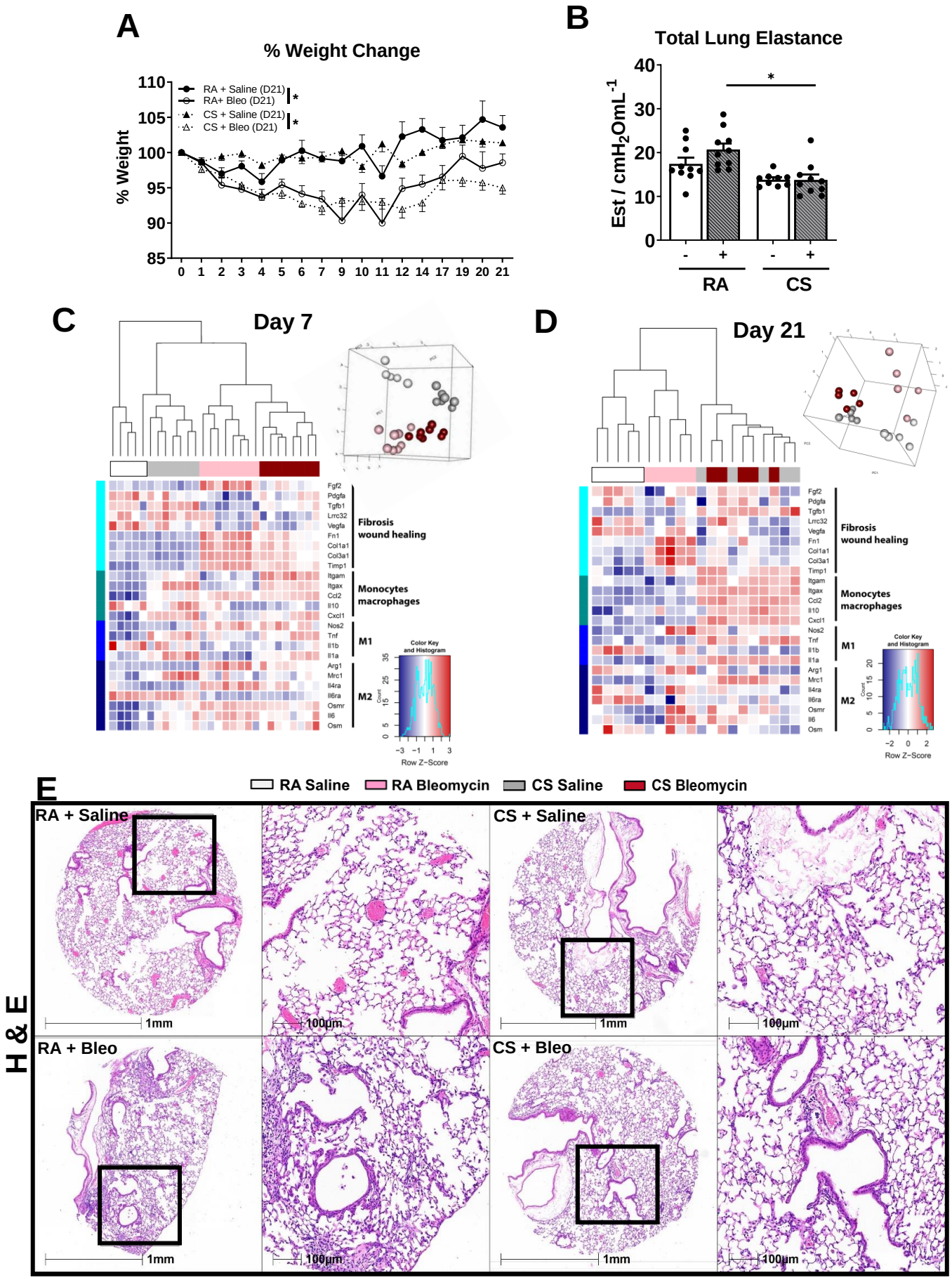
A
% Weight Change
% Weight
RA + Saline (D21)
RA+ Bleo (D21)
CS + Saline (D21)
CS + Bleo (D21)
B
Total Lung Elastance
Est / cmH2OmL-1
RA
CS
C
Day 7
D
Day 21
Fibrosis wound healing
Monocytes macrophages
M1
M2
Color Key and Histogram
Row Z-Score
E
RA Saline
RA Bleomycin
CS Saline
CS Bleomycin
H & E
RA + Saline
CS + Saline
RA + Bleo
CS + Bleo
1mm
100µm

Figure S5

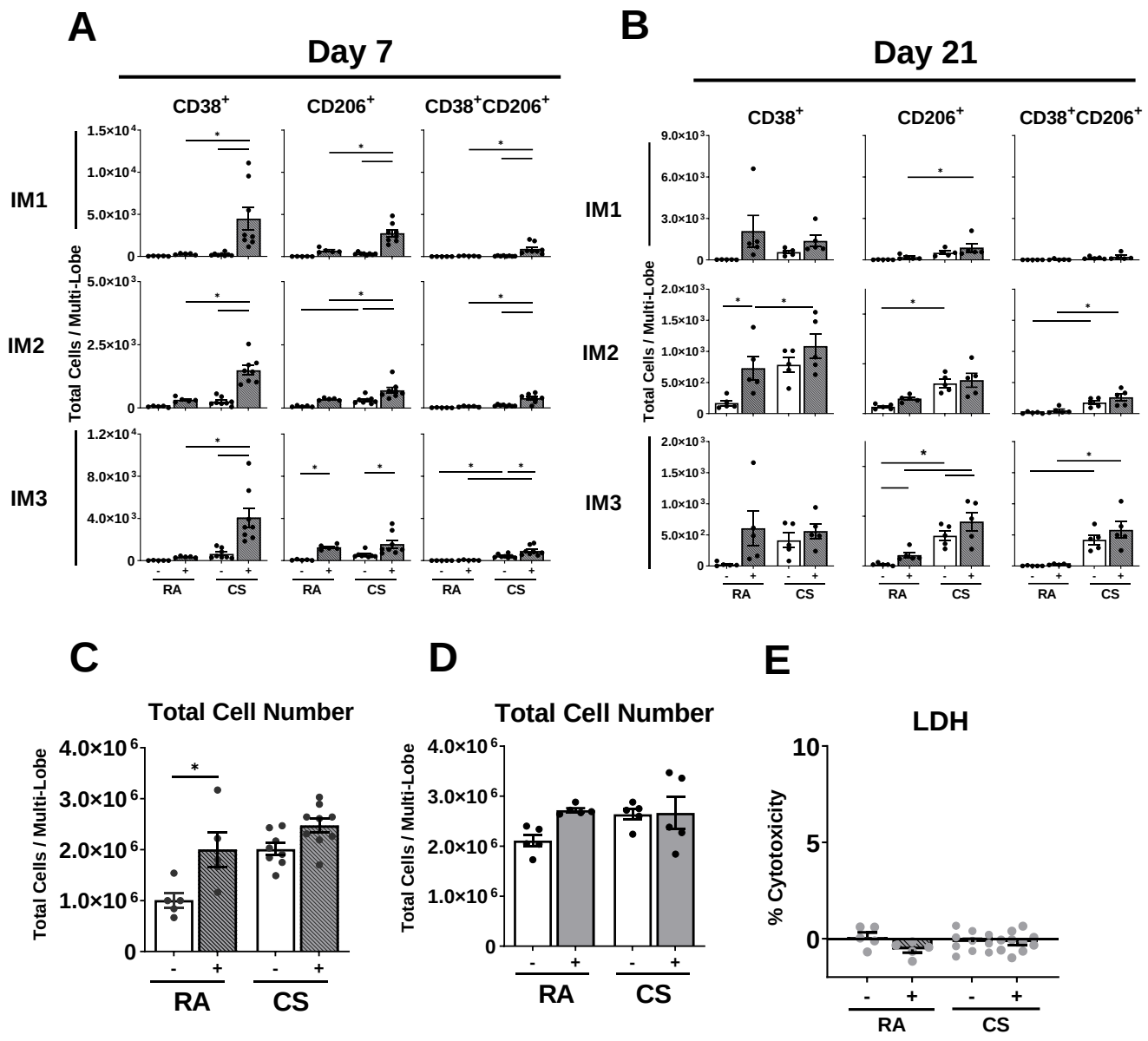
A
Day 7
CD38+
CD206+
CD38+CD206+
IM1
IM2
IM3
Total Cells / Multi-Lobe
RA
CS
B
Day 21
C
Total Cell Number
Total Cells / Multi-Lobe
D
Total Cell Number
E
LDH
% Cytotoxicity

Figure S6

Chapter 4

Myeloid-specific deletion of activating transcription factor 6 alpha increases CD11b^{+} macrophage subpopulations and aggravates lung fibrosis

Olivia Mekhael[1], Spencer D. Revill[1,2], Aaron I. Hayat[1], Steven P. Cass[1], Kyle MacDonald[3], Megan Vierhout[1], Anmar Ayoub[2], Amir Reihani[2], Manreet Padwal[1], Jewel Imani[1], Ehab Ayaub[1], Anna Dvorkin-Gheva[3], Anthony Rullo[3], Jeremy A. Hirota[2,3], Carl D. Richards[3], Darren Bridgewater[4], Martin R. Stämpfli[2,3], Nathan Hambly[2], Asghar Naqvi[4], Martin R.J. Kolb[2], and Kjetil Ask[#2,3]

[1]Medical Sciences Graduate Program, McMaster University, Hamilton, ON, Canada, [2]Department of Medicine, Firestone Institute for Respiratory Health, McMaster University and The Research Institute of St. Joe's Hamilton, Hamilton, ON, Canada, [3]Department of Medicine, McMaster Immunology Research Centre, McMaster University, Hamilton, ON, Canada, [4]Department of Pathology and Molecular Medicine, McMaster University Hamilton, ON, Canada.

Submitted to Journal:
Manuscript is in review in Immunology and Cell Biology

Article type:
Original Research Article

Received on:
29 Jul 2021

Myeloid-specific deletion of activating transcription factor 6 alpha increases CD11b$^+$ macrophage subpopulations and aggravates lung fibrosis

Olivia Mekhael[1], Spencer D. Revill[1,2], Aaron I. Hayat[1], Steven P. Cass[1], Kyle MacDonald[3], Megan Vierhout[1], Anmar Ayoub[2], Amir Reihani[2], Manreet Padwal[1], Jewel Imani[1], Ehab Ayaub[1], Anna Dvorkin-Gheva[3], Anthony Rullo[3], Jeremy A. Hirota[2,3], Carl D. Richards[3], Darren Bridgewater[4], Martin R. Stämpfli[2,3], Nathan Hambly[2], Asghar Naqvi[4], Martin R.J. Kolb[2], and Kjetil Ask[#2,3]

1. *Medical Sciences Graduate Program, McMaster University, Hamilton, ON, Canada.*
2. *Department of Medicine, Firestone Institute for Respiratory Health, McMaster University and The Research Institute of St. Joe's Hamilton, Hamilton, ON, Canada.*
3. *Department of Medicine, McMaster Immunology Research Centre, McMaster University, Hamilton, ON, Canada.*
4. *Department of Pathology and Molecular Medicine, McMaster University Hamilton, ON, Canada.*

[#]**Corresponding author:** Dr. Kjetil Ask, Department of Medicine, McMaster University and The Research Institute of St. Joe's Hamilton, Firestone Institute for Respiratory Health, Luke Wing, Rm L314-5, 50 Charlton Ave East, Hamilton, Ontario, Canada L8N 4A6, Ph. (905) 522 1155 ext. 33683; Fax (905) 521 6183; E-mail: askkj@mcmaster.ca.

Running head: ATF6α-deficient macrophage in lung fibrosis.

Key words: Myeloid-derived cells, macrophage, unfolded protein response, endoplasmic reticulum stress, ATF6α, CHOP, apoptosis, immunopathology.

Abbreviations:

Activating transcription factor 6 alpha - **ATF6α**

Alpha-Smooth muscle actin - **α-SMA**

Alveolar epithelial cells - **AECs**

Alveolar macrophage - **AM**

Arginase-1 - **Arg-1**

Bone marrow-derived macrophages - **BMDMs**

Broncheoalveolar lavage - **BAL**

CCAAT/enhancer binding proteins (C/EBP) homologous protein - **CHOP**

Deoxyribonuclease I from bovine pancreas - **DNase I**

Dimethylsulfoxide - **DMSO**

Endoplasmic reticulum - **ER**

Extracellular matrix - **ECM**

Fluorescence minus one - **FMO**

Fluorescent *in situ* hybridization - **FISH**

Formalin-fixed paraffin-embedded - **FFPE**

Glucose-regulated protein 78kDA - **GRP78**

Hematoxylin & eosin - **H&E**

Hypoxia inducible factor 1 alpha - **HIF-1α**

Idiopathic pulmonary fibrosis - **IPF**

Immunohistochemistry - **IHC**

Inositol-requiring protein-1 alpha - **IRE1α**

Interstitial lung disease - **ILD**

Interstitial macrophage - **IM**

Lactose dehydrogenase - **LDH**

Macrophage colony-stimulating factor - **M-CSF**

Masson's Trichrome - **MTri**

Metaphyseal chondrodysplasia type Schmid - **MCDS**

Paraformaldehyde - **PFA**

Phenylmethylsulfonyl fluoride - **PMSF**

Protein kinase R (PKR)-like endoplasmic reticulum kinase - **PERK**

Polymerase chain reaction - **PCR**

Radioimmunoprecipitation assay - **RIPA**

RNA sequencing - **RNA-seq**

Single-cell RNA sequencing - **scRNA-seq**

Smooth muscle cell - **SMC**

Tissue microarray - **TMA**

Total macrophages - **MΦ**

Transforming growth factor beta 1 - **TGF-β1**

Unfolded protein response - **UPR**

Wild-type - **WT**

X-box-binding protein-1 - **XBP1**

1,4-Dithiothreitol – **DTT**

ABSTRACT

Idiopathic pulmonary fibrosis (IPF) is a chronic, progressive, fibrotic interstitial lung disease of unknown etiology. The accumulation of macrophages is associated with disease pathogenesis. The unfolded protein response (UPR) has been linked to macrophage activation in pulmonary fibrosis. To date, the impact of activating transcription factor 6 alpha (ATF6α), one of the UPR mediators, on the composition and function of pulmonary macrophage subpopulations during lung injury and fibrogenesis is not fully understood. We began by examining the expression of *Atf6α* in IPF patients' lung single-cell RNA sequencing dataset, archived surgical lung specimens, and $CD14^+$ circulating monocytes. To assess the impact of ATF6α on pulmonary macrophage composition and pro-fibrotic function during tissue remodelling, we conducted an *in vivo* myeloid-specific deletion of *Atf6α*. Flow cytometric assessments of pulmonary macrophages were carried out in C57BL/6 and myeloid specific ATF6α-deficient mice in the context of bleomycin-induced lung injury. Our results demonstrated that *Atf6α* mRNA was expressed in pro-fibrotic macrophages found in IPF patient lung and in $CD14^+$ circulating monocytes obtained from IPF patient blood. Following bleomycin administration, the myeloid-specific deletion of *Atf6α* altered pulmonary macrophage composition, expanding $CD11b^+$ subpopulations with dual polarized $CD38^+CD206^+$ expressing macrophages. Compositional changes were associated with an aggravation of fibrogenesis including increased myofibroblast and collagen deposition. Further mechanistic *ex vivo* investigation revealed that ATF6α was required for CHOP induction and for the apoptotic death of bone marrow-derived $CD11b^+$

macrophages. Overall, our findings suggest a detrimental role for the ATF6α-deficient $CD11b^{+}$ macrophages which had altered function during lung injury and fibrosis.

INTRODUCTION

Idiopathic pulmonary fibrosis **(IPF)**, the most common idiopathic interstitial pneumonia, is a chronic, progressive, fibrotic interstitial lung disease **(ILD)** of unknown cause, that occurs primarily in older adults[1]. The prognosis of IPF is poor with a mean life expectancy of 2.5-5 years post diagnosis[2], and limited response to current therapies[1,3]. While IPF pathogenesis remains unknown, recruited monocyte-derived macrophages are considered central orchestrators in lung fibrosis pathogenesis[4]. Particularly, a distinctive population of macrophages was shown to be associated with altered tissue remodelling in pulmonary fibrosis lung explants[5–7]. Further, an expansion of monocyte-derived macrophage populations was associated with enhanced fibrogenesis in mouse models of lung fibrosis[4,8,9]. Notably, macrophage function is influenced by the immune environment. In particular, depending upon the specific mediators, macrophages are polarized toward the "alternatively activated", also known as "M2-like" phenotype, which resolve wound healing processes and suppress inflammatory responses in the lung[10]. In fibrotic lung diseases, this wound-healing cascade is altered causing aberrant tissue remodelling and studies provide evidence of the contributions of pro-fibrotic M2-like macrophages to this pathogenic fibrogenesis[10–14]. However, the mechanisms which alter pulmonary macrophage function during tissue remodelling and fibrogenesis are not well understood.

A growing body of evidence supports the impact of endoplasmic reticulum **(ER)** stress and the unfolded protein response **(UPR)** on pro-fibrotic macrophage activation[15,16]. ER stress is triggered by the accumulation of misfolded proteins in the ER which

subsequently activates the UPR signaling pathway[17]. UPR initially aims to restore proteostasis via three ER transmembrane proteins: 1) protein kinase R (PKR)-like endoplasmic reticulum kinase **(PERK)**, 2) activating transcription factor 6 alpha **(ATF6α)**, and 3) spliced x-box-binding protein-1 **(XBP1)**-inositol-requiring protein-1 alpha **(IRE1α)**[17]. Failing successful restoration, prolonged UPR signal induces apoptotic cell death through CCAAT/enhancer binding proteins (C/EBP) homologous protein **(CHOP)** induction[17]. It was previously shown in transgenic knockout mouse models that the modulation of the UPR results in either protection or aggravation of the fibrotic responses via the regulation of M2-like macrophage activation[18]. The haploinsufficiency of glucose-regulated protein 78kDA **(GRP78)**, an essential regulator of the UPR sensors, resulted in apoptosis of M2-like macrophages and protection against fibrosis[18]. In contrast, CHOP deficiency led to an accumulation of the M2-like macrophage populations and an increase in fibrosis[18]. The role of each UPR-associated protein in fibrosis is still to be determined.

UPR is believed to be critical in the differentiation of a wide array of cell types from inactive states to synthetic cells with highly secretory capacities, including macrophages, plasma cells, adipocytes, and myofibroblasts[18]. We previously demonstrated that the addition of IL-6 to macrophages led to a hyperpolarized pro-fibrotic M2 phenotype associated with increases in the activation of both IRE1-XBP1 and cleaved ATF6 pathways[19]. Inhibition studies targeting the IRE1-XBP1 arm of the UPR reduced the ER expansion program of macrophages and inhibited their activation toward the hyperpolarized phenotype[19].

p90ATF6α, encoded by the *Atf6* gene[20], is a type II transmembrane glycoprotein localized in the ER and is synthesized as a precursor protein in unstressed cells before undergoing proteolytic cleavage into the soluble nuclear active form p50ATF6α in response to ER stress[20,21]. The overexpression of ATF6 upregulates myocardin expression and its depletion reduces myocardin induction during the differentiation of embryonic stem cell towards the smooth muscle cell **(SMC)** lineage[22]. Further studies indicate that ATF6α might have a role in cell differentiation and phenotypic modulation, likely via the ER expansion program[23]. Furthermore, ATF6α induces the expansion of the ER in mouse embryo fibroblasts in the absence of XBP-1[24]. However, the contribution of ATF6α is yet to be investigated in the context of macrophage pro-fibrotic activation.

Here, we examined the expression of ATF6α in control subjects and in patients diagnosed with IPF, using a publicly available lung single-cell RNA sequencing **(scRNA-seq)** dataset, archived surgical lung specimens, and CD14 positive circulating monocytes. To specifically investigate whether ATF6α was required for macrophage activation towards the pro-fibrotic functional status, we generated transgenic mice with an ATF6α specific deletion in the myeloid compartment. Pulmonary macrophage subpopulations composition and functional status, lung injury, and subsequent fibrosis were examined during tissue remodelling processes. In an experimental mouse model of bleomycin-induced lung fibrosis, we observed that the myeloid-specific deletion of ATF6α increased the number of pro-fibrotic $CD11b^{+}$ macrophages, and increased susceptibility to bleomycin-induced tissue remodelling and subsequent pulmonary fibrosis. Mechanistic

studies *ex vivo* revealed that the absence of ATF6α prevented the activation of CHOP and CHOP-induced apoptotic death in macrophages. These data suggest that ATF6α was not required for macrophage transition toward a pro-fibrotic phenotype but required and responsible for UPR-mediated CHOP activation and subsequent apoptosis.

RESULTS

Atf6α mRNA is expressed in IPF patient monocytes and macrophages. To characterize *Atf6α* mRNA expression in various cell types in the lung, we first used publicly available scRNA-seq data derived from patients diagnosed with IPF[25]. No significant differences were present in *Atf6α* mRNA expression levels across the 27 cell populations, which supports that *Atf6α* is ubiquitously expressed in all cell types examined in IPF patients and control subjects including monocytes and macrophages **(Figure 1A)**. These findings were validated in human surgical lung biopsies examined using fluorescent *in situ* hybridization **(FISH)** RNAscope® technology. Using FISH, *Atf6α* was shown to be colocalized with the pan-macrophage marker *CD68* and *Mrc1* (gene name for CD206), a well-known marker of pro-fibrotic macrophages **(Figure 1B)**. Furthermore, using bulk RNA sequencing **(RNA-seq)** analysis, *Atf6α* was shown to be expressed at a detectable level in $CD14^+$ circulating monocytes isolated from blood obtained from IPF patients and control subjects **(Figure 1C)**, demonstrating the presence of *Atf6α* in macrophage precursor cells in the circulation. "All genes" grey violin shown in **Figure 1C** reflected the distribution of all genes in the 62 samples in order to show the relative expression of *Atf6α* in the groups of interest (control subjects and IPF patients). Taken together, the *Atf6α* gene is expressed in pro-fibrotic macrophages found in IPF patient lungs and in $CD14^+$ circulating monocytes obtained from IPF patient blood.

Development of a myeloid specific Atf6α-deficient mouse model. To investigate the contribution of ATF6α to pulmonary macrophage pro-fibrotic function in the context of

lung fibrogenesis, we developed a transgenic myeloid specific ATF6α-deficient mouse model **(LyM-*Atf6α*$^{fl/fl}$)** using Cre-LoxP recombination system. LyM-*Atf6α*$^{fl/fl}$ DNA genotype was verified using standard polymerase chain reaction **(PCR)** and FISH RNAscope® technology. PCR showed that broncheoalveolar lavage **(BAL)** macrophages obtained from LyM-*Atf6α*$^{fl/fl}$ mice were ATF6α deficient **(Figure 2A)**. In addition, FISH RNAscope® assay performed on mouse lung tissues did not detect *Atf6α* mRNA co-localized with *CD68* mRNA in LyM-*Atf6α*$^{fl/fl}$ mice **(Figure 2B, circles)**, as opposed to the wild-type **(WT)** C57BL/6 **(*Atf6α*$^{+/+}$)** control mice which clearly showed positivity for *Atf6α* mRNA in both epithelial cells and in macrophages **(Figure 2B, arrows and circles, respectively)**. Of note, epithelial cells found in LyM-*Atf6α*$^{fl/fl}$ mice were positive for *Atf6α* mRNA (**Figure 2B, arrows)**.

Myeloid-specific deletion of Atf6α increases pro-fibrotic macrophages and is associated with an exacerbated fibrogenesis.To examine the effect of the deletion of ATF6α in the myeloid compartment on pro-fibrotic macrophage activation during mild acute lung injury and tissue remodelling, we first exposed female LyM-*Atf6α*$^{fl/fl}$ and *Atf6α*$^{+/+}$ mice to a single suboptimal dose of bleomycin (0.04 units/mouse), a dose previously shown to result in a modest level of weight loss, lung injury, and fibrosis[26]. Histological examinations of extracellular matrix **(ECM)** deposition including collagen (Masson's Trichrome, **MTri**) and myofibroblast accumulation (alpha smooth muscle actin, **α-SMA**) on lung serial sections were performed at day 21 (peak tissue remodelling and repair). Data indicated that bleomycin-treated LyM-*Atf6α*$^{fl/fl}$ mice had increased percentage of MTri and α-SMA

positive areas at day 21 **(Figures 2C-D)**. To characterize macrophage pro-fibrotic activation and accumulation, we performed immunostaining on serial sections of the same lungs. LyM-*Atf6α*$^{fl/fl}$ mice had significantly higher percentage of CD206^{+} cells compared to their respective controls and to bleomycin exposed *Atf6α*$^{+/+}$ mice at day 21 post bleomycin administration **(Figure 2E)**. Overall, the changes in CD206^{+} cells, collagen, and α-SMA deposition were associated with changes in pulmonary mechanics and increased quasistatic lung elastance in LyM-*Atf6α*$^{fl/fl}$ mice at day 21 post bleomycin administration **(Figure 2F)**. Combined, these results suggest that LyM-*Atf6α*$^{fl/fl}$ mice are more susceptible to bleomycin (0.04U/mouse)-induced tissue remodelling compared to *Atf6α*$^{+/+}$ mice and this aggravated fibrogenesis is associated with pro-fibrotic macrophage accumulation.

Myeloid-specific deletion of Atf6α expands CD11b^{+} macrophage subpopulations, with a dual CD38^{+}CD206^{+} expression during bleomycin-induced lung injury. To further examine the role of ATF6α deficiency, we assessed the impact of that genetic deletion on pulmonary macrophage composition and function during lung injury and fibrogenesis using flow cytometry-based techniques. Flow cytometric assessments were carried out on enzymatically digested multi-lobe lungs at two timepoints, day 7 (peak injury and inflammation) and day 21 (peak tissue remodelling and repair). Using established markers and flow cytometry gating strategies shown in **Figure 3A**, pulmonary macrophages were stratified into two broad populations, SiglecF^{+} populations associated with alveolar macrophages **(AM)** and CD11b^{+} populations associated with interstitial macrophages **(IM)**. The M1/M2 functional status of macrophage populations was determined based on

the expression of CD38, a marker associated with pro-inflammatory M1 macrophages and based on the expression of arginase-1 **(Arg-1)** and CD206, markers associated with pro-fibrotic M2 macrophages. To note, markers used to identify the different macrophage subpopulations were selected based on findings previously reported by Misharin *et al.* (2013)[13], Jablonski *et al.* (2015)[27], and Gibbings *et al.* (2017)[28]. We first assessed the number of $F4/80^{+}CD64^{+}$ total lung macrophages which were higher in lungs of both LyM-*Atf6α*$^{fl/fl}$ and *Atf6α*$^{+/+}$ 7 days after bleomycin administration (**Figure 3B**). Furthermore, the majority of the macrophage pool was $CD11b^{+}$ and not $SiglecF^{+}$, suggesting that bleomycin exposure led to a robust increase in $CD11b^{+}$ IM in both myeloid specific ATF6α-deficient and WT mice at day 7 (**Figure 3B**). At day 7, bleomycin-treated LyM-*Atf6α*$^{fl/fl}$ mice had significantly higher number of $CD11b^{+}$ macrophage subpopulations compared to bleomycin-treated *Atf6α*$^{+/+}$ mice and to their respective controls **(Figure 3B)**.

Next, we determined the relative distribution of activated polarized macrophages in these populations, using CD38 (M1-like marker) and Arg-1/CD206 (M2-like markers) or a mixed population using CD38/CD206 (mixed phenotype). $SiglecF^{+}$ macrophages were mostly unpolarized and no differences could be observed in their M1 or M2 or mixed phenotype between LyM-*Atf6α*$^{fl/fl}$ and *Atf6α*$^{+/+}$ mice at day 7 post bleomycin instillation **(Figure 4A)**. $CD11b^{+}$ populations had increased levels of all macrophage phenotypes in bleomycin-exposed LyM-*Atf6α*$^{fl/fl}$ and *Atf6α*$^{+/+}$ mice at day 7 **(Figure 4A)**. At day 7 post bleomycin instillation, LyM-*Atf6α*$^{fl/fl}$ mice had a significantly higher number of $CD38^{+}$ cells as compared to wild-type mice **(Figure 4A)**. Notably, at day 7 post bleomycin

administration, both polarized LyM-*Atf6α*$^{fl/fl}$ and *Atf6α*$^{+/+}$ CD11b^{+} subpopulations were pre-dominantly pro-fibrotic Arg-1^{+}CD206^{+} macrophages **(Figure 4A)**. These results demonstrated that at day 7 post bleomycin administration, the majority of lung CD11b^{+} subpopulations were pro-fibrotic Arg-1^{+}CD206^{+} macrophages, with fewer cells expressing CD38^{+} alone or having a CD38^{+}CD206^{+} dual expression. These findings were shown in both myeloid specific ATF6α-deficient and WT mice.

We subsequently examined the macrophage composition and phenotype in the fibrotic phase, at day 21. In contrast to the injury phase at day 7, the numbers of F4/80^{+}CD64^{+} total lung macrophages, SiglecF^{+} and CD11b^{+} macrophages were significantly reduced in *Atf6α*$^{+/+}$ mice exposed to bleomycin compared to their saline-treated groups at day 21 **(Figure 3C)**. Conversely, the number of total macrophages, pre-dominantly CD11b^{+} subpopulations, remained expanded and significantly increased in LyM-*Atf6α*$^{fl/fl}$ mice compared to WT mice following 21 days of bleomycin exposure **(Figure 3C)**. Notably, the total number of macrophages in bleomycin-treated LyM-*Atf6α*$^{fl/fl}$ mice seemed to be reduced at day 21 compared with day 7 **(Figures 3B-C)**. No differences were detected in the M1/M2 functional status of SiglecF^{+} subpopulations between LyM-*Atf6α*$^{fl/fl}$ and *Atf6α*$^{+/+}$ mice at day 21 **(Figure 4B)**. In addition, no differences were detected in the M1/M2 functional status of CD11b^{+} subpopulations between bleomycin-treated *Atf6α*$^{+/+}$ mice and their saline-treated respective controls at day 21 **(Figure 4B)**. In contrast, LyM-*Atf6α*$^{fl/fl}$ CD11b^{+} subpopulations expressing CD38 alone, Arg-1/CD206, or dual CD38/CD206 remained elevated at day 21 post bleomycin administration **(Figure 4B)**. To

note, LyM-*Atf6α*$^{fl/fl}$ polarized CD11b^{+} subpopulations remained pre-dominantly of the pro-fibrotic M2-like phenotype at day 21 post bleomycin administration **(Figure 4B)**. Overall, these findings suggest that a mixed M1/M2 population of CD11b^{+} macrophages contributed to the repair process in both WT and myeloid specific ATF6α-deficient mice. Of note, the main difference between the resolving WT mice at day 21 and the fibrotic myeloid specific ATF6α-deficient mice was the continuous presence of "Arg-1^{+}CD206^{+}" and to a lesser extent mixed "CD38^{+}CD206^{+}" CD11b^{+} macrophages, contributing to aggravated tissue remodelling and fibrogenesis.

Myeloid-specific deletion of Atf6α inhibits bone marrow-derived macrophages from producing CHOP and undergoing apoptosis during ex vivo chronic ER stress. To investigate the molecular mechanisms associated with the accumulation of CD11b^{+} macrophages in LyM-*Atf6α*$^{fl/fl}$ mice, we next assessed their capacity to undergo UPR-mediated apoptosis. Bone marrow-derived macrophages **(BMDMs)** were isolated from LyM-*Atf6α*$^{fl/fl}$ and *Atf6α*$^{+/+}$ mice to assess UPR-mediated apoptosis using immunofluorescence, western blotting, and flow cytometry-based approaches. To artificially stimulate ER stress, UPR-mediated CHOP activation and apoptotic cell death, BMDMs were treated with either tunicamycin which blocks protein glycosylation, or thapsigargin which depletes ER calcium stores[29] and incubated for 8 or 16 hours. While neither wild-type or ATF6α-deficient BMDMs exposed to tunicamycin or thapsigargin for 8 hours led to increased CHOP protein expression, CHOP was highly expressed after 16 hours of exposure only in wild-type BMDMs **(Figure 5A)**. As expected, no CHOP signal

was observed in any of the control or vehicle-treated groups **(Figure 5A)**. When BMDMs from both genotypes were exposed to tunicamycin for 24 hours, a reduced CHOP expression in LyM-*Atf6α*$^{fl/fl}$ BMDMs was detected **(Figures 5B-C).** These observations were validated by assessing lactate dehydrogenase **(LDH)** cytotoxicity activity in the supernatant of LyM-*Atf6α*$^{fl/fl}$ and *Atf6α*$^{+/+}$ macrophages exposed to tunicamycin for 24 hours **(Figure 5D)**. Cytotoxicity assay indicated that ATF6α-deficient BMDMs were markedly protected from cell death as shown by the significant reduced level of LDH in the supernatant of tunicamycin-treated LyM-*Atf6α*$^{fl/fl}$ cells compared to tunicamycin-exposed *Atf6α*$^{+/+}$ cells **(Figure 5D)**.

To investigate whether ATF6α-deficient CD11b^{+} macrophage subpopulations lack the ability to undergo apoptosis, we assessed Annexin V staining by flow cytometry. Following 16 hours of treatment, thapsigargin-exposed LyM-*Atf6α*$^{fl/fl}$ BMDMs had a significantly decreased percentage of CD11b^{+}Annexin V^{+} apoptotic macrophages compared to thapsigargin-exposed *Atf6α*$^{+/+}$ BMDMs **(Figure 5E)**. *Atf6α*$^{+/+}$ BMDMs had a significantly higher percentage of CD11b^{+}Annexin V^{+} apoptotic macrophages compared to their vehicle group **(Figure 5E)**. No differences were detected in the percentage of CD11b^{+}Annexin V^{+} cells between any of the tunicamycin-exposed BMDM groups at 16 hour of treatment **(Figure 5E)**. Overall, these data suggest that ATF6α deficiency prevents UPR-mediated apoptosis in macrophages, through a likely requirement of ATF6α for the activation of CHOP.

Myeloid-specific deletion of Atf6α is associated with CHOP-deficient macrophages in fibrotic conditions. To determine the expression level of CHOP in macrophages in lungs of wild-type and LyM-*Atf6α*$^{fl/fl}$ mice in both normal and fibrotic conditions, we used triplex FISH RNAscope® technology and examined *Atf6α*, *CD68*, and *CHOP* mRNA co-localization. In line with the *ex vivo* assessments, we observed that ATF6α-deficient CD68^{+} macrophages were also CHOP deficient *in vivo* **(Figure 6)**. This data further suggests that ATF6α is required for CHOP induction in macrophages.

DISCUSSION

While IPF pathogenesis remains unknown, the current paradigm is that IPF is triggered by recurrent microinjuries and damage to the alveolar epithelium[30,31]. Consequential epithelial and immune cell release of fibrogenic mediators then promote the recruitment of bone marrow–derived cells and mediate fibroblast differentiation into activated myofibroblasts in the lungs[30]. Together these processes promote excessive extracellular matrix deposition and ultimately fibrosis[30]. Chronic ER stress and UPR have been reported to have important roles in fibrotic processes in numerous organs including lung, heart, kidney, liver, and gastrointestinal tract[32,33]. Particularly, an association between ER stress mediators and IPF has been previously reported. Korfei *et al.* (2008) have found that the protein levels of p50ATF6, ATF4, and CHOP, as well as transcript levels of XBP-1, were significantly higher in lung homogenates and type II alveolar epithelial cells **(AECIIs)** of IPF patients compared to control donors[34]. Moreover, Yao *et al.* (2016) previously demonstrated that CHOP expression was significantly elevated in $CD206^+$ M2-like macrophages found in IPF lungs compared to control subjects[16]. We here investigated whether the ATF6α arm of the UPR is required for the regulation of pulmonary macrophage composition and pro-fibrotic function in the context of lung injury, fibrosis, and repair.

M2-polarized alternatively activated macrophages perform a vital role in tissue remodelling and fibrogenesis[11–14]. Consequently, we first assessed the localization of *Atf6α* mRNA in macrophages found in IPF patient lung and in circulating monocytes isolated from IPF patient blood. Subsequently, we developed a novel transgenic mouse model,

where *Atf6* gene, encoding ATF6α protein, was specifically deleted in the myeloid compartment. Myeloid specific ATF6α-deficient mice were administered bleomycin to induce lung injury and fibrogenesis. Our results demonstrated that at a low dose of bleomycin (0.04 units/mouse), myeloid lineage ATF6α-deficient mice exhibited an exacerbated fibrotic response. This was shown by increases in myofibroblast and collagen deposition in the lung. This elevated fibrogenesis was associated with an accumulation of $CD11b^{+}$ macrophage subpopulations with a pre-dominant M2 profile and to a lesser extent a mixed M1/M2 phenotype. These findings shed light on examining the role of ATF6α-mediated apoptosis of macrophages, a mechanism that might be important in the resolution of injury and fibrogenesis.

Macrophages are highly plastic cells that can switch from one functional phenotype to another depending on the stimuli and signals from the environment[10] which make their isolation challenging. Nevertheless, the well-established flow cytometry-based approaches presented here enabled the identification of the various macrophage subpopulations in healthy and fibrotic mouse lungs. Assessing macrophage composition at the different timepoints following bleomycin administration suggested that although macrophage infiltration peaked during the injury phase (day 7) in wild-type mouse lung tissues, cellular composition was restored after 21 days of chronic ER stress/UPR. In contrast, ATF6α-deficient macrophages peaked during the inflammatory phase and persisted until the fibrotic phase (day 21). This macrophage accumulation was associated with aggravated bleomycin-induced tissue remodelling. Consequently, we postulated that macrophage

accumulation at day 21 might be caused by an inability to undergo apoptosis during prolonged ER stress associated with bleomycin-induced lung injury. Further investigations revealed that ATF6α was required for macrophage CHOP-induced apoptotic death during chronic ER stress *ex vivo*. Overall, targeting $CD11b^{+}$ macrophage subpopulations through the ATF6α arm of UPR might offer a potential therapeutic approach to halt IPF progression.

To the best of our knowledge, this is the first report to identify that the ATF6α arm of the UPR is required for CHOP induction and the apoptotic death of bone marrow-derived $CD11b^{+}$ macrophages *ex vivo.* In line with our findings, data obtained from Bommiasamy *et al.* (2009) provided evidence that CHOP was highly expressed in the ATF6α-expressing Chinese hamster ovary cells, whereas cells expressing the other UPR sensors (ATF6β, XBP-1, and ATF4) had much lower levels of CHOP[24]. ATF6α was also found to be required for CHOP-independent apoptosis of myoblast cells during ER stress and that the co-expression of a dominant negative form of ATF6α suppressed apoptosis[35]. Lastly, Forouhan *et al.* (2018) have shown that the knockdown of ATF6α halted the expression of GRP78 and CHOP mRNAs in cells expressing p.N617K (metaphyseal chondrodysplasia type Schmid **(MCDS)** cell culture model)[36]. Taken together, these findings imply that ATF6α is likely required for CHOP production and subsequent apoptosis of different cell types including macrophages as reported in our present studies.

While ATF6α contribution to pulmonary fibrosis has not been fully elucidated, the role of CHOP has been well studied. Our group has previously shown that full body CHOP knockout **($CHOP^{-/-}$)** mice exposed to a single intratracheal dose of bleomycin had increased

lung fibrosis and an accumulation of Arg-1^{+} M2 like macrophages[18]. This suggests that blocking the ability of macrophages to undergo UPR-mediated apoptosis during chronic ER stress can lead to macrophage accumulation in the lung resulting in an increased fibrotic response. In contrast, Burman *et al.* (2018) used repetitive intratracheal bleomycin injury model to induce lung fibrosis in full body CHOP$^{-/-}$ mice and found that CHOP$^{-/-}$ mice were significantly protected from the development of lung fibrosis, shown by a reduction in fibrotic area, decreased soluble collagen content and fibronectin level[37]. In addition, the number of TUNEL^{+} alveolar epithelial cells was significantly lower in repetitive bleomycin-treated CHOP$^{-/-}$ mice compared to wild-type controls. This suggests that in the repetitive bleomycin model, CHOP deficiency protects from lung fibrosis by reducing AEC apoptosis[37]. In another study conducted by Delbrel *et al.* (2018), it was shown that localized hypoxia and hypoxia inducible factor 1 alpha **(HIF-1α)** promote ER stress and CHOP-mediated apoptosis of AEC, indicating their potential role in epithelial cell damage in IPF[38]. Combined with our observations, these data indicate that cell-specific apoptotic modulation, via ATF6α and CHOP-mediated pathways results in different outcomes, depending on the experimental system. CHOP deficiency prevents the excessive apoptosis of the epithelial barrier when using low repetitive doses of bleomycin and this subsequently protects from downstream fibrogenesis. Conversely, ATF6α/CHOP deficiency in the myeloid compartment results in the accumulation of pro-fibrotic macrophages and leads to enhanced fibrotic response. Therefore, the data shed light on compartment specificity knockdown studies rather than full body knock-out animal models. While AEC excessive apoptosis triggers fibrotic processes, macrophage inability to undergo apoptosis is

detrimental. This suggests that cell-specific delivery of therapeutics may be required for the treatment of chronic fibrotic lung diseases as recently proposed[39].

In conclusion, the data presented indicate that the myeloid-specific deletion of ATF6α promotes lung fibrosis by attenuating macrophage CHOP-mediated apoptosis. This results in the persistent expansion of $CD11b^+$ macrophage subpopulations with aberrant function. The specific enhancement of the activity of ATF6α/CHOP arm in $CD11b^+$ macrophage subpopulations through targeted drug delivery to specifically induce apoptosis in this compartment might be a potential therapeutic approach to halt pulmonary fibrosis.

MATERIALS AND METHODS

Single-cell RNA sequencing. Data pre-processed using the cell ranger pipeline (10x Genomics) were obtained from GSE135893, containing samples collected from 12 IPF patients and 10 control subjects. Post-processing was performed using Seurat package in R[40]. The same pipeline described in the source paper (Habermann *et al*, 2020)[25] was followed. Visualizations were created using Seurat. Cell populations were defined using the markers found in the source paper (Habermann *et al*, 2020)[25].

$CD14^+$ cells isolation and bulk RNA sequencing. Approximately 10 mL of fresh whole blood was collected from 12 control subjects and 50 IPF patients. Upon collection, $CD14^+$ cells were isolated directly from whole blood via immunomagnetic negative selection using the EasySep™ Direct Human Monocyte Isolation Kit (STEMCELL Technologies Inc., REF #19669). Cells were subsequently lysed for RNA extraction. The obtained libraries were used for bulk RNA-seq using the Illumina HiSeq 1500. The samples were sequenced with single end reads of 75 base pairs, at an average depth of 9.1 million clusters (ranging from 6 million to 14 million). The reads were filtered based on quality, selecting only the reads with at least 90% of bases having quality score of 20 and higher. Remaining reads were aligned using HISAT2[41] with hg38 (UCSC) reference genome and the reads were counted using HTSeq count[41]. Next, genes exhibiting more than 10 counts in more than 9 samples were selected using filterByExpr (EdgeR package in R[42,43]), resulting in 13,243 genes. These count values were then normalized with TMM normalization method[44] and transformed with voom transformation[45]. Differential expression analysis was performed

using limma package package[46] in R; p-value was corrected with BH correction for multiple testing[47], and corrected values <0.05 were considered to be significant. Violin plot was created using ggplot2 package in R.

Human lung tissue and RNAscope® Assay. All work conducted using human tissues was approved by the Hamilton Integrated Research Ethics Board (11-3559 and 13-523-C). Formalin-fixed paraffin-embedded **(FFPE)** human lung tissues were obtained from a biobank for interstitial lung diseases at St. Joseph's Healthcare in Hamilton, Ontario, Canada. IPF lung biopsies were selected based on clinical, radiological, and a pattern of usual interstitial pneumonia determined by a trained molecular pathologist. Non-cancerous tissues from lung cancer cases were used as controls. Fibrotic regions in IPF patients and non-tumour areas in control subjects were selected to be placed into a tissue microarray **(TMA)** block. The TMA was processed for RNAscope® fluorescent *in situ* hybridization multiplex assay (Advanced Cell Diagnostics **(ACD)**, Inc.) to assess the co-localization of human *Atf6α* (ACD, Cat# 555298), *CD68* (ACD, Cat# 560598), and *Mrc1* (ACD, Cat# 583928) mRNAs. The bacterial probe dapB was used as a negative control to ensure that there is no background staining related to the assay and that the tissue specimen is appropriately prepared. High definition images were acquired using the Olympus VS120 Slide Scanner at a 40× magnification as previously described[14,18,48].

Animals. Female and male wild-type C57BL/6 **(*Atf6α*$^{+/+}$)** mice were commercially obtained from either Charles River Laboratories (PQ, Canada) or The Jackson Laboratories (Maine, USA). Myeloid specific ATF6α-deficient **(LyM-*Atf6α*$^{fl/fl}$)** mice were developed

utilizing Cre-LoxP recombination system and were bred in-house. In the present studies, *Atf6α*$^{+/+}$ mice were age-matched with LyM-*Atf6α*$^{fl/fl}$ mice with ages falling between 6 and 14 weeks at day 0. Two female *Atf6*$^{fl/fl}$ floxed mice **B6(cg) – *Atf6*^{tm1Hota}/J** which were homozygous for *Atf6* gene were bred with one male **B6.129P2-*Lyz2* $^{tm1(cre)Ifo}$/J** (also known as LysMcre). The *Atf6*$^{fl/fl}$ floxed mice had the *Atf6* gene which codes for "p90ATF6α" protein[20], being flanked by LoxP sites. LysMcre mouse had the Cre recombinase gene being inserted into the lysozyme 2 **(Lyz2)** which is a promoter region found in all cells of the myeloid lineage. After 1-2 months of breeding, the entire F1 generation born was heterozygous. One male from F1 was bred with two new unbred female *Atf6*$^{fl/fl}$ floxed mice. After 1-2 months of breeding, 4 different genotypes of F2 generation were produced. Only 25% of F2 generation had the *Atf6* gene being deleted from the myeloid lineage. Mice were genotyped to select the desired genotype. B6(cg) – *Atf6*^{tm1Hota}/J and B6.129P2-*Lyz2* $^{tm1(cre)Ifo}$/J (both with C57BL/6 background) were purchased from The Jackson Laboratories (Maine, USA) (Cat# 028253 and 004781, respectively). All strains of mice were housed in the Central Animal Facility at McMaster University (Hamilton, ON, Canada). The animals were kept on a 12 h light/12 h dark cycle and fed *ad libitum*. All animal work was approved by the Animal Research Ethics Board at McMaster University (# 19-08-23).

DNA genotyping and standard polymerase chain reaction. Broncheoalveolar lavage cells were collected from male and female *Atf6α*$^{+/+}$ and LyM-*Atf6α*$^{fl/fl}$ mice (n=5-7) and macrophages were cultured. DNA genotyping was performed on adhered macrophages according to the KAPA Mouse Genotyping Kit protocol (Millipore Sigma, cat# KK7302).

The following primers (prepared by Integrated DNA technologies) were used for standard PCR: *Atf6* forward primer with a sequence of **5'- TGC ATC TGG GAA GAG AAC CA -3'**, *Atf6* WT reverse primer with a sequence of **5'- TGC CAT GAA CTA CCA TGT CAC -3'**, and *Atf6* mutant reverse primer with a sequence of **5'- AGA CTG CCT TGG GAA AAG CG -3'**. Cells from a heterozygous mouse having both the mutant **(KO)** (160 bp) and the WT (101 bp) bands and cells from a mouse being homozygous to the mutant gene (160 bp) were used as controls.

Intratracheal administration of bleomycin. Experimental pulmonary fibrosis was induced with a single intratracheal instillation of a suboptimal dose of bleomycin (0.04 units/mouse in a volume of 50 µl sterile saline). Control animals received vehicle (sterile saline) alone (50 µl per mouse). Weights of animals were monitored regularly, and endpoint measures were conducted following 7 (inflammatory phase) or 21 (fibrotic phase) days of bleomycin intubation.

Measurement of respiratory mechanics. Lung function assessments were conducted using a flexiVent® mechanical respirator (flexiVent®, SCIREQ, Montreal, PQ, Canada) according to SCIREQ Scientific Respiratory Equipment Inc.'s published protocols[49]. FlexiVent® enabled the measurement of lung elastance which is a functional parameter derived from the pressure-driven pressure–volume loops.

Single lobe-lung processing for histopathology. Mouse left lungs were inflated, fixed in 10% formalin for 48 hours, and processed for subsequent immunohistochemistry (**IHC**) and RNAscope® fluorescent *in situ* hybridization staining. Briefly, lungs were cut, placed

into histology cassettes, embedded in paraffin wax, and a TMA was generated. Following the development of a TMA containing mouse lung tissues[48], 5 µm lung sections were cut and stained on a Bond RX fully automated research Stainer (Leica Biosystems)[14,18]. IHC staining on lung serial sections was performed for α-smooth muscle actin, Masson's trichrome, and CD206. In addition, RNAscope® fluorescent *in situ* hybridization multiplex assay was conducted to assess the co-localization of mouse *Atf6α* (ACD, Cat# 555278), *CD68* (ACD, Cat# 316618), and CHOP (*Ddit3*) (ACD, Cat# 317668) mRNAs. Lastly, IHC and FISH stained-microscope slides were digitalised using an Olympus VS120-L100-W slide scanner at a 20× (IHC) or 40× (FISH) magnification and IHC stained-slides were quantified using HALO™ Image Analysis Software (Halo Plus 3.2, Indica Labs)[48].

Multi-lobe-lung processing for flow cytometric assessment. To obtain single cell suspensions, mouse right superior, middle, inferior, and post-caval lobes were enzymatically digested (0.3 mg/mL collagenase type I, 50 units/mL Deoxyribonuclease I from bovine pancreas **(DNase I),** and 1000 units/mL Hyaluronidase from bovine testes) for 2-3 hours shaking at 37°C. Digested lung was crushed through 40 µm filter. Cell count was performed using Countess™ automated cell counter (Invitrogen, Cat# C10281). Trypan blue stain 0.4% (Invitrogen, cat# T10282) was used to test for cellular viability. Single cell suspensions were suspended in cell staining buffer (0.5% BSA in PBS), non-antigen-specific binding of immunoglobulins to Fcγ II/ III receptor was blocked using purified rat anti-mouse CD16/32 antibody (mouse FC block), and cells were subsequently stained for

flow cytometric analysis using antibodies shown in **Table S1**. All samples were run on a BD LSRFortessa (BD Biosciences, ON, Canada).

Processing of mouse bone marrow-derived macrophages for protein analysis. BMDMs were isolated and cultured as previously described[50]. In brief, bone marrow cells were obtained from the femur, tibia, hib, and spine of female or male *Atf6α*$^{+/+}$ (n=3-5) and LyM-*Atf6α*$^{fl/fl}$ (n=3-5) mice and cultured with 20 ng/mL macrophage colony-stimulating factor **(M-CSF)** (PeproTech, Cat# AF-315-02) for 5-7 days to differentiate them into macrophages. Next, adhered macrophages were lifted using Accutase™ (Stemcell™, Cat# 07920) and cell scraper, counted, and plated in either 60 × 15 mm petri dishes with a density of 6-8 × 10^6 cells for flow cytometry assessment, in 6-well plates with a density of 2-3 × 10^6 cells for western blotting, or with a density of 300,000 cells/well on glass coverslips that were previously placed in 12-well plates for immunofluorescence analysis. Adhered macrophages were then treated with either tunicamycin (2 or 20 μg/mL) (Sigma Life Science, Cat # T7765), thapsigargin (20 μg/mL) (Sigma Life Science, Cat # T9033), or control media alone. Since tunicamycin and thapsigargin were dissolved in dimethylsulfoxide **(DMSO)**, DMSO was used as vehicle control. Following 8, 16, and 24 hours of treatment, stimulated macrophages were processed for either western blotting or immunofluorescence. Following 16 hours of treatment, stimulated adhered macrophages were lifted and stained for flow cytometry assessment of CD11b$^+$Annexin V$^+$ cells **(Table S1)**. Annexin V flow cytometry staining was performed according to the manufacturer's protocol (Thermo Fisher Scientific).

Western blotting. Cells were lysed with either Radioimmunoprecipitation assay **(RIPA)** buffer containing protease inhibitor (Na_3VO_4 (200 mM), aprotinin, phenylmethylsulfonyl fluoride **(PMSF)** (0.1 mM), and 1,4-Dithiothreitol **(DTT)** (1 M) or with TRIzol. Protein was extracted from cells treated with TRIzol according to the manufacturer's protocol (Thermo Fisher Scientific). Cell lysates were loaded onto 12% SDS-PAGE gels (20 µg of protein/well) and separated by electrophoresis at 90V for 90 minutes, then transferred to nitrocellulose membranes at 400 mA for 60 minutes. Blots were blocked using Odyssey Blocking Buffer (LI-COR Biosciences, Lincoln, NE, USA) for 1 hour at room temperature, then probed using the following antibodies overnight at 4°C: actin (C-4, Santa Cruz Biotechnology), diluted 1:1000, and CHOP (L63F7, Cell signalling Technology, Whitby, ON, Canada), diluted 1:1000. Following 24 hours, blots were washed with TBS + 0.15% Tween20, and IRDye® goat anti-mouse secondary antibodies (LI-COR, Biosciences, Lincoln, NE, USA) was added to the blots for 60 minutes at room temperature. After subsequent washes, blots were imaged using Odyssey LI-COR Imaging System (Lincoln, NE, USA). Protein band signals of interest were quantified by densitometry using Image Studio Lite.

Immunofluorescence staining and quantification. Immunofluorescence was conducted as previously described[19]. In brief, cells were fixed with 4% Paraformaldehyde **(PFA)** solution in PBS (Boster Biological Technology, Cat# AR1068) and permeabilized using 0.1% Triton X. Cells were then stained with Alexa Fluor 488-labeled anti-GADD153/CHOP (Novus Biologicals, Cat# NB600-1335AF488). ProLong™ Gold

Antifade Mountant with DAPI (Thermo Fisher Scientific, Cat# P36931) was used and 3-5 images (at least 5-92 cells per image) per each condition were taken at 40× magnification using fluorescence microscopy. Exposure time was kept constant during imaging at 300 milliseconds (ms) for CHOP and 20 ms for DAPI for all slides. ImageJ software (National Institutes of Health, Bethesda, MD, USA) was used to analyze and quantify antibody expression. The number of cells was counted, and thresholding was used to detect percent of positive cells. CHOP and DAPI were analyzed at threshold levels of 55 and 53, respectively. The % of positive cells for each image was calculated and graphed.

Cytotoxicity assay. Following 24 hours of treatment, supernatants from adhered macrophages were collected and stored for lactate dehydrogenase measurements using "Pierce LDH cytotoxicity assay" which was conducted according to the manufacturer's protocol (Thermo Fisher Scientific, Cat# 88954).

Statistical analysis. All results were expressed as mean ± standard error of the mean. All graphs and statistical tests were performed using GraphPad Prism 9.1 (GraphPad Software, Inc). Two-way ANOVA followed by Tukey's multiple comparisons test was used to determine significance. A $p < 0.05$ was considered statistically significant.

Data availability. The current study datasets are available upon request from the corresponding author.

ACKNOWLEDGMENTS

We sincerely thank Mary Jo Smith and Mary Bruni at McMaster Immunology Research Centre John Mayberry histology facility (McMaster University, ON, Canada) for their technical help in immunohistochemistry and RNAscope® fluorescent *in situ* hybridization. We thank Christine King (Farncombe Metagenomics Facility, McMaster University, ON, Canada) for assistance with bulk RNA-seq experiments. This work was funded by the Canadian Pulmonary Fibrosis Foundation and the Lung Health Foundation.

AUTHOR CONTRIBUTIONS

Conception and design: OM and KA; Performed experiments: OM, SDR, AIH, KM, MV, AA, aR, MP, JI, EA; Analysis and interpretations: OM, SPC, ADG, AR, JAH, CDR, DB, MRS, NH, AN, MRJK, and KA; Drafting the manuscript: OM; Edited and revised manuscript: OM, SDR, SPC, MV, and KA. All authors read and approved the final version.

FIGURE LEGENDS

Figure 1. *Atf6α* mRNA is expressed in human macrophages and circulating monocytes associated with fibrotic lung diseases. (A) Expression level of *Atf6α* mRNA across cell populations in both healthy and IPF subjects. ScRNA-seq was performed on samples obtained from peripheral lung tissues removed at the time of lung transplant surgery from patients with IPF (n = 12) and from non-fibrotic controls (n = 10)**. Left panel:** UMAP plot showing all identified cell populations. **Middle panel:** UMAP plot showing level of expression of *Atf6α*. **Right panel:** Violin plot showing level of expression of *Atf6α* in the identified cell populations. **(B)** FISH representative images showing the co-localization of *Atf6α*, *CD68*, and *Mrc1* mRNA (puncta) in lung tissues obtained from non-fibrotic control subject and IPF patient. Negative controls for each region are shown. **(C)** Bulk RNA-seq analysis showing RNA expression of *Atf6α* in $CD14^{+}$ circulating monocytes. Violin plot showing normalized expression levels of 12 control subjects and 50 IPF patients. Medians are marked by red dots within the violin shapes.

Figure 2. Myeloid-specific deletion of *Atf6α* results in an enhanced bleomycin-induced tissue remodelling associated with increased pro-fibrotic macrophage subpopulations. Transgenic myeloid specific *Atf6α*-deficient mouse model (LyM-$Atf6\alpha^{fl/fl}$) was developed and DNA genotype was verified using **(A)** PCR and **(B)** FISH RNAscope® technology. $Atf6\alpha^{+/+}$ and LyM-$Atf6\alpha^{fl/fl}$ mice were intubated intratracheally with a suboptimal single dose of bleomycin (0.04 units/mouse) and fibrosis was assessed

after 21 days using immunohistochemistry staining on generated TMA and biomechanical measurements. Collagen deposition, myofibroblast and pro-fibrotic macrophage accumulation are shown respectively by serial sections of **(C-E [left panel])** representative Masson's Trichrome, α-SMA, and CD206-stained lung images of sterile saline-, and bleomycin-exposed animals. The figure also shows representative images generated by HALO™ Image Analysis Software used to quantify the different IHC stain through cytonuclear and area quantification modules (Halo Plus 3.2, Indica Labs). **(C-E [right panel])** Halo quantification from saline- and bleomycin-exposed lung tissues. **(F)** Total lung elastance measurement. Data shown mean ± SEM, n = 4-5; *p<0.05; **p<0.01; ***p<0.001; *represent a difference between the indicated groups. Two-way ANOVA followed by Tukey's multiple comparisons test.

Figure 3. Myeloid-specific deletion of *Atf6α* results in increased CD11b$^+$ macrophage subpopulations. *Atf6α*$^{+/+}$ and LyM-*Atf6α*$^{fl/fl}$ mice were intubated intratracheally with a suboptimal single dose of bleomycin (0.04 units/mouse), and multi-lobe-right lungs were enzymatically digested and processed for flow cytometry after 7 and 21 days. **(A)** Flow cytometry gating strategy used to identify total macrophages **(MΦ)**, alveolar macrophages **(AM)**, and interstitial macrophages **(IM)**. Single cells were gated from all cells to exclude doublets and debris, then CD45.2$^+$ immune cells were obtained. F4/80$^+$CD64$^+$ total MΦ populations were gated from CD45.2$^+$ immune cells. Total MΦ populations were further divided into IM and AM based on the expression of CD11b and CD11c. SiglecF$^+$ AM was also gated from CD11c$^+$CD11b$^-$ AM. Fluorescence minus one **(FMO)** was used to gate

each of the population of interest. **(B-C)** Graphs showing the absolute numbers of F4/80^{+}CD64^{+} total MΦ, SiglecF^{+} AM, and CD11b^{+} IM following 7 or 21 days of bleomycin administration. Data shown mean ± SEM, n = 3-5; *p<0.05; **p<0.01; ***p<0.001; *represent a difference between the indicated groups. Two-way ANOVA followed by Tukey's multiple comparisons test.

Figure 4. Myeloid-specific deletion of *Atf6α* results in increased CD11b^{+} macrophage subpopulations with dual CD38^{+}CD206^{+} expression. *Atf6α*$^{+/+}$ and LyM-*Atf6α*$^{fl/fl}$ mice were intubated intratracheally with a suboptimal single dose of bleomycin (0.04 units/mouse), and multi-lobe-right lungs were enzymatically digested and processed for flow cytometry after 7 and 21 days. **(A-B)** Graphs showing the absolute numbers of SiglecF^{+} macrophages expressing CD38, Arg-1/CD206, or dual CD38/CD206, and CD11b^{+} macrophages expressing CD38, Arg-1/CD206, or dual CD38/CD206 following 7 or 21 days of bleomycin administration. Data shown mean ± SEM, n = 3-5; *p<0.05; **p<0.01; ***p<0.001; *represent a difference between the indicated groups. Two-way ANOVA followed by Tukey's multiple comparisons test.

Figure 5. Myeloid-specific deletion of *Atf6α* inhibits CHOP induction and halts the apoptotic death of bone marrow-derived CD11b^{+} macrophages during *ex vivo* chronic ER stress. Following *Atf6α*$^{+/+}$ and LyM-*Atf6α*$^{fl/fl}$ BMDM exposure to tunicamycin or thapsigargin for 8, 16, and 24 hours, cells were subjected to western blotting, immunofluorescence staining, or flow cytometry assessments. **(A)** Representative western

blot image, analysis, and densitometry of CHOP and actin. Samples (n=3 per group) were derived from the same experiment and run on blots in parallel. **(B)** Representative images showing immunofluorescence staining of CHOP. **(C)** Graph demonstrating immunofluorescence quantification of CHOP. **(D)** LDH cytotoxicity assay performed on cell supernatant. **(E)** Annexin V assessment of $CD11b^+$ BMDMs using flow cytometry. Data shown mean ± SEM, n = 3-10; *p<0.05; **p<0.01; ***p<0.001; **** p<0.0001; *represent a difference between the indicated groups. Two-way ANOVA followed by Tukey's multiple comparisons test.

Figure 6. Myeloid-specific deletion of *Atf6α* is associated with CHOP deficiency in macrophages during bleomycin-induced tissue remodelling. FISH representative images showing the co-localization of *Atf6α* and *Chop* mRNAs in $CD68^+$ macrophages in lung tissues obtained from *Atf6α*$^{+/+}$ and LyM-*Atf6α*$^{fl/fl}$ mice following 21 days of saline or bleomycin instillation.

SUPPLEMENTAL TABLE LEGENDS

Table S1. Flow cytometry panel. A panel of surface and intracellular markers designed to examine the different macrophage subpopulations in single mononuclear mouse lung cells.

REFERENCES

1. Lederer, D. J. & Martinez, F. J. Idiopathic Pulmonary Fibrosis. *New England Journal of Medicine* **378**, 1811–1823 (2018).
2. Fujimoto, H., Kobayashi, T. & Azuma, A. Idiopathic Pulmonary Fibrosis: Treatment and Prognosis. *Clin Med Insights Circ Respir Pulm Med* **9s1**, CCRPM.S23321 (2015).
3. Kalchiem-Dekel, O., Galvin, J. R., Burke, A. P., Atamas, S. P. & Todd, N. W. Interstitial Lung Disease and Pulmonary Fibrosis: A Practical Approach for General Medicine Physicians with Focus on the Medical History. *J Clin Med* **7**, (2018).
4. Misharin, A. V. *et al.* Monocyte-derived alveolar macrophages drive lung fibrosis and persist in the lung over the life span. *The Journal of Experimental Medicine* **214**, 2387–2404 (2017).
5. Adams Taylor S *et al.* Single Cell RNA-seq reveals ectopic and aberrant lung resident cell populations in Idiopathic Pulmonary Fibrosis. *Science Advances* **6**, 1–28 (2020).
6. Morse, C. *et al.* Proliferating SPP1/MERTK-expressing macrophages in idiopathic pulmonary fibrosis. *European Respiratory Journal* **54**, (2019).
7. Reyfman, P. A. *et al.* Single-cell transcriptomic analysis of human lung provides insights into the pathobiology of pulmonary fibrosis. *American Journal of Respiratory and Critical Care Medicine* **199**, 1517–1536 (2019).

8. Joshi, N. *et al.* A spatially restricted fibrotic niche in pulmonary fibrosis is sustained by M-CSF/M-CSFR signalling in monocyte-derived alveolar macrophages. *The European respiratory journal* **55**, (2020).
9. McCubbrey, A. L. *et al.* Deletion of c-FLIP from CD11bhi Macrophages Prevents Development of Bleomycin-induced Lung Fibrosis. *Am J Respir Cell Mol Biol* **58**, 66–78 (2018).
10. Zhang, L. *et al.* Macrophages: friend or foe in idiopathic pulmonary fibrosis? *Respir Res* **19**, 170 (2018).
11. Prasse, A. *et al.* A Vicious Circle of Alveolar Macrophages and Fibroblasts Perpetuates Pulmonary Fibrosis via CCL18. *Am J Respir Crit Care Med* **173**, 781–792 (2006).
12. Gibbons, M. A. *et al.* Ly6Chi Monocytes Direct Alternatively Activated Profibrotic Macrophage Regulation of Lung Fibrosis. *Am J Respir Crit Care Med* **184**, 569–581 (2011).
13. Misharin, A. V., Morales-Nebreda, L., Mutlu, G. M., Budinger, G. R. S. & Perlman, H. Flow Cytometric Analysis of Macrophages and Dendritic Cell Subsets in the Mouse Lung. *Am J Respir Cell Mol Biol* **49**, 503–510 (2013).
14. Ayaub, E. A. *et al.* Overexpression of OSM and IL-6 impacts the polarization of pro-fibrotic macrophages and the development of bleomycin-induced lung fibrosis. *Scientific Reports* **7**, 1–16 (2017).
15. Oh, J. *et al.* Endoplasmic Reticulum Stress Controls M2 Macrophage Differentiation and Foam Cell Formation. *J Biol Chem* **287**, 11629–11641 (2012).

16. Yao, Y. *et al.* Chop Deficiency Protects Mice Against Bleomycin-induced Pulmonary Fibrosis by Attenuating M2 Macrophage Production. *Mol Ther* **24**, 915–925 (2016).
17. Burman, A., Tanjore, H. & Blackwell, T. S. Endoplasmic reticulum stress in pulmonary fibrosis. *Matrix Biol* **68–69**, 355–365 (2018).
18. Ayaub, E. A. *et al.* GRP78 and CHOP modulate macrophage apoptosis and the development of bleomycin-induced pulmonary fibrosis. *The Journal of Pathology* **239**, 411–425 (2016).
19. Ayaub, E. A. *et al.* IL-6 mediates ER expansion during hyperpolarization of alternatively activated macrophages. *Immunol Cell Biol* **97**, 203–217 (2019).
20. Haze, K. *et al.* Identification of the G13 (cAMP-response-element-binding protein-related protein) gene product related to activating transcription factor 6 as a transcriptional activator of the mammalian unfolded protein response. *Biochem J* **355**, 19–28 (2001).
21. Haze, K., Yoshida, H., Yanagi, H., Yura, T. & Mori, K. Mammalian transcription factor ATF6 is synthesized as a transmembrane protein and activated by proteolysis in response to endoplasmic reticulum stress. *Mol Biol Cell* **10**, 3787–3799 (1999).
22. Wang, X., Karamariti, E., Simpson, R., Wang, W. & Xu, Q. Dickkopf Homolog 3 Induces Stem Cell Differentiation into Smooth Muscle Lineage via ATF6 Signalling. *J Biol Chem* **290**, 19844–19852 (2015).
23. Krawczyk, K. K. *et al.* Assessing the contribution of thrombospondin-4 induction and ATF6α activation to endoplasmic reticulum expansion and phenotypic modulation in bladder outlet obstruction. *Sci Rep* **6**, 32449 (2016).

24. Bommiasamy, H. *et al.* ATF6alpha induces XBP1-independent expansion of the endoplasmic reticulum. *J Cell Sci* **122**, 1626–1636 (2009).
25. Habermann, A. C. *et al.* Single-cell RNA sequencing reveals profibrotic roles of distinct epithelial and mesenchymal lineages in pulmonary fibrosis. *Science Advances* **6**, eaba1972 (2020).
26. Tat, V. *et al.* FK506-Binding Protein 13 Expression Is Upregulated in Interstitial Lung Disease and Correlated with Clinical Severity. A Potentially Protective Role. *Am J Respir Cell Mol Biol* **64**, 235–246 (2021).
27. Jablonski, K. A. *et al.* Novel Markers to Delineate Murine M1 and M2 Macrophages. *PLoS One* **10**, (2015).
28. Gibbings, S. L. *et al.* Three Unique Interstitial Macrophages in the Murine Lung at Steady State. *Am J Respir Cell Mol Biol* **57**, 66–76 (2017).
29. Li, Y., Guo, Y., Tang, J., Jiang, J. & Chen, Z. New insights into the roles of CHOP-induced apoptosis in ER stress. *Acta Biochim Biophys Sin (Shanghai)* **46**, 629–640 (2014).
30. Fernandez, I. E. & Eickelberg, O. The Impact of TGF-β on Lung Fibrosis: From Targeting to Biomarkers. *Proc Am Thorac Soc* **9**, 111–116 (2012).
31. Sgalla, G. *et al.* Idiopathic pulmonary fibrosis: pathogenesis and management. *Respir Res* **19**, (2018).
32. Lenna, S. & Trojanowska, M. The role of endoplasmic reticulum stress and the unfolded protein response in fibrosis. *Curr Opin Rheumatol* **24**, (2012).

33. Tanjore, H., Lawson, W. E. & Blackwell, T. S. Endoplasmic reticulum stress as a pro-fibrotic stimulus. *Biochim Biophys Acta* **1832**, 940–947 (2013).
34. Korfei, M. *et al.* Epithelial endoplasmic reticulum stress and apoptosis in sporadic idiopathic pulmonary fibrosis. *Am J Respir Crit Care Med* **178**, 838–846 (2008).
35. Morishima, N., Nakanishi, K. & Nakano, A. Activating Transcription Factor-6 (ATF6) Mediates Apoptosis with Reduction of Myeloid Cell Leukemia Sequence 1 (Mcl-1) Protein via Induction of WW Domain Binding Protein 1 *. *Journal of Biological Chemistry* **286**, 35227–35235 (2011).
36. Forouhan, M., Mori, K. & Boot-Handford, R. P. Paradoxical roles of ATF6α and ATF6β in modulating disease severity caused by mutations in collagen X. *Matrix Biol* **70**, 50–71 (2018).
37. Burman, A. *et al.* Localized hypoxia links ER stress to lung fibrosis through induction of C/EBP homologous protein. *JCI Insight* **3**, (2018).
38. Delbrel, E. *et al.* HIF-1α triggers ER stress and CHOP-mediated apoptosis in alveolar epithelial cells, a key event in pulmonary fibrosis. *Scientific Reports* **8**, 17939 (2018).
39. Naiel, S. *et al.* Protein Misfolding and Endoplasmic Reticulum Stress in Chronic Lung Disease: Will Cell-Specific Targeting Be the Key to the Cure? *Chest* **157**, 1207–1220 (2020).
40. Satija, R., Farrell, J. A., Gennert, D., Schier, A. F. & Regev, A. Spatial reconstruction of single-cell gene expression data. *Nature Biotechnology* **33**, 495–502 (2015).
41. Anders, S., Pyl, P. T. & Huber, W. HTSeq--a Python framework to work with high-throughput sequencing data. *Bioinformatics* **31**, 166–169 (2015).

42. Robinson, M. D., McCarthy, D. J. & Smyth, G. K. edgeR: a Bioconductor package for differential expression analysis of digital gene expression data. *Bioinformatics* **26**, 139–140 (2010).
43. McCarthy, D. J., Chen, Y. & Smyth, G. K. Differential expression analysis of multifactor RNA-Seq experiments with respect to biological variation. *Nucleic Acids Res* **40**, 4288–4297 (2012).
44. Robinson, M. D. & Oshlack, A. A scaling normalization method for differential expression analysis of RNA-seq data. *Genome Biology* **11**, R25 (2010).
45. Law, C. W., Chen, Y., Shi, W. & Smyth, G. K. voom: precision weights unlock linear model analysis tools for RNA-seq read counts. *Genome Biology* **15**, R29 (2014).
46. Ritchie, M. E. *et al.* limma powers differential expression analyses for RNA-sequencing and microarray studies. *Nucleic Acids Res* **43**, e47 (2015).
47. Benjamini, Y. & Hochberg, Y. Controlling the False Discovery Rate: A Practical and Powerful Approach to Multiple Testing. *Journal of the Royal Statistical Society: Series B (Methodological)* **57**, 289–300 (1995).
48. Mekhael, O. *et al.* Mouse Models of Lung Fibrosis. in *Myofibroblasts: Methods and Protocols* (eds. Hinz, B. & Lagares, D.) 291–321 (Springer US, 2021). doi:10.1007/978-1-0716-1382-5_21.
49. McGovern, T. K., Robichaud, A., Fereydoonzad, L., Schuessler, T. F. & Martin, J. G. Evaluation of respiratory system mechanics in mice using the forced oscillation technique. *Journal of Visualized Experiments* **75**, (2013).

50. Zhang, X., Goncalves, R. & Mosser, D. M. The isolation and characterization of murine macrophages. *Curr Protoc Immunol* **Chapter 14**, Unit 14.1 (2008).

TABLES

Antibody Specificity	Conjugate	Clone	Supplier
CD11b	BV650	M1/70	Biolegend
F4/80	PE-CF594	T45-2342	BD Biosciences
CD45.2	APC-Cy7	104	Biolegend
CD64	PE-Cy7	X54-5/7.1	Biolegend
CD11c	BV510	N418	Biolegend
SiglecF	BV421	E50-2440	BD Biosciences
Arginase-1	PE	-	R&D systems
CD206	Alexa Fluor 700	C068C2	Biolegend
CD38	BV605	90	BD Biosciences
CD16/CD32 (Fc block)	-	-	BD Biosciences
Annexin V	APC	-	Thermo Fisher Scientific

Table S1

FIGURES

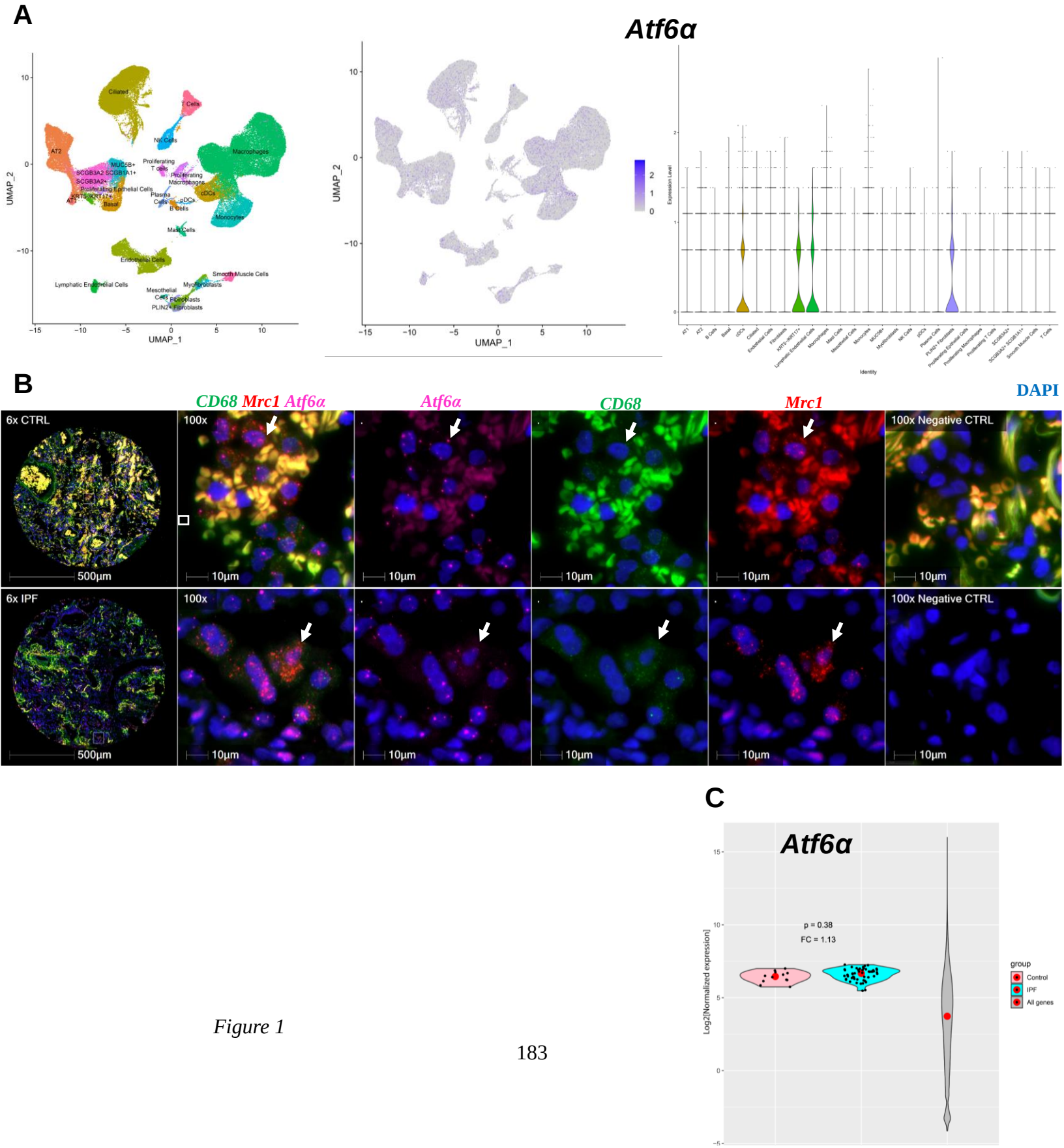

Figure 1

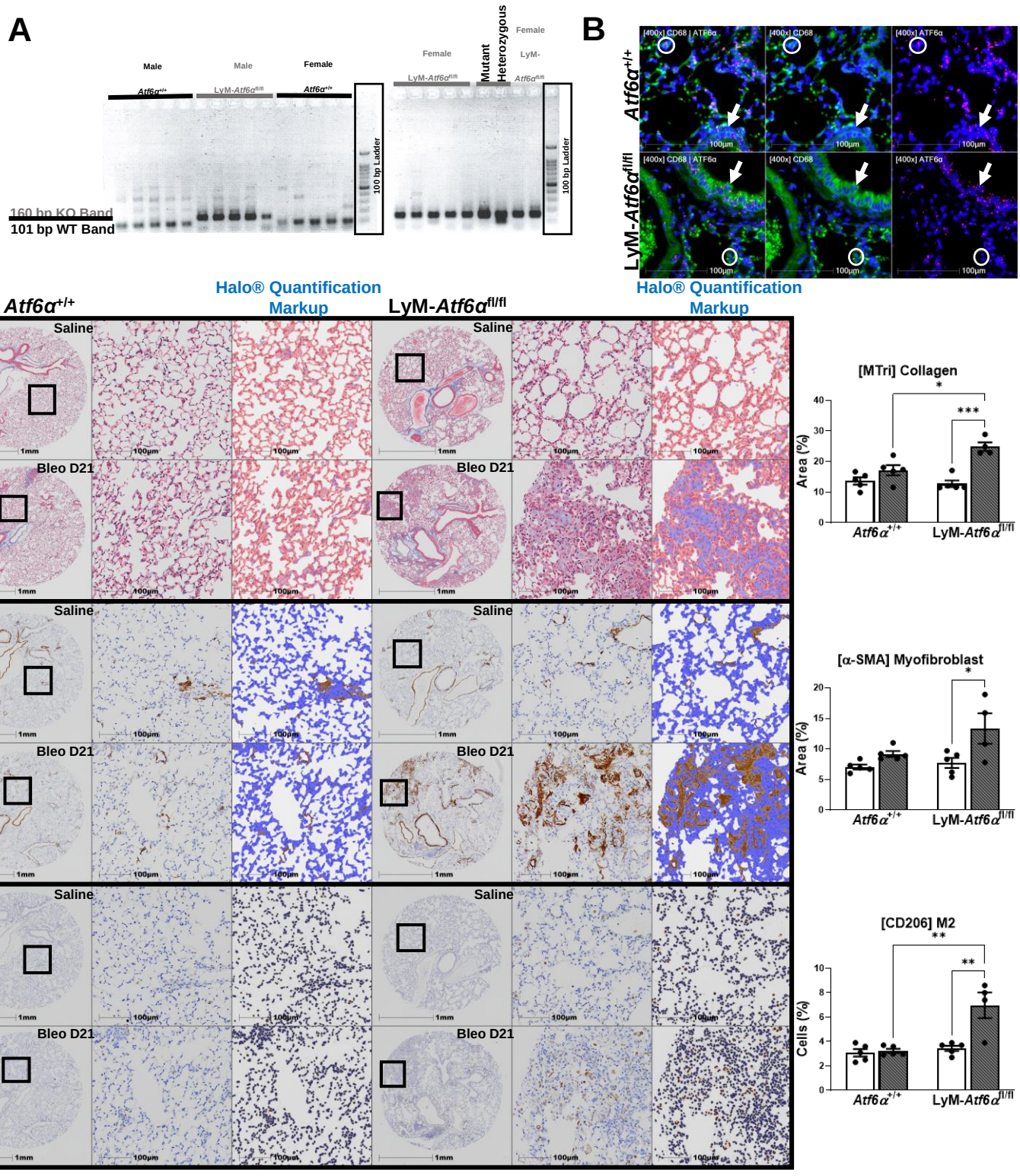
A
Male
Male
Female
Female
Mutant
Heterozygous
Female
LyM-
100 bp Ladder
160 bp KO Band
101 bp WT Band
B
Atf6α+/+
LyM-Atf6αfl/fl
[400x] CD68 | ATF6α
[400x] CD68
[400x] ATF6α
100µm
C
Masson's Trichrome
Atf6α+/+
LyM-Atf6αfl/fl
Halo® Quantification Markup
Saline
Bleo D21
1mm
100µm
[MTri] Collagen
Area (%)
Vehicle
Bleomycin D21
D
α-SMA
[α-SMA] Myofibroblast
E
CD206
[CD206] M2
Cells (%)
F
Total Lung Elastance
Est (cmH2O/mL)

Figure 2

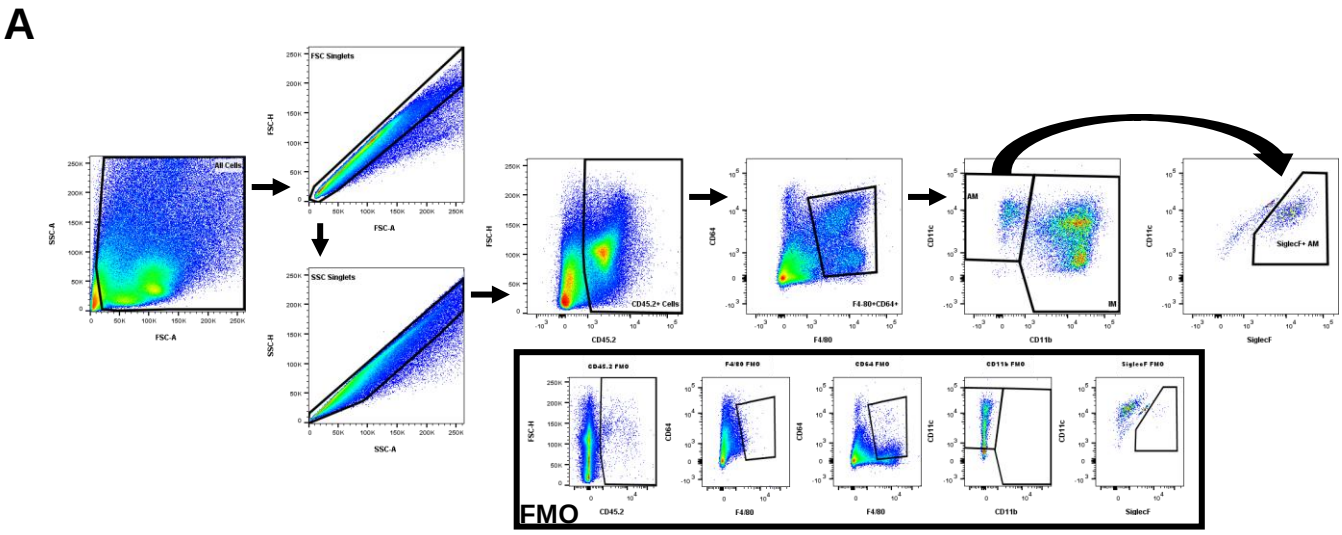
A
All Cells
FSC Singlets
SSC Singlets
CD45.2+ Cells
F4/80+CD64+
AM
IM
SiglecF+ AM
FMO

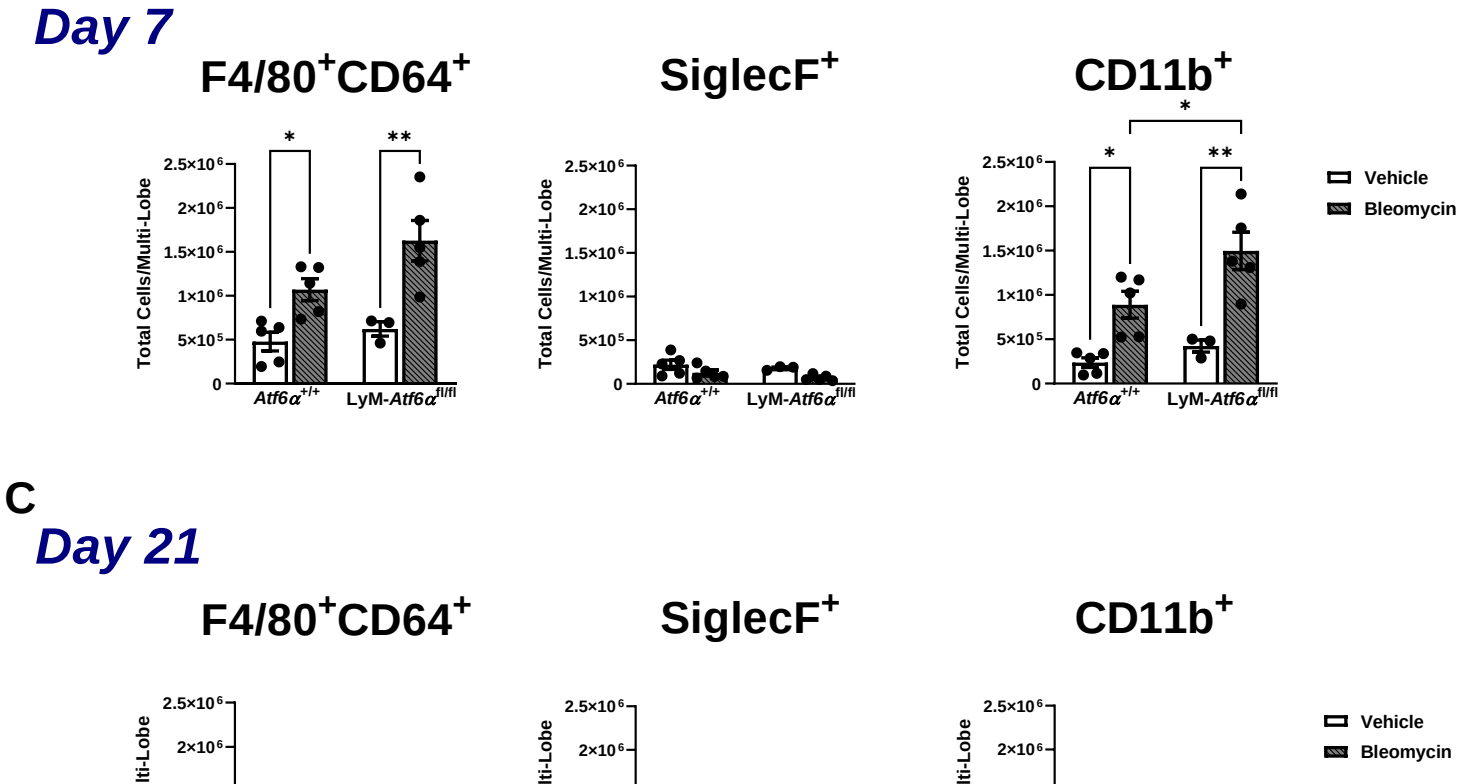
B
Day 7
F4/80+CD64+
SiglecF+
CD11b+
Total Cells/Multi-Lobe
Atf6α+/+
LyM-Atf6αfl/fl
Vehicle
Bleomycin
C
Day 21
F4/80+CD64+
SiglecF+
CD11b+
Total Cells/Multi-Lobe
Atf6α+/+
LyM-Atf6αfl/fl
Vehicle
Bleomycin

Figure 3

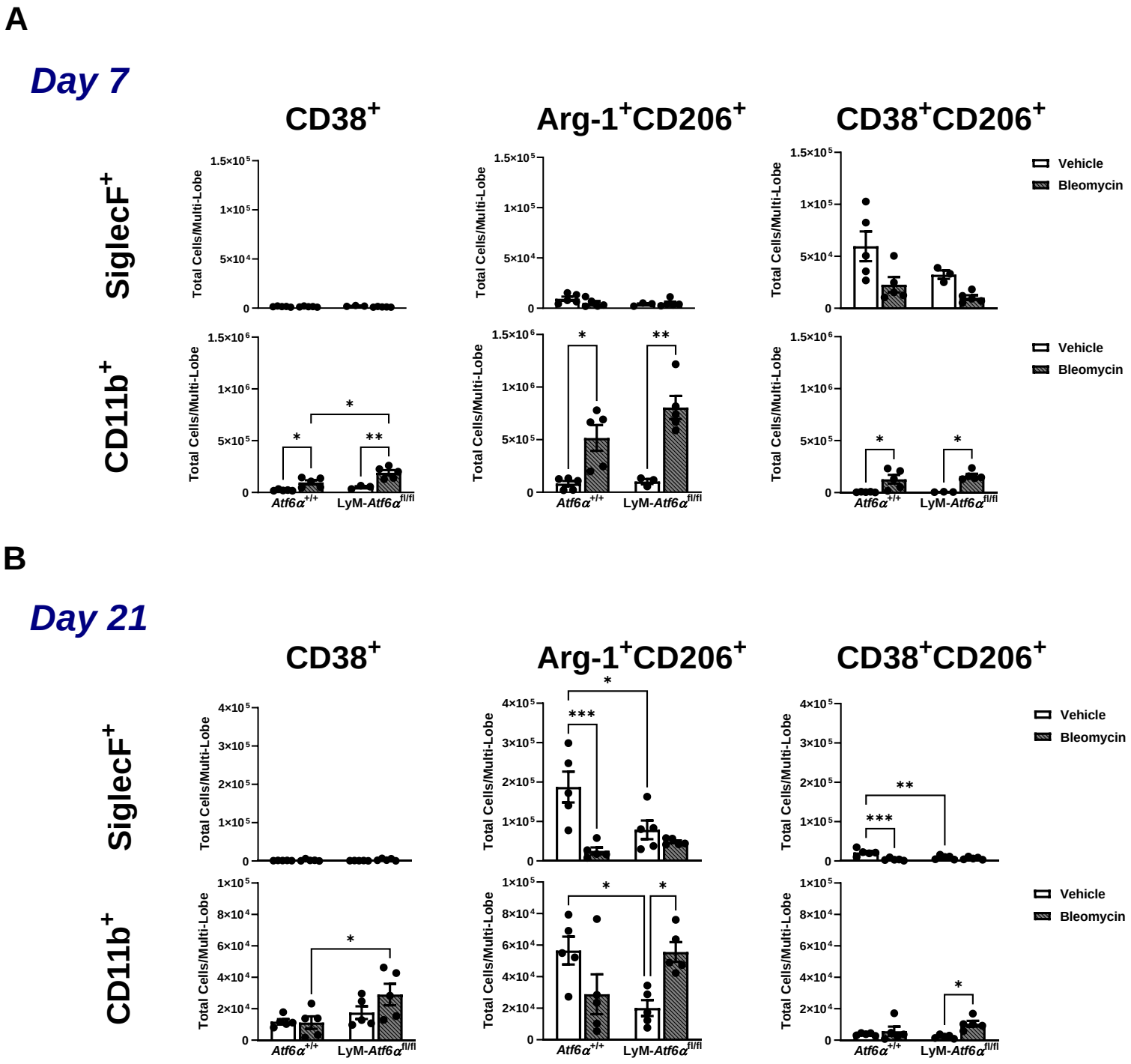
A
Day 7
CD38+
Arg-1+CD206+
CD38+CD206+
SiglecF+
CD11b+
Total Cells/Multi-Lobe
Vehicle
Bleomycin
Atf6α+/+
LyM-Atf6αfl/fl
B
Day 21
CD38+
Arg-1+CD206+
CD38+CD206+
SiglecF+
CD11b+
Total Cells/Multi-Lobe
Vehicle
Bleomycin
Atf6α+/+
LyM-Atf6αfl/fl

Figure 4

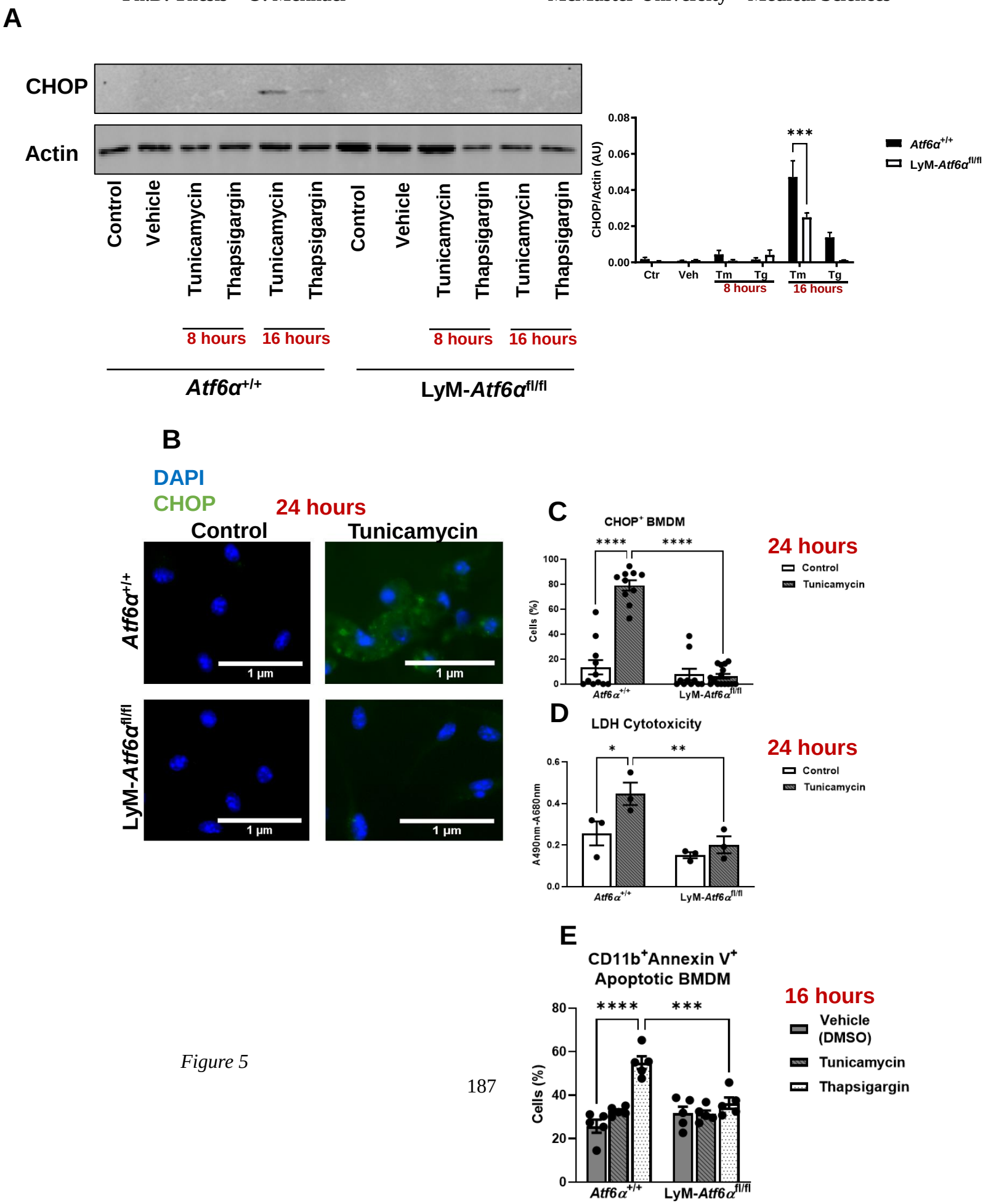
A
CHOP
Actin
Control
Vehicle
Tunicamycin
Thapsigargin
Tunicamycin
Thapsigargin
Control
Vehicle
Tunicamycin
Thapsigargin
Tunicamycin
Thapsigargin
8 hours
16 hours
8 hours
16 hours
Atf6α+/+
LyM-Atf6αfl/fl
CHOP/Actin (AU)
0.08
0.06
0.04
0.02
0.00
***
Ctr
Veh
Tm
Tg
Tm
Tg
8 hours
16 hours
Atf6α+/+
LyM-Atf6αfl/fl
B
DAPI
CHOP
24 hours
Control
Tunicamycin
Atf6α+/+
LyM-Atf6αfl/fl
1 µm
C
CHOP+ BMDM
****
****
Cells (%)
24 hours
Control
Tunicamycin
D
LDH Cytotoxicity
*
**
A490nm-A680nm
24 hours
Control
Tunicamycin
E
CD11b+Annexin V+
Apoptotic BMDM
****
***
Cells (%)
16 hours
Vehicle (DMSO)
Tunicamycin
Thapsigargin

Figure 5

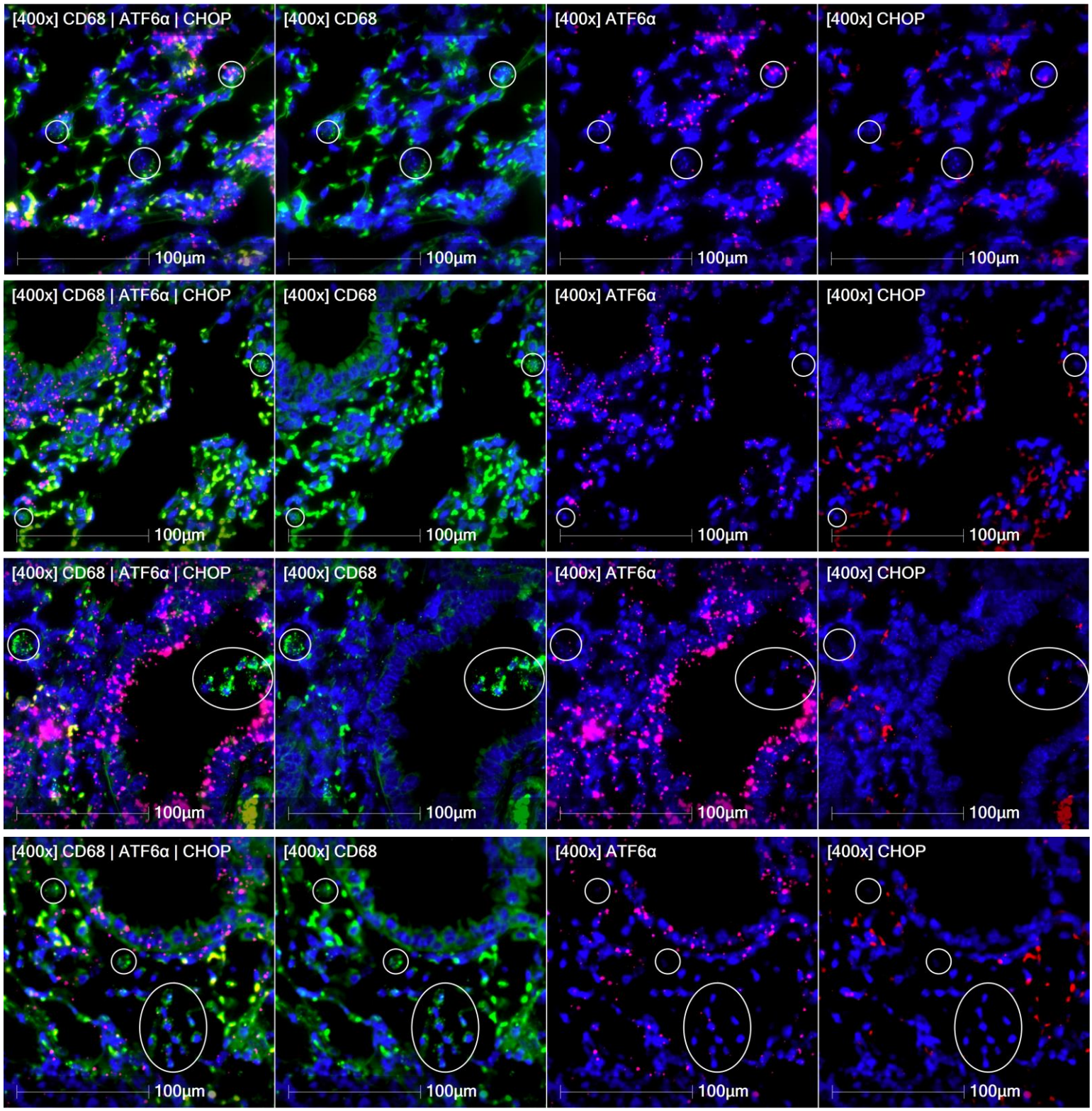
Atf6α+/+ + Saline
LyM-Atf6αfl/fl + Saline
Atf6α+/+ + Bleo D21
LyM-Atf6αfl/fl + Bleo D21
[400x] CD68 | ATF6α | CHOP
[400x] CD68
[400x] ATF6α
[400x] CHOP
100µm

Figure 6

Chapter 5

Discussion

Interplay of major findings obtained from Chapters 2-4

Monocyte-derived, but not tissue-resident macrophages, contribute to tissue remodelling

Role of cigarette smoke in tissue remodelling

Role of cigarette smoke in endoplasmic reticulum stress and the unfolded protein response

Clinical implications

Interplay of major findings obtained from Chapters 2-4

Firstly, the findings from chapter 2 provided novel clinical insights from the prospective Canadian registry for pulmonary fibrosis. To the best of our knowledge, this is the first report to study the impact of smoking status on the survival and pulmonary function outcome using a Canadian registry for fibrotic ILDs. Our clinical investigations have revealed that IPF patients were more likely to have a smoking history compared to the other fibrotic ILDs and that CTD-ILD, HP, and U-ILD patients had lower mortality than IPF patients whether they belong to the never smoker or smoker category. Furthermore, subgroup analysis showed that there was a significant interaction between smoking and fibrotic ILD diagnosis, with respect to mortality, with smoking affecting the risk of death in CTD-ILD and U-ILD more than IPF and HP. The data suggest that IPF patients are more likely to have a smoking history and a higher mortality rate compared to the other fibrotic ILD patients. However, the higher mortality rate detected in IPF patients might not necessary be directly linked to smoking. To shed light upon these clinical observations and to better understand the mechanisms by which continuous smoking affects tissue remodelling and fibrotic processes, we used a preclinical experimental mouse model of concurrent CS exposure and acute lung injury in the subsequent study. Unravelling cigarette smoke-mediated mechanisms in fibrotic ILD is warranted to shed light on clinical controversies.

Macrophages perform a vital role in the pathogenesis of several cigarette smoke-associated respiratory diseases including chronic obstructive pulmonary disease and

interstitial lung disease. However, the composition and functional capacity of pulmonary macrophage subpopulations following CS exposure have not been elucidated. In chapter 3, we utilized a whole-body cigarette smoke exposure system to investigate the impact of CS exposure on macrophage subpopulations in C57BL/6 mice using flow cytometry-based approaches. Furthermore, to assess the functional consequences of CS-induced altered macrophage composition, we used a model of concurrent bleomycin-induced lung injury and cigarette smoke exposure to examine macrophage polarization, tissue remodelling and fibrogenesis processes. We showed that CS altered pulmonary macrophage composition, expanding monocyte-derived $CD11b^+$ subpopulations at multiple CS exposure timepoints. The increase in $CD11b^+$ subpopulations was IL-1α dependent and likely reflective of elevated cell recruitment. These compositional changes were exacerbated in a model of lung injury and functionally became predominately M1-polarized with attenuated MMP9 release. These macrophage compositional and functional changes were associated with attenuated fibrogenesis and impaired tissue remodelling in CS-exposed mice. Collectively, our data propose that CS exposure skews pulmonary macrophage subpopulation composition and function predisposing the lung to impaired tissue remodelling and wound healing processes. To the best of our knowledge, this is the first report to investigate the impact of cigarette smoke exposure on pulmonary macrophage composition and function during lung injury, tissue remodelling, and fibrosis.

Protein misfolding, ER stress, and the UPR have been linked to macrophage activation in pulmonary fibrosis. To date, the impact of ATF6α, one of the UPR mediators,

on the composition and function of pulmonary macrophage subpopulations during lung injury and fibrogenesis has not been investigated. In Chapter 4, we began by examining the expression of *Atf6α* in IPF patients' lung single-cell RNA sequencing dataset, archived surgical lung specimens, and CD14 positive circulating monocytes. To assess the impact of ATF6α on pulmonary macrophage composition and pro-fibrotic function during tissue repair processes, we conducted an *in vivo* myeloid-specific deletion of *Atf6α*. Flow cytometric assessments of pulmonary macrophage subpopulations were carried out in C57BL/6 and myeloid specific ATF6α-deficient mice in the context of bleomycin-induced lung injury. The findings of chapter 4 showed that *Atf6α* gene was expressed in pro-fibrotic macrophages found in IPF patient lung and in $CD14^+$ circulating monocytes obtained from IPF patient blood. Following bleomycin administration, the myeloid-specific deletion of ATF6α expanded $CD11b^+$ subpopulations with dual polarized $CD38^+CD206^+$ expressing macrophages. Compositional changes were associated with an aggravation of fibrogenesis including increased myofibroblast and collagen deposition. Further mechanistic *ex vivo* investigation revealed that ATF6α is required for CHOP induction and for the apoptotic death of bone marrow-derived $CD11b^+$ macrophages. Taken together, our findings suggest a detrimental role for the ATF6α-deficient $CD11b^+$ macrophages which had altered functional status during lung injury and fibrosis. Targeting these $CD11b^+$ macrophage populations through the ATF6α arm of UPR might offer a potential therapeutic approach to halt fibrotic ILD progression. To the best of our knowledge, this is the first report to identify that the ATF6α arm of the UPR is required for CHOP induction and the apoptotic death of bone marrow-derived $CD11b^+$ macrophages *ex vivo*.

Collectively, CS and aberrant ER stress/UPR processes disturbed pulmonary macrophage subpopulation composition and function, expanding $CD11b^+$ macrophages, and resulted in alterations in wound healing and tissue remodelling. Further investigation of $CD11b^+$ macrophages in clinical samples obtained from fibrotic ILD patients enrolled in CARE-PF is required. The exact mechanism by which CS skews pulmonary macrophage composition and modulates their functional status is yet to be elucidated. Lastly, the specific enhancement of the activity of ATF6α/CHOP arm in $CD11b^+$ macrophage populations through targeted drug delivery to specifically induce apoptosis in this compartment might be a potential therapeutic approach to halt pulmonary fibrosis.

Monocyte-derived, but not tissue-resident macrophages, contribute to tissue remodelling

Tissue-resident alveolar macrophages, long-lived cells with developmental origins in the fetal liver[94], differentiate shortly after birth and persist over the lifespan via self-renewal, with no contribution from circulating bone marrow–derived monocytes[94]. At steady state, Res-AMs remove apoptotic cells, environmental particulates, and pathogens while ensuring normal gas-exchanging functions of the alveolus[94]. Nevertheless, severe environmental insults recruit circulating monocytes to the lung, where they differentiate into "monocyte-derived" alveolar macrophages and coordinate pro-inflammatory and pro-fibrotic responses. Furthermore, interstitial macrophage, a third macrophage population, has been shown to originate from an embryonic yolk-sac-derived origin and they are being maintained by postnatal bone marrow-derived cells[30,35]. Interstitial macrophages are

important for tissue remodelling and maintenance, as well as antigen presentation[29,30]. To date, whether these ontologically distinct macrophages play distinct roles or act synergistically during lung injury and fibrosis is not fully understood[94].

The findings from chapter 3 have shown that cigarette smoke expands monocyte-derived $CD11b^{+}$ macrophages, including Mo-AM as well as (IM)1, -2 and -3 during the early acute inflammatory phase of bleomycin-induced lung injury. However, we observed attenuated tissue remodelling following CS exposure which was associated with decreased Res-AM and Mo-AM populations at peak fibrogenesis. Chapter 3 of the present thesis provides novel evidence of the contribution of cigarette smoke exposure to altered macrophage composition during fibrogenesis. Given that chapter 2 showed that cigarette smoking might be strongly associated with the development of some fibrotic ILDs, a comprehensive understanding of the mechanism by which CS affects lung fibrosis immunopathogenesis, development, and progression is crucial. Furthermore, chapter 4 of the thesis demonstrated that following bleomycin administration, the myeloid-specific deletion of ATF6α expanded $CD11b^{+}$ macrophage populations and that was associated with aggravated fibrogenesis. In line with preclinical findings shown in chapters 3 and 4, McCubbrey *et al.* (2018) genetically depleted monocyte-derived $CD11b^{hi}$ macrophages during fibrosis by deleting the antiapoptotic protein cellular FADD-like IL-1β–converting enzyme–inhibitory protein **(c-Flip)** from those populations[62]. Consequently, $CD11b^{hi}$ macrophages became more susceptible to apoptosis[62]. They showed that the deletion of c-Flip reduced the number of $CD11b^{hi}$ macrophages in the lung, and subsequently prevented

the development of bleomycin-induced lung fibrosis[62]. Similarly, Misharin *et al.* (2017) showed that the genetic deletion of monocyte-derived alveolar macrophages via necroptosis following their recruitment to the lung attenuated bleomycin-induced lung fibrosis, whereas tissue-resident alveolar macrophages did not contribute to fibrogenesis[42]. Targeted lineage tracing experiments are warranted to validate the ontogeny of the expanded macrophage subpopulations found in our concurrent cigarette smoke and bleomycin-induced tissue remodelling preclinical experimental model and in bleomycin treated myeloid-specific ATF6α-deficient mice.

Role of cigarette smoke in tissue remodelling

Chapter 3 of this thesis demonstrated that CS significantly attenuated fibrogenesis and tissue remodelling processes in a model of bleomycin-induced lung injury. We also found altered MMP9 secretion in isolated adherent lung $CD45^+$ cells from 12-week CS-exposed mice. These data suggest an inability for CS-exposed adherent $CD45^+$ cells to contribute to α-SMA^+ myofibroblast deposition during the fibrotic phase of bleomycin-induced lung injury. Studies that aim to investigate the mechanisms which contribute to CS-mediated halted myofibroblast expansion during tissue remodelling are required.

The effect of CS on fibrotic measures has been previously addressed in multiple different experimental models of pulmonary fibrosis. For instance, Zhou *et al.* (2019) continuously exposed C57BL/6J mice to smoke for 1h each day (12 cigarettes/day, 5 days/week) over 40 days. Pulmonary fibrosis was induced in the CS-exposed mice by multiple intraperitoneal injections of bleomycin (4 mg/mL) at a dose of 40 mg/kg at days

1, 5, 8, 11 and 15. The mice were euthanized at day 40[95]. Their results illustrated that CS aggravated bleomycin-induced pulmonary fibrosis, shown by increased lung collagen deposition and that the activation of TGF-β-Smad2/3 and -Akt signaling was involved in the process[95]. Similarly, Cisneros-Lira *et al.* (2003) have shown that CS exposure increased bleomycin-induced lung fibrosis in guinea pigs. In their experimental model, guinea pigs were first exposed to smoke (20 cigarettes/day, 5 days/week) for 6 weeks, then bleomycin (3 units) was administered by single intratracheal instillation and animals were euthanized 6 weeks after bleomycin treatment[96]. A separate group was also included where guinea pigs were first given bleomycin, and simultaneously exposed to smoke for 6 weeks[96]. Although lung collagen deposition was found to be significantly higher in both CS-exposed groups treated with bleomycin compared with the control group exposed to RA and treated with saline, significant increases in lung hydroxyproline (collagen) were only detected in those guinea pigs that received tobacco smoke first and bleomycin after, compared with the group that received bleomycin alone[96]. Contrarily, Osanai *et al.* (1988) highlighted that CS ameliorated the effect of bleomycin-induced lung fibrosis in Golden hamster[97]. Animals were exposed to the smoke (4 cigarettes) for 15 min (5-min aliquots, twice a day, 5 days/week). On day 30 (day 0 of Bleo) from the start of housing and exposure to smoke, a single instillation of 0.5 mg of bleomycin per 100g body weight in saline was endotracheally administered[97]. Following 40 days of CS exposure (10 days of bleomycin instillation), quantitative morphometry of the lungs showed that CS-inhaled animals treated with bleomycin had less lung fibrotic change compared with animals treated with bleomycin alone, however, based on qualitative observation, the fibrotic

lesions of (CS+Bleo) group were merged with emphysematous changes[97]. Given the current conflicting research findings, we conclude that it is challenging to mimic human smoking fibrotic ILD conditions in experimental animal models as it was shown that the outcome of CS exposure depends on the experimental model used. Therefore, further studies are required to identify an experimental animal model that closely recapitulates fibrotic ILD patients who are smokers to be able to unravel the disease pathogenesis and subsequently yield more effective therapies[98]**.** Although the current animal models do not fully mimic the physiological features of IPF or the histopathologic pattern of UIP[99], several clinical trials relied on preclinical studies in animals and have resulted in the FDA approval of two drugs, pirfenidone and nintedanib[98,100,101]. The current IPF therapies slow down disease progression, however, they do not cure fibrosis. This suggests the need to further investigate the cellular and molecular mechanisms involved in IPF. In chapter 3 of the thesis, we administered a single intratracheal instillation of bleomycin (0.05U/mouse) in female C57BL/6 mice using the oral pharyngeal method. Bleomycin is an antibiotic that was shown to treat squamous cell carcinomas and skin tumors, however, it was found to cause pro-fibrotic side effects in lymphoma patients[98,102]. Bleomycin is considered to be the most extensively used experimental model to induce lung fibrosis in mice[98,103]**.** The consensus view of a recent American Thoracic Society workshop report proposed that the murine intratracheal bleomycin model in animals of both genders, is the *"best-characterized animal model available for preclinical testing"* and the view recognized hydroxyproline quantification for collagen deposition and the histopathology examination as best-characterized measurements[99].

Role of cigarette smoke in endoplasmic reticulum stress and the unfolded protein response

The potential link between CS, UPR, and macrophage dysfunction is yet to be established. While it is currently believed that smoke exposure can alter protein folding and result in pulmonary ER stress, the mechanisms associating smoke with ER stress are not fully understood[104]. *In vitro* exposure of cells to cigarette smoke has been shown to stimulate ER stress and UPR[105–107]. Interestingly, exposure of human bronchial epithelial cells **(hBEC)** to CS extract **(CSE)** *in vitro* induced GRP78 and CHOP expression and stimulated apoptosis[108]. Additionally, *in vivo* exposure of mice to CS triggered GRP78 and CHOP expression in the lung[108]. In chapter 3, we found that following 21 days of bleomycin administration, cigarette smoke significantly reduced Res-AM and Mo-AM populations. Given the role of CS in CHOP-mediated apoptosis[108], we further speculate that the depletion of macrophages detected in our preclinical model of concurrent CS exposure and bleomycin-induced lung injury at day 21 might be caused by CS-mediated apoptosis. Lastly, Kelsen *et al.* (2008) demonstrated that a number of UPR proteins were up-regulated in the lungs of chronic cigarette smokers[109]. Given that the role of CS in ER stress/UPR processes has been reported and that the contribution of ER stress/UPR mediators to macrophage activation has been shown, studies that investigate the potential impact of CS exposure on UPR-mediated macrophage dysfunction in the context of fibrogenesis are required.

Clinical implications

Chapter 3 data provided evidence that CS impaired tissue remodelling and wound healing processes. These findings are novel and support current thoughts in the literature that clinically, smokers with wounds resulting from trauma, disease, or surgical procedures have slow wound healing[110]. Cigarette smoking alters the function of neutrophils and macrophages required for inflammatory and bactericidal activity and compromises oxygen delivery to tissues, hence, underlying the pathobiology of chronic wounds[111]. Furthermore, cigarette smoke has been demonstrated to halt fibroblast proliferation, chemotaxis[112], and survival[113]. Impaired fibroblast migration and activation could be one of the mechanisms through which cigarette smoke impairs wound healing and tissue remodelling. A better understanding of the mechanisms and cell type which are directly altered by smoking is crucial to identify potential therapeutic targets. Specifically targeting pathways and cells that are overactivated or suppressed by smoking will potentially mitigate smoking-associated diseases. Moreover, chapter 4 of the present thesis showed that ATF6α was required for $CD11b^{+}$ macrophage CHOP-induced apoptotic death, a process required for the attenuation of fibrogenesis during chronic ER stress. Enhancing ATF6α activity in macrophages might offer a potential therapeutic approach to halt pulmonary fibrosis progression. Using drugs that activate ATF6 has been a therapeutic strategy for many human diseases associated with disrupted proteostasis including senile systemic amyloidosis, familial amyloid polyneuropathy, A1AD-associated emphysema, and liver

cirrhosis[114]. Our studies showed that cell-specific delivery of therapeutics may be required for the treatment of fibrotic lung diseases.

REFERENCES (for Chapters 1 (except for "Mouse models of lung fibrosis, a published book chapter" section), 2, and 5)

1. Wijsenbeek, M. & Cottin, V. Spectrum of Fibrotic Lung Diseases. *New England Journal of Medicine* **383**, 958–968 (2020).

2. Selman, M. & Pardo, A. When things go wrong: Exploring possible mechanisms driving the progressive fibrosis phenotype in interstitial lung diseases. *European Respiratory Journal* (2021) doi:10.1183/13993003.04507-2020.

3. Tzouvelekis, A. & Bouros, D. Endotyping of progressive fibrotic interstitial lung diseases: It is the final destination that matters and not the journey. *EBioMedicine* **51**, (2020).

4. Macneal, K. & Schwartz, D. A. The Genetic and Environmental Causes of Pulmonary Fibrosis. *Proc Am Thorac Soc* **9**, 120–125 (2012).

5. Ryerson, C. J. *et al.* The Canadian Registry for Pulmonary Fibrosis: Design and Rationale of a National Pulmonary Fibrosis Registry. *Canadian Respiratory Journal* **2016**, 1–7 (2016).

6. Travis, W. D. *et al.* An Official American Thoracic Society/European Respiratory Society Statement: Update of the International Multidisciplinary Classification of the Idiopathic Interstitial Pneumonias. *Am J Respir Crit Care Med* **188**, 733–748 (2013).

7. Lederer, D. J. & Martinez, F. J. Idiopathic Pulmonary Fibrosis. *N. Engl. J. Med.* **379**, 797–798 (2018).

8. Sack, C. & Raghu, G. Idiopathic pulmonary fibrosis: unmasking cryptogenic environmental factors. *Eur Respir J* **53**, 1801699 (2019).

9. Sgalla, G. *et al.* Idiopathic pulmonary fibrosis: pathogenesis and management. *Respir Res* **19**, (2018).

10. Martinez, F. J. *et al.* Idiopathic pulmonary fibrosis. *Nat Rev Dis Primers* **3**, 1–19 (2017).

11. Klingberg, F., Hinz, B. & White, E. S. The myofibroblast matrix: implications for tissue repair and fibrosis. *J Pathol* **229**, 298–309 (2013).

12. Hinz, B. *et al.* The Myofibroblast. *Am J Pathol* **170**, 1807–1816 (2007).

13. Prevention (US), C. for D. C. and, Promotion (US), N. C. for C. D. P. and H. & Health (US), O. on S. and. *A Vision for the Future*. *How Tobacco Smoke Causes Disease: The Biology and Behavioral Basis for Smoking-Attributable Disease: A Report of the Surgeon General* (Centers for Disease Control and Prevention (US), 2010).

14. Prevention (US), C. for D. C. and, Promotion (US), N. C. for C. D. P. and H. & Health (US), O. on S. and. *Pulmonary Diseases*. *How Tobacco Smoke Causes Disease: The Biology and Behavioral Basis for Smoking-Attributable Disease: A Report of the Surgeon General* (Centers for Disease Control and Prevention (US), 2010).

15. Prevention (US), C. for D. C. and, Promotion (US), N. C. for C. D. P. and H. & Health (US), O. on S. and. *Chemistry and Toxicology of Cigarette Smoke and Biomarkers of Exposure and Harm*. *How Tobacco Smoke Causes Disease: The Biology and*

Behavioral Basis for Smoking-Attributable Disease: A Report of the Surgeon General (Centers for Disease Control and Prevention (US), 2010).

16. Houghton, A. M., Mouded, M. & Shapiro, S. D. Common origins of lung cancer and COPD. *Nat Med* **14**, 1023–1024 (2008).

17. Cigarette smoking and health. American Thoracic Society. *Am J Respir Crit Care Med* **153**, 861–865 (1996).

18. Margaritopoulos, G. A., Vasarmidi, E., Jacob, J., Wells, A. U. & Antoniou, K. M. Smoking and interstitial lung diseases. *Eur Respir Rev* **24**, 428–435 (2015).

19. Baumgartner, K. B., Samet, J. M., Stidley, C. A., Colby, T. V. & Waldron, J. A. Cigarette smoking: a risk factor for idiopathic pulmonary fibrosis. *Am J Respir Crit Care Med* **155**, 242–248 (1997).

20. Baumgartner, K. B. *et al.* Occupational and environmental risk factors for idiopathic pulmonary fibrosis: a multicenter case-control study. Collaborating Centers. *Am J Epidemiol* **152**, 307–315 (2000).

21. Taskar, V. S. & Coultas, D. B. Is Idiopathic Pulmonary Fibrosis an Environmental Disease? *Proc Am Thorac Soc* **3**, 293–298 (2006).

22. Kishaba, T., Nagano, H., Nei, Y. & Yamashiro, S. Clinical characteristics of idiopathic pulmonary fibrosis patients according to their smoking status. *J Thorac Dis* **8**, 1112–1120 (2016).

23. King, T. E., Tooze, J. A., Schwarz, M. I., Brown, K. R. & Cherniack, R. M. Predicting survival in idiopathic pulmonary fibrosis: scoring system and survival model. *Am. J. Respir. Crit. Care Med.* **164**, 1171–1181 (2001).

24. Antoniou, K. M. *et al.* Idiopathic Pulmonary Fibrosis. *Am J Respir Crit Care Med* **177**, 190–194 (2008).

25. Kärkkäinen, M. *et al.* Effect of smoking and comorbidities on survival in idiopathic pulmonary fibrosis. *Respiratory Research* **18**, 160 (2017).

26. Wells, A. U. *et al.* Idiopathic Pulmonary Fibrosis. *Am J Respir Crit Care Med* **167**, 962–969 (2003).

27. Song, J. W., Hong, S.-B., Lim, C.-M., Koh, Y. & Kim, D. S. Acute exacerbation of idiopathic pulmonary fibrosis: incidence, risk factors and outcome. *European Respiratory Journal* **37**, 356–363 (2011).

28. Vassallo, R. & Ryu, J. H. Smoking-related interstitial lung diseases. *Clin Chest Med* **33**, 165–178 (2012).

29. Evren, E., Ringqvist, E. & Willinger, T. Origin and ontogeny of lung macrophages: from mice to humans. *Immunology* **160**, 126–138 (2020).

30. Tan, S. Y. S. & Krasnow, M. A. Developmental origin of lung macrophage diversity. *Development* **143**, 1318–1327 (2016).

31. Lugg, S. T., Scott, A., Parekh, D., Naidu, B. & Thickett, D. R. Cigarette smoke exposure and alveolar macrophages: mechanisms for lung disease. *Thorax* thoraxjnl-2020-216296 (2021) doi:10.1136/thoraxjnl-2020-216296.

32. Gibbings, S. L. *et al.* Three Unique Interstitial Macrophages in the Murine Lung at Steady State. *Am J Respir Cell Mol Biol* **57**, 66–76 (2017).

33. Hu, G. & Christman, J. W. Editorial: Alveolar Macrophages in Lung Inflammation and Resolution. *Front. Immunol.* **10**, (2019).

34. Guilliams, M. *et al.* Alveolar macrophages develop from fetal monocytes that differentiate into long-lived cells in the first week of life via GM-CSF. *J Exp Med* **210**, 1977–1992 (2013).

35. Schyns, J., Bureau, F. & Marichal, T. Lung Interstitial Macrophages: Past, Present, and Future. *J Immunol Res* **2018**, (2018).

36. Jenkins, S. J. *et al.* Local Macrophage Proliferation, Rather than Recruitment from the Blood, Is a Signature of TH2 Inflammation. *Science* **332**, 1284–1288 (2011).

37. Schulz, C. *et al.* A lineage of myeloid cells independent of Myb and hematopoietic stem cells. *Science* **336**, 86–90 (2012).

38. Hashimoto, D. *et al.* Tissue-resident macrophages self-maintain locally throughout adult life with minimal contribution from circulating monocytes. *Immunity* **38**, 792–804 (2013).

39. Gibbings, S. L. *et al.* Transcriptome analysis highlights the conserved difference between embryonic and postnatal-derived alveolar macrophages. *Blood* **126**, 1357–1366 (2015).

40. Yona, S. *et al.* Fate mapping reveals origins and dynamics of monocytes and tissue macrophages under homeostasis. *Immunity* **38**, 79–91 (2013).

41. Janssen, W. J. *et al.* Fas determines differential fates of resident and recruited macrophages during resolution of acute lung injury. *Am J Respir Crit Care Med* **184**, 547–560 (2011).

42. Misharin, A. V. *et al.* Monocyte-derived alveolar macrophages drive lung fibrosis and persist in the lung over the life span. *J Exp Med* **214**, 2387–2404 (2017).

43. Misharin, A. V., Morales-Nebreda, L., Mutlu, G. M., Budinger, G. R. S. & Perlman, H. Flow Cytometric Analysis of Macrophages and Dendritic Cell Subsets in the Mouse Lung. *Am J Respir Cell Mol Biol* **49**, 503–510 (2013).

44. Zhang, L. *et al.* Macrophages: friend or foe in idiopathic pulmonary fibrosis? *Respir Res* **19**, 170 (2018).

45. Wynn, T. A. & Vannella, K. M. Macrophages in tissue repair, regeneration, and fibrosis. *Immunity* **44**, 450–462 (2016).

46. Jablonski, K. A. *et al.* Novel Markers to Delineate Murine M1 and M2 Macrophages. *PLoS One* **10**, (2015).

47. Qiu, F. *et al.* Impacts of cigarette smoking on immune responsiveness: Up and down or upside down? *Oncotarget* **8**, 268–284 (2016).

48. Karimi, R., Tornling, G., Grunewald, J., Eklund, A. & Sköld, C. M. Cell recovery in bronchoalveolar lavage fluid in smokers is dependent on cumulative smoking history. *PLoS One* **7**, e34232 (2012).

49. Gaschler, G. J. *et al.* Cigarette Smoke Exposure Attenuates Cytokine Production by Mouse Alveolar Macrophages. *Am J Respir Cell Mol Biol* **38**, 218–226 (2008).

50. Chen, H., Cowan, M. J., Hasday, J. D., Vogel, S. N. & Medvedev, A. E. Tobacco smoking inhibits expression of proinflammatory cytokines and activation of IL-1R-associated kinase, p38, and NF-kappaB in alveolar macrophages stimulated with TLR2 and TLR4 agonists. *J Immunol* **179**, 6097–6106 (2007).

51. Dewhurst, J. A. *et al.* Characterisation of lung macrophage subpopulations in COPD patients and controls. *Scientific Reports* **7**, 7143 (2017).

52. Morissette, M. C., Shen, P., Thayaparan, D. & Stämpfli, M. R. Disruption of pulmonary lipid homeostasis drives cigarette smoke-induced lung inflammation in mice. *Eur Respir J* **46**, 1451–1460 (2015).

53. Nikota, J. K. *et al.* Cigarette smoke primes the pulmonary environment to IL-1α/CXCR-2-dependent nontypeable Haemophilus influenzae-exacerbated neutrophilia in mice. *J Immunol* **193**, 3134–3145 (2014).

54. Shaykhiev, R. *et al.* Smoking-dependent Reprogramming of Alveolar Macrophage Polarization: Implication for Pathogenesis of COPD. *J Immunol* **183**, 2867–2883 (2009).

55. Karimi, K. *et al.* Toll-like receptor-4 mediates cigarette smoke-induced cytokine production by human macrophages. *Respir Res* **7**, 66 (2006).

56. Eapen, M. S. *et al.* Abnormal M1/M2 macrophage phenotype profiles in the small airway wall and lumen in smokers and chronic obstructive pulmonary disease (COPD). *Sci Rep* **7**, (2017).

57. Adams Taylor S *et al.* Single Cell RNA-seq reveals ectopic and aberrant lung resident cell populations in Idiopathic Pulmonary Fibrosis. *Science Advances* **6**, 1–28 (2020).

58. Morse, C. *et al.* Proliferating SPP1/MERTK-expressing macrophages in idiopathic pulmonary fibrosis. *European Respiratory Journal* **54**, (2019).

59. Reyfman, P. A. *et al.* Single-cell transcriptomic analysis of human lung provides insights into the pathobiology of pulmonary fibrosis. *American Journal of Respiratory and Critical Care Medicine* **199**, 1517–1536 (2019).

60. Ayaub, E. A. *et al.* Single Cell RNA-seq and Mass Cytometry Reveals a Novel and a Targetable Population of Macrophages in Idiopathic Pulmonary Fibrosis. *bioRxiv* 2021.01.04.425268 (2021) doi:10.1101/2021.01.04.425268.

61. Joshi, N. *et al.* A spatially restricted fibrotic niche in pulmonary fibrosis is sustained by M-CSF/M-CSFR signalling in monocyte-derived alveolar macrophages. *Eur Respir J* **55**, (2020).

62. McCubbrey, A. L. *et al.* Deletion of c-FLIP from CD11bhi Macrophages Prevents Development of Bleomycin-induced Lung Fibrosis. *Am J Respir Cell Mol Biol* **58**, 66–78 (2018).

63. Prasse, A. *et al.* A Vicious Circle of Alveolar Macrophages and Fibroblasts Perpetuates Pulmonary Fibrosis via CCL18. *Am J Respir Crit Care Med* **173**, 781–792 (2006).

64. Gibbons, M. A. *et al.* Ly6Chi Monocytes Direct Alternatively Activated Profibrotic Macrophage Regulation of Lung Fibrosis. *Am J Respir Crit Care Med* **184**, 569–581 (2011).

65. Ji, W.-J. *et al.* Temporal and spatial characterization of mononuclear phagocytes in circulating, lung alveolar and interstitial compartments in a mouse model of bleomycin-induced pulmonary injury. *J. Immunol. Methods* **403**, 7–16 (2014).

66. Ayaub, E. A. *et al.* Overexpression of OSM and IL-6 impacts the polarization of pro-fibrotic macrophages and the development of bleomycin-induced lung fibrosis. *Scientific Reports* **7**, 1–16 (2017).

67. Lodyga, M. *et al.* Cadherin-11–mediated adhesion of macrophages to myofibroblasts establishes a profibrotic niche of active TGF-β. *Sci. Signal.* **12**, (2019).

68. Naiel, S. *et al.* Protein Misfolding and Endoplasmic Reticulum Stress in Chronic Lung Disease: Will Cell-Specific Targeting Be the Key to the Cure? *Chest* **157**, 1207–1220 (2020).

69. Hu, H., Tian, M., Ding, C. & Yu, S. The C/EBP Homologous Protein (CHOP) Transcription Factor Functions in Endoplasmic Reticulum Stress-Induced Apoptosis and Microbial Infection. *Front. Immunol.* **9**, (2019).

70. Corazzari, M., Gagliardi, M., Fimia, G. M. & Piacentini, M. Endoplasmic Reticulum Stress, Unfolded Protein Response, and Cancer Cell Fate. *Front Oncol* **7**, (2017).

71. Bradley, K. L., Stokes, C. A., Marciniak, S. J., Parker, L. C. & Condliffe, A. M. Role of unfolded proteins in lung disease. *Thorax* **76**, 92–99 (2021).

72. Burman, A., Tanjore, H. & Blackwell, T. S. Endoplasmic reticulum stress in pulmonary fibrosis. *Matrix Biol* **68–69**, 355–365 (2018).

73. Wei, J., Rahman, S., Ayaub, E. A., Dickhout, J. G. & Ask, K. Protein misfolding and endoplasmic reticulum stress in chronic lung disease. *Chest* **143**, 1098–1105 (2013).

74. Oyadomari, S. & Mori, M. Roles of CHOP/GADD153 in endoplasmic reticulum stress. *Cell Death Differ* **11**, 381–389 (2004).

75. Burman, A. *et al.* Localized hypoxia links ER stress to lung fibrosis through induction of C/EBP homologous protein. *JCI Insight* **3**, (2018).

76. Delbrel, E. *et al.* HIF-1α triggers ER stress and CHOP-mediated apoptosis in alveolar epithelial cells, a key event in pulmonary fibrosis. *Scientific Reports* **8**, 17939 (2018).

77. Ayaub, E. A. *et al.* GRP78 and CHOP modulate macrophage apoptosis and the development of bleomycin-induced pulmonary fibrosis. *The Journal of Pathology* **239**, 411–425 (2016).

78. Ayaub, E. A. *et al.* IL-6 mediates ER expansion during hyperpolarization of alternatively activated macrophages. *Immunol Cell Biol* **97**, 203–217 (2019).

79. Bommiasamy, H. *et al.* ATF6alpha induces XBP1-independent expansion of the endoplasmic reticulum. *J Cell Sci* **122**, 1626–1636 (2009).

80. Baek, H. A. *et al.* Involvement of Endoplasmic Reticulum Stress in Myofibroblastic Differentiation of Lung Fibroblasts. *Am J Respir Cell Mol Biol* **46**, 731–739 (2012).

81. Ghavami, S. *et al.* Autophagy and the unfolded protein response promote profibrotic effects of TGF-β1 in human lung fibroblasts. *Am J Physiol Lung Cell Mol Physiol* **314**, L493–L504 (2018).

82. Haze, K., Yoshida, H., Yanagi, H., Yura, T. & Mori, K. Mammalian transcription factor ATF6 is synthesized as a transmembrane protein and activated by proteolysis in response to endoplasmic reticulum stress. *Mol Biol Cell* **10**, 3787–3799 (1999).

83. Haze, K. *et al.* Identification of the G13 (cAMP-response-element-binding protein-related protein) gene product related to activating transcription factor 6 as a transcriptional activator of the mammalian unfolded protein response. *Biochem J* **355**, 19–28 (2001).

84. Forouhan, M., Mori, K. & Boot-Handford, R. P. Paradoxical roles of ATF6α and ATF6β in modulating disease severity caused by mutations in collagen X. *Matrix Biol* **70**, 50–71 (2018).

85. Adachi, Y. *et al.* ATF6 is a transcription factor specializing in the regulation of quality control proteins in the endoplasmic reticulum. *Cell Struct Funct* **33**, 75–89 (2008).

86. Yamamoto, K. *et al.* Transcriptional induction of mammalian ER quality control proteins is mediated by single or combined action of ATF6alpha and XBP1. *Dev Cell* **13**, 365–376 (2007).

87. Okada, T., Yoshida, H., Akazawa, R., Negishi, M. & Mori, K. Distinct roles of activating transcription factor 6 (ATF6) and double-stranded RNA-activated protein kinase-like endoplasmic reticulum kinase (PERK) in transcription during the mammalian unfolded protein response. *Biochem J* **366**, 585–594 (2002).

88. Wang, X., Karamariti, E., Simpson, R., Wang, W. & Xu, Q. Dickkopf Homolog 3 Induces Stem Cell Differentiation into Smooth Muscle Lineage via ATF6 Signalling. *J Biol Chem* **290**, 19844–19852 (2015).

89. Krawczyk, K. K. *et al.* Assessing the contribution of thrombospondin-4 induction and ATF6α activation to endoplasmic reticulum expansion and phenotypic modulation in bladder outlet obstruction. *Sci Rep* **6**, 32449 (2016).

90. Rosas, I. O. *et al.* Interstitial Lung Disease: NHLBI Workshop on the Primary Prevention of Chronic Lung Diseases. *Ann Am Thorac Soc* **11**, S169–S177 (2014).

91. Kalchiem-Dekel, O., Galvin, J. R., Burke, A. P., Atamas, S. P. & Todd, N. W. Interstitial Lung Disease and Pulmonary Fibrosis: A Practical Approach for General Medicine Physicians with Focus on the Medical History. *J Clin Med* **7**, (2018).

92. Attili, A. K. *et al.* Smoking-related Interstitial Lung Disease: Radiologic-Clinical-Pathologic Correlation. *RadioGraphics* **28**, 1383–1396 (2008).

93. Fisher, J. H. *et al.* Baseline characteristics and comorbidities in the CAnadian REgistry for Pulmonary Fibrosis. *BMC Pulm Med* **19**, 223 (2019).

94. McQuattie-Pimentel, A. C., Budinger, G. R. S. & Ballinger, M. N. Monocyte-derived Alveolar Macrophages: The Dark Side of Lung Repair? *Am J Respir Cell Mol Biol* **58**, 5–6 (2018).

95. Zhou, L.-L. *et al.* Cigarette smoking aggravates bleomycin-induced experimental pulmonary fibrosis. *Toxicol. Lett.* **303**, 1–8 (2019).

96. Cisneros-Lira, J., Gaxiola, M., Ramos, C., Selman, M. & Pardo, A. Cigarette smoke exposure potentiates bleomycin-induced lung fibrosis in guinea pigs. *Am. J. Physiol. Lung Cell Mol. Physiol.* **285**, L949-956 (2003).

97. Osanai, K. *et al.* The effect of cigarette smoke on bleomycin-induced pulmonary fibrosis in hamsters. *Am. Rev. Respir. Dis.* **138**, 1276–1281 (1988).

98. Tashiro, J. *et al.* Exploring Animal Models That Resemble Idiopathic Pulmonary Fibrosis. *Front Med (Lausanne)* **4**, (2017).

99. Jenkins, R. G. *et al.* An Official American Thoracic Society Workshop Report: Use of Animal Models for the Preclinical Assessment of Potential Therapies for Pulmonary Fibrosis. *Am J Respir Cell Mol Biol* **56**, 667–679 (2017).

100. King, T. E. *et al.* A phase 3 trial of pirfenidone in patients with idiopathic pulmonary fibrosis. *N. Engl. J. Med.* **370**, 2083–2092 (2014).

101. Richeldi, L. *et al.* Efficacy and safety of nintedanib in idiopathic pulmonary fibrosis. *N. Engl. J. Med.* **370**, 2071–2082 (2014).

102. Moore, B. B. & Hogaboam, C. M. Murine models of pulmonary fibrosis. *Am. J. Physiol. Lung Cell Mol. Physiol.* **294**, L152-160 (2008).

103. Degryse, A. L. *et al.* Repetitive intratracheal bleomycin models several features of idiopathic pulmonary fibrosis. *Am J Physiol Lung Cell Mol Physiol* **299**, L442–L452 (2010).

104. Dickens, J. A., Malzer, E., Chambers, J. E. & Marciniak, S. J. Pulmonary endoplasmic reticulum stress—scars, smoke, and suffocation. *The FEBS Journal* **286**, 322–341 (2019).

105. Jorgensen, E. *et al.* Cigarette smoke induces endoplasmic reticulum stress and the unfolded protein response in normal and malignant human lung cells. *BMC Cancer* **8**, 229 (2008).

106. Hengstermann, A. & Müller, T. Endoplasmic reticulum stress induced by aqueous extracts of cigarette smoke in 3T3 cells activates the unfolded-protein-response-dependent PERK pathway of cell survival. *Free Radic Biol Med* **44**, 1097–1107 (2008).

107. Kenche, H. *et al.* Adverse Outcomes Associated with Cigarette Smoke Radicals Related to Damage to Protein-disulfide Isomerase. *J Biol Chem* **291**, 4763–4778 (2016).

108. Tagawa, Y. *et al.* Induction of apoptosis by cigarette smoke via ROS-dependent endoplasmic reticulum stress and CCAAT/enhancer-binding protein-homologous protein (CHOP). *Free Radic Biol Med* **45**, 50–59 (2008).

109. Kelsen, S. G. *et al.* Cigarette smoke induces an unfolded protein response in the human lung: a proteomic approach. *Am J Respir Cell Mol Biol* **38**, 541–550 (2008).

110. Silverstein, P. Smoking and wound healing. *Am J Med* **93**, 22S-24S (1992).

111. McDaniel, J. C. & Browning, K. K. Smoking, Chronic Wound Healing, and Implications for Evidence-Based Practice. *J Wound Ostomy Continence Nurs* **41**, 415-E2 (2014).

112. Nakamura, Y. *et al.* Cigarette smoke inhibits lung fibroblast proliferation and chemotaxis. *Am J Respir Crit Care Med* **151**, 1497–1503 (1995).

113. Wong, L. S. & Martins-Green, M. Firsthand cigarette smoke alters fibroblast migration and survival: implications for impaired healing. *Wound Repair Regen* **12**, 471–484 (2004).

114. Plate, L. & Wiseman, R. L. Regulating Secretory Proteostasis Through the Unfolded Protein Response: From Function to Therapy. *Trends Cell Biol* **27**, 722–737 (2017).

APPENDIX- COPYRIGHT INFO

Author of this Springer Nature content	yes
Title	Mouse Models of Lung Fibrosis
Institution name	McMaster University
Expected presentation date	Jun 2021
Order reference number	978-1-0716-1382-5
Requestor Location	Miss. Olivia Mekhael 5468 Tenth Line West MISSISSAUGA, ON L5M 0G5 Canada Attn: Miss. Olivia Mekhael
Total	0.00 CAD

Terms and Conditions

Springer Nature Customer Service Centre GmbH
Terms and Conditions

This agreement sets out the terms and conditions of the licence (the **Licence**) between you and **Springer Nature Customer Service Centre GmbH** (the **Licensor**). By clicking 'accept' and completing the transaction for the material (**Licensed Material**), you also confirm your acceptance of these terms and conditions.

1. Grant of License

1. 1. The Licensor grants you a personal, non-exclusive, non-transferable, world-wide licence to reproduce the Licensed Material for the purpose specified in your order only. Licences are granted for the specific use requested in the order and for no other use, subject to the conditions below.

1. 2. The Licensor warrants that it has, to the best of its knowledge, the rights to license reuse of the Licensed Material. However, you should ensure that the material you are requesting is original to the Licensor and does not carry the copyright of another entity (as credited in the published version).

1. 3. If the credit line on any part of the material you have requested indicates that it was reprinted or adapted with permission from another source, then you should also seek permission from that source to reuse the material.

2. Scope of Licence

2. 1. You may only use the Licensed Content in the manner and to the extent permitted by these Ts&Cs and any applicable laws.

2. 2. A separate licence may be required for any additional use of the Licensed Material, e.g. where a licence has been purchased for print only use, separate permission must be obtained for electronic re-use. Similarly, a licence is only valid in the language selected and does not apply for editions in other languages unless additional translation rights have been granted separately in the licence. Any content owned by third parties are expressly excluded from the licence.

2. 3. Similarly, rights for additional components such as custom editions and derivatives require additional permission and may be subject to an additional fee. Please apply to Journalpermissions@springernature.com/bookpermissions@springernature.com for these rights.

2. 4. Where permission has been granted **free of charge** for material in print, permission may also be granted for any electronic version of that work, provided that the material is incidental to your work as a whole and that the electronic version is essentially equivalent to, or substitutes for, the print version.

2. 5. An alternative scope of licence may apply to signatories of the STM Permissions Guidelines, as amended from time to time.

3. Duration of Licence

3. 1. A licence for is valid from the date of purchase ('Licence Date') at the end of the relevant period in the below table:

Scope of Licence	Duration of Licence
Post on a website	12 months
Presentations	12 months
Books and journals	Lifetime of the edition in the language purchased

4. Acknowledgement

4. 1. The Licensor's permission must be acknowledged next to the Licenced Material in print. In electronic form, this acknowledgement must be visible at the same time as the figures/tables/illustrations or abstract, and must be hyperlinked to the journal/book's homepage. Our required acknowledgement format is in the Appendix below.

5. Restrictions on use

5. 1. Use of the Licensed Material may be permitted for incidental promotional use and minor editing privileges e.g. minor adaptations of single figures, changes of format, colour and/or style where the adaptation is credited as set out in Appendix 1 below. Any

other changes including but not limited to, cropping, adapting, omitting material that affect the meaning, intention or moral rights of the author are strictly prohibited.

5. 2. You must not use any Licensed Material as part of any design or trademark.

5. 3. Licensed Material may be used in Open Access Publications (OAP) before publication by Springer Nature, but any Licensed Material must be removed from OAP sites prior to final publication.

6. Ownership of Rights

6. 1. Licensed Material remains the property of either Licensor or the relevant third party and any rights not explicitly granted herein are expressly reserved.

7. Warranty

IN NO EVENT SHALL LICENSOR BE LIABLE TO YOU OR ANY OTHER PARTY OR ANY OTHER PERSON OR FOR ANY SPECIAL, CONSEQUENTIAL, INCIDENTAL OR INDIRECT DAMAGES, HOWEVER CAUSED, ARISING OUT OF OR IN CONNECTION WITH THE DOWNLOADING, VIEWING OR USE OF THE MATERIALS REGARDLESS OF THE FORM OF ACTION, WHETHER FOR BREACH OF CONTRACT, BREACH OF WARRANTY, TORT, NEGLIGENCE, INFRINGEMENT OR OTHERWISE (INCLUDING, WITHOUT LIMITATION, DAMAGES BASED ON LOSS OF PROFITS, DATA, FILES, USE, BUSINESS OPPORTUNITY OR CLAIMS OF THIRD PARTIES), AND
WHETHER OR NOT THE PARTY HAS BEEN ADVISED OF THE POSSIBILITY OF SUCH DAMAGES. THIS LIMITATION SHALL APPLY NOTWITHSTANDING ANY FAILURE OF ESSENTIAL PURPOSE OF ANY LIMITED REMEDY PROVIDED HEREIN.

8. Limitations

8. 1. ***BOOKS ONLY:*** Where **'reuse in a dissertation/thesis'** has been selected the following terms apply: Print rights of the final author's accepted manuscript (for clarity, NOT the published version) for up to 100 copies, electronic rights for use only on a personal website or institutional repository as defined by the Sherpa guideline (www.sherpa.ac.uk/romeo/).

8. 2. For content reuse requests that qualify for permission under the STM Permissions Guidelines, which may be updated from time to time, the STM Permissions Guidelines supersede the terms and conditions contained in this licence.

9. Termination and Cancellation

9. 1. Licences will expire after the period shown in Clause 3 (above).

9. 2. Licensee reserves the right to terminate the Licence in the event that payment is not received in full or if there has been a breach of this agreement by you.

Appendix 1 — Acknowledgements:

For Journal Content:
Reprinted by permission from [**the Licensor**]: [**Journal Publisher** (e.g. Nature/Springer/Palgrave)] [**JOURNAL NAME**] [**REFERENCE CITATION** (Article name, Author(s) Name), [**COPYRIGHT**] (year of publication)

For **Advance Online Publication papers:**
Reprinted by permission from [**the Licensor**]: [**Journal Publisher** (e.g. Nature/Springer/Palgrave)] [**JOURNAL NAME**] [**REFERENCE CITATION** (Article name, Author(s) Name), [**COPYRIGHT**] (year of publication), advance online publication, day month year (doi: 10.1038/sj.[JOURNAL ACRONYM].)

For Adaptations/Translations:
Adapted/Translated by permission from [**the Licensor**]: [**Journal Publisher** (e.g. Nature/Springer/Palgrave)] [**JOURNAL NAME**] [**REFERENCE CITATION** (Article name, Author(s) Name), [**COPYRIGHT**] (year of publication)

Note: For any republication from the British Journal of Cancer, the following credit line style applies:

Reprinted/adapted/translated by permission from [**the Licensor**]: on behalf of Cancer Research UK: : [**Journal Publisher** (e.g. Nature/Springer/Palgrave)] [**JOURNAL NAME**] [**REFERENCE CITATION** (Article name, Author(s) Name), [**COPYRIGHT**] (year of publication)

For **Advance Online Publication** papers:
Reprinted by permission from The [**the Licensor**]: on behalf of Cancer Research UK: [**Journal Publisher** (e.g. Nature/Springer/Palgrave)] [**JOURNAL NAME**] [**REFERENCE CITATION** (Article name, Author(s) Name), [**COPYRIGHT**] (year of publication), advance online publication, day month year (doi: 10.1038/sj.[JOURNAL ACRONYM])

For Book content:
Reprinted/adapted by permission from [**the Licensor**]: [**Book Publisher** (e.g. Palgrave Macmillan, Springer etc) [**Book Title**] by [**Book author**(s)] [**COPYRIGHT**] (year of publication)

Other Conditions:

Version 1.3

Questions? customercare@copyright.com or +1-855-239-3415 (toll free in the US) or +1-978-646-2777.